James Ayres

Galvanised Ultra High Strength Steels for Cold Formed Automotive Body in White Applications

Submitted to Swansea University, in fulfilment of the requirements for the Degree of

Doctor of Engineering

2022

Prifysgol Abertawe
Swansea University

Declaration

This work has not previously been accepted in substance for any degree and is not being concurrently submitted in candidature for any degree.

[redacted].....

Date.....21/12/2022.....

This thesis is the result of my own investigations, except where otherwise stated. Other sources are acknowledged by footnotes giving explicit references. A bibliography is appended.

[redacted].....

Date.....21/12/2022.....

I hereby give consent for my thesis, if accepted, to be available for electronic sharing **after expiry of a bar on access approved by the Swansea University.**

[redacted].....

Date.....21/12/2022.....

The University's ethical procedures have been followed and, where appropriate, that ethical approval has been granted.

[redacted].....

Date.....21/12/2022.....

Abstract

The requirement of automotive manufacturers to downgauge material to save weight and lower vehicular emissions has led to the development of ever more complex advanced and ultra-high strength steels (AHSS/UHSS). Dual Phase (DP) steels have come to the fore in recent years due to their high strength and initial strain hardening whilst achieving good elongation. Microstructurally these properties are achieved with a combination of a hard martensitic phase combined with a soft and ductile ferrite phase.

This thesis focusses on silicon's role on the microstructure and mechanical properties of DP steels whilst also optimizing the processing windows at Tata Steel's continuous annealing processing line (CAPL), and the galvanising line, ZODIAC. Lab casts of DP800 steel with 0wt%, 0.2wt% and 0.4wt% silicon were cast and rolled to match industrial specifications, it was found that the increased silicon content led to a refined hot rolled microstructure with an increased volume fraction of pearlite. The finely dispersed pearlite allows for an increase in nucleation sites where it can transform to austenite during the soak section of the annealing cycle. This led to a more finely dispersed and higher volume fraction of austenite which on cooling transforms to martensite in the final product. The result was an increase in tensile strength from 790MPa to 900MPa with no marked change in elongation.

Additionally, a DP cast chemistry with an increase in silicon produced and used in Tata Steel's IJmuiden plant was trialled to achieve a viable DP1000 product through Zodiac. Whilst the grade did achieve the requirements in some trials, the variability when scaling to industrial processing would likely lead to mechanical property failures, outweighing the benefits. Trialling the same cast chemistry using optimized CAPL cycles led to the development of a novel high yield variant of DP1000, and a potential successful replacement to the current cast chemistry used to produce DP1000 at Tata Steel's UK site.

Acknowledgements

Firstly, I would like to thank my academic supervisor Professor David Penney for his endless support and guidance throughout these last five years, keeping me on track and always pushing me when I needed it. Secondly, I would also thank my industrial supervisors Dr Peter Evans and Dr Richard Underhill for their invaluable knowledge of both product and processes.

I would also like to thank Peter's NPD team, Andrew, Geraint, Tom and in particular Lee for their help rolling material, cutting material as well as assisting whatever requirements I've needed for this project. You guys have been instrumental in getting things done over the years, and it's been very much appreciated!

Additional thanks to the M2A team who have been helped and supported me through the program, and the teams at Swansea such as MACH1 and AIM who have been instrumental in dilatometry and imagery. Further thanks go to Mark and Callum at SaMI, for the help with several rounds of tensile testing, bake hardening and block cutting.

And finally to my family, friends and in particular to my wife Emily. This work has been one of the most challenging things I have had to do, during some of the most difficult times we have gone through. Your patience and support in getting me through this has been so very much appreciated, and I hope that I have done you proud.

Contents

List of Tables / Figures

1. Introduction

With ever increasing concerns about human induced global warming through release of greenhouse gases, stringent targets are being set by global legislators to reduce the effects humans are having on the climate. Initial reports have suggested that industrialised countries should look to reduce greenhouse gas emissions by 50-75% by 2050 (1). To support this, automotive manufacturers are searching for new materials to help save weight in vehicles, bringing about a reduction in the emissions produced. Ever more complex geometries being built into automotive vehicles, combined with the requirement for weight saving, has led to the development of novel ultra-high strength steels (UHSS). These materials often combine high strength with good formability and allow automotive manufacturers to meet the diverse functional requirements that are in today's vehicles (2).

An advantage of downgauging UHSS material is that the fuel efficiency can be increased, or in the case of electric vehicles an increase in range would be achieved. UHSS can be made thinner than traditional high strength steels, therefore giving the automotive manufacturer the same strength to weight ratio. An example of this is the FutureSteelVehicle (FSV) program produced with steel members in the WorldAutoSteel group, the program achieved a 39% mass reduction of the vehicle through optimisation of the body structure (2). Another study has shown that for every 10% reduction in vehicle weight, a 3.5% improvement in fuel efficiency can occur. As for the greenhouse gas effect, a 100kg weigh reduction can result in CO_2 reductions of approximately 3.5gCO_2/km of cars driven (3).

Further advantages to the UHSS materials mean the light-weighting of the vehicle required less power to accelerate and to brake, leading to further emissions savings because the power unit required to drive the vehicle is lessened (3).

A life cycle assessment (LCA) is also high on automotive manufacturers list. Steel has come under ever increasing challenge from other materials such as aluminium, magnesium and composites such as carbon fibre. The LCA can give an estimate on the environmental impact that a product may have over its life span, this is called cradle-to-grave. It assesses the materials impact from raw materials to its final disposal, also including how the material is extracted, processed, manufactured, used, maintained and then either recycled or sent to landfill (4).

With advances in other materials, steels share in the automotive body in white (BIW) looks to be under threat. Reducing the weight of an automotive vehicle will have a significant effect on its cost over the lifetime. The biggest advantage of steel is that it is comparatively cheap to manufacture per ton, especially when comparing to aluminium and carbon fibre. However, due to its lightweight nature, aluminium has become a big competitor. Research has shown over its lifetime that replacing traditional steel components with aluminium has a payback period of 9 years from virgin material, where it would have been more cost effective, this is due to the much larger cost of extraction and production of primary aluminium comparative to steel (5)(6).

It also shows that if both materials were to have 75% of its components recycled come from recycled material, it would only require 4 years or 57,970 miles to offset the cost of aluminium versus steel, though the final conclusion to the review was that both materials should be considered rather than a complete replacement (5). Due to the higher costs of aluminium over an equivalent steel part, the use of aluminium tends to be kept to luxury automotive manufactures, who can recover the costs in the higher selling price of the vehicles.

In the past 30 years, innovation has led to development of new UHSS which are allowing automotive manufacturers to downgauge the components whilst not compromising strength and crashworthiness. This family of steels include Dual Phase (DP), Complex-Phase (CP), Ferritic-Bainitic (FB), Martensitic (MS), Transformation-Induced Plasticity (TRIP), Hot-Formed (HF), and Twinning-Induced Plasticity (TWIP). Each of these materials has unique properties which differentiates itself from the normal range high strength steels. This range of steels are known as 1st and 2nd generation UHSS steels.

The 3rd generation is looking to take innovation further. The trend of increase strength typically means a decrease in ductility, the 3rd generation is looking to ‘plug the gap’ by increasing the ductility of these UHSS without sacrificing strength. The aims of the 3rd generation mechanical properties are shown diagrammatically in figure 1.1. Cutting edge steels products such as carbide-free bainite, medium manganese (Medium Mn) and quench and partitioned (Q&P) have been produced, but the complexity required in some cases has meant large scale commercialisation can be difficult.

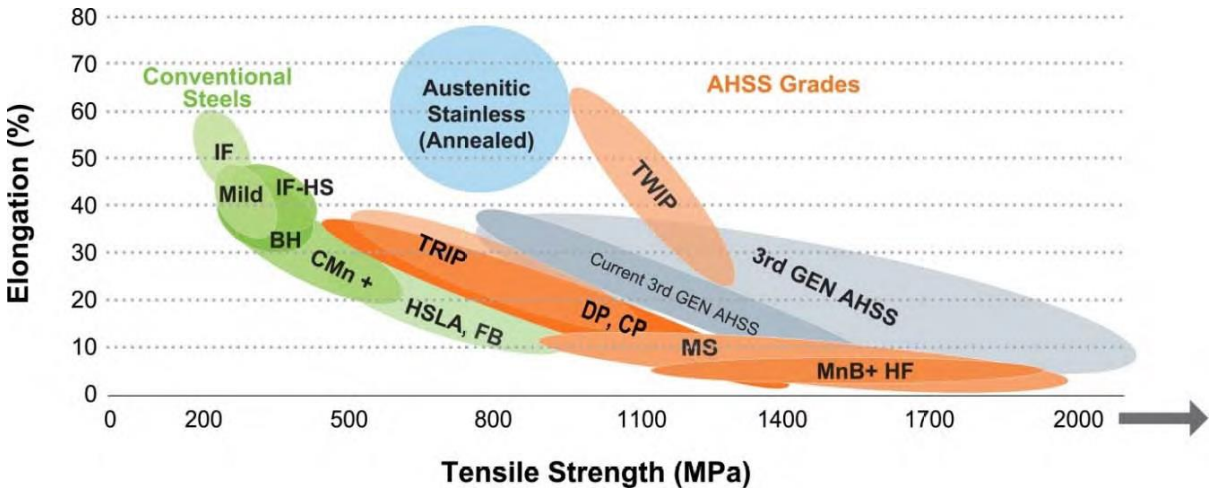

Figure 1.1 Steel strength vs. ductility curve, or 'banana' diagram showing current range of AHSS, with 3rd generation AHSS (grey region) the goal for many automotive manufacturers (2)

Tata Strip Products UK currently offer UHSS materials in their product range, the current commercialised products include a FB grade as well as DP600, DP800 and DP1000. Trials have been attempted for some of the more complex UHSS grades, such as TRIP and TWIP. The body of work in this thesis will focus on developments for both DP800 and DP1000, adjusting the processing conditions to bring about the best mechanical properties and to potentially expand the product offering for these grades.

2. Literature Review

2.1. Dual Phase Steels

Dual Phase steels (DP) were one of the first grades to be produced in the UHSS family. It is thought that their development first arose in around 1975 with the grade producing around 600MPa of strength combined with good ductility (7). The material consists primarily of two phases, ferrite for ductility and martensite for its strength. Ferrite makes up most of the matrix of the steel combined with high strength martensite islands within the structure, as shown in figure 2.1. It is not uncommon for other phases to be present in the steel, for example retained austenite and bainite may be present, which will also change the mechanical properties of the material (8). Commercially the number after DP reflects the tensile strength of the steel, so for example DP800 steel would be a dual phase steel with 800MPa tensile strength.

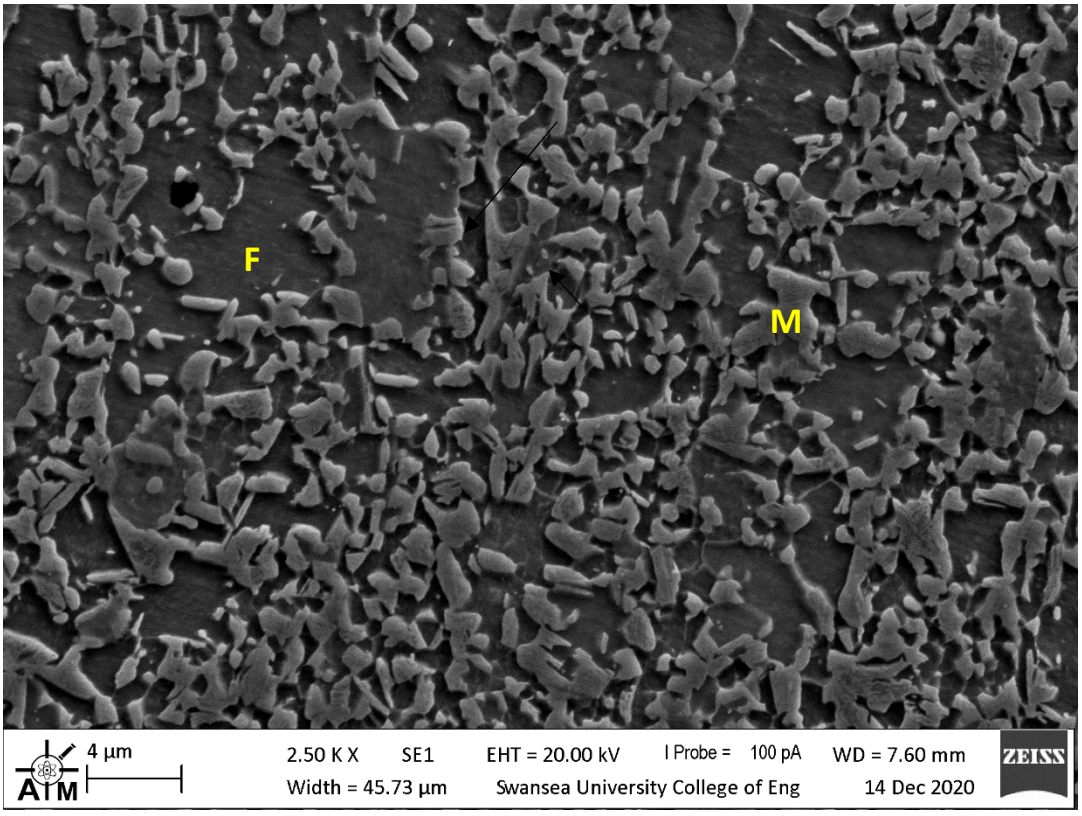

Figure 2.1 Scanning Electron Microscope (SEM) image of DP800. Microstructure consists of ductile ferrite (F) background and hard martensite (M) islands.

DP steels comprise of high tensile strength, low yield to tensile strength ratio, high work hardening rate, continuous yielding and good ductility (9). This combination is what make it a commonly used

UHSS for structural automotive parts. The other advantage of DP steels is that they tend to be low carbon and low alloy containing, which is a cost saving benefit for manufacturers, achieving the excellent mechanical properties by means of specific heat treatment (10) rather than expensive chemical alloying. It is the inter-critical annealing between the A_{c1} and A_{c3} temperatures on the Fe-C phase diagram, that is used to obtain the final mechanical properties, which will be described in further detail in this thesis.

Another advantage to automotive manufacture is the bake hardenability of the DP steels. Bake hardening gives a significant increase in the yield strength of a component once it is subjected to the paint baking operation of automotive body parts (11). This is one of the areas that will be investigated in this project and will also be described in more detail later in this chapter.

2.2. Dual Phase applications

DP steel is increasingly replacing heavier gauges of high strength steels, allowing for downgauging of components which allows weight savings to be made in the body in white of a vehicle.

Components made of advanced and ultra-high strength steel allow for greater absorption of energy in the event of a crash and prevent better intrusion when compared to lower strength steels (12). An example of this is a range of AHSS DP steels developed by Tata called HyperForm. These products can allow for a 23% reduction in gauge when compared to equivalent high strength low alloy components when used in complex structural car parts, whilst offering the same level of crash performance (13).

Typical applications for DP steels in body in white application includes door pillars, box girders in chassis, crash boxes, crossbeam and cross members and door and sill reinforcements. Figure 2.2 shows examples of where DP steels are used in BIW.

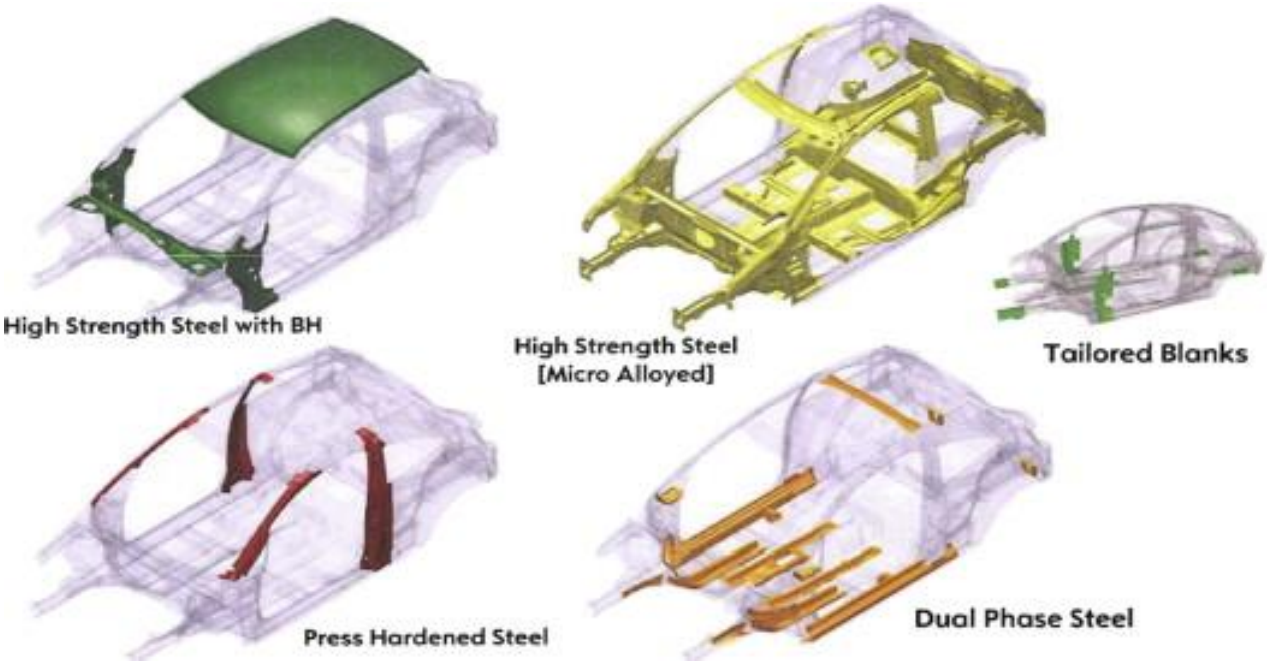

Figure 2.2. Examples of steel grades used in body in white of an automotive vehicle. Dual phase steel is typically used for structural components such as pillars, where high strength is required (14)

As automotive manufacturers move away from fossil fuel powered vehicles, there will still be a drive for weight reduction in body in white to help improve battery performance in electric vehicles. This will mean a likely increase in use of DP steels, replacing further components made of traditional high strength low alloy steels. Whilst the method of powering automotive vehicles may change, the crashworthiness of AHSS and UHSS will still be required to protect passengers and the energy storage system during any incidents.

2.3. Properties governed by phases and microstructures

The phase structure of DP materials is critical. The two primary phases consist of a background of soft ferrite combined with islands of harder martensite. Whilst these are the two phases that are make up a DP steel, chemistry and temperature plays a critical role in how much of each phase appears in the final product.

2.3.1. Ferrite

When pure iron is heated, it experiences two changes in crystal structures before it melts. At room temperature its stable form is α ferrite with a body centre cubic (BCC) structure. At a temperature of around 912°C and above it transforms into a face centre cubic structure (FCC) called γ austenite. This changes again at 1538°C, where the iron reverts to another BCC structure called δ ferrite (15).

To produce steel, carbon is added. Even a small amount of carbon added the steel can have a profound impact. Iron is a very soft, ductile metal, and with a small amount of carbon added it will become a much stronger material (16). Carbon is an interstitial atom in the iron matrix and the amount of carbon that the α ferrite can hold in solution is limited due to its BCC structure. It has been shown that carbon's solubility in the α ferrite phase is around 0.1wt%, compared to the γ austenite, which allows up to 9-10wt% solubility (16). Figure 2.3 shows the iron rich portion of the iron-iron carbon phase diagram.

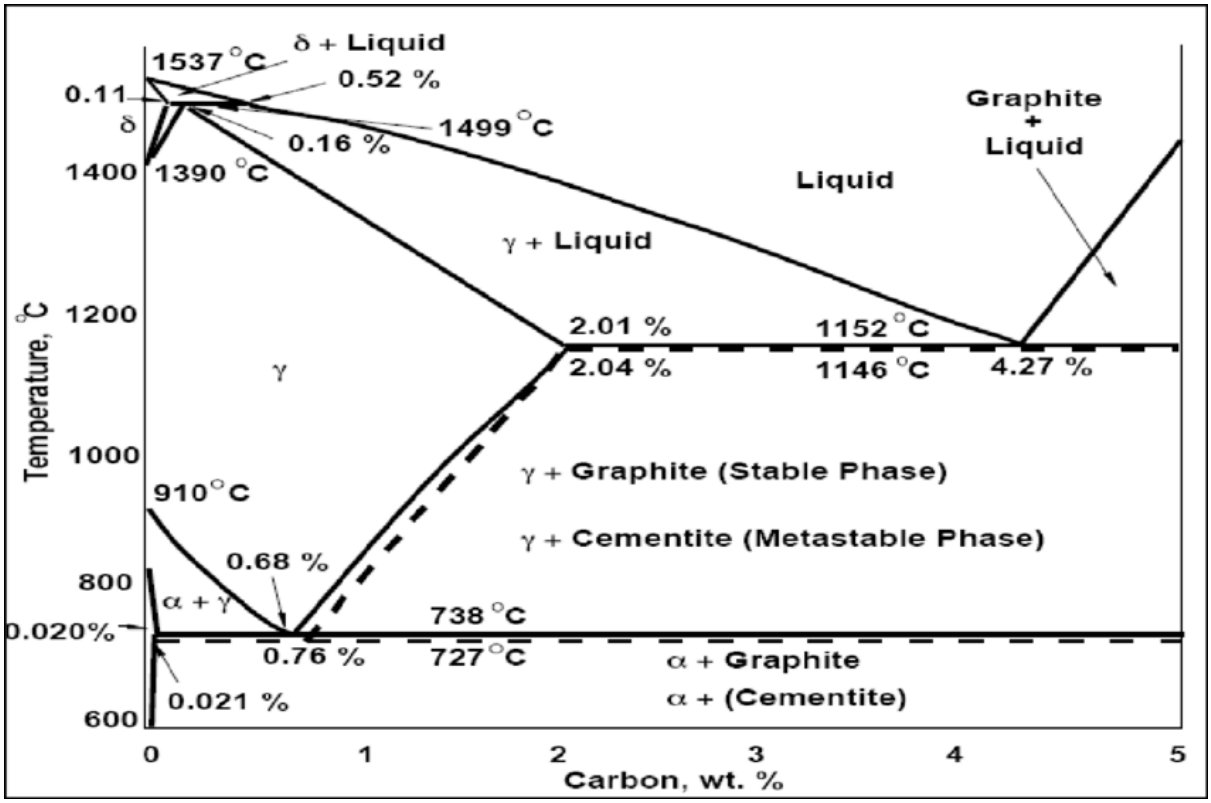

Figure 2.3 Iron-Iron Carbon Equilibrium Phase Diagram, α represents ferrite whilst γ indicates austenite (17)

On figure 2.3, its noted that the 'steel' section is on the far left of the diagram, with most steels typically produced with up to around 0.8wt% C. It also shows the different structures that iron goes through and how an addition of carbon changes the phases during equilibrium cooling.

The low carbon content typically used in a dual phase steel means that when the steel gets heated back up for intercritical annealing, it passes into the austenite / ferrite (α+γ) phase field.

The morphology and properties of ferrite can play a key role in the final mechanical properties of the steel. The way the material is heated, held at temperature and then cooled can affect its final grain size and how it has recovered and recrystallised. A high level of interstitial carbon in ferrite during rapid quenching can lead to embrittlement, with the yielding behaviour depending upon the interaction of carbon and cementite (Fe_3C) and the mobile dislocations that occur in ferrite (18).

2.3.2. Pearlite

Pearlite is two phase mixture of both ferrite and cementite, which forms in alternative layers or bands. It's this formation that gives it a mother of pearl like appearance to which it owes its name and is shown in figure 2.4.

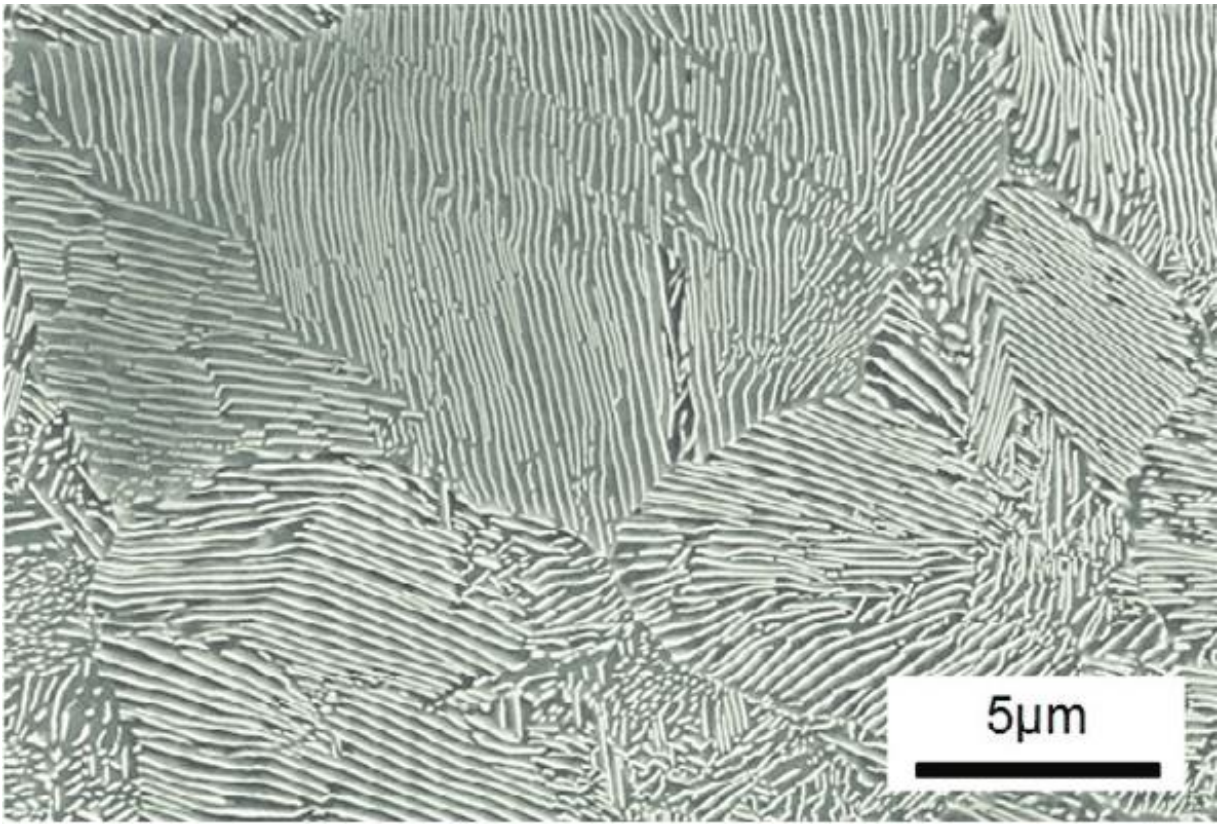

Figure 2.4. Pearlite microstructure consisting of ferrite (dark region) and cementite (light region) to form a mother of pearl appearance (19)

The formation of pearlite is a diffusive one and occurs typically on slow cooling by a eutectoid reaction when austenite cools below the transformation temperature of around 727°C, the microstructure of which can be seen in figure 2.4.

The ferrite in pearlite is body centre cubic iron, whereas the cementite layers consist of Fe_3C carbides with orthogonal structure in the undeformed state.

Typically, the higher the carbon content the higher volume fraction of pearlite, until the eutectoid composition is reached at around 0.8wt% carbon. Most steel grades, particularly in the steel industry, will be hypoeutectoid. This means on slow cooling relatively pure ferrite grains will accompany pearlite in the microstructure.

For the final microstructure in a dual phase steel, pearlite is typically avoided in the microstructure with the aim of cooling sufficiently rapidly enough to form martensite, which is a diffusionless-transformation. This however is not always the case throughout the steel processing, because the strength and hardness of pearlite is typically much lower than martensite, it requires much lower

rolling forces to process a microstructure consisting of ferrite and pearlite compared to ferrite and martensite. This is typically employed during the hot rolling to cold rolling process, where a microstructure of ferrite and pearlite allows for lower rolling forces to cold roll the steel to its final thickness. An example of the differences in hardness between pearlite, bainite and martensite are shown in figure 2.5.

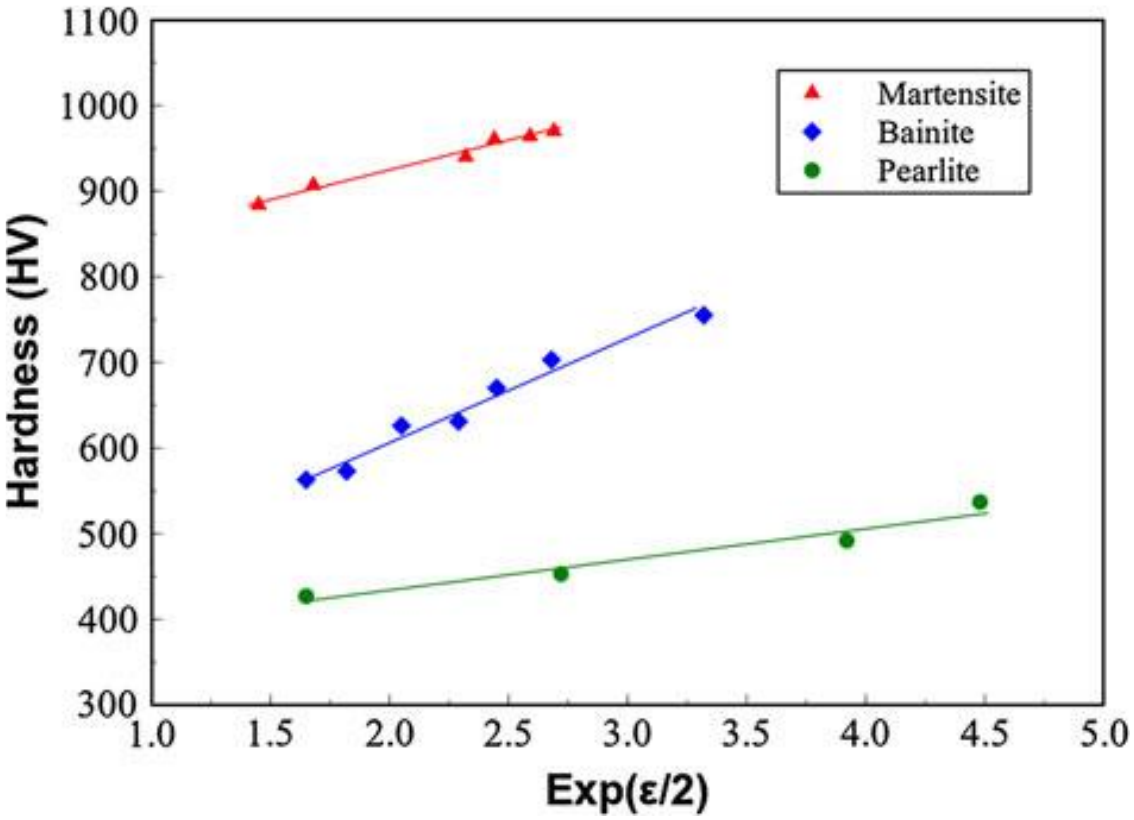

Figure 2.5. Hardness of pearlite, bainite, and martensite as a function of the cold-rolling strain plotted as exp(e/2). Pearlite showing the lowest hardness, followed by bainite and martensite with the highest hardness (20)

2.3.3. Austenite

Austenite, also known as γ austenite, is a nonmagnetic allotrope of iron, typically alloyed with carbon (21). The austenite that appears in steel is only stable above the A_{c1} temperature, which is the boundary between the ferrite-cementite and the regions containing austenite and ferrite or austenite and cementite on the Fe-C phase diagram. Austenite strongly influences the transformation and deformation behaviour of heat treatment in steels (22).

The annealing of dual phase steels takes advantage of the high solubility of carbon in austenite. This strongly influences the final ferrite / martensite microstructure. In DP steel, the final microstructure is produced by heating to partial austenitisation within the α+γ phase field of the phase diagram, followed by a specified cooling regime to achieve the final microstructure. Again, it is the combination of heating and cooling, time and alloy content that is also critical to achieve the required phases (23).

Austenite grain size is also critical for the martensite transformation kinetics, the size of the grain can affect the martensite start (M_s) temperatures on cooling. The finer the austenite grains the greater the shear resistance of the austenite to martensite transformation, which in turn stabilises the austenite and lowers the martensite start temperature (22).

Austenite in DP steels typically transforms to martensite on rapid cooling. However sufficiently alloyed DP steels can retain austenite down to room temperature. Alternatively, austenite that is not sufficiently alloyed, or is cooled slowly, can transform to other phases such as bainite.

2.3.4. Martensite

The term martensite was coined from the pioneering German metallurgist Adolf Martens, and has long since been used to describe the hard microstructure that is often found in quenched carbon steels (24). In steels, martensite typically comes from the cooling of austenite, and is called a diffusionless reaction, by which the martensite contains the exact same chemical composition as the austenite. The rapid cooling often associated with martensite leads to a different structure called body centre tetragonal (BCT), this is because the solubility of carbon typically far exceeds that which ordinary body centre cubic (BCC) would form on a slower cool.

The carbon gets trapped within the BCT structure leaving high levels of residual stress in and around the martensite phase. This leaves martensite as a metastable phase, present only because diffusion has been suppressed (24). An example of the BCT structure is shown in figure 2.6.

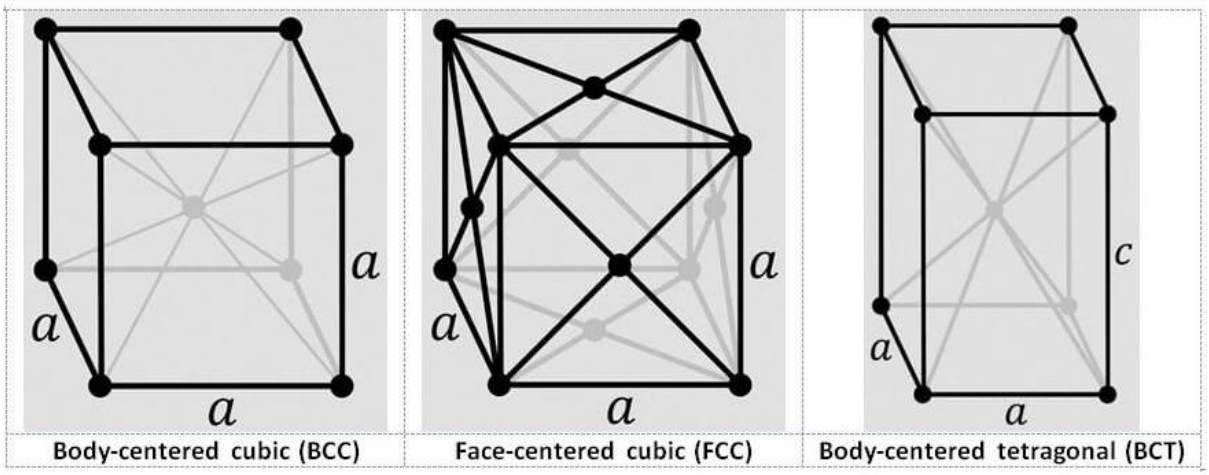

Figure 2.6 Examples of typical atomic arrangements in steel. BCC representing ferrite, FCC representing austenite and BCT for martensite. The elongated structure of BCT allowing more carbon to be retained in the matrix (25)

It is the martensite in the DP steel that gives this grade its strength. The effect of carbon being trapped in the BCT structure is an indication as to why this microstructure gives great strength to the properties of steel. Adjustment of chemistry and cooling rates can alter the amount of martensite present in DP steels.

Martensite can also be tempered, heat treating the martensite improves formability by relaxing the stresses and allowing for carbon diffusion. The tempering of martensite can be categorised into stages, the first stage is excess carbon segregating to defects or forming clusters within solid solution. It then precipitates as cementite or iron carbides, dependant on the carbon within the steel. Further annealing leads to almost all excess carbon being precipitated and the carbides are converted into a more stable form, cementite. The ageing and tempering of martensite and the precipitation of iron carbide typically occurs between room temperature and 423 K (26).

During extensive time and temperature continued tempering would lead to retained austenite decomposing, and then coarsening of carbide and recrystallisation of ferrite plates into equiaxed grains (27). It is worth noting however that this process reduces the strength from the microstructure (28) making it useful for potential property adjustment post annealing. During the industrial annealing cycle, material can be held at elevated temperatures, typically during the overage section, at which point the material temperature is sufficiently high enough that tempered martensite is formed. The overage section used on continuous annealing lines can range from around 250°C up to around 350°C, whereas on a continuous galvanising line the overage temperatures would be higher, in the range of 450-500°C, due to the requirement to coat in a bath of molten zinc.

2.3.5. Bainite

Work from Robertson, Davenport and Bain (29) led to an observation of a unique type of morphology in steel during intermediate temperature isothermal heat treatment. Some twenty years later the decomposition of austenite below the austenite to pearlite and above the martensite start formation temperature was termed bainite, in the memory of Bain. The formation of bainite occurring between ferrite and martensite is shown in an example of a continuous cooling transformation diagram (CCT) in figure 2.7.

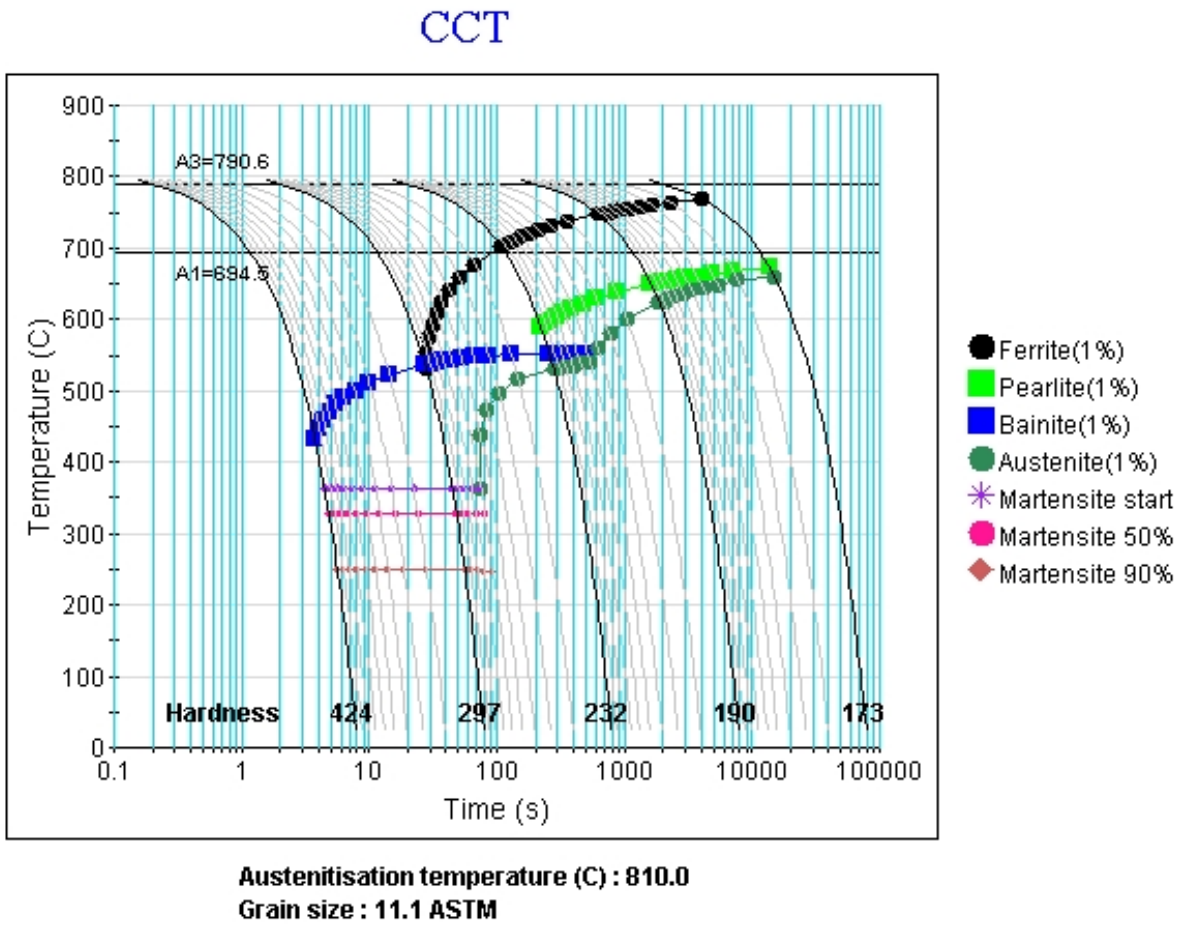

Figure 2.7. Continuous Cooling Transformation curve showing expected starting temperatures of each phase during cooling of a DP1000 grade steel, using JMatPro software. Example shows that cooling from 800°C to room temperature would generate bainite formation at approximately 425°C if cooling within 10 seconds

Further work from Mehl in 1939 broke down bainite into two distinct forms, upper and lower bainite (30). This distinction of upper or lower bainite is dependant on whether the carbides are distributed between individual ferrite regions or within them, respectively. The difference between upper and lower bainite is also based on the approximate temperature of around 350°C. Upper bainite is typically lathlike in appearance, whilst lower bainite is generally seen to have a platelike morphology (31).

For lower bainite, cementite carbides will form with carbides laying in the same orientation, typically around 60° to the ferritic plate as shown in figure 2.8. Due to the more refined intra-lath carbides, an increase in strengthening occurs when compared to upper bainite (32) which consists of larger cementite carbides between the plates. The overall differences between upper and lower bainite are summarised in table 2.1.

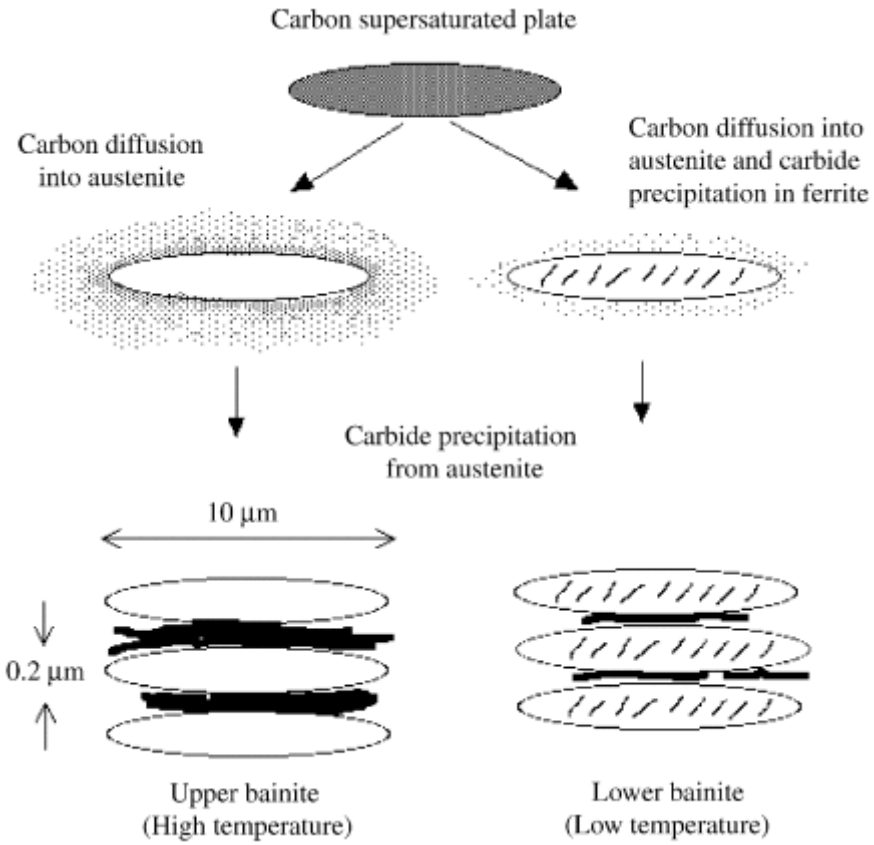

Figure 2.8. Summary of the mechanism and microstructure of bainite in steel and the differences in their appearance (33)

Bainite forms as a displacive mechanism of transformation and occurs at a relatively high temperature when compared to martensite (34). Upper bainite consists of clusters of platelets of ferrite which are identical in orientation as austenite when it grows. Cementite particles are along the boundaries of these platelets. When the temperature is reduced, some of the carbon precipitates within the ferrite plates, leading to the lower bainite structure (35). The transformation temperatures at which upper and lower bainite occur are shown in table 2.1.

Table 2.1. Differences between upper and lower bainite for low carbon steel (36)

Structure	Carbide Location within laths	Carbide Distribution	Transformation Temperature (°C)
Upper Bainite	Carbide-free Retained austenite or carbides between laths	Along the lath interface	550 – 400
Lower Bainite	Lath – like, with lenticular carbides present at ~60° to the long axis of the ferrite laths	Within laths and lath interface	400 – 250

The microstructure of tempered martensite and bainite are often difficult to distinguish apart. One of the most effective ways of establishing a difference is the alignment of the carbides in the microstructure, with tempered martensite having more randomly orientated carbides compared to lower bainite which has carbides orientated at around 60° to the ferrite laths, an example of this is shown in figure 2.9.

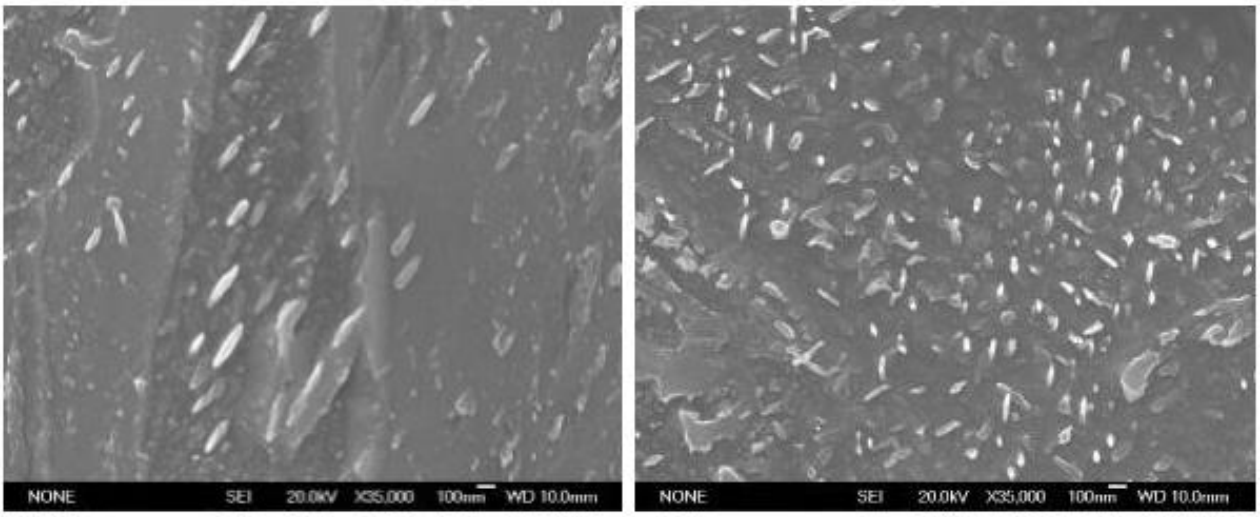

Figure 2.9 Lower bainite (left) and tempered martensite (right) with orientated carbides visible in the bainite compared to multiple carbide orientation of tempered martensite (36)

2.4. Chemistry in the microstructure

The chemistry plays a key role in how the phases / microstructures appear when the material is firstly heated and then cooled on a run out table for hot rolling, or during the annealing process. The elements below are those most commonly added to influence the final microstructural outcome of the DP steel.

2.4.1. Carbon

Carbon is one of the main alloying elements in steel. It is virtually insoluble in the body centre cubic (BCC) α ferrite phase; however, it is soluble in the face centre cubic (FCC) γ austenite. Carbon lowers the solidification temperature of iron and broadens the temperature range over which austenite is stable, thereby lowering the temperature at which α ferrite occurs upon heating. For this reason carbon is known as an austenising element (37). Carbon also has a large effect on the intercritical $A_{c1} – A_{c3}$ temperature range. In a DP steel containing chromium, manganese, silicon and boron, it was found that reducing the carbon content from 0.18% to 0.07% reduced the amount of γ-phase from 6%/^{o}C to 2.3%/^{o}C respectively in the temperature range of 760-850^{o}C (7).

Higher carbon content controls the hardness of the martensitic phase, hence affecting the final mechanical properties. Investigation has shown there is a range of martensitic fractions between 35-50% where the properties for dual phase steel are optimised (38), and this constitutes a carbon content of approximately 0.1-0.15wt%, which gives approximately 50% martensite in a consistent chemistry range (39).

2.4.2. Manganese

At approximately 1.5-2wt% of the composition of DP steels, manganese (Mn) is typically the largest alloying addition. Mn is traditionally added to steel because it acts as a deoxidizer and desulphurizer. It also strongly retards the transformation of austenite to ferrite upon cooling, allowing deep hardening in heat treatable steels. It also lowers the transformation temperature and the eutectoid carbon content (40). In a DP steel, Mn is beneficial for the formation of martensite. This comes in part from Mn enrichment in cementite in the form of Mn-Fe carbides, which is then partly inherited by the austenite that undergoes the martensitic transformation. The benefit of these carbides is to give a higher fraction of effectively pinned grain boundaries, resulting in a finer, stronger material (41).

The DP hardenability is also controlled by Mn partitioning between the ferrite and austenite allowing the transformation of austenite to martensite during inter-critical annealing (42).

2.4.3. Aluminium

Aluminium (Al) has the opposite effect to carbon, it is a strong ferrite former and is also a grain refiner like Mn, and combines readily with interstitials like nitrogen (40)(43). It is kept in low quantity in DP steels, this may be because it can decrease the volume fraction of austenite and hence martensite after its been cooled (7).

Another feature of Al is that it can prevent the precipitation of carbides in bainite (43), though most DP steels avoid the generation of bainite and try to achieve a ferrite-martensite structure only.

2.4.4. Chromium

Chromium (Cr) is most commonly known for being the primary alloy addition in stainless steel, to give high stress corrosion and pitting corrosion resistance (44). Cr is used to retard the pearlite and bainite formation. The addition of Cr also helps to stabilise the austenite, slow down the kinetics of ferrite and to modify the microstructure and to also improve the overall mechanical properties (7)(45).

2.4.5. Titanium / Niobium

Titanium (Ti) and niobium (Nb) can add additional strength by grain refinement and precipitation hardening. The primary reason for these additions in DP steel is to tie up interstitial nitrogen and form nitrides, which is typically achieved at the higher temperatures during hot rolling. This is important because nitrogen remaining in solid solution would increase strength, reduce formability and lead to the potential of strain ageing (46).

2.5. Effect of Processing

DP steels created by Tata are for the strip steel market. This means their typical gauge range for cold rolled coil is between 0.8 – 1.6mm. To get to this gauge, material is cast, hot rolled down to gauges of around 3-4mm, and then cold rolled to produce a cold rolled unannealed product, known as ‘hard iron’. The following sections describe how a cast of DP steel is rolled and annealed to produce the final product.

2.5.1. Hot Rolling

A steel slab, typically 234mm thickness by 10m length is reheated in a furnace to approximately 1150-1250°C. This furnace then pushes the slab onto a set of rollers which pass the slab to a set of scale breakers. At such a high temperature, oxidation of the surface of the steel occurs causes a

build-up of scale which, if not removed, can then get rolled into the surface of the steel causing defects. Rollers and high velocity water jets break up and remove the scale before the first rolling sequence occurs.

Once through the scale breaking section, a set of reversing roughing rolls passes the strip backwards and forward several times, each time the roll height is decreased which reduces the gauge of the material whilst elongating it in length.

Once through the roughing mill, the strip then gets coiled into a coil box, or hot box. Whilst there is no additional heating element applied at this stage, the material being coiled allows for a more uniform temperature of the strip across the profile before passing through the finishing mill, stopping the edges of the coil cooling too rapidly.

From the coil box, the strip is fed through the finishing mill. The finishing mill consists of seven individual stands, each stand consisting of a work roll and a backup roll. The work rolls provide the strip reduction, whilst the larger backup rolls provide the force to keep the work rolls from bending too greatly, ensuring the strip profile is maintained. Each of these stands subjects the strip to further deformation, reducing the strip gauge to between 2.5-5mm thickness.

Once through the finishing mill, the cooling of the strip is controlled via overhead water sprays which are set up in banks. Each of these banks of cooling water sprays can be turned on or off whilst the strip is passing through them, this enables the temperature of the strip to be controlled before it is coiled. An example of a typical hot strip mill layout is shown in figure 2.10.

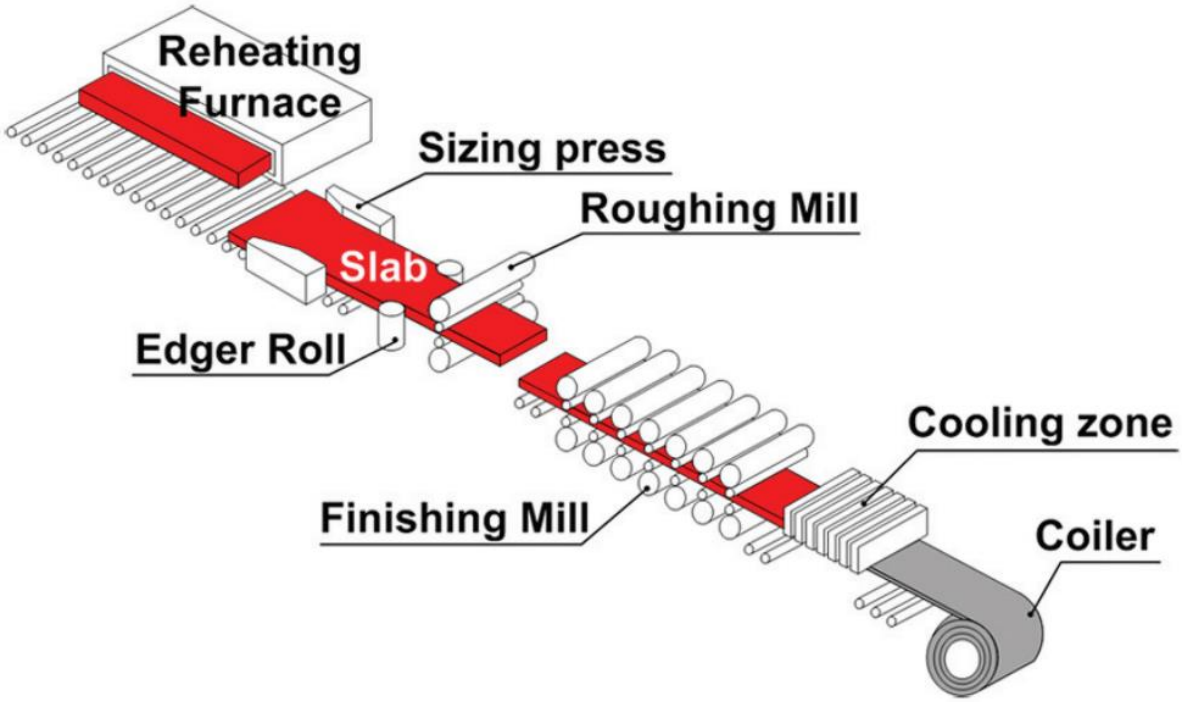

Figure 2.10 Typical hot strip mill set up. Slabs are reheated, edges rolled before being reduced at the roughing mill and rolled to the final thickness through the finishing mill. The cooling zone, or run out table (ROT) reduces the temperature to around 500-600°C before coiling (47)

For cold rolled DP steels, the aim at the hot mill is to achieve a product that is as soft as possible. Therefore, the aim microstructure is a ferrite and pearlite mix which is lower in strength compared to the final annealed microstructural aim of ferrite and martensite (20). An example of the cooling pattern required is shown in figure 2.11.

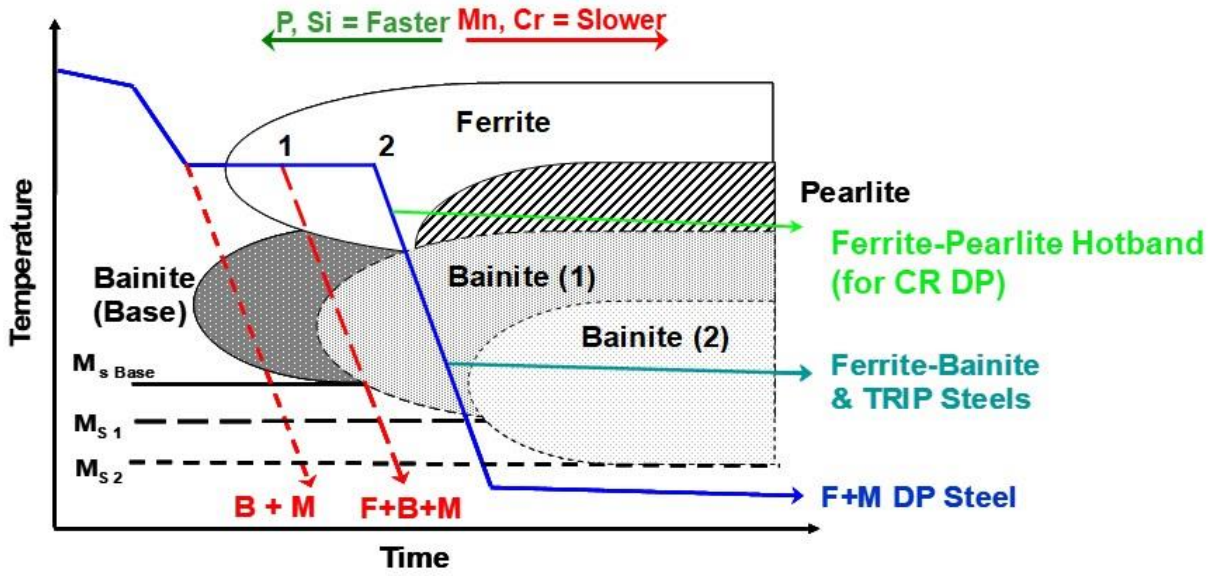

Figure 2.11. Continuous cooling diagram for DP production. Note the green pathway for hot rolling to achieve a ferrite-pearlite mix compared to the final annealing temperature profile in blue, to achieve a ferrite-martensite microstructure (M_s – martensite start / B – bainite / M – martensite / F – ferrite) (48)

Due to the high rolling loads that are experienced during the cold rolling of a DP product, it is necessary to aim for a product with the softest mechanical properties as possible. Therefore the aim for cooling on the run out table to is maximise the amount of ferrite and pearlite within the microstructure, by aiming to cool to around 650°C to achieve ferrite, and then apply a small amount of further cooling to coil at around 600°C to achieve a pearlitic microstructure (48).

Achieving uniformity of temperature across the strip is also key, due to the narrow window in which the ferrite/pearlite microstructure is achieved. Certain sections of the coil such as the coil ends or edges can cool more rapidly than the centre, this would give the potential of bainite formation on the run-out table leading to harder coil extremities with different properties compared to the main body of the coil. These temperatures are closely monitored through the hot rolling process, and regions of the coil that may become excessively hard can be discarded before being cold rolled, to ensure uniformity of phase structure and hence mechanical properties throughout the coil.

2.5.2. Cold Rolling

To achieve thinner gauges that automotive manufacturers require, further rolling of the steel is required. Before the material can be processed on the cold mill the strip surface needs to be pickled.

Due to the higher temperatures experienced on the hot mill, the strip surface oxidizes leaving a build up of scale. To remove this, the steel is uncoiled and processed through a set of hydrochloric acid baths. The rollers break the scale up as the strip moves along whilst the acid removes the scale build up from the surface of the strip.

The strip then moves through the cold mill. Similar to the hot mill, a set of rolling stands featuring a work roll and back up roll reduce the gauge of the material from between 2.5-5mm to the final thickness which can vary from 0.5-2mm, dependant on the final customer gauge requirement.

Due to the high strength nature of DP steels, there is a finite amount of cold reduction that can be achieved on the cold mill, even with a ferritic/pearlitic microstructure. Rolling load limitations mean that as much reduction that can be achieved on the hot mill is required, and around 50-60% cold reduction can be achieved to obtain the final customer gauge requirements.

2.5.3. Annealing Cycles – Uncoated and coated

Unlike hot rolling, where the steel strip recovers and recrystallises as it is rolled due to the high temperatures used, cold rolling occurs at room temperature. Because of this, the microstructure is elongation and pressed in the direction of rolling, as shown in figure 2.12.

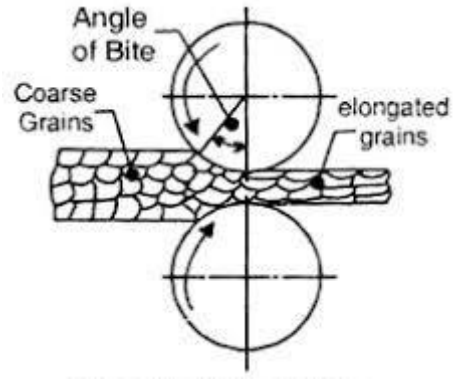

Figure 2.12 Example of cold rolling process distorting microstructure in direction of rolling (49)

Cold rolled, or hard iron steel will have very high strengths but will have very low ductility (50), therefore to correct this a heat treatment cycle must be applied. The annealing cycle determines the temperatures and rate at which the material is heating, held and cooled, to achieve the final

microstructure and mechanical properties. Due to demand, a single chemistry is used to satisfy both the continuous annealing line and the galvanising line for DP products. Each of these mills has a different configuration, so therefore there is increased complexity in producing the same end mechanical properties from two different annealing cycles.

Zodiac

Figure 2.13 shows a schematic of the Zodiac processing line.

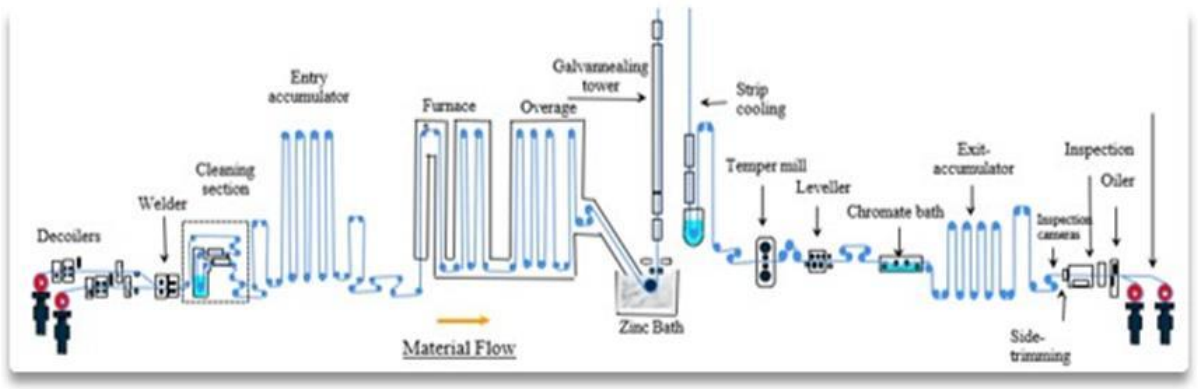

Figure 2.13. Schematic of Zodiac line. Material is uncoiled, welded to the end of the previous coil, passes through a cleaning section before passing through the furnace. The material is then coated, cooled and then passes through additional processing of temper mill, passivation section, inspection and trimming and oiling before being recoiled.

Zodiac is a continuous processing line, so the material is uncoiled, the ends cut using a shear, and resistance welded to the back end of the previous coil that is being processed. The material then passes through an accumulator which allows for the entry of the line to stop and weld, whilst the critical part of the line between the two accumulators can keep running at a continuous speed.

Before the furnace, a small cleaning section allows for the strip to be cleaned, using sodium hydroxide solution and a set of Hotani brush rolls to remove any dirt or debris that has been picked up from the previous cold rolling operation. The material then passes into the furnace.

Figure 2.14 shows a typical annealing cycle that would be used in industry to anneal a steel product via a galvanising line.

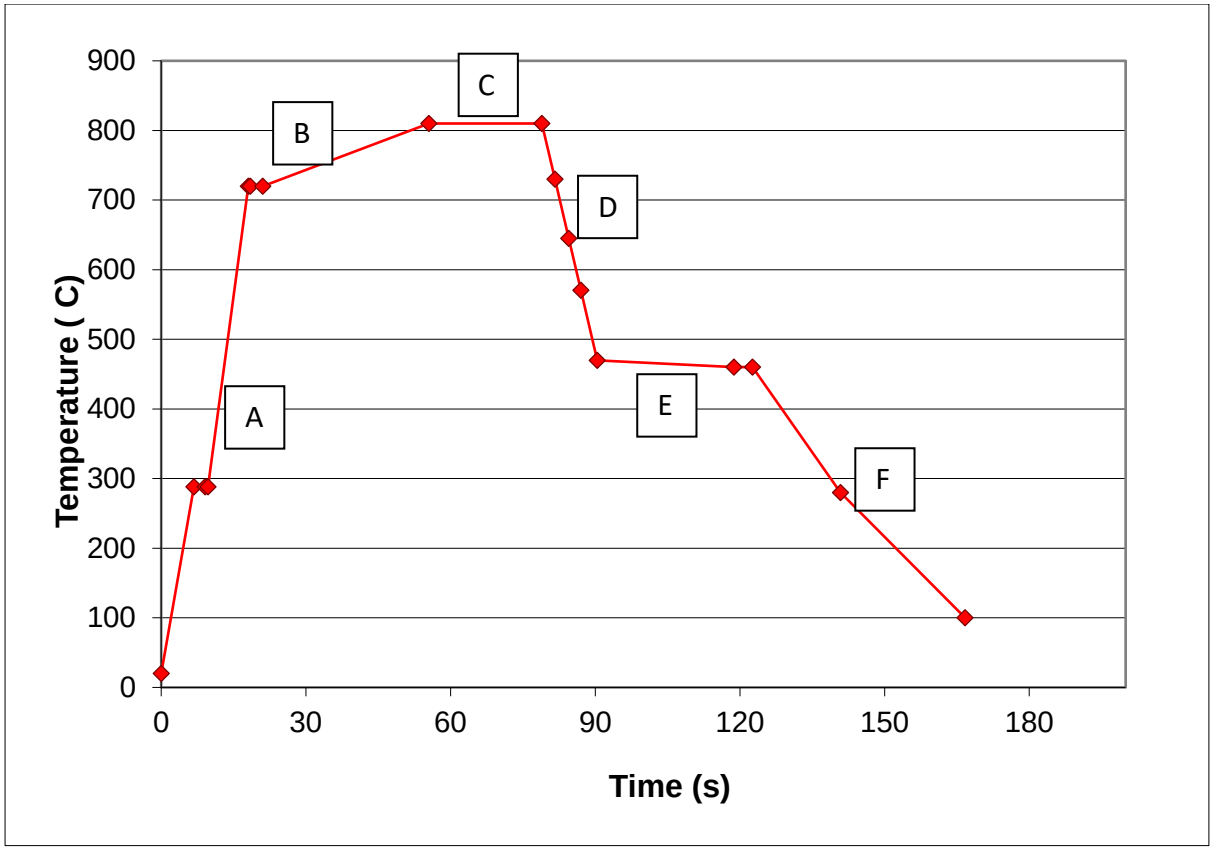

Figure 2.14. Typical DP annealing cycle for a galvanised steel product at Tata Strip UK, heating for recrystallisation and grain growth, before cooling to be galvanised, then rapidly cooled post galvanising allowing for the zinc to solidify (Zodiac)

The annealing cycle comes under several stages, and temperature changes. These stages are shown on Figure 2.14, and consist of the following:

Stage A – C - Heating

There are three stages of heating that occur on Tata's galvanising line, the pre-heat, the direct fire furnace (DF) and the radiant tube furnace (RT). In the initial pre-heat, exhaust gases from the DF are circulated around the steel strip, this pre-heats the steel before it enters the DF furnace (A). The DF utilises natural gas burners which rapidly and directly heat the strip to bring it up to temperature. The temperature in this section is raised from ambient temperature to around 700-750°C in a single pass. The fuel to air ratio is tightly controlled in this section, as the strip passes through the ratio is stoichiometrically controlled to prevent excessive oxidising of the strip as well as removing any remaining surface oils.

Because the steel strip gets coated with a protective layer of zinc, it is critical that the surface allows for correct adhesion. Therefore, before the strip enters the RT furnace, an oxybar provides a small layer of oxygen to the strip. The oxybar is a series of pipework that fits around the steel strip as it passes through the bottom of the DF furnace. A carefully controlled ratio of air and nitrogen is delivered through this bar onto the strip during processing of DP material, with the ratio varied dependant on the thickness of the steel. This is done only for DP steels, and is due to poor wettability of zinc that is encountered due to the high levels of external oxidation from Mn and Cr. Applying oxygen to the strip allows for selective oxidation of Mn and Cr internally, leading to improved wettability on the surface of the strip (51), this will be discussed further in chapter 2.8.

The strip then enters the RT furnace (B). The RT furnace consists of tubes with burners that burn natural gas within the tube. The strip passes by these tubes and the heat radiates out which indirectly increases the strip temperature, allowing for a consistent heat profile to be maintained during the soak section (C). Temperatures in this region typically vary between 750-850°C allowing for recrystallisation to the steel strip to occur. In this region the atmosphere is inert, made up typically of 95% nitrogen and 5% hydrogen and a dew point of around -40°C. The hydrogen in the atmosphere reduces the oxide layer that was formed during the DF section allowing for a good coating quality due to a clean strip surface.

Stage D – Cooling

The cooling section on the galvanising line consists of three cooling sections, the slow cool section (SJC), rapid cooling section (RJC) and gas cooling section (GJC). Here the strip is cooled from the soak temperature of around 750-850°C to the temperatures just above the galvanising pot, of around 470°C. The achieve this, furnace gasses are drawn into water cooled heat exchangers which cools the nitrogen/hydrogen mix before being forced onto the strip, reducing its temperature.

Stage E = Overage

The overage section allows for carbon to precipitate out of solid solution. The carbon will preferentially precipitate at defects such as dislocations, the correct precipitation of carbon leads to a reduction in the ageing effect of the steel (52). The overage section on Zodiac is much smaller than CAPL due to a furnace upgrade, where the initial 12 passes in the overage section has been reduced

to just a single pass. This has been driven primarily from a change in product mix, allowing for an increase in speed of work through the furnace without detriment to the remaining products Zodiac produce.

Stage F = Pot and Cooling,

The steel passes from the end of the overage at 465°C and into the molten zinc pot. This galvanising bath holds around 250 tons of molten zinc with a small addition (~0.3wt%) Aluminium. This forms the galvanised layer with the thickness of the coating being controlled with a set of nitrogen knives. The strip is then cooled through three coolers in one vertical pass, before passing through a water quench to take the temperature down to around 30-40°C.

CAPL

Whilst many of the overall process of annealing is similar between Zodiac and CAPL, differences exist between the two. Figure 2.15 shows a basic schematic of CAPL with the main processes that the material goes through.

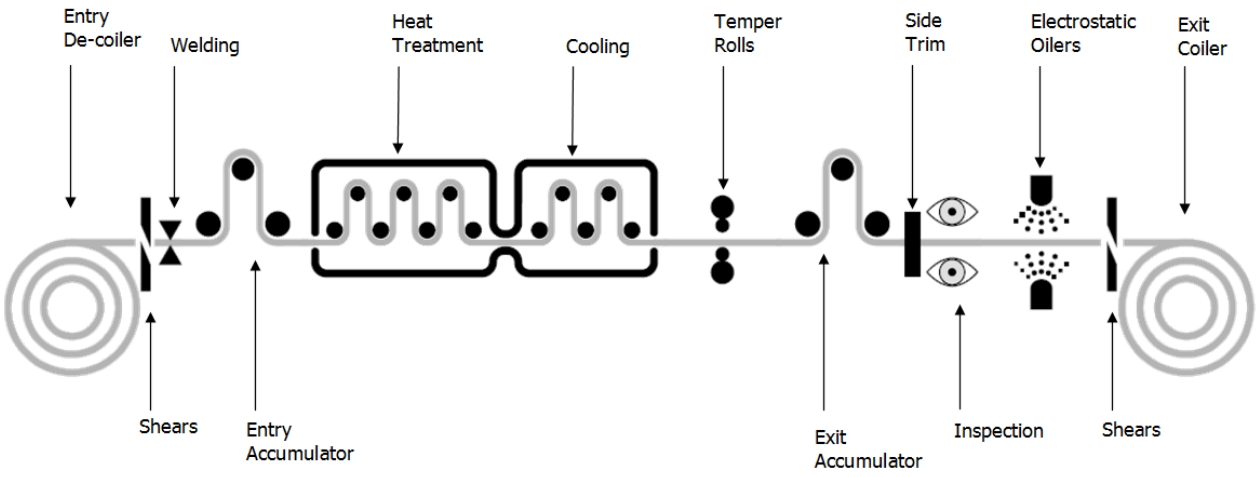

Figure 2.15. Basic schematic of processing through CAPL. Material is uncoiled, welding, cleaned before passing through the furnace, temper rolling and trimming before recoiling (52)

To keep the line continuous, the material is uncoiled and resistance welded to the back end of the previous coil that is being processed. The material then passes through an accumulator which allows for the entry of the line to stop and weld, whilst the critical part of the line between the two accumulators can keep running at a continuous speed. A cleaning section similar to Zodiac cleans the strip of rolling oils and ensure the strip is as clean as possible before entering the furnace.

Figure 2.16 shows a typical DP annealing cycle on CAPL.

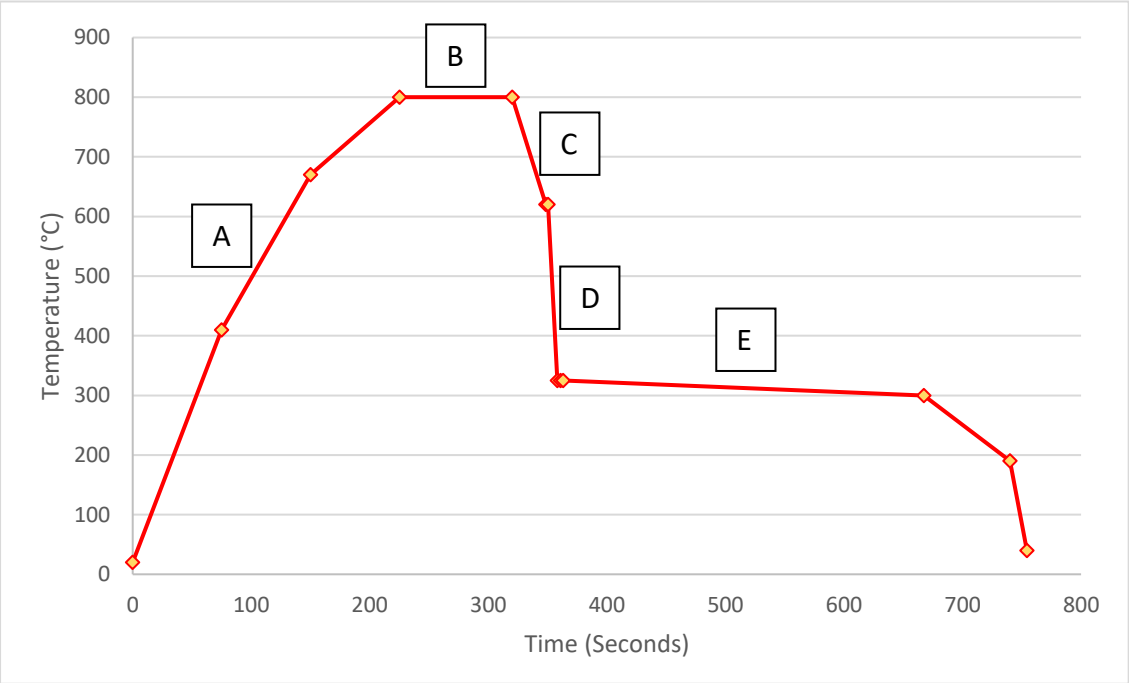

Figure 2.16. Typical annealing cycle for a continuous annealing line (CAPL) to produce a DP product. Similarly to Zodiac, material is heated for recrystallisation and grain growth to obtain the mechanical properties, before being cooled before existing the furnace

Stage A – B - Heating

The heating stages for Tata's continuous annealing line, CAPL, are all achieved via radiant tube furnace. Unlike the galvanising line, which uses an initial direct fire furnace, the continuous annealing line heats solely with radiant tubes. The annealing atmosphere that is typically used through the heating and cooling stages is 95% Nitrogen and 5% Hydrogen and a dew point of around -40°C. This atmosphere is used to prevent oxidation of the strip as it passes through the annealing process at higher temperatures. As with the galvanising line, stage B is the soaking stage, here the strip is exposed to an intercritical temperature that, in the case of dual phase steel, will determine the amount of ferrite and austenite phase fraction in the material.

Stage C – CGJC (Conventional Gas Jet Cooling)

Two distinct areas of cooling exist on Tata's continuous annealing line, the slow cool section and the rapid cool section. The initial slow cooling section cools the strip from the soak region at around 5°C/s, this slow cooling allows for new ferrite growth to occur.

Stage D – HGJC (Hydrogen Gas Jet Cooling)

The HGJC is the rapid cooling section. In this section, the annealing atmosphere can be adjusted to allow for more rapid cooling to take place. Typically, the cooling that can be achieved is around 40°C/s, for DP steels this is to try and avoid the onset of bainite and to cool the material to retain austenite in the microstructure throughout the overage section.

The advantage of this cooling section over Zodiac is that the temperature can reduced to between 250-350°C because there is no requirement to coat the material in zinc. This allows for direct cooling to the martensite transformation temperature, whereas the Zodiac cycle is held at temperatures in excess of 460°C during coating, relying on after pot cooling to achieve martensite.

Stage E - Overage

As with Zodiac, the overage section on CAPL allows for carbon to precipitate out of solid solution. The carbon will preferentially precipitate at defects such as dislocations, the precipitation of carbon leads to a reduction in the ageing effect of the steel (52). For DP steels, its critical at this stage that the austenite is sufficiently saturated by carbon to delay the transformation to martensite for the final cooling stage to room temperature, avoiding tempering of martensite which can occur at these elevated temperatures (53).

Temper Mill

The final processing section on both CAPL and Zodiac which is important for mechanical properties, as well as shape, is the temper mill. The temper mill applies typically between 0.5-1.5% extension to

the strip which improves the shape, imparts a surface roughness to the strip and increases the yield strength of the steel.

Additionally on Zodiac is a set of tension levelling cassettes. These cassettes are a set of rolls that utilises bending forces to straighten the strip and level it. It can also help improve the yield strength of the material.

Protection and trimming

Both CAPL and Zodiac provide additional protection to the coils. Electrostatic oilers at the end of the line allow for a thin layer of oil to be applied, which acts as a barrier on the surface of the material to stop corrosion occurring. Zodiac also has the capability to provide a passivation layer to the material, applying a thin layer of phosphate based passivate to stop white rust formation during storage and transportation. Typically this is applied as an alternative to oiling for the construction industry.

A set of trimming heads can also be brought in to trim the material to the final customer width at the end of the line before the material is recoiled.

2.6. Method Analysis

2.6.1. Dilatometry

When a steel is heated, it thermally expands. Dilatometry is a powerful technique that allows the study of solid-solid phase transformation. Dilatometry allows for the real time monitoring of the evolution of the microstructure within steel, by recording the changes in expansion and contraction. The monitoring of such thermal differences can then allow the plotting of phase transformation diagrams, both for the heating and the cooling part of the thermal cycle.

Another useful aspect is being able to plot the A_{c1} and A_{c3} temperature. There are currently various computer software programs that utilise experimentation results to plot various expected phase transformations that take place, dependant on the chemistry and the heat treatment being used.

The dilatometry results can then be used to indicate whether initial results that have been plotted on these types of software match up to the actual real world heat treatment results.

The Gleeble 3500 is a thermomechanical simulator, it is this machine that will primarily be used to anneal the steel samples in this thesis. The Gleeble also comes with a linear variable differential transformer (LVDT) type dilatometer. This dilatometer uses glass rods which attach to the steel sample and record, highly accurately, any changes in specimen length.

Due to iron's two crystal forms at atmospheric pressure (BCC and FCC), the transformation from ferrite to austenite is accompanied with a change in atomic volume of approximately 1% (54). This means that when during the heating cycle a significant contraction is seen in the dilatometry, which is the change in length at a given temperature.

There are certain values that can be associated, and the nomenclature of these points vary dependant on how the material is being heated and cooled. A_{e1} and A_{e3} temperatures are the points at which the eutectoid reaction occurs (A_{e1}) and for the ferrite to austenite transformation (A_{e3}). These values would typically sit at 723°C and 910°C on the iron carbon equilibrium diagram, however because steel is rarely pure iron and carbon, and not cooled in equilibrium conditions, these values will vary dependant on the heating, cooling and chemical composition.

Therefore, A_c is typically assigned for heating, A_r is assigned for cooling, and A_e is used for equilibrium conditions. The former is two conditions will more typically be applied during this thesis, as replicating mill conditions is not done under equilibrium conditions.

Thermal expansions and contractions allow for the A_{c1} and A_{c3} temperatures to be plotted during the heating of the material. Furthermore, the dilatometry can also show the changes occurring during the cooling of the material, allowing for the changes in phases from austenite to ferrite, bainite and martensite to be observed. The sensitivity of the material to changes in chemical composition and cooling rates and temperatures means that changes to the microstructure can be linked to what is seen under the microscope, as well as on the macroscopic level in terms of mechanical property changes.

2.6.2. Transformation Diagrams

There are two main types of transformation diagrams that can be used to help design an optimum processing route for a set of given properties, these are CCT (continuous cooling transformation) and TTT (time temperature transformation) curves.

TTT diagrams are useful in measuring the rate in which transformation occurs at a constant temperature. An example of this in steel would be to fully austenise the steel, and then hold it at a certain temperature. This can be done by using dilatometry, so the rate of transformation can be plotted. A large volume of testing can be done to build up a full picture of the phases that are produced at different times and temperatures.

As holding material for a long time at a set temperature is not typically applicable industrially, CCT diagrams are more commonly adopted. These diagrams show the extent of transformation for a continuous decreasing temperature. This is particularly useful in the case of annealing, to indicate the phase structure during the cooling part of an annealing cycle to room temperature. Another example of CCT use is in chemistry design. Different chemical elements can move the starting position of the resultant phases during cooling, helping alloy designers to determine the effect that each of the elements will have on the final microstructure.

An example of moving the nose of the austenite / ferrite start temperature is shown in figure 2.17. It shows the impact of molybdenum (Mo) on the cooling rate. Molybdenum is one of the strongest austenite stabilisers (55), which would explain the retardation of the ferrite / pearlite nose, pushing it to the right. This means that the high addition of Mo would allow for a slower cool, retaining the austenite phase for longer into the cool before it drops into the bainite / martensite region. This has advantages by allowing a longer time to achieve the required martensitic temperature, so a less rapid quench would be required.

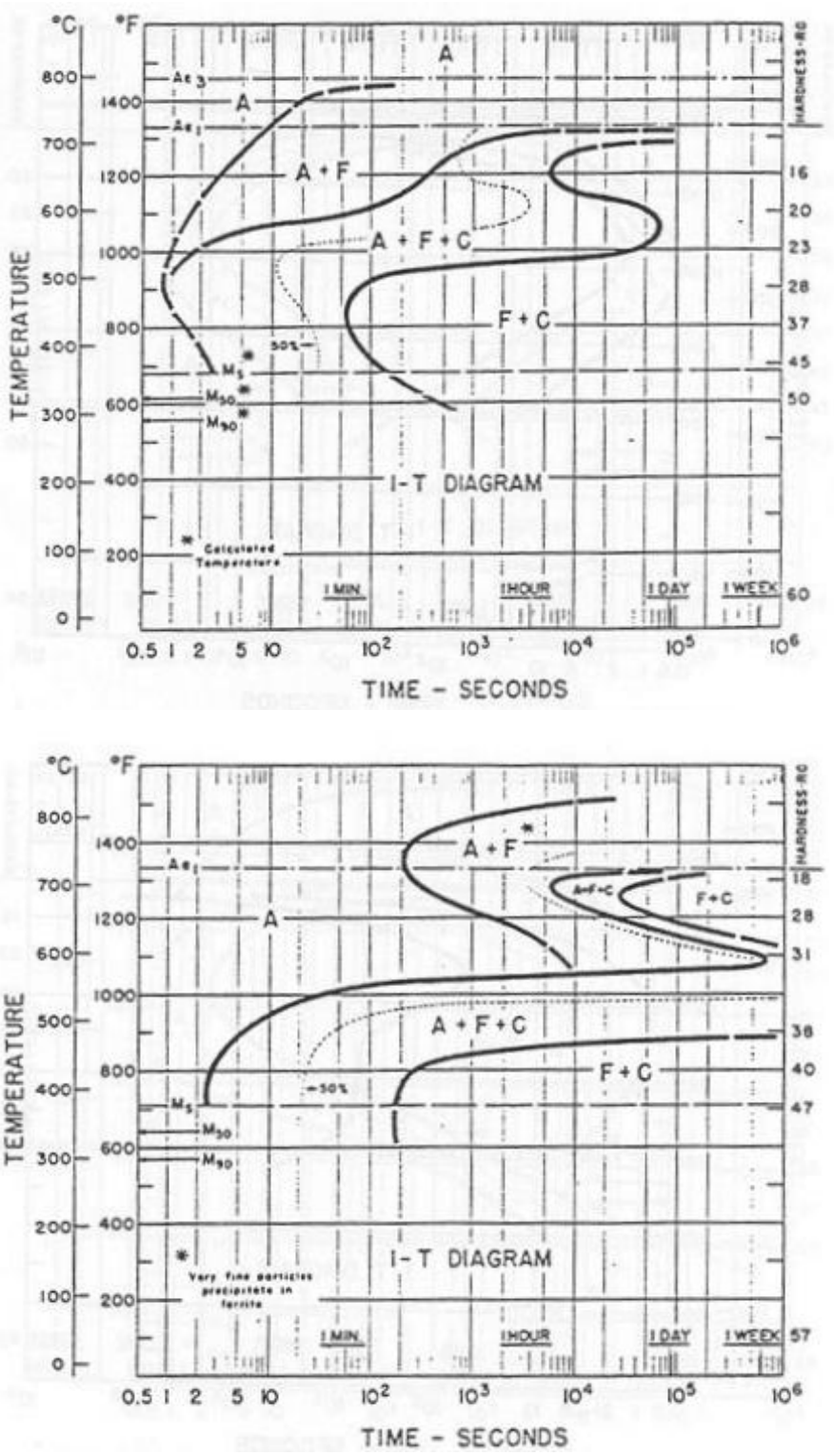

Figure 2.17. Example of a hypothetical CCT curve containing Mo steel. The diagram on the top has 0.2wt% Mo whilst the bottom has approximately 2.0wt% Mo. Note the curve being pushed right as Mo content increases (56)

Understanding these CCT diagrams allows manufacturers to design a chemistry which will give them the phases they require. Additions of Mo enhance the hardenability of austenite suppressing pearlite and ferrite formations, slowing the kinetics of ferrite transformation and lowering the transformations start temperatures. The inhibition effect of Mo on ferrite formation results in promotion of bainite formation (57). Due to its high costs, Mo tends to be substituted with Cr where possible (57). So, whilst Mo may be added to the steel in small percentages, it is the use of other chemical elements which drive the ferrite / martensite structure that is required.

2.7. Critical Mechanical Properties

Manufacturers require the mechanical property performance of steels to design their products. DP steels have designations that they must achieve to be sold. For Tata, they typically benchmark their material to the European Standards (Euro-norm) or the American Standard (ASTM). Some customers will specify their own standards, these tend to be a variant on the Euro-norm or ASTM. Table 2.2 shows what the aims are to achieve each of the type of DP steels. As an example, DP600 would be represented as HCT590X in the nomenclature of the Euro-norm.

Table 2.2 Typical property requirements from the Euro-norm Standard EN10338

Specification	**Proof Strength** $R_{p\,0.2}$ *(MPa) min*	**Tensile Strength** R_m *(MPa) min*	**Elongation** *A80 % min*	**Bake Hardening** BH_2 *(MPa) min*
HCT590X	290 - 380	590	20	30
HCT780X	440 - 550	780	14	30
HCT980X	590 - 740	980	10	30

Each of these properties are important, as well as others such as the ‘n-value’, a materials response to cold working, and the ‘r-value’, a measurement of a materials drawability. Typically, a tensile test is used to obtain the mechanical properties above. Whilst this will not cover all mechanical

properties, it can cover yield and proof strength, tensile strength and elongation which are the three major characteristics that can determine a materials mechanical behaviour.

The yield strength of a component is the maximum stress that can be applied before the shape of the material is permanently changed. The ultimate tensile strength is the maximum stress that a material can withstand before breaking. Elongation can be measured at two main points of a tensile test. First is the uniform elongation, which is the elongation at maximum load, and better represents the materials ductility in uniaxial deformation. Secondly is total elongation, which is the elongation at fracture and is more typically used to indicate a materials ductility overall.

During a tensile test, a sample is gripped on opposite ends within a load frame of a testing machine, a tensile force is then applied to the sample. This force is increased, resulting in the gradual elongation and eventual fracture of the sample material. During the pulling, force-extension data records how the material deforms under the applied force (58) using an extensometer.

For flat sheet steel, the most common shape for the test piece is ‘dog-bone’ shape. The reasoning for using this is because it allows each end of the sample to be gripped by the machine, the narrow section in the centre reduces the likelihood of fracture at each of the ends, essentially allowing the failure to occur in the narrower section. The size of this test piece is kept at a given standard, whether that be governed by Euro-norm, ASTM or customer requirements.

Typical dog-bone tensile samples come in differing sizes. Typical industrial samples are called ‘A80’ samples and have 80mm gauge length. Smaller 50mm gauge length (A50) samples are typically used at Tata on the CASIM (Continuous Annealing SIMulator), as the smaller size enables multiple samples to be taken from a CASIM test. Different size tensile specimens shouldn’t affect yield and tensile strength for a given cross sectional area and gauge length, however the elongation properties may be affected. To eliminate these differences, conversion factors can be made to allow direct comparison between different specimen geometries, for example ISO 2566 (59) Further explanation of the sample sizes used in this work are described in section 4.4.1.

2.7.1. Yield point and continuous yielding

Most materials have a region in which, when a stress is applied, the material behaves elastically. In most low carbon steels, and indeed some other materials, there is a point where the load verses

extension are no longer proportional, this is the onset of plastic flow and is called the yield point phenomenon (60). It is past this point that the material will begin to behave plastically.

Some steels experience both an upper and a lower yield point, including a phenomenon called Lüders bands. An example of typical mild steel behaviour is shown in figure 2.18.

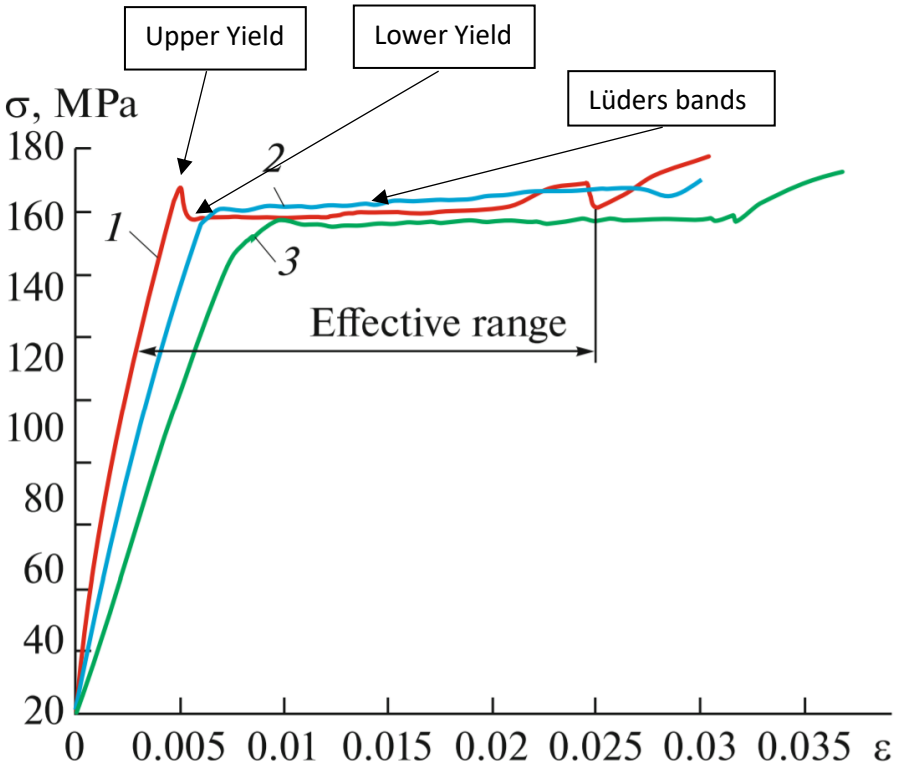

Figure 2.18 Examples of elastic portion of stress strain curve for mild steel. Note the peak of upper yield, followed by a lowering of stress for the lower yield with a plateau region where Lüders banding occurs (61)

At the upper yield point, plastic deformation occurs with an apparent decrease in engineering stress. Continued deformation fluctuates slightly with a constant stress value which is where the lower yield point occurs. Steels with this effect have the average stress associated with the lower yield point (15).

The Lüders bands, or stretcher-strain marks, are part of the specimen which has undergone plastic deformation to the full extent of the Lüders strain, which is the horizontal section of the yield curve. Here, the specimen is inhomogeneous, and further straining causes 'bands' to appear through the remaining material (60).

DP steels typically lack a distinct yield point, this is called continuous yielding. The excellent mechanical properties of DP steels, including the continuous yielding and high strain hardening rate are thought to have been a consequence of the austenite to martensite transformation which involves a volume expansion (62). The large volume of unpinned mobile dislocations in the microstructure that occur during this volume expansion have been attributed to the continuous yielding behaviour (63). Figure 2.19 shows a typical DP800 tensile test curve, noting the continuous yielding behaviour of the material.

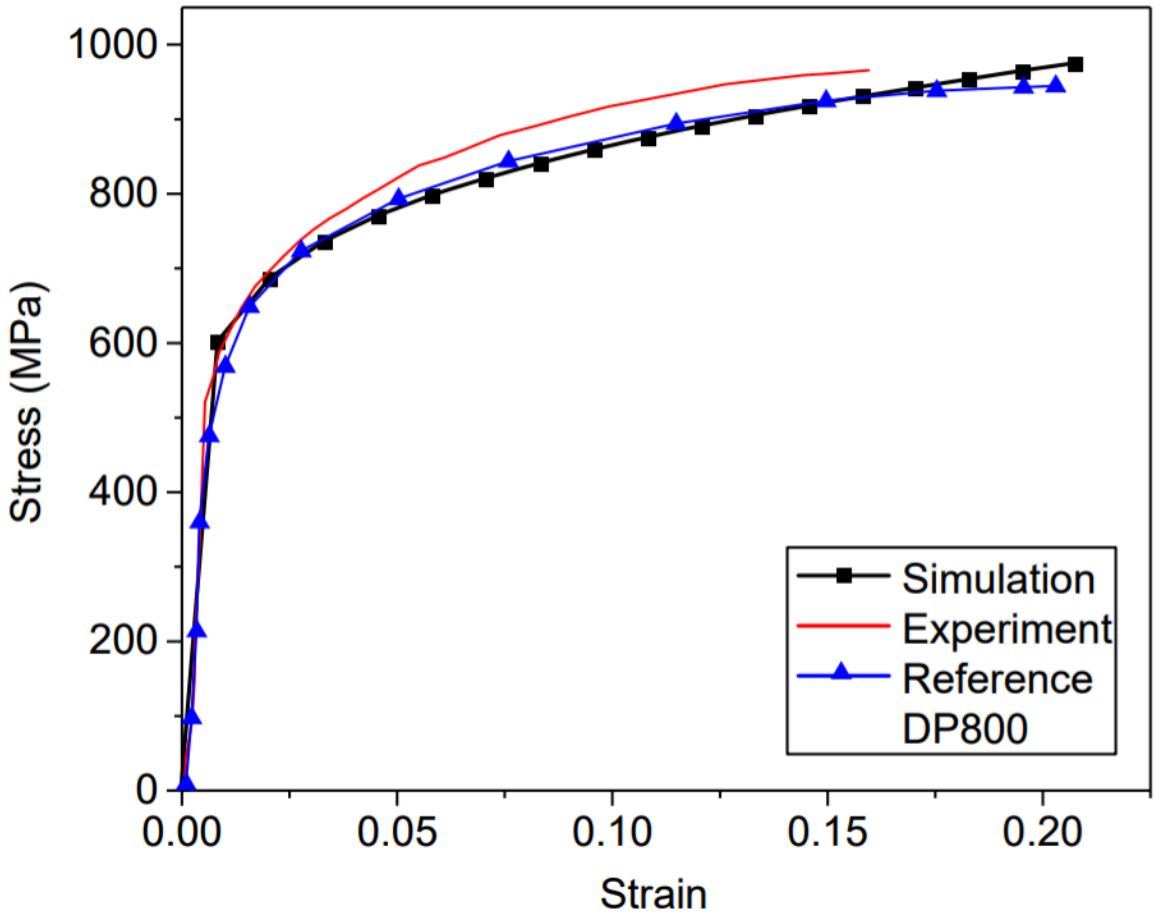

Figure 2.19. Typical stress strain curve of a DP800 material with no distinct yielding point present (64)

It is believed the formation of martensite is important to introduce a high density of dislocations into the ferrite. These dislocation move on the application of stress, and thereby give the continuous yielding that is associated with DP steels (22).

To determine the yield strength in a material that does not have an obvious yield point, a value called proof strength is used. To determine this, a stress is applied that will produce a permanent plastic extension of approximately 0.2% in the gauge length of the test piece, though this may vary up to 0.5% depending on the material in question (65).

2.7.2. Bake Hardening

Bake hardening is achieved in the automotive industry by painting and baking the parts for automobiles. Once the part is formed into its required shape, it is painted and then baked at around 150-200^{o}C to cure the paint, it is this secondary post-processing temperature increase that causes the bake hardening increase in strength. Due to the nature of its microstructure, DP steels can increase in yield strength during this final forming and curing process, an attribute which most high strength steels are unable to achieve.

Typically, bake hardening requires sufficient interstitial atoms present within the steel for dislocation pinning. There also needs to be a sufficient dislocation density, these defects tend to be built up primarily in the ferrite phase of a DP steel. When a stress is applied to a material, these dislocations can move, causing the lattice to slip. It is this slip that allows plastic deformation to occur. The interstitial atoms in solid solution will migrate towards these mobile edge dislocations in the right conditions and pin them in place.

The grain size is also a factor for bake hardening. Research into the effect of grain size on bake hardening is contradicting. Research has suggested that the bake hardening response increases with a decreasing grain size as shown in figure 2.20. Conversely, research has shown that an increase in grain size leads to an increase in carbon content, which can result in cementite formation and a lower bake hardening response (66). The latter research is likely to have limited impact for this thesis, due to DP steels avoiding the cementite formation in favour of martensite, though in other grades of steel this may pose an interesting debate as to which mechanism enhances bake hardenability.

During the forming of the part, the strain, typically applied in the region of 2 to 5%, can lead to an increase in dislocation density. The Snoek effect and can influence the mechanical response of the material (11). It is related to the preferential occupation of interstitial sites by atoms under elastic stress orientated in the stress direction. Once the load that was applied is then removed, the atoms

distribute themselves randomly. The Snoek process involves atoms essentially ‘jumping’ between neighbouring sites (11).

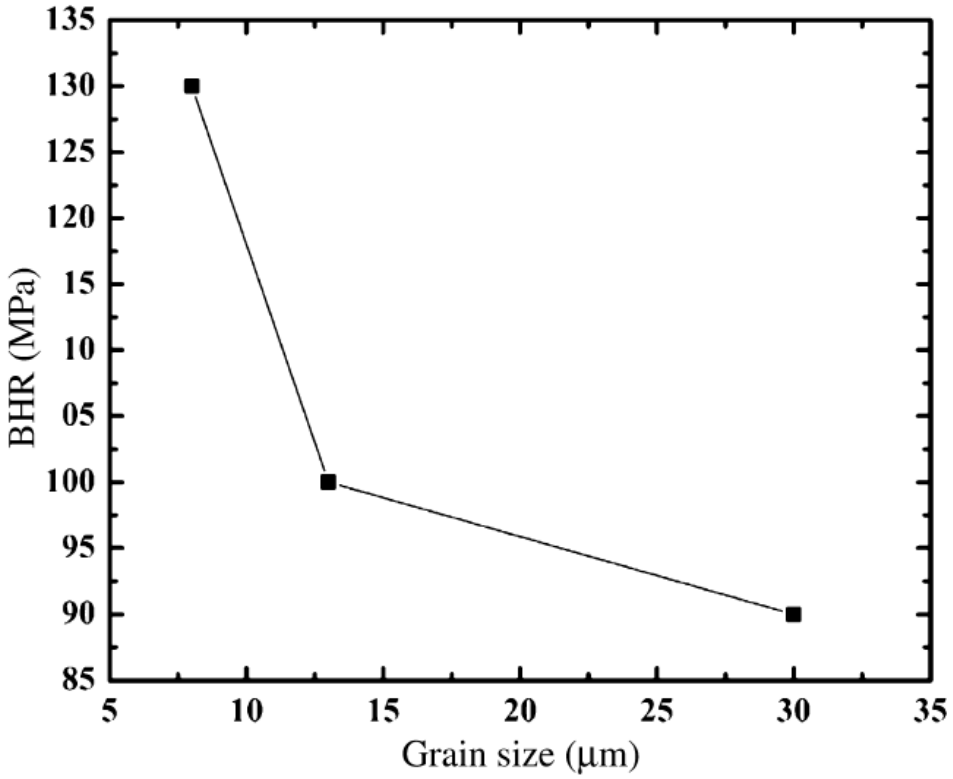

Figure 2.20. Increasing grain size showing decrease in bake hardening response, data taken from mechanisms and modelling of bake-hardening steel (67)

The site for the primary bake hardening response occurs in the ferrite phase. Whilst ferrite contains a low level of carbon in solid solution, the small amount that is dissolved can pin the free dislocations during the forming and heating operation (68).

The mechanisms associated with bake hardening in the ferrite region are suggested to occur in three stages. The first mechanism, developed by Cottrell and Bilby, suggest that interstitial atoms such as carbon and nitrogen diffuse to regions where freshly formed dislocation occur, due to previous deformation. It is these interstitials that form ‘atmospheres’ around the dislocation, essentially pinning them to inhibit further movement (69). Once these dislocations are pinned, a further increase in applied stress is required to allow further movement of the dislocations, breaking free of the pinning by the interstitial atoms, thereby increasing the measured yield strength.

The precipitation of carbides is the second stage, this is dependent on the concentration of interstitial carbon present. Due to the high level of dislocations present in the DP steel, and the large number of dislocation-dislocation interactions, there are numerous precipitation sites. These precipitation site allow the nucleation of excess carbon to form carbon clusters, or carbides in the ferrite matrix. This is responsible for the increase in strength after the Cottrell atmosphere stage (70).

The tempering of martensite is thought to be the final stage. The volume fraction of martensite present tends to decrease due to the formation of carbon clusters or transition carbides, this allows for a reduction of internal stresses within the ferrite. This in combination with the presence of pinned dislocations in the ferrite leads to an increase in yield strength. Whilst tempered martensite would show a decrease in tensile strength, the fact that the low temperature precipitates remain coherent in the ferrite means the yield strength increases (70). The three stages are best shown in a diagram form, as seen in figure 2.21.

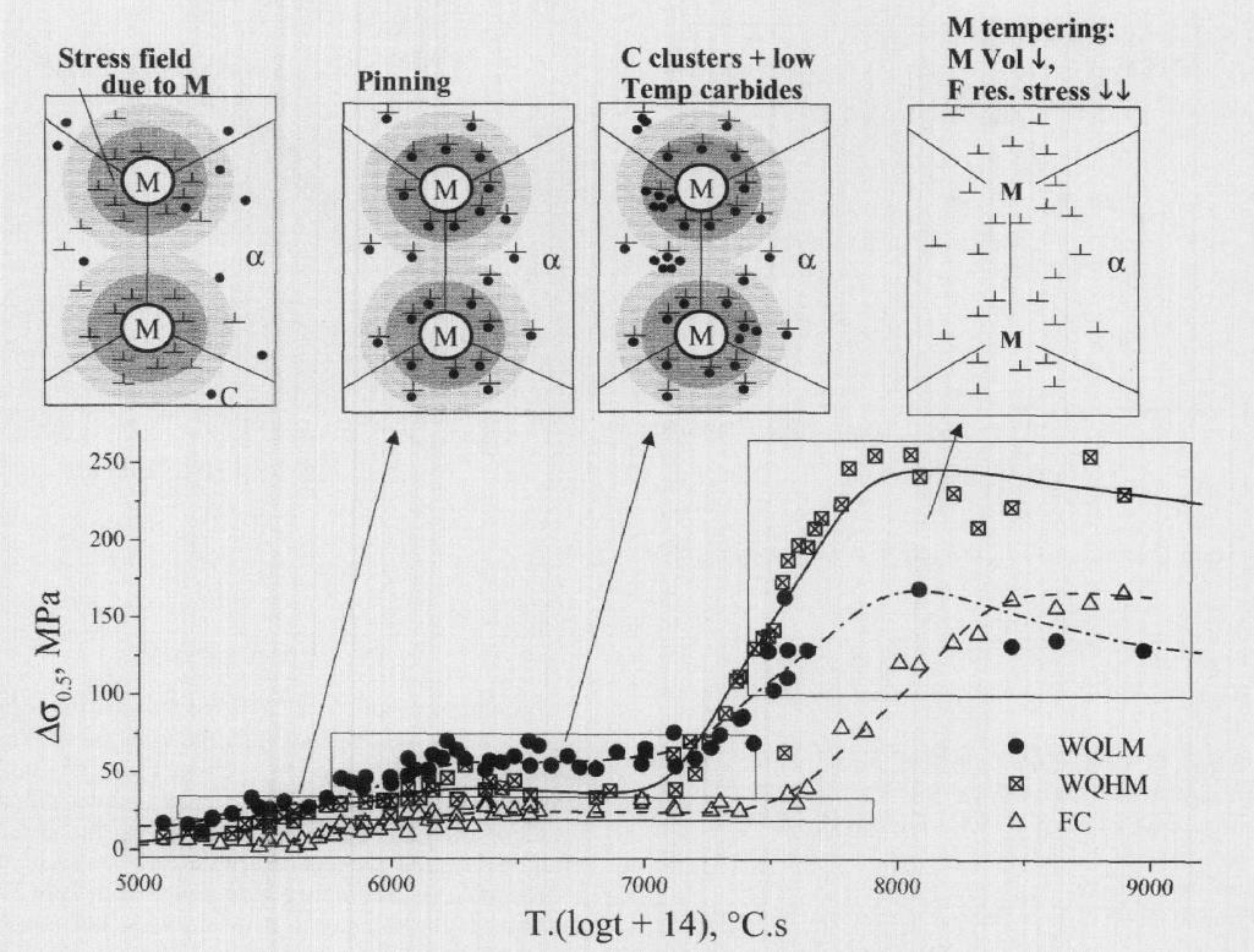

Figure 2.21. Three stages of BHR increase over time: (1) formation of Cottrell's atmospheres pinning, (2) carbide clustering and then (3) tempering of martensite, each stage showing an increase in yield strength. Water quenched low martensite (WQLM) water quenched high martensite (WQHM) as examples. (70)

Whilst the bake hardening mechanism increases the strength, it lowers the elongation and, in most cases for DP steels, it can also bring about the return of the yield point. The yield point is not usually present in a DP steel, as shown in figure 2.22 and this is because dislocations are not pinned post intercritical anneal. The bake hardening process will pin these dislocations in place. Therefore under load, and once the yield point has been surpassed, the unlocking of the dislocations in the material will allow plastic deformation to occur (71). This shows as a defined yield point that is reflected in figure 2.22.

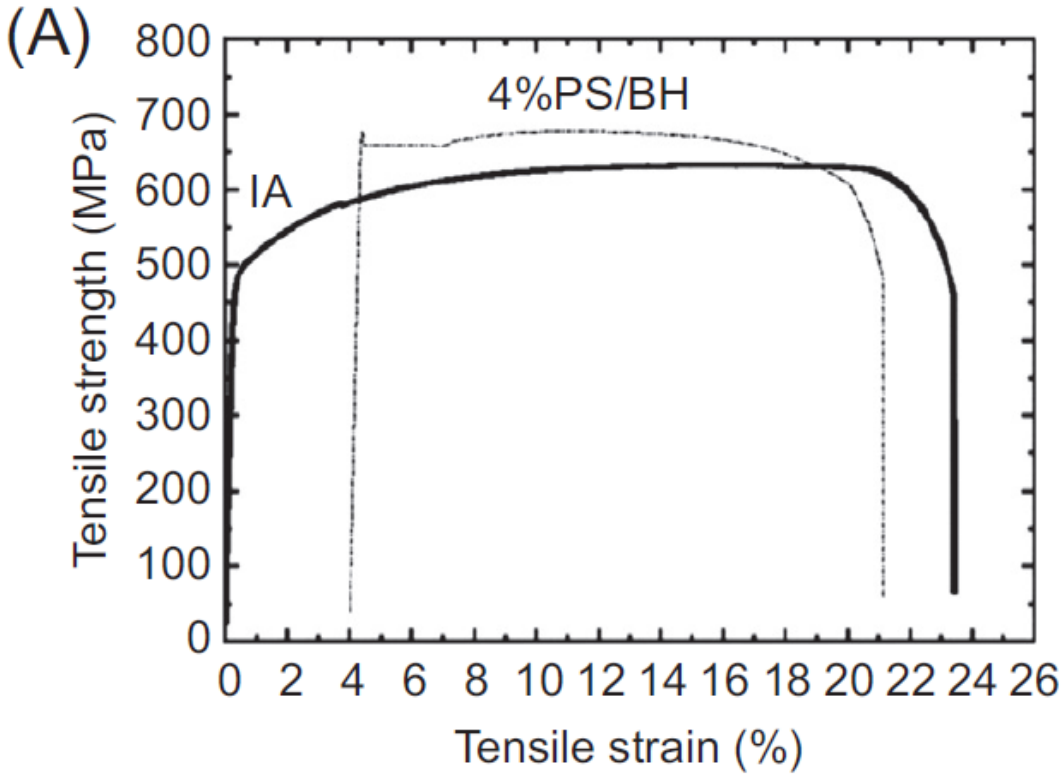

Figure 2.22. Example of post-strained bake hardened DP steel (dashed line). Note the increase in tensile strength but loss of tensile strain compared to the pre-strain specimen (solid line). Nomenclature as follows: IA (intercritical anneal), PS (pre-strain) and BH (bake hardening) (72)

2.8. Coating Wettability

During the hot dip galvanising process, zinc is applied to the surface of the material. This provides the base steel with a protective coating against corrosion. Galvanising poses its own unique challenge during the DP annealing process, as it requires liquid zinc to be applied. This dictates the limits on the overage temperature which must be kept within a tight temperature range to allow for the zinc to be applied to the strip.

The wettability of the coating to the strip surface is dependent on the contact angle on the deposition of the coating material. The contact angle can be determined from the balance of the surface tensions of the solid and liquid surface with respect to the interfacial tension between the solid and liquid phases, with a contact angle smaller than 90^{o} tending to reflect a good surface wettability (73).

A known issue with DP steels face is oxidation of the minor elements during the annealing process, even with a reducing atmosphere. Selective oxidation of elements such as Mn and Si can cause poor wetting of the steel surface, meaning bare patches can form with the liquid zinc (74). These oxides can change the contact angle on the surface, increasing the angle meaning the wettability of the zinc coating can decrease, which in turn can be the reason for these bare patches appearing on the steel substrate surface.

The highest percentage alloying component for DP steels is the Mn, typically between 1.7-2.2wt%. Depending on the concentration of Mn, specific oxides will form, these are $MnSiO_3$, Mn_2SiO_4, MnO respectively. Each of these oxides has a different effect on the contact angle of the coating. The reason for these oxide formations is because Mn preferentially oxidises during the annealing process, and research has shown that the increase in the amount of Mn increases the surface oxidants in the range in which a DP steels Mn content would lie, up to 2.6wt% (75).

This research also shows an increase in the contact angle from 101% to 110% from the oxides respectively, this increase would cause a reduction in the wettability of the substrate surface, leading to bare spots on the strip surface (75).

By applying a controlled amount of oxygen to the steel strip surface and allowing selective oxidation of manganese and chromium, it has been shown that an improvement of surface wettability can be achieved by promoting selective internal oxidation (51). This internal oxidation means that when the strip passes through the reducing atmosphere of the radiant tube furnace, the oxygen on the strip can be reduced and leave a clean surface for zinc adhesion.

2.9. Investigating DP literature

A wide body of academic research has focused on the production and development of dual phase steel over the last 30-40 years. From the initial cold rolled microstructure, through to heating and cooling, each stage can have a huge impact on the final product that is produced. Section 2.9 summarizes some key points that each stage can have on a DP product.

2.9.1. Initial Microstructure

The effect of the cold rolled unannealed microstructure can play an important role in the final mechanical properties of the annealed material. Industrially, a ferrite and pearlite microstructure is typically adopted due to high rolling loads that are experienced during the industrial cold rolling process. If the initial hot rolled material has been quenched to form a bainitic or martensitic microstructure, then there would be difficulties in reducing the materials gauge to obtain the final customer ordered thickness.

However, several bodies of research have found that by achieving a martensitic or tempered martensitic microstructure before annealing, then the resultant mechanical properties and work hardening response are improved (76)(77). This has been linked to well defined and uniformly distributed martensite islands in the final microstructure post annealing, compared to the conventional ferritic-pearlitic banded microstructure which performed poorer in mechanical property tests.

Similarly work from Yong-gang et al. (78) found that comparing ferrite-pearlite, ferrite-martensite and completely martensite initial microstructures yielded the same results, with higher volume fractions of martensite in the initial microstructure leading to significantly refined ferritic phases in the final annealed microstructure, improving strength whilst total elongation remained unaffected.

2.9.2. Heating and heating rate

The rate at which the unannealed DP steel is heated influences the morphology and grain size of the final microstructure. Increasing the heating rate to the intercritical annealing temperature region has shown to refine the final grain size of the microstructure (79)(80).

At increased heating rates it has been shown that both fine recrystallised and larger non-recrystallised ferritic grains can be present, whereas a conventional heating rate of 10°C/s produced equiaxed, recrystallised grains (81). This is in agreement with work from Mohanty et al. (82), which suggests that faster heating delays the recrystallisation kinetics in DP steel.
It can be expected that recrystallisation is complete in ferrite before the nucleation of austenite, therefore with high heating rates the recrystallisation of ferrite at higher temperatures can occur concurrently with the formation of austenite (83).

2.9.3. Intercritical annealing

Heating a DP steel to intercritical annealing requires heating between the A_{c1} and A_{c3} temperatures. At this point, both ferrite and austenite are produced, both of which are key for the final annealed ferrite and martensite microstructure. An example of cooling through the intercritical region is shown in figure 2.23.

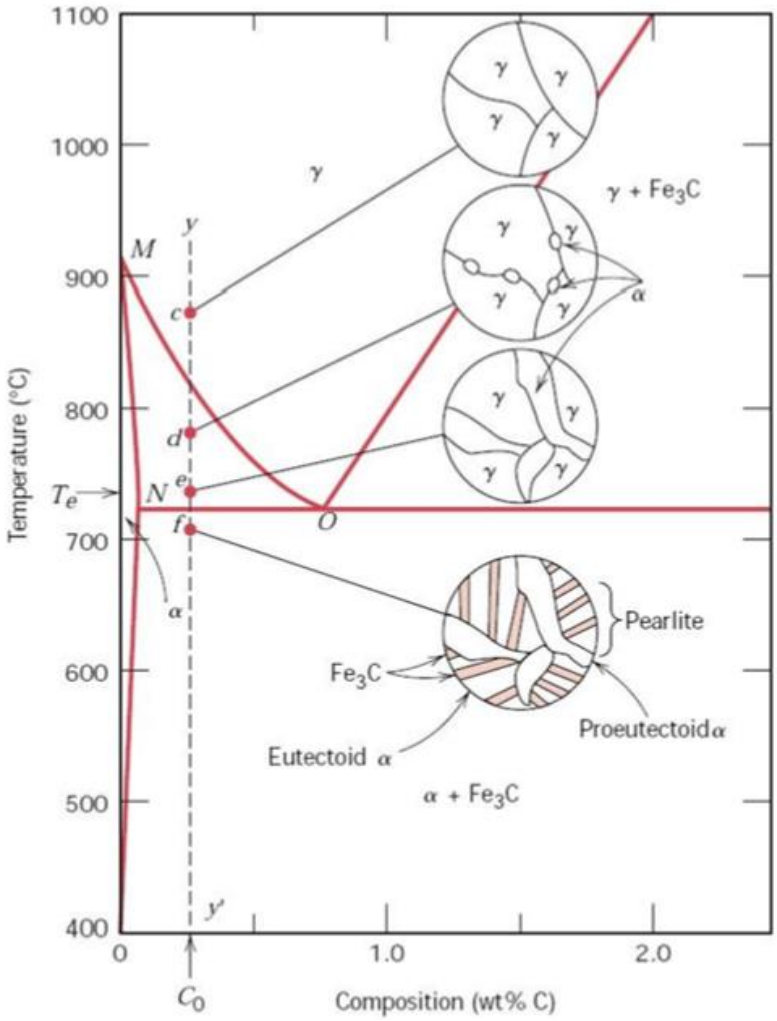

Figure 2.23. Schematic of iron carbon diagram with an example of cooling through the intercritical region, creating a hypoeutectoid steel (C_O). From points M to O represent the A_{c3} line, where N to O is the A_{c1} line. Between these lines is the intercritical region. Points d and e on the dashed line show two examples of the microstructure during cooling through this region (15)

Most literature agrees that increasing the temperature close to the A_{c3} will lead to an increase in the yield and tensile strength of DP steels, this is primarily down to the increase in higher austenite volume fraction which in turn leads to an increase in the martensite volume fraction of the final material (84)(85)(86)(87).

Annealing within the intercritical region provides austenite with a higher carbon content, compared to annealing within the completely reaustenitised region above A_{c3}. This in turn gives higher stability to the austenite, promoting transformation to martensite rather than bainite during cooling (88).

Speich et al. (89) showed three distinct stages of austenitisation during the intercritical stage. First is the growth of austenite phase within the pearlite regions, until consumed. Second stage is the slow growth of austenite into the former ferrite regions, typically controlled by carbon diffusion in the short term or by manganese diffusion at extended soak times. The final stage is achievement of equilibrium controlled primarily by manganese in austenite, though the author suggests this would be around 2000-4000 hours. Whilst this shows the theoretical stages, the nature of processing on a continuous annealing line would have the material in the intercritical annealing temperature for a matter of minutes, rather than hours, therefore the latter stage is unlikely to take effect.

The recrystallisation of ferrite can occur typically before the intercritical temperature is reached. However, the increase in alloying elements such as manganese, chromium and niobium typically seen in higher quantities of a DP steel can lead to a slow down in the recrystallisation rate. A couple of authors noted that increasing these elements can lead to a recovery of the initial cold rolled ferrite rather than the recrystallisation of it (90).

The recovery of ferrite rather than the recrystallisation leads to a presence of large dislocation boundaries within the ferrite, which creates a diffusion path network for solute atoms such as carbon and manganese. This allows austenite to grow along the directionally aligned fragmented pearlite colonies and recovery bands (91).

As has already been described earlier in the body of work, chemistry plays a critical role in the creation of a DP microstructure. Work from Andrews (92) provides a good indication for the effect that chemistry (wt%) will have on the increase or decrease in A_{c1}/ A_{c3} temperatures.:

$$A_{c3} = 910 - 203\sqrt{C} - 15.2Ni + 44.7Si + 104V + 31.5Mo + 13.1W \quad \text{(Eq 1.1)}$$

$$A_{c1} = 723 - 10.7Mn - 16.9Ni + 29.1Si + 16.9Cr + 290As + 6.38W \quad \text{(Eq 1.2)}$$

Adjusting each of these elements can show its theoretical effect on the A_{c1} and A_{c3} temperature. The short time during the soak that is seen on an industrial processing line also leads to a non-uniform distribution of carbon and other alloying elements (89). Increasing the carbon content of a DP steels leads to an increase in the austenite volume fraction during heating in the intercritical region, leading to an increase in the strength and hardness (39).

The other major contributing element added at large quantity is manganese. Calcagnotto et al. (42) showed that manganese decreases the A_{c1} temperature, refines cementite in the initial microstructure which leads to a pinning effect and reduces grain boundary mobility due to the solute drag effect. As well as this it has been shown to substantially enhance grain size stability during intercritical annealing and enhances the martensitic phase transformation upon cooling.

2.9.4. Effect of cooling

The cooling path determines the transformation of the microstructure from austenite to its different room temperature constituents, in a DP chemistry that can typically include retained austenite, martensite, bainite or pearlite.

The first region of cooling on CAPL is slow cooling. This region allows enough time for the generation of new precipitate free ferrite, which in turn promotes the enrichment of the surrounding austenite (93). This enrichment further delays the transformation of austenite to bainite, allowing the potential for slower cooling rates to be used to achieve a martensite / ferrite microstructure.

Sufficiently rapid cooling is then required to avoid the formation of bainite and to transform to martensite, this also has the benefit of decreasing the sensitivity of the mechanical properties to annealing temperature (88).

Kong et al. (53) found that during the overage section, lower temperatures improved the phase transformation dynamics, which led to an increase in the martensite content. As overage temperatures are increased, so too was the percentage of tempered martensite in the microstructure. This increase in tempered martensite would lower the overall strength of the material and cause a precipitation of carbides, therefore reducing distortion in the martensite lattice and decrease residual stress (83).

2.10. Investigating the effect of silicon

Silicon is a widely used alloying addition in DP steels. Silicon (Si) in solid solution will increase the strength, raises the tensile stress to yield stress ratio and aids the removal of discontinuous yielding (94). Even with this added strength, research has shown that it also has a minimal effect on the ductility losses associated with strength increase. The presence of Si enhancing the partitioning of carbon to austenite during intercritical annealing provides increased ductility to ferrite and the overall ductility of DP steel (95).

Further work by Fonstein et al. (96) shows that there is a general improving trend between the tensile strength and the elongation when increased Si additions are made. This is shown in figure 2.24, where increasing amounts of Si were added to a base chemistry. This improvement in the tensile strength and ductility was also noted in work from Cai et al. (97), who put the increase in the balance between strength and ductility due to an increase in the strain hardening rate.

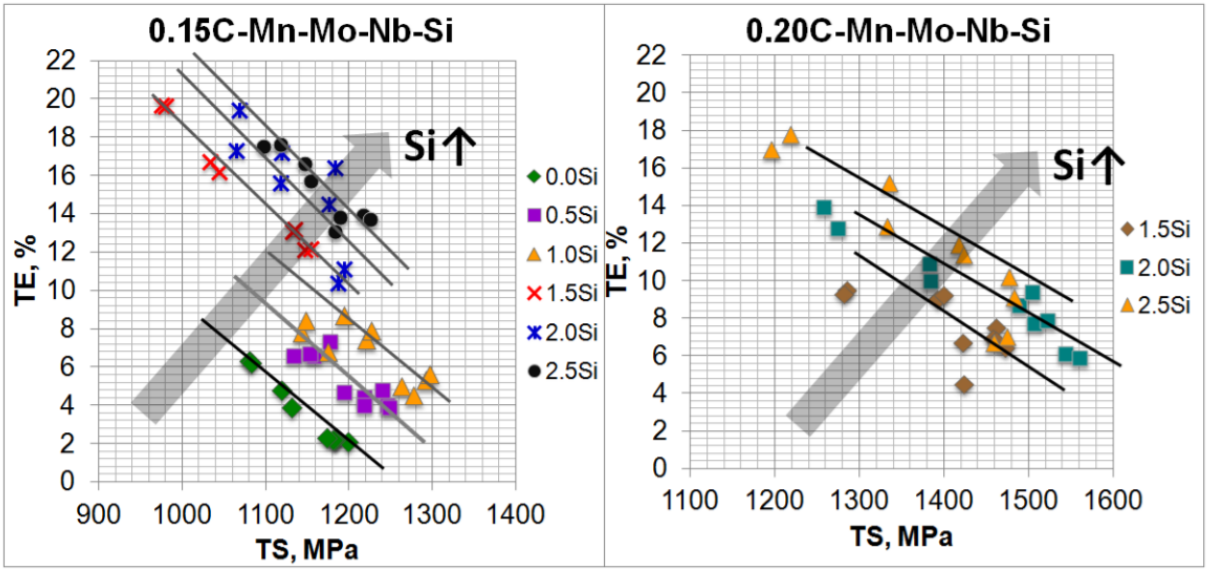

Figure 2.24 Effect of Si for strength vs ductility in DP steels. The left graph shows 0.15wt% C addition with the right graph containing 0.20wt% C, both showing an increase in elongation/strength as Si content increases (96)

This is also suggested by Davies et al. (98), where additional Si also allows for a more ductile ferrite due to dispersion of carbon from the ferrite to the surrounding austenite, enhancing the strength of the martensite. It is reported that this is achieved by the Si driving the carbon from ferrite to the

martensite, therefore leaving a ferrite phase with less interstitial carbon and further saturating the martensite phase, increasing its strength and stability on cooling (99). This additional stability can be critical during the cooling of austenite, if the austenite remains supersaturated with carbon, it will delay the onset of bainite formation during rapid cooling and over-aging on the continuous annealing process.

Increasing Si will increase the A_{c1}/ A_{c3} start temperatures during intercritical annealing. For this reasoning, it can be expected that Si would promote the formation of ferrite nuclei and growth. Work by Drumond et al. (100) shows that varying the Si content from 0wt% to 0.3wt% allowed the recrystallisation process to start earlier, so when the austenite formation begins, ferrite grains are already recrystallised. This means multiple austenite nuclei are formed, therefore smaller more uniform distribution of austenite can be expected in the microstructure.

Si will also provide increased solid solution of strengthening, primarily in ferrite. As described by Mein et al. (101), this solid solution strengthening will decrease the difference in hardness between the ferrite and martensite, and this should promote an improved hole expansion value. Increasing the amount of silicon has also shown to provide the best combination of tensile strength and stretch flangeability, this was shown in work by Cai et al. (97) where Si was varied in a DP steel from 0-0.95wt%.

Work from Saleh et al. (102) showed that increasing the Si content to 1.44% results in a high work hardening rate, high uniform elongation and high tensile strength. This was attributed to the increased amount of retained austenite which transformed to high strain martensite upon cooling(102). The same work also showed that any further increase in Si lowered the work hardening, uniform elongation and decreased the tensile strength.

Whilst an increase in Si has shown to be beneficial to the overall mechanical properties, it's increase is likely to be detrimental to coating. Si, like Mn, is preferential for generating oxides in the furnace. It's worth noting that the Mn and Si oxides tend to bond with each other when both are present in the steel. Research on Si content has shown small amounts up to 0.5wt% worsens the wettability of the coating, which is within the region of a DP steel, by generating those oxides previously mentioned, $MnSiO_3$ and Mn_2SiO_4 (103).

If all Si were to be removed from the steel, whilst retaining Mn, the formation of MnO would occur as the preferential oxide. This would cause a decrease in the contact angle, which has been explained due to the reduction of the MnO with the soluble Al present in the zinc bath (103).

An issue with coating highly alloyed steels AHSS is liquid metal embrittlement (LME). For the majority of automotive manufacturers, the joining technique most commonly used is resistance spot welding (RSW). During RSW of AHSS, cracks on the sheet surface have been observed in and around the weld area. It has been theorised that the cracks are initiated by liquified low melting zinc phases, which then infiltrate the grain boundaries of the steel and lead to brittle fracture (104).

Si is thought to play a role in LME cracking. Work from Kalashami et al. (105) focussed on the effect Si has on LME and found that increasing the Si content from 0.7wt% to 1.8wt% increased LME crack length significantly. The same body of work also found that at 1.8wt% Si there was increased surface ferrite grain size, decarburization layer and internal oxide density, all of which were shown to result in an increase crack LME crack susceptibility.

As this body of work will look at the effect increasing Si has on the mechanical properties of DP steels, coating adhesion will need to be investigated to show that any benefit of mechanical property improvement will not lead to a degradation of the galvanised products coating.

3. Aims & Objectives

As automotive manufacturers strive to lower emissions from the vehicles they produce, steel manufacturers look to deliver a generation of steel that provides increased strength and formability. Over the past decade, Tata has made steady progress in the advanced high strength steels arena by producing both commercialised DP600 and DP800 through the continuous annealing line CAPL and more recently DP800 on the galvanising line Zodiac. DP1000 is currently produced through CAPL, and trial work has looked at producing a viable DP1000 offering at Zodiac.

A lot of research has been undertaken to enhance the understanding of the effect of chemistry and heat treatment of DP steels, which has been shown in chapter 2. However, this research tends to have been limited in the main to small scale or laboratory manufacturing. There is considerably less published research for large scale industrial processing.

This body of work will focus on enhancing the knowledge of processing at Tata's UK annealing units with a view towards commercialising new DP grades through both CAPL and Zodiac, whilst enhancing the scientific understanding of industrial scale processing and the challenges it presents, bridging the gap between lab scale production to full scale industrial production.

Effect of annealing process on DP steels

This section of work will look at the current DP800 product that is produced through CAPL and establish what effect that each region of the industrial annealing cycle plays in the final microstructure and mechanical properties of the steel.

Effect of Silicon on DP800

Silicon plays an important role in the effect of mechanical properties of DP steels. This section of work will look at the effect that silicon plays when processed through CAPL, and what level of silicon provides the best overall mechanical properties with a view to improving the bake hardenability of the final product.

Processing DP1000 on Zodiac

This section will look an existing chemistry used on Tata Ijmuiden's galvanising lines and see if the processing parameters can be trialled to produce a viable DP1000 galvanised product on the UK galvanising line Zodiac.

High yield DP1000

To look at improving the DP1000 product offering through CAPL, a DP1000 high yield variant could be produced. This section of work will use a cold rolled substrate from Tata Ijmuiden to investigate whether CAPL's processing conditions can be adjusted to produce a viable DP1000 high yield product.

4. Experimental Procedures

4.1. Casting of Material

Three 50kg casts of a DP steel chemistry were made with varying silicon content as show in table 4.1. The material melted in a vacuum induction melting furnace (VIM) in a Al_2O_3 crucible. Iron is added melted and a Celox measurement is taken to check the oxygen levels. Aluminium is then added to 'kill' the steel, reducing the oxygen content of the melt to around 3.7 PPM. Following this the other elements are added, shown in table 4.1, the Celox measures the temperature throughout, which was kept at 1550°C, before it is cast and rolled to what is known as a transfer bar thickness of 34cm.

Table 4.1 Alloy content of low, medium and high silicon DP steel that was VIM cast (wt%). Remainder of alloy was kept as similar as possible to limit potential variability.

Alloy	C	Mn	Si	Ti	Cr	Nb
Low Si	0.14	1.838	0.013	0.029	0.547	0.025
Med Si	0.137	1.825	0.253	0.031	0.54	0.026
High Si	0.139	1.826	0.407	0.03	0.549	0.026

Whilst the international specification EN10338 (106) has a maximum limit of 0.8wt% limit, the silicon content of this material reflects the reasonable limits for DP800 cast at Tata, therefore keeping the chemistry industrially relevant.

4.2. Rolling

The transfer bars were received in the UK, the bars were cut to 70mm x 70mm blocks. Cutting the transfer bars to blocks allows for the material to be hot and cold rolled on a laboratory mini mill. The blocks are reheated in a Carbolite furnace to 1250°C in air for two hours to ensure a homogenous

temperature is achieved throughout the material. Following the reheat, the blocks are moved from the furnace and scale build up is mechanically removed from the surface, the block is then placed in front of the two high reversing mill where it will then be rolled.

During the rolling process, the material is passed through the stand a total of seven times to achieve the final thickness. The initial pass is called the roughing pass. Control of the roll gap, the distance between the two rolls, is controlled manually by a transducer and a motor. By adjusting the down switch, the roll gap will decrease, therefore decreasing the gauge of the material as it passes through. This process is repeated for seven passes, aiming for a final hot rolled gauge of approximately 3.5mm thickness. Throughout the rolling process real time data is recorded giving rolling loads determined by two load cells each side of the mill and temperature readings from pyrometers.

The samples are then transferred to the run-out table, the sample passes through the set of water sprays at a controlled speed. Pyrometers are used to record the run-out table gap, entry and exit temperatures. This ensures that the temperature profile during the process matches the same processing parameters that would be seen on an industrial hot mill.

Once processed through the run-out table, the samples are transferred to a furnace set at the appropriate coiling temperature, the furnace is then switched off to simulate coil cooling on the industrial processing line.

4.3. Annealing Simulation

4.3.1. Continuous Annealing Simulator (CASIM)

The CASIM is an ideal way of replicating large scale mill annealing, utilising cold rolled unannealed substrate of approximately 360mm x 100mm length and width. The sample is cleaned using acetone and a scrubbing cloth, this removes oxide build up from the strip sample. The steel is then tightened between a set of metal grips with six thermocouples spot welded to the surface of the strip. These thermocouples provide temperature readings of the strip as it is heated and cooled, with the control thermocouple providing a continuous feedback loop to control the temperature. An example of the thermocouple welded sample is shown in figure 4.1.

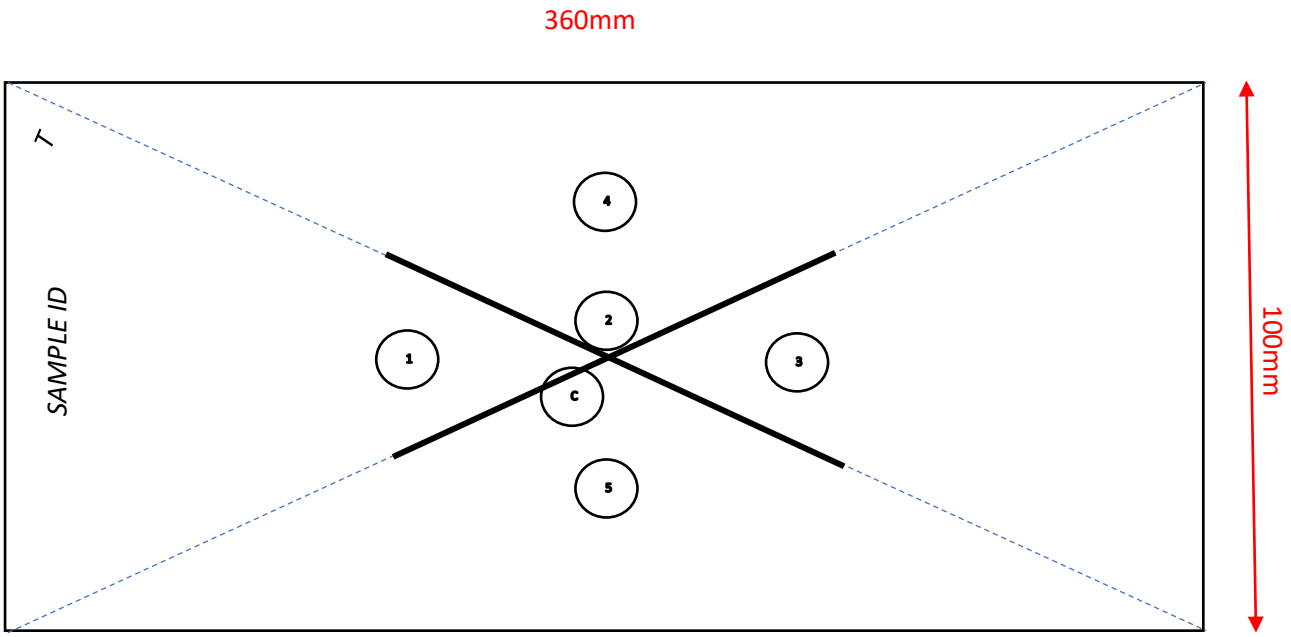

Figure 4.1 CASIM sample set up, each circle represents where a thermocouple would be welded to feedback strip temperature during heating and cooling cycle.

The program temperatures and times set up on the computer linked to the CASIM, temperatures and times reflective of a typical continuous annealing cycle are input and are sent from the computer software to the CASIM, the temperature is increased by resistive heating through the grips and then controlled through continuous feedback from the thermocouples.

Compressed air is forced through quench heads in front and behind the strip sample provide the cooling necessary to mimic the rapid cooling rates achieved on a large-scale annealing mill. The position of the thermocouples across the strip sample provides feedback of the temperature profile. Figure 4.2 shows the sample in the CASIM, the door is then closed and locked before the annealing cycle is started.

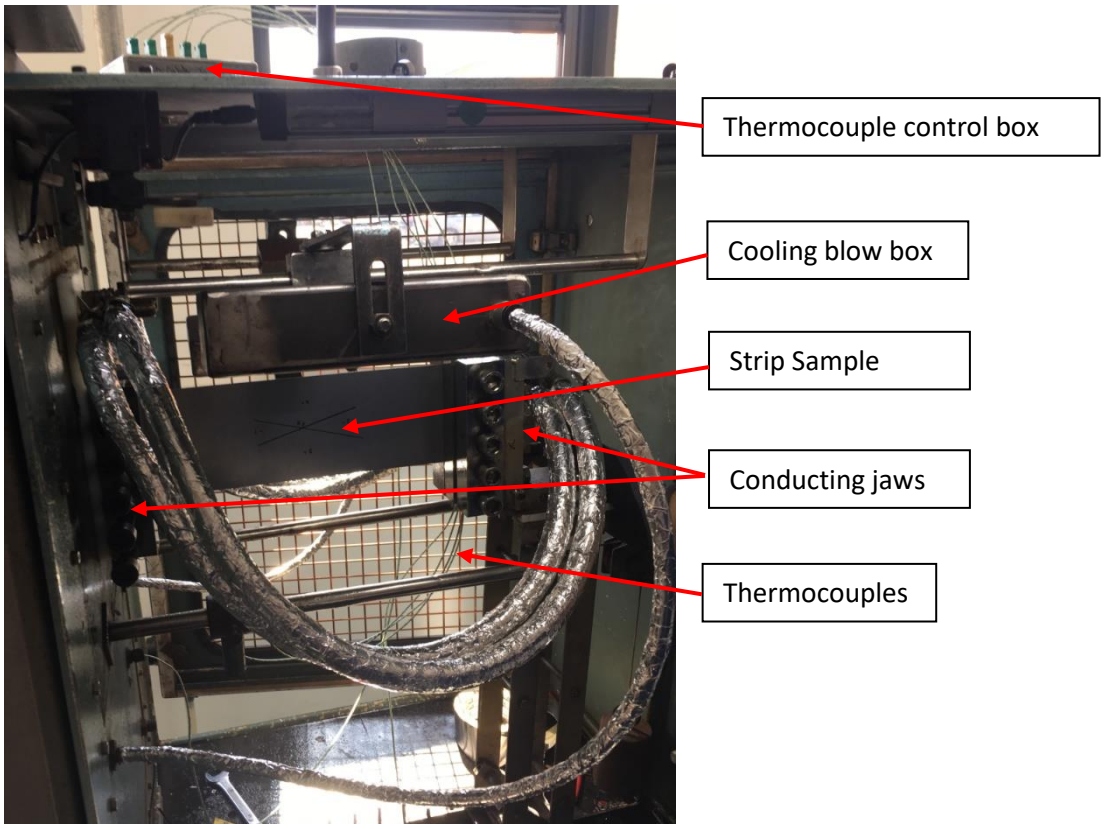

Figure 4.2 Set up of CASIM. Steel sample inserted between conductive jaws, thermocouples are welded to the front of the strip and the blow box is lowered to cool the strip during the annealing cycle.

Once annealed, the sample is large enough to provide two samples that can be machined for tensile testing, as well as taking a small strip from the centre of the sample which can be used for metallographic purposes.

4.3.2. Gleeble 3500

Similarly to the CASIM, the Gleeble 3500 is a thermomechanical simulator that uses resistive heating via stainless steel jaws to heat the steel. An external cooling head can be applied within the Gleeble

which provides sufficient air or water mist cooling to the strip surface to match that of a continuous annealing cycle.

Strip samples are much smaller than that of the CASIM, each sample is typically 18mmx180mm. Each sample has the surface ground using sandpaper to around 600 grit finish before cleaned with ethanol. This is to ensure a clean contact between the steel jaws and to provide a clean area for thermocouple welding. Each sample has two thermocouples welded to the centre of the strip, and this provides continuous feedback to the control machine.

The sample is clamped between the stainless steel jaws, the cooling head is attached to the frame and connected to the air cooling tanks. The pressure of air cooling can be adjusted dependant on the degree of cooling required.

As with the CASIM, the programmed times and temperatures are entered in the control machine computer and then the program is transferred to the Gleeble with real time temperature feedback provided by the thermocouples on the strip. An example of the program using times and temperatures is shown in figure 4.3.

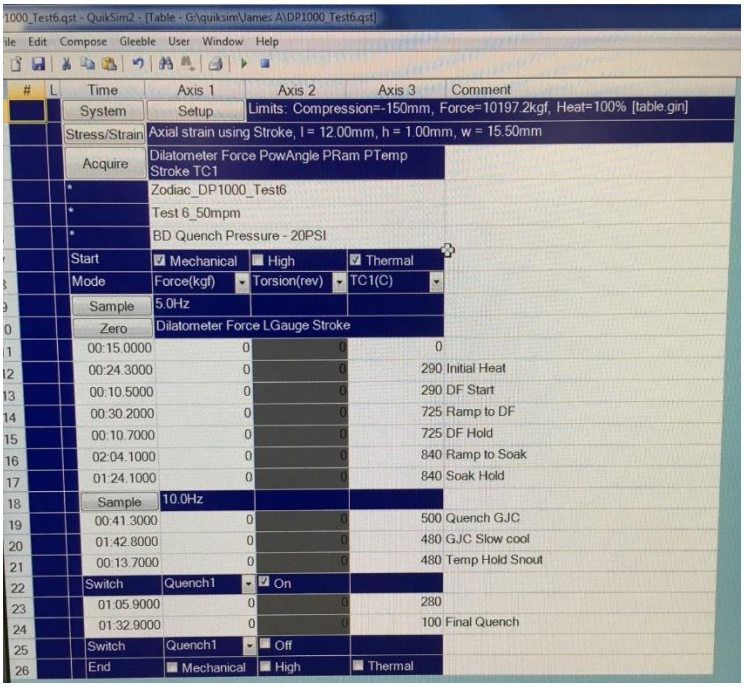

Figure 4.3 Image showing QuickSim software. Time and temperature is entered and the program is sent to the Gleeble control which initiates the cycle run. Thermocouples provide the feedback to the temperatures being achieved in relation to the entered information.

Unlike the CASIM, the Gleeble does have the capacity for a controlled atmosphere and can run in a vacuum. As all the samples using Gleeble and CASIM were tensile tested, each experiment was performed in air and thoroughly cleaned before testing to remove strip oxidation using a combination of acetone and sandpaper. Figure 4.4 shows the test chamber of the Gleeble in operation.

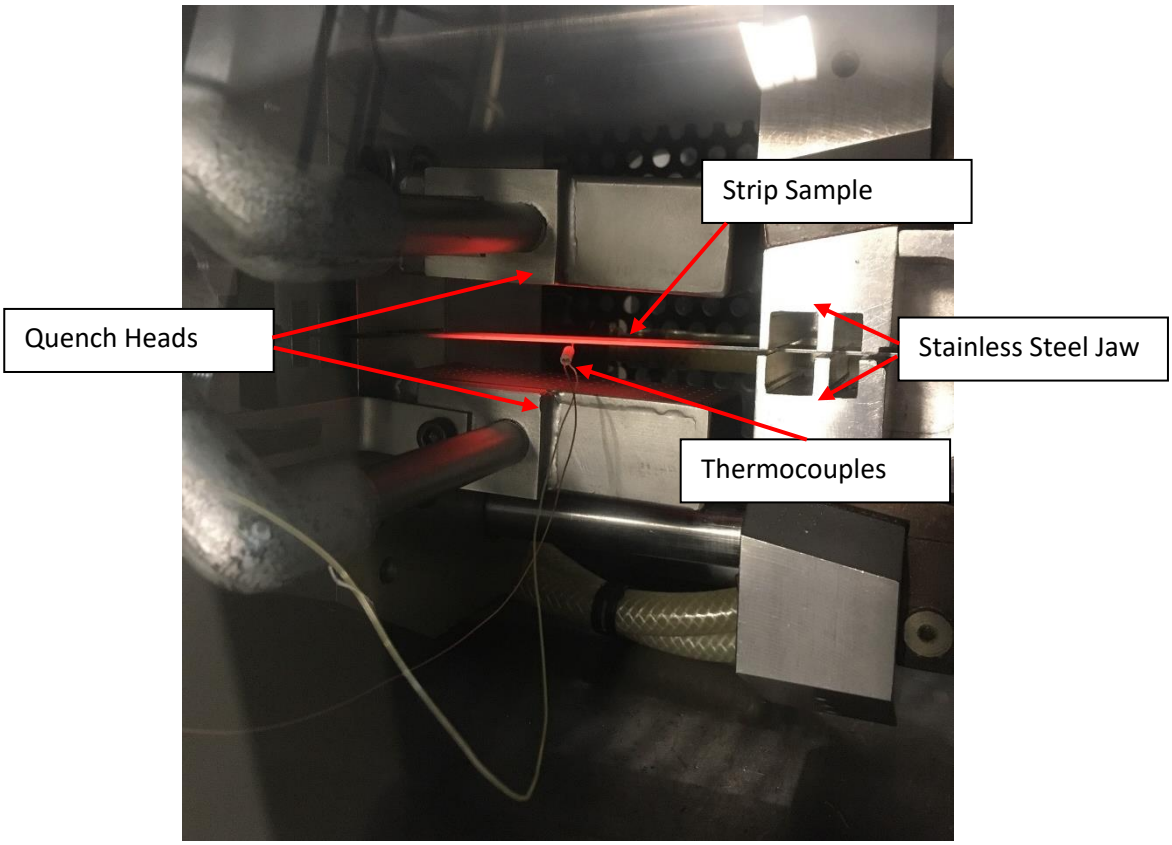

Figure 4.4. Inside test chamber of Gleeble, strip being resistively heated whilst running an annealing cycle.

4.3.3. Surtec A5 Hot Dip Process Simulator (HDPS)

The HDPS is a continuous annealing and galvanising simulator. Unlike the CASIM and Gleeble, an A5 sheet steel sample can be heated in a controlled atmosphere containing nitrogen and hydrogen in the combinations found in continuous annealing and galvanising lines. It also has a 35kg zinc bath of liquid zinc or zinc alloy which can be dipped.

Similarly to the other simulators, a temperature and time profile is entered into the machine computer to mimic an industrial annealing cycle. The temperature profile is controlled by infra-red

lamps compared to resistive heating for the CASIM and Gleeble. The annealing atmosphere can be controlled with differing ratios of hydrogen and nitrogen to also replicate a continuous galvanising line.

Dew points can be controlled between -60 to +70 allowing for internal and external oxidation reactions and to see its influence on coating and mechanical property performance.

The atmosphere of the pot can be controlled as well as utilising nitrogen gas knives to control the applied zinc coating weight. The A5 sheet is sufficiently large enough to produce a dog bone sample of the same size as is produced from a CASIM sample.

4.4. Mechanical Testing

4.4.1. Tensile Test

The tensile test is a universal method of assessing a materials' mechanical properties. Tensile testing allows for reliable predictions of how a material performs under loading other than just uniaxial tension (107).

In this body of work, all tensile testing will be prepared as a dogbone shaped sample, which is the most widely used method used for testing sheet steel samples. An example of a dogbone sample used is shown figure 4.5.

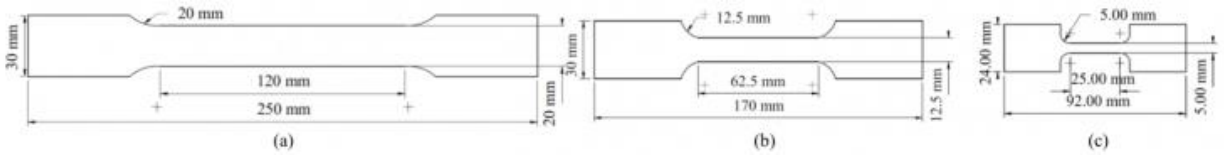

Figure 4.5 Examples of dog bone tensile specimens. Specimen (b) is the typical A50 size sample used in this thesis, testing in accordance to ISO 6892 (8)

The sample consists of wider shoulder sections, this is to allow the tensile testing machine jaws to grip the sample for it to be pulled. The centre section has a reduced gauge area region, it is here that measurements are made. The reduced gauge area should also be sufficiently small in diameter compared to the shoulders, which constrains the deformation to within the gauge area.

Two different sample dimensions were used for tensile testing. Due to the CASIM samples being much larger in size, industrial sized A50 samples can be achieved as per the European testing standard ISO 6892. These samples are machine cut out of the CASIM sample and are then pickled in HCl 30% for 15 minutes to remove any oxide. The sample are then washed in water with diluted sodium carbonate solution which then neutralises any remaining HCl acid. Once pickled, the samples are deburred to limit edge defects which may adversely affect the tensile test results, where the tensile test extensometer attaches to the sample.

Due to the much smaller sample size achieved for Gleeble testing, a subsize sample was used. These samples were also machine cut and pickled in similar conditions to remove the oxide layer, before being deburred. The dimensions of the dog bone sample is shown in figure 4.6.

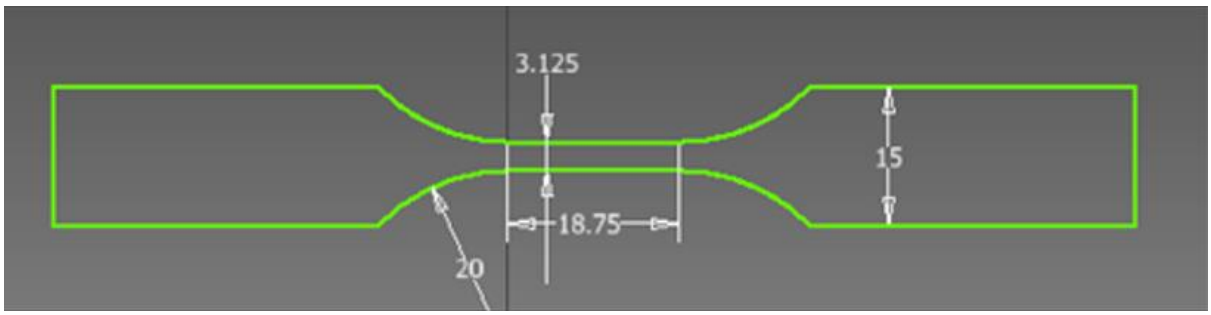

Figure 4.6 Subsize Gleeble sample used for tensile testing. Measurements shown in mm. This sample was used due to the small uniform region where temperatures were consistent. Larger samples would have caused temperature variability across the strip.

The main tensile tester used throughout this work was the Zwick 1474. This machine is a floor standing hydraulic tensile testing machine with test loads of 100kN. It is equipped with gauge and width extensometers which allow for additional measurements of r-value and n-value.

Once pickled, a 50mm bar is used to scribe marks along the gauge length. This is key to allow for a manual elongation measurement should the specimen break outside of the extensometer.

Three measurements of the sample thickness and the sample width in the reduced gauge area are taken, and the mean of these measurements is used. This information is then entered in the Zwick software and allows for accurate calculation of the mechanical properties.

The sample is then positioned vertically between the two clamps and aligned within the centre of the jaws, a small amount of tension is placed on the sample and the system reset to account for the

correct sample size. The extensometers are brought on to the strip to ensure they are correctly attaching to the sample surface.

The tensile test adheres to the ISO 6892 tensile testing of metallic materials standard. At the start of the tensile test the initial test speed is applied at 0.00025mm/s, up to 2% strain where the test speed is then increased to 0.0067mm/s, with the test running until material fracture. The tensile test will provide direct measures of ultimate tensile strength (UTS), uniform elongation, taken at UTS point, and total elongation.

Due to DP steels having a lack of definitive yield point, the measurement of proof strength is taken at 0.2% strain. After the test is completed, the samples are removed from the jaws and manual measurement of the samples can be done if necessary to obtain the elongation at fracture.

Due to capability on the Zwick, a second tensile testing machine was used for the smaller ASTM Gleeble samples. The Instron 8516 is a servo-hydraulic controlled fatigue system using a 50kN load cell. It can be used in the same method as a universal tensile testing machine, achieving a broad range of mechanical properties.

The process of tensile testing was the same as for the Zwick. The samples have the gauge length scribed for elongation measurements, and have the thickness and width measured three times within the gauge length area and the mean taken. The test itself is the same with the initial test speed of 0.00025mm/s up to 2% strain, then increasing the test speed to 0.0067mm/s until material fracture. Tensile test results in this thesis are either duplicated, or where material allows, three tests taken for each result. Errors are min/max of these results.

4.4.2. Bake Hardening

The purpose of a bake hardening test is to replicate the paint curing conditions experienced by automotive components. A steel blank is pressed into the final automotive component, it is then painted. After the paint baking cycle, an increase in the yield strength of the part is seen. This increase is not seen in all grades of steel, but is present in DP steels (108).

Classification of bake hardenability is determined by the bake hardening index (BHI). Using the Zwick 1474, samples are prepared in the same way as a conventional tensile test is, by producing a dog bone sample which is deburred and pickled.

The sample is placed in the machine and pulled to a 2% strain, also known as a pre-strain. Once this is achieved, the sample is removed from the grips and placed in a Carbolite oven at 170°C for 20 minutes. The sample is removed after 20 minutes and is left to cool down to room temperature.

The sample is then placed back in the tensile testing machine and is pulled to fracture using the same test parameters as stated in the conventional tensile test. The BHI index is calculated by taking the ultimate tensile stress at 2% pre-strain and subtracting from the yield point post bake hardening, as shown in figure 4.7.

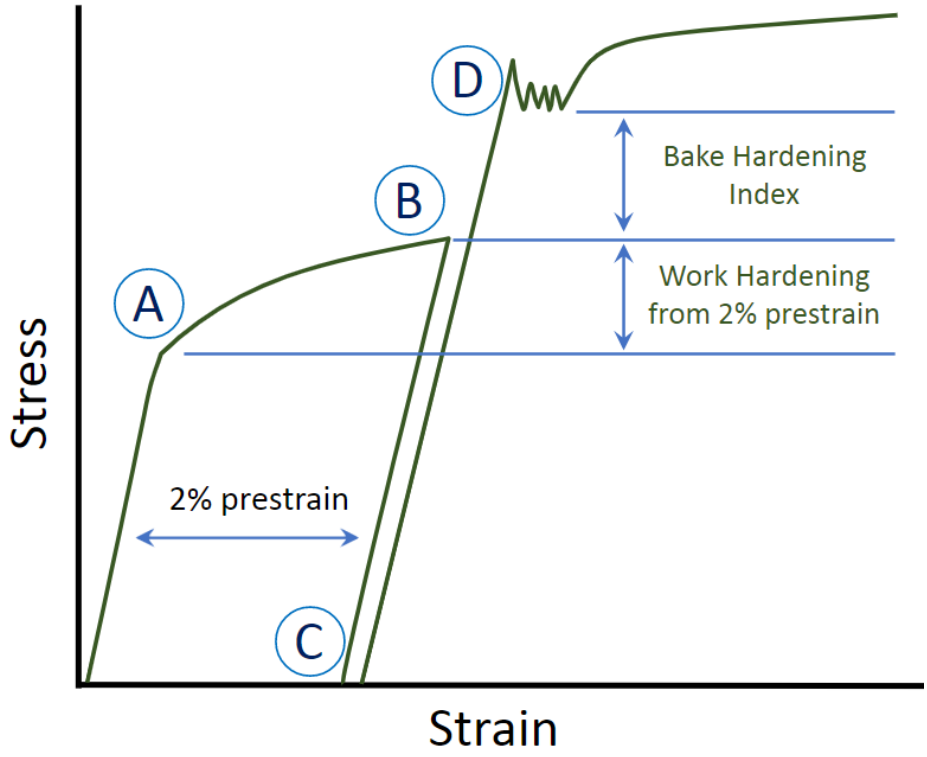

Figure 4.7 Example of stress strain curve linked to the BH test. The initial pre-strain test is to point B, the sample is unloaded (C), then the sample is placed in an oven to replicate the baking process. The sample is tested again to destruction. B - A reflects work hardening increase, with the bake hardening calculated from D - B

All BH testing was done in accordance with EN 10325, which governs the times and temperatures that must be followed for the test. BH testing is a mechanical property requirement in both EN 10338 (cold rolled multiphase steel) and EN 10346 (continuously hot dip coated steel) for DP steels, where the requirement for DP material is to achieve a 30MPa increase in BHI after BH testing.

4.4.3. Nano-Hardness

Hardness testing is a popular method of evaluating a material's mechanical characteristics. It allows a measurement of a materials resistance to deformation by applying a local penetrative force on the sample surface. The indents in standard hardness testing are typically in the mm range and provides bulk hardness properties. Nano hardness testing allows for indentations of around 50nm, allowing mechanical properties of discrete phases to be elucidated. This is ideal for DP microstructures that are typically very refined.

Preparation for nano-hardness involves cutting small strip steel samples to around 20mm and mounting them in bakelite. These samples are then ground with three different grit papers, before being polished to a 0.04-micron finish. This will be described in more detail in section 4.5.

The final 0.04-micron stage is achieved using a colloidal silica finish and polish for 7 minutes. The sample is then thoroughly cleaned using deionised water to remove any excess silica and washed using a soap solution before finally being cleansed with ethanol. This process allowed for a smooth and flat surface finish for the nano-hardness testing.

The Bruker Hysitron Ti950 was used for all nano-hardness testing. A Berkovich tip was used for the indenting and an accelerated mechanical property map (XPM) was created mapping a 10x10 array with a load of 1000uN and 3um spacing. This was chained into a 2x2 matrix and gave 400 indent measurements per sample.

Scanning probe microscopy (SPM) was used over each of the areas and the plots of the XPM measurements allowed for a generation of mechanical properties across the surface of the material. Examples of the nano-hardness outputs are shown in figure 4.8 and 4.9.

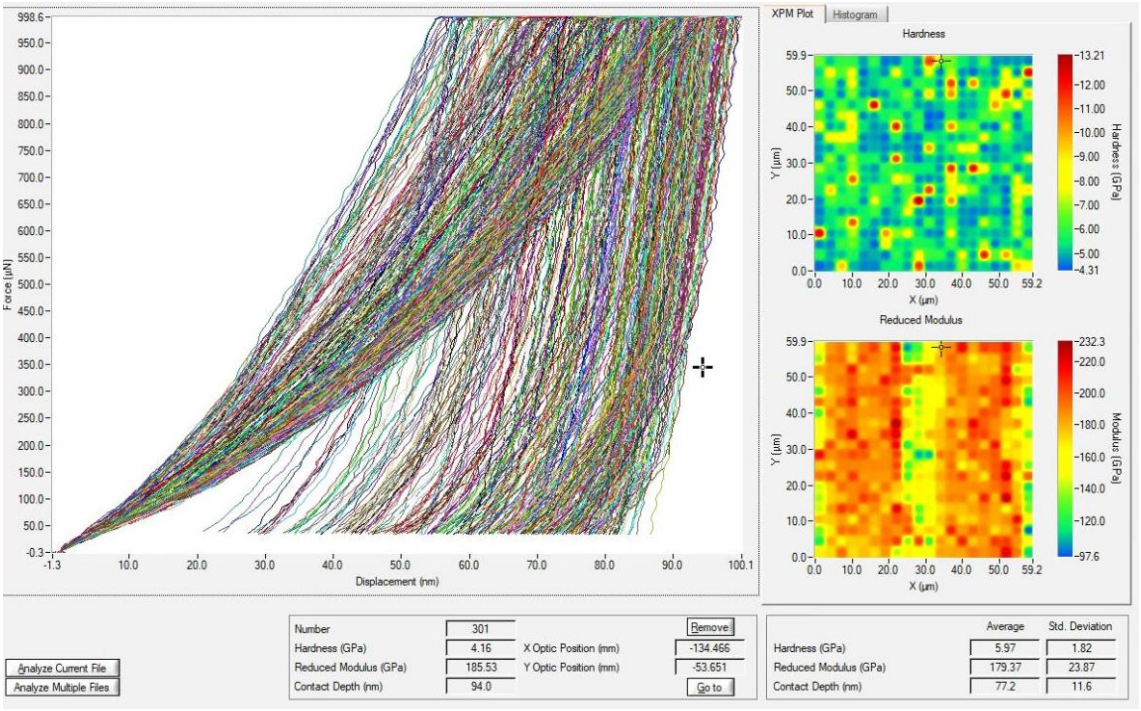

Figure 4.8. XPM showing individual hardness tests (left), the hardness plots (top right image) and the reduced modulus (bottom right image). The hardness plots show areas of high hardness (red) and low hardness (green), the image indicating a mixed microstructure

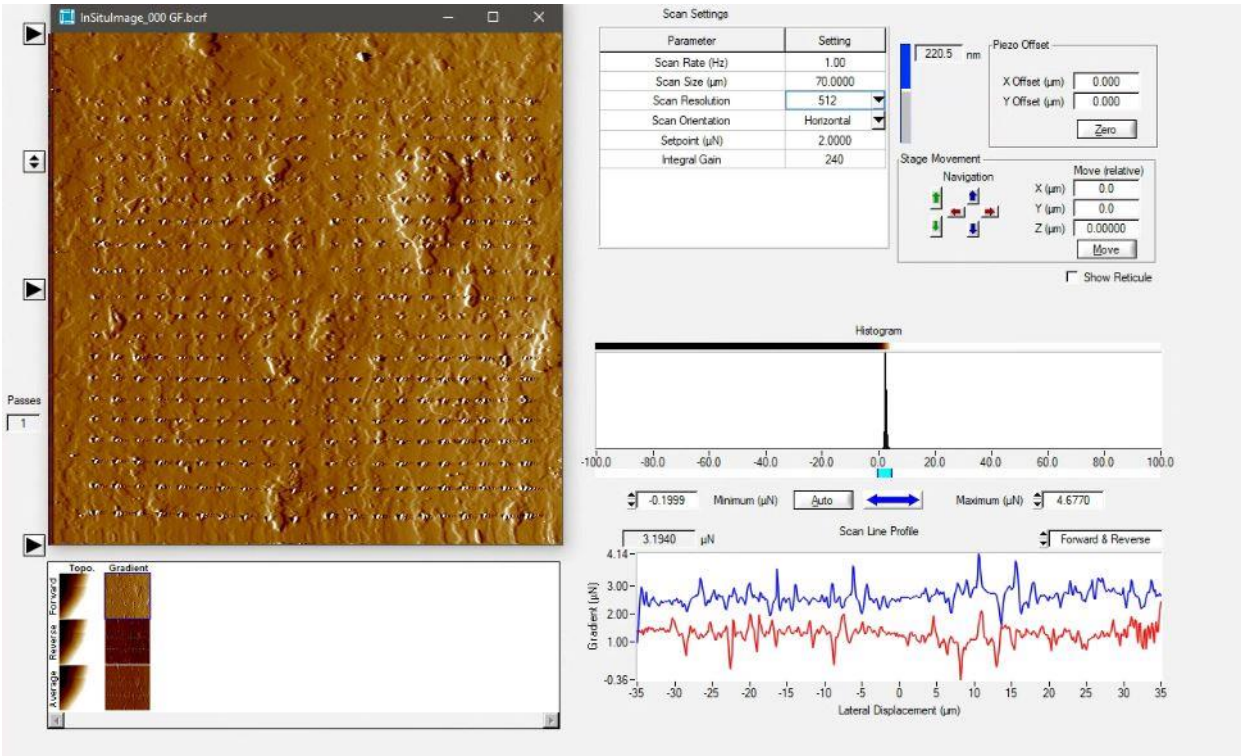

Figure 4.9. Example of the SPM output. The image shows the four 10x10 chain of indents to have 400 nano-indents.

4.5. Metallography and Microscopy

Changes to the microstructure of a material can have a profound effect on the final mechanical properties at the macro scale. Therefore, metallography plays a vital role in understanding a materials behaviour.

4.5.1. Metallography Preparation

Steel strips of approximately 20mm x 300mm are cut to 10mm x 20mm using a Brillant 220 cut off machine, these samples are then hot mounted in Bakelite or Formvar powder. The Struers Prontopress is then used to set the Bakelite or Formvar powder. The machine is shown in figure 4.10.

Figure 4.10. Struers Prontopress used for sample mounting. Sample placed in the top of machine, lowered, then a heating cycle is applied and a sample such as that in figure 4.11 is produced.

Once the cycle has completed, the sample can be removed. An example of a mounted metallography sample is shown in figure 4.11.

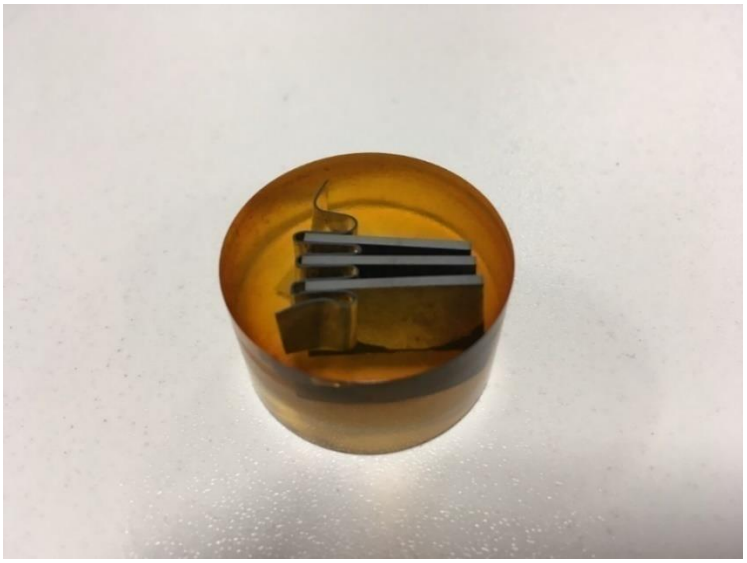

Figure 4.11. Mounted steel samples in Formvar. Grinding, polishing and etching stages are applied to the top of the sample to produce a flat and clean surface for microscopy

Three different grinding papers are applied to the sample first, each stage taking 5 minutes. A Struers LaboPol 20 is used for both the grinding and the polishing stage, with the grinding stages having water applied to the grinding paper. A coarse 120-grit paper is applied to the sample first, the sample is then washed with soapy water and rinsed with ethanol before being dried with a hand dryer.

The next stage is a 600-grit paper, which is then washed as in the previous step. The final grinding stage uses a finer 1200 grit paper. At each stage the sample is checked under a microscope to check for any heavy scratching or defects that have occurred from the previous stage.

Three different levels of polishing pads are used for the final polishing stage, each stage has its own diamond suspension solution which is applied to the pad to provide a high-quality surface finish. These stages take between 3-5 minutes. The first stage is using a 6-micron pad with a 6-micron diamond suspension, once polishing is complete the sample is washed in soapy water, rinsed with ethanol and dried with a hand drier.

The next stage applies a 3-micron pad, with 3-micron diamond suspension. Again, this is washed with soapy water, rinsed with ethanol and dried. The final stage used a 1-micron pad with 1 micron diamond suspension with the same cleaning procedure. As with the grinding, each polishing stage is checked under the microscope to ensure no defects occur in the surface.

Once polished, the sample is left with flat, smooth, mirror like appearance. The final stage to see the microstructure under the microscope is to etch the surface. Etching was done with 2% Nital, typically etching for 10-15 seconds to reveal the grain boundaries. The sample was then thoroughly washed with water and ethanol before drying with a nitrogen air drier.

4.5.2. Light Microscopy (LOM)

Light microscopes allow for a magnified image of smaller objects using visible light. This allows for quick microstructural evaluation and imaging to be taken. Two main light microscopes have been used for this work, Zeiss Axio Observer and the Keyence Vhx7000.

The Zeiss Observer Z1M microscope is an inverted microscope with a 1.3MP camera. It has a range of objective lenses that achieve magnification from 2.5x through to 100x, with manual control for sample focus. Due to the nature of DP steels refined microstructure, the majority of imaging is taken at maximum magnification of 100x, allowing for grain size and phase fraction analysis.

The samples are placed on the top of the microscope, and the monitor on the microscope controls the imaging mode and magnification. Once the sample image is focussed, an image can be taken using the Zeiss software on the computer, with the magnification bar applied.

The VHX7000 has a 3.19MP 4K camera with a fully integrated head that can automatically change from 20x to 6000x magnification. The sample is placed on the observation platform and the VHX automatically scans to achieve the correct image focus. Images can then be saved on the Keyence software with the magnification bar applied.

4.5.3. Scanning Electron Microscopy (SEM)

The SEM uses a focussed electron beam to scan a sample surface and produce an image. The electrons in the beam interact with the sample and produces various signals that can then be used to obtain information about the surface composition and topography (109).

This allows for much greater magnification of the sample surface, up to 1,000,000x, and can produce high quality images for microstructural analysis. For this body of work a Zeiss Evo LS25 SEM was used, imaging using the secondary electron detector (SE).

The Bakelite samples are placed on the SEM mount and then have copper conducting paper attached around the samples to ensure conductivity. The SEM chamber is then vented, once the chamber is depressurized the sample can be attached to the sample holder within the chamber and the chamber is pumped to achieve vacuum. Using the SE camera view at the lowest mag, the sample target can be found and the stage lifted aiming for a working distance of 10mm.

Small adjustments are likely to be made using the aperture, to allow the beam to reach the objective lens and the stigmator to correct beam astigmatism. Once an image is correctly focussed and the magnification achieved, a picture of the image can be taken and stored using the Zeiss software.

4.6. Data and Image Analysis

4.6.1. Dilatometry

The solid-state transformation of austenite to ferrite is a change from a face centre cubic (FCC) to a body centre cubic (BCC) lattice structure. This change in crystal structure leads to a volume change in the steel.

Dilatometry allows us to measure the change in dimensions as a function of temperature. A sample can be accurately heated and cooled in a controlled environment to allow for determination of critical phase changes that occur during an annealing cycle.

For the A_{c1} / A_{c3} intercritical temperatures, a Netzsch 402C pushrod dilatometer was used. A linear voltage differential transducer (LVDT) continuously measures the expansion and contraction of the specimen during the test, recording the temperature and length changes which allows for a temperature over length plot to be produced.

Samples of 5x20mm were cut from cold rolled unannealed material. This was then heated in an inert argon atmosphere at a rate of 35°C per minute to 1200°C and the measurements of the A_{c1} and A_{c3} point taken, an example of which is shown in figure 4.12.

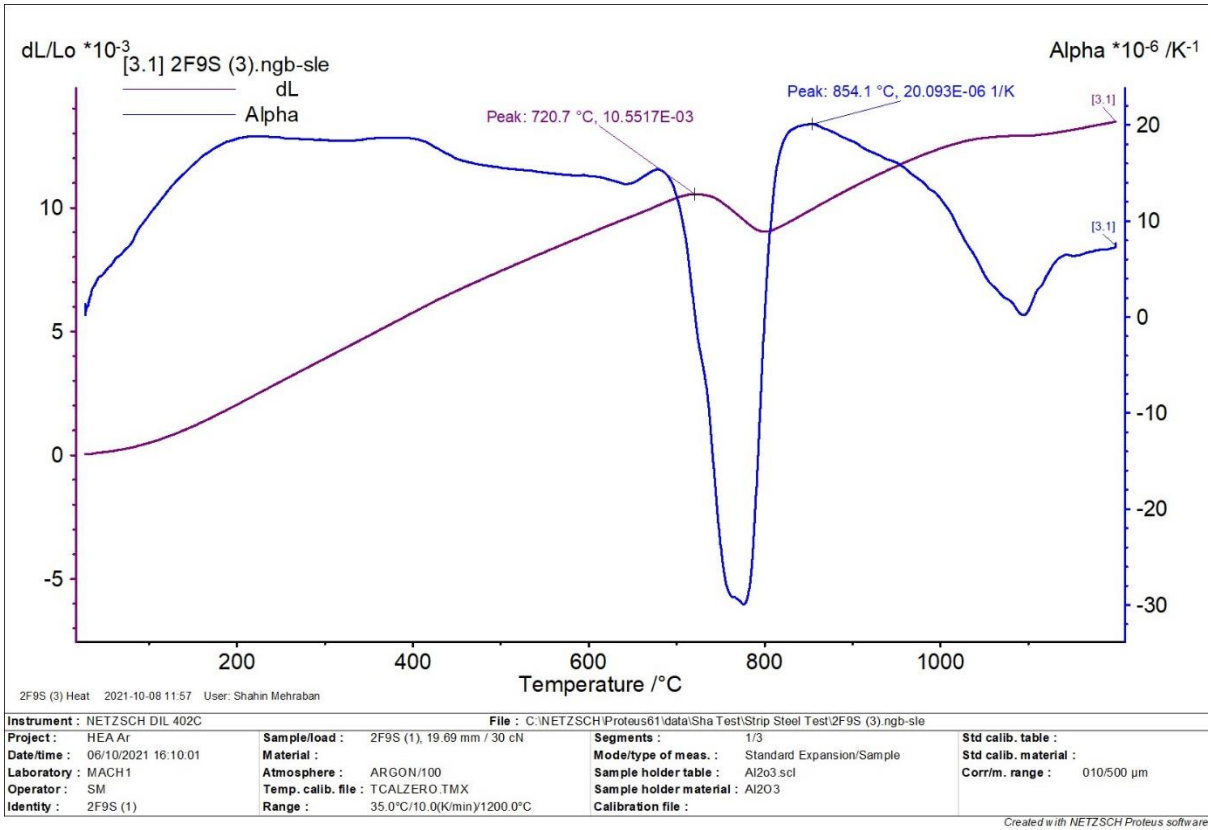

Figure 4.12 Example of the A_{c1}/ A_{c3} points taken by calculating the inflection point on the curve readings. Each test was done three times and the average values taken. Peak 720°C represents A_{c1} value, whilst peak 854°C represents A_{c3} value for this sample.

To achieve continuous cooling transformation (CCT) diagrams, a Bahr 805 A/D quenching dilatometer was used. Flat samples of 5x10mm were EDM cut from the cold rolled unannealed sheets of the VIM cast material.

Similarly to the annealing simulators, the quench dilatometer allows for a precise program of heating and cooling to be applied under vacuum, allowing the prevention of oxidation. The samples are heated using an induction heating coil and helium gas used to achieve rapid cooling to mimic a continuous annealing line.

Similar to the Netzsch, a linear voltage differential transducer (LVDT) continuously measures the expansion and contraction of the specimen during the test and records length and temperature changes which allows for a temperature over length plot to be produced. Put together on a graph the various cooling times allow for a CCT curve to be built, an example of which is shown in figure 4.13.

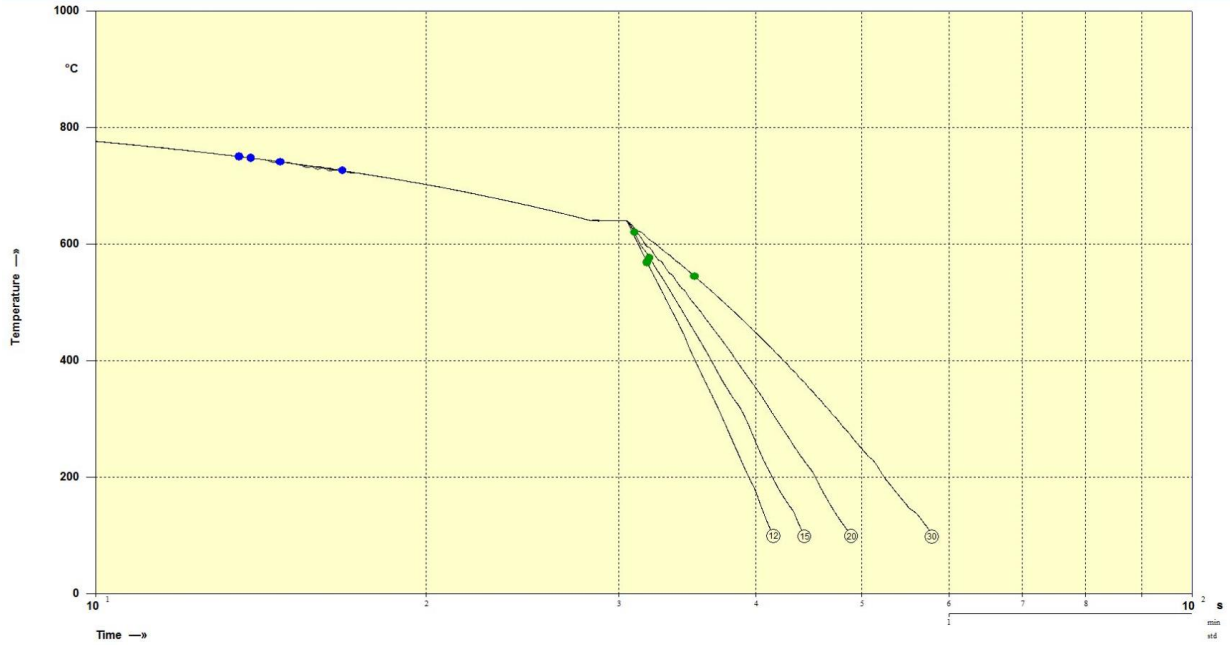

Figure 4.13. Example of CCT curve produced, with temperature on Y axis and time on the X axis. Example shows temperature dropping to reflect slow cooling of annealing cycle, followed by rapid cooling at different speeds to 100°C

These CCT curves can then be combined with metallographic analysis to determine the phase fractions being produced within each sample, and to measure the temperature at which each phase occurs.

4.6.2. JMatPro

JMatPro is a simulation software that allows for the calculation of a wide range of material properties, and in particular for multi-component alloys that are used in industrial practise (110). The software allows for a particular chemical composition to be entered and for various thermophysical and physical properties to be obtained.

This software has been used in this thesis to give an indication of expected temperatures at which transformations take place, including time temperature transformation (TTT) and continuous cooling transformation (CCT) diagrams. Further to this the phase start temperatures can be assumed, for example martensite, bainite and ferrite start temperature.

This information, combined with dilatometry, provides a solid foundation for the range of temperatures that were used during experimentation to achieve expected mechanical properties.

4.6.3. Phase Fraction Analysis

Using phase fraction analysis allows for an evaluation of the amount of each phase of material is present in the microstructure, allowing for an indication of mechanical property behaviour. For this thesis, phase fraction analysis was achieved using ImageJ software.

Within ImageJ there an analysis tool called WEKA trainable segmentation. This plugin is a machine learning tool that uses a limited number of manual annotations on an image in order to train a classifier and segment the clusters to identify certain required image features (111).

The images used for analysis were from optical microscopy, where etching has allowed for differentiation between the primary white phase of ferrite, and the darker brown phase of martensite.

The image is uploaded into WEKA segmentation with the magnification bar removed. The image can then have classes assigned to each phase that requires measurement. By default only two classes can be picked, however additional can be added if further phases are present in the material.

An SEM image example is shown in figure 4.14, with a selection for class 1 (ferrite) and class two (martensite). Marking each phase allows for the classifier to predict which phase belongs in which class to a good degree of accuracy.

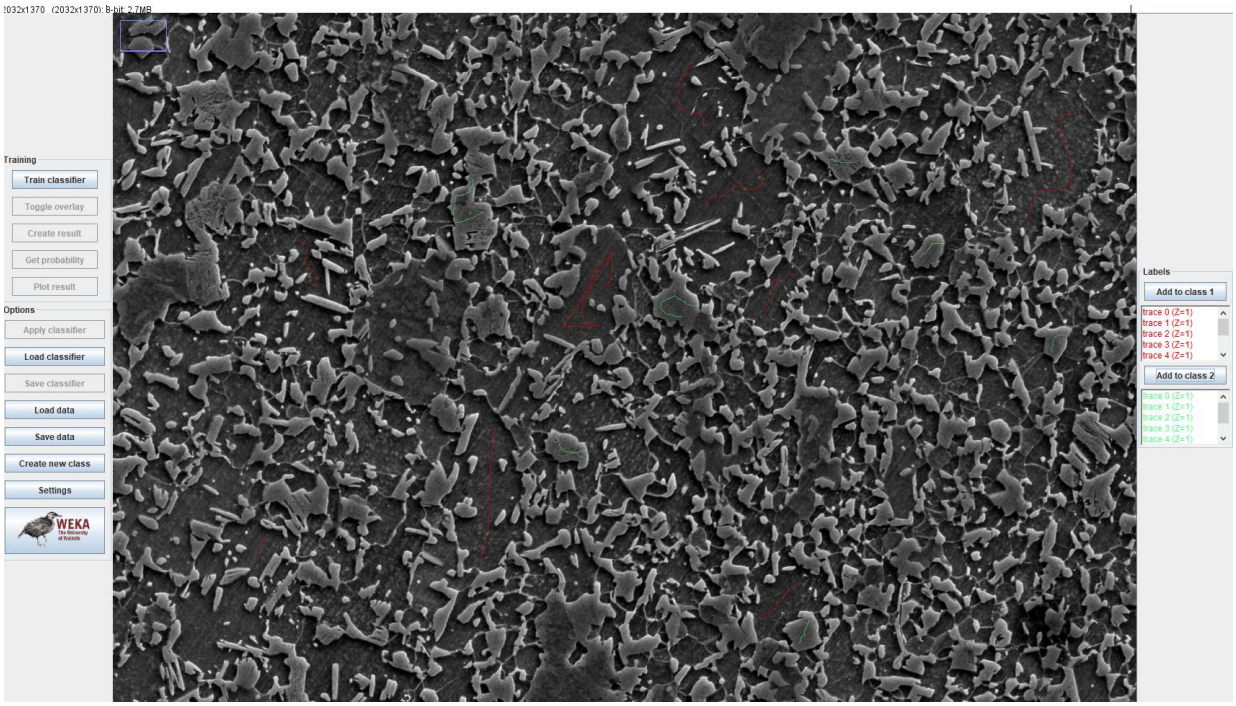

Figure 4.14 SEM image on WEKA Segmentation classifier. Red lines highlight ferrite phase, whilst green lines highlight martensite. The classifier then produces an image based on the input classification, seen in figure 4.15.

Once the image has been classed, pressing the train classifier allows for image analysis, the results of which are shown in figure 4.15.

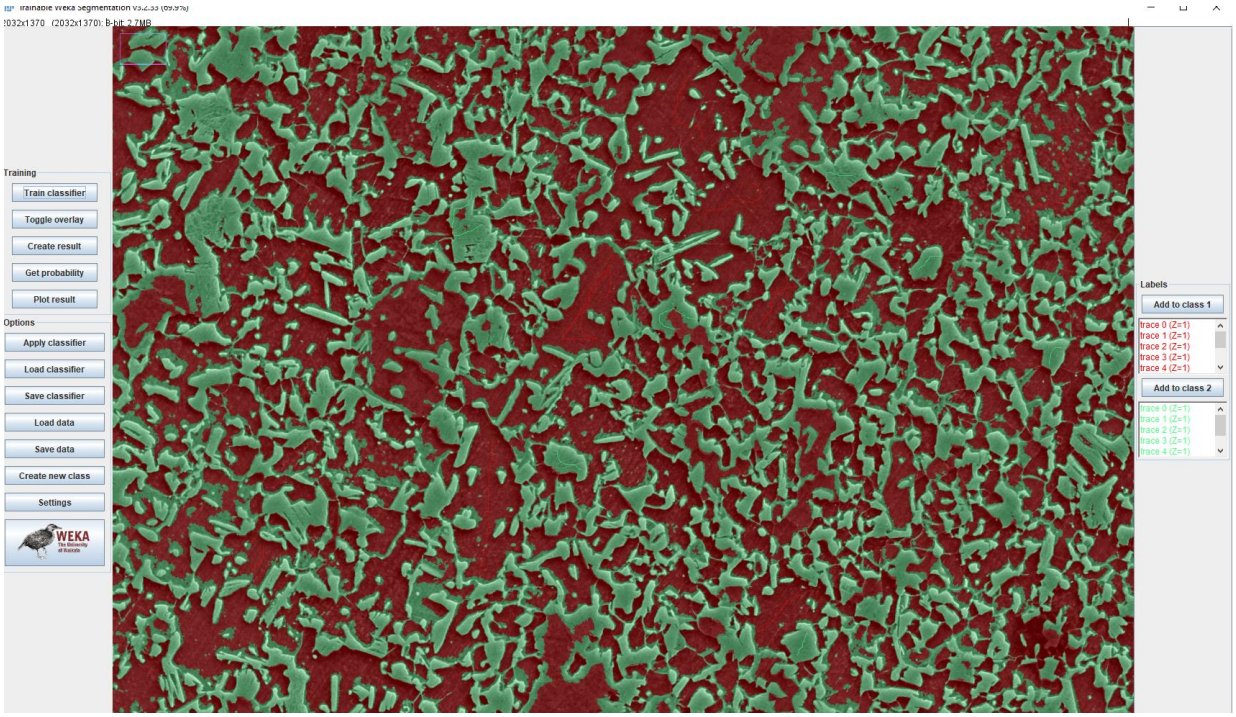

Figure 4.15. A 'trained' image showing red region as ferrite with green region as martensite

Selecting create result allows produces a two-colour image, if two classifications were used. From here the image can be transformed in ImageJ to an 8-bit image, and under the analyse section the analyse particles option allows for a calculated phase percentage.

Additional trace lines may be added to increase the accuracy of each phase classification until satisfactory coverage of each phase is achieved. For each sample, three images were typically used, with an average phase fraction taken to give accurate representation across a sample width.

4.6.4. Grain Size Analysis

For grain size analysis the mean linear intercept method, or Heyn intercept method, was adopted. The analysis was carried out in ImageJ using optical microscope images at 100x magnification. A line of known length was placed along the image, and the number of grain boundaries intersected measured. Determining the grain size is achieved by the following calculation from the ISO standard ISO 643 (112):

$$P_L = P \,/\, L_T$$

Where P is the mean value of number of intersections and L_T is the true length of the test line.

Each sample had three images taken. Each of these images had three lines drawn across them at random points to give an average over nine different points per sample to give a true representation of the grain size across the width of each sample.

4.7. Processing conditions – Line speed

Throughout this work, referencing will be made to line speed. This is the speed at which the steel passes through the CAPL / Zodiac line. The speed in which material passes through the line, in particular the furnace section, can have a big impact on the final mechanical properties of the steel. Whilst the aim of both units is to anneal cold rolled material to achieve final properties, the addition of a zinc pot on Zodiac means the way in which they achieve that through the furnace differs.

The table 4.2 shows the list of line speeds that will be investigated throughout the following chapters, along with the timing it takes for the material to pass through the CAPL and Zodiac lines if it were running at this processing speed.

Typically, the thicker the material, the slower the line speed. This is due to the material requiring more time to heat uniformly and to 'soak' at these temperatures, to achieve the required microstructure.

Table 4.2. Line Speed vs. time for CAPL and Zodiac. Calculations show that time in the CAPL furnace is 3.5 times as long as if it was passing through Zodiac.

Speed (mpm)	**CAPL Annealing Cycle (min.secs)**	**Zodiac Annealing Cycle (min.secs)**
50	35.12	10.00
90	19.33	5.55
100	17.36	5.00
120	14.40	4.16
150	11.44	3.33

As can be seen from the table, the time at which the material is in the furnace is significantly different between CAPL and Zodiac, this is primarily down to the differences in furnaces. As CAPL utilises radiant tubes in the furnace only, the strip is not in direct contact with the heat source and therefore takes longer to heat up to temperature.

Conversely, Zodiac's direct fired furnace section heats the strip from ambient temperature to around 700°C in one pass, before utilising the radiant tube section for the soak section. Typically, CAPL operate at a much higher line speed for DP products when compared to Zodiac, average speeds for Zodiac for a 1mm DP product would be around 100mpm, whilst CAPL would process around 120mpm.

5. Effect of annealing process parameters on dual phase steel

This chapter focusses on the effect of industrial continuous annealing, and the effect that the annealing process has on the final mechanical properties and microstructure of a DP steel. Sections of this chapter have also formed part of a published journal article (113).

An increasing body of research has looked at improvements of DP steels over the last few years, particularly around intercritical annealing. Movahed et al. (114) investigated the effect of intercritical annealing on the tensile properties and work hardening behaviour of DP steel, suggesting equal amounts of ferrite and martensite exhibit optimum mechanical properties. Further developments were made by producing intercritically annealing a cold rolled DP chemistry with a starting martensitic microstructure, the work done has shown to improve the strength-ductility balance through the refined final microstructure (115)(116)(117).

Other bodies have work have focused on the effect that the holding time has on the microstructure and the mechanical properties of DP steels during the intercritical annealing stage, some suggest that the effect of increased holding times does not greatly affect the microstructure (118)(119), whilst others showed an improvement in tensile strength compared to other commercially available DP steels (120).

Increasing the intercritical temperature increases austenite formation, which can lead to an increase in the final martensite start temperature (86)(53). This start temperature is important for austenite transformation, and whether it transforms to martensite or bainite on rapid cooling (121). Additional challenges exist for DP production, particularly on an industrial annealing line which would incorporate an overage section which aids production of different steel grades. Therefore, it's important to understand the effect that each region of an industrial annealing cycle can have on the final microstructure and mechanical properties.

This chapter focuses on the influence of intercritical temperature, also known as soak temperature, and the rapid cooling section, and the effect this has on the final mechanical properties of a DP steel processed using a similar annealing cycle that would be used on an industrial continuous annealing line.

5.1. Continuous annealing cycle and achieving a DP steel

A 50kg cast of a DP steel chemistry, shown in table 5.1, was made using a vacuum induction melting furnace (VIM). This material was then rolled to transfer bar thickness of 340mm.

Table 5.1. VIM Cast chemistry of DP steel. Values shown in weight %

Alloy	C	Mn	Si	Ti	Cr	Nb
DP	0.13-0.15	1.80-1.90	0.25-0.26	0.03-0.04	0.50-0.60	0.020-0.030

The bars were then cut to 70mm x 70mm blocks using a band saw before being reheated to 1250^{o}C for two hours and hot rolled to a target thickness of 3.5mm. The hot rolling process was controlled to achieve a ferrite / pearlite microstructure. The material was subsequently pickled in HCl to remove mill scale before being cold rolled to achieve a 55% reduction.

The annealing process was simulated on a continuous annealing simulator (CASIM), which has been described in chapter 4.3.2. The annealing cycles used for this investigation are shown schematically in figure 5.1 and 5.2, and replicates what is seen on a modern continuous annealing line.

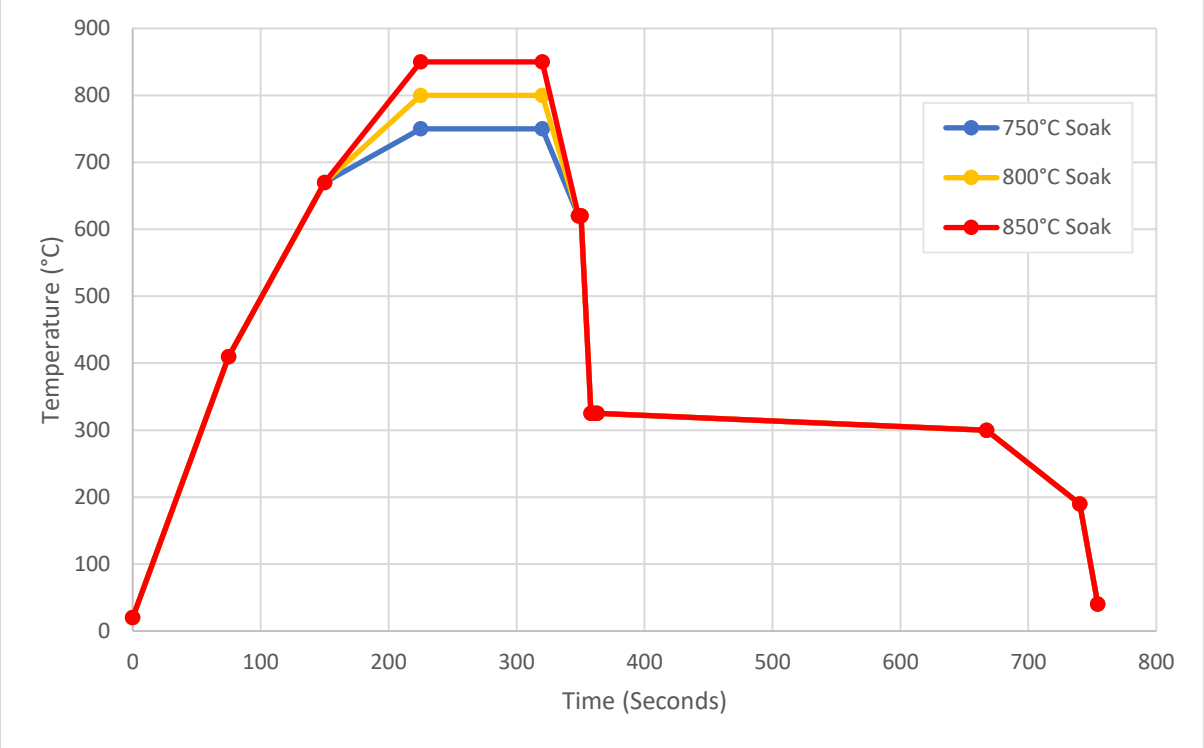

Figure 5.1. Continuous Annealing cycle showing variations in intercritical temperature, also known as soak temperature.

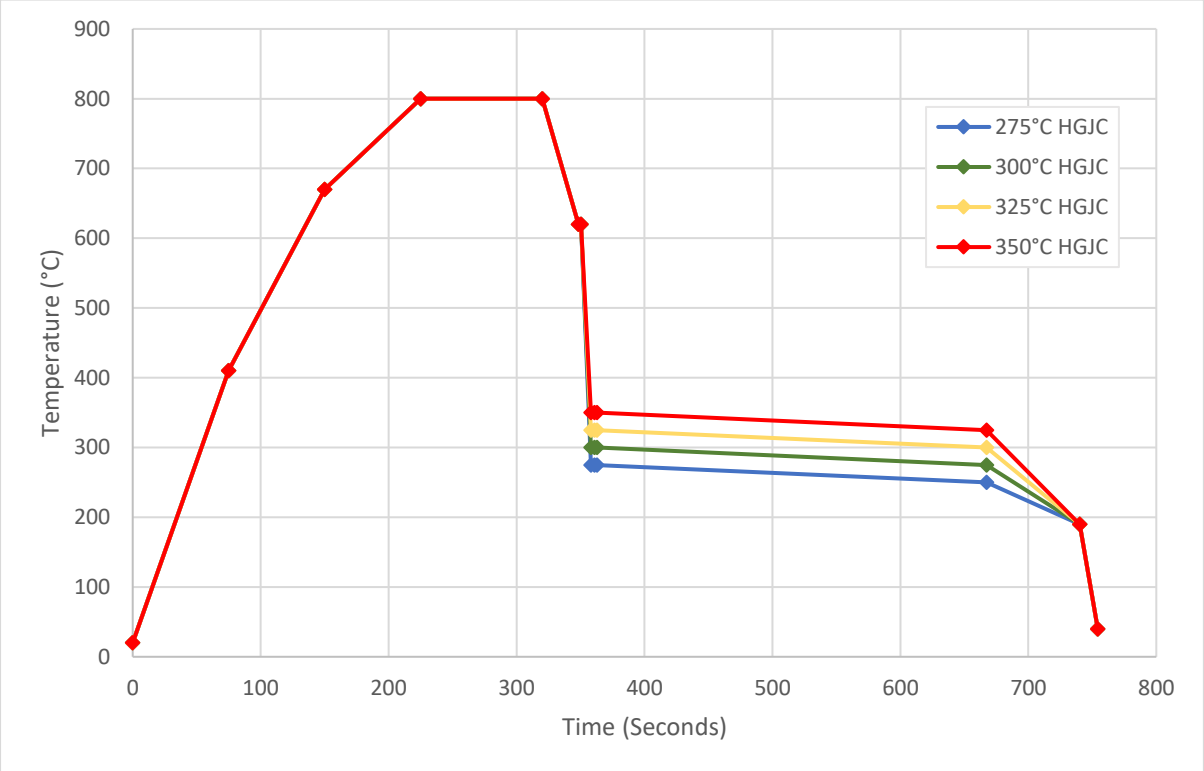

Figure 5.2. Continuous annealing cycle showing variations of HGJC.

Once annealed, the material was cut to tensile sample sizes with a gauge length of 50mm, gauge width of 12.5mm and total length of 180mm, and tensile tested on a Zwick 1474 tensile testing machine. Testing was performed in accordance with ISO 6982. For bake hardening, the samples were subjected to a 2% pre-strain then baked at 170°C for 20 minutes in accordance with standard EN10325. The samples were then tensile tested in accordance with the ISO 6892 standard to measure the BH effect.

Metallographic analysis was achieved as described in chapter 4.5.1, and samples were then imaged under a Zeiss Observer light microscope and a Zeiss Evo LS25 scanning electron microscope (SEM). Volume fractions of constituent phases and grain size analysis was obtained using ImageJ imaging software.

One of the areas of influence on the final microstructure of dual phase steels comes from the variations in the intercritical, or soak temperature. The intercritical temperature range is held between A_{c1} and A_{c3}, it is within this region that new ferrite (α) and austenite (γ) nucleate. In DP steels, the typical industrial cooling section rapidly reduces the temperature that the austenite transforms to martensite (α'), producing the dual phase structure.

A number of variables can affect the microstructure and the final mechanical properties of the material. The stability of austenite is key to whether martensite, tempered martensite or bainite is produced in the final microstructure. Carbon content within the austenite can change depending on the volume fraction of austenite in the microstructure. Typically, the higher the volume fraction of austenite, the less carbon is present within the austenite, so during cooling it becomes less stable with an increased chance of transformation to bainite rather than martensite during the overage section. Therefore microalloying additions are added to stabilise the microstructure so the desired phase of martensite, rather than bainite, forms (88).

As well as the carbon content of austenite, the soak region also influences the final grain size of the ferrite and martensite. At lower soak temperatures, recrystallisation takes place at a slow rate, so therefore it can be expected that the grain sizes present in the final microstructure would be refined compared to heating to higher soak temperatures, particularly the martensite (122).

The temperatures at which the A_{c1} and A_{c3} exist can also shift, dependant on the chemistry and the rate of heating. To get an indication of what these values would be for this chemistry, an empirical calculation can be made using the Andrews' formula (24).

$A_{c3} = 910 - 203\sqrt{C} – 15.2Ni + 44.7Si + 104V + 31.5Mo + 13.1W$ (Eq 1.1)

$A_{c1} = 723 – 10.7Mn – 16.9Ni + 29.1Si + 16.9Cr + 290As + 6.38W$ (Eq 1.2)

From these calculations it can be determined that the A_{c1} and A_{c3} temperatures are 720°C and 847°C respectively. Therefore, subjecting the steel to temperatures at the low, middle, and high end of this range will determine which soak temperature produces the best final mechanical properties if processed using a typical industrial annealing cycle, when all other parameters are kept constant.

To predict the final phases from these soak temperatures, a material simulation software called JMatPro was utilised. Inputting the chemistry and the temperatures of the soak, the software simulates the expected phases that occur during cooling and are plotted in a continuous cooling transformation (CCT) diagram.

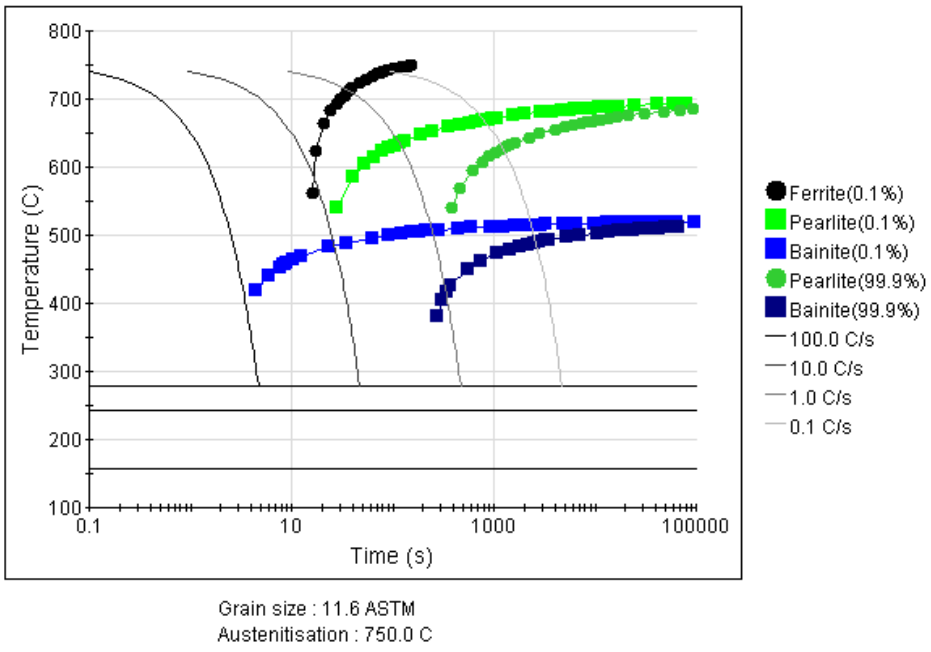

Figure 5.3 Predicted CCT diagram of cooling from 750°C soak temperature

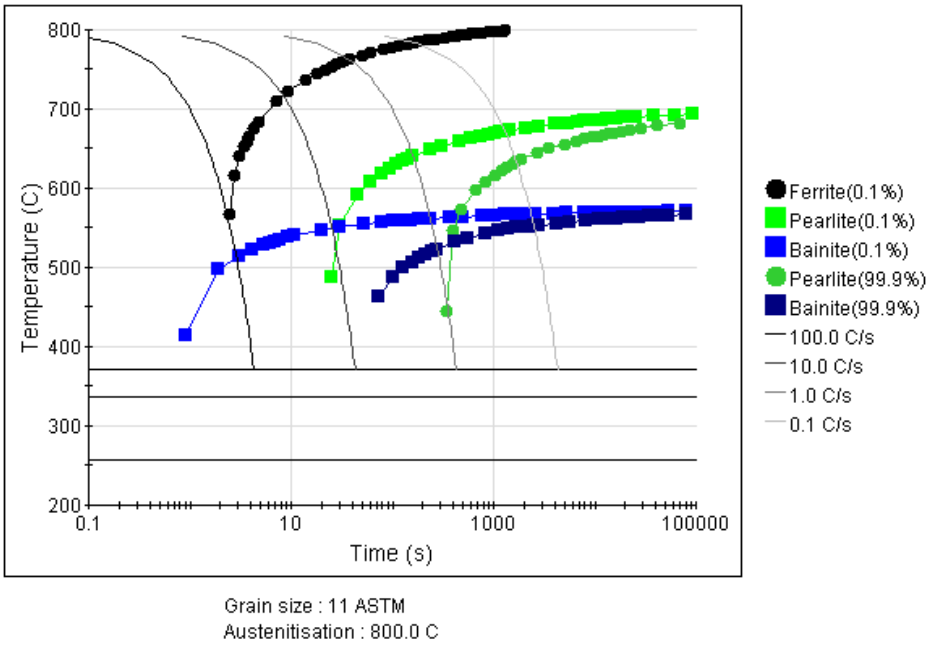

Figure 5.4 Predicted CCT diagram of cooling from 800°C soak temperature

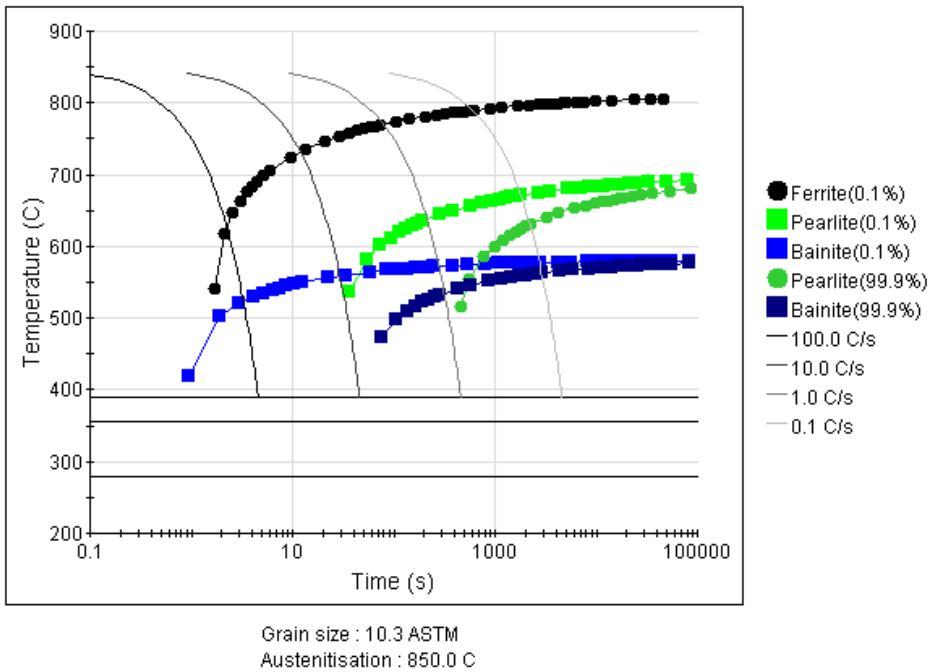

Figure 5.5 Predicted CCT diagram of cooling from 850°C soak temperature

From these CCT diagrams it is also possible to estimate the bainite and martensite start temperature. These temperatures are critical to the final mechanical properties, and the rate of cooling that needs to be achieved to determine the final phase composition.

Table 5.2 Effect of soak temperature on martensite and bainite start temperatures. Martensite and bainite start temperature are higher as soak temperature is increased.

Soak Temperature (°C)	Martensite Start (M_s) (°C)	Bainite Start (B_s) (°C)
750	279	521
800	371	572
850	389	582

Both M_s and B_s increase as the soak temperature is increased. This would indicate that an increased cooling rate would be required at a higher soak temperature to avoid bainite or to form tempered martensite when the material reaches the overage temperature. Subtle changes in the secondary hard phase of a DP steel can lead to a substantial change in the final mechanical properties. Therefore not only is the intercritical temperature a key variable, so too is the rapid cooling and overage section on a continuous annealing line.

To keep as much continuity as possible between the samples, and to replicate production on a continuous annealing line, each of the samples have been hot rolled to produce a ferrite and pearlite microstructure. The hot rolled microstructure is shown in figure 5.6.

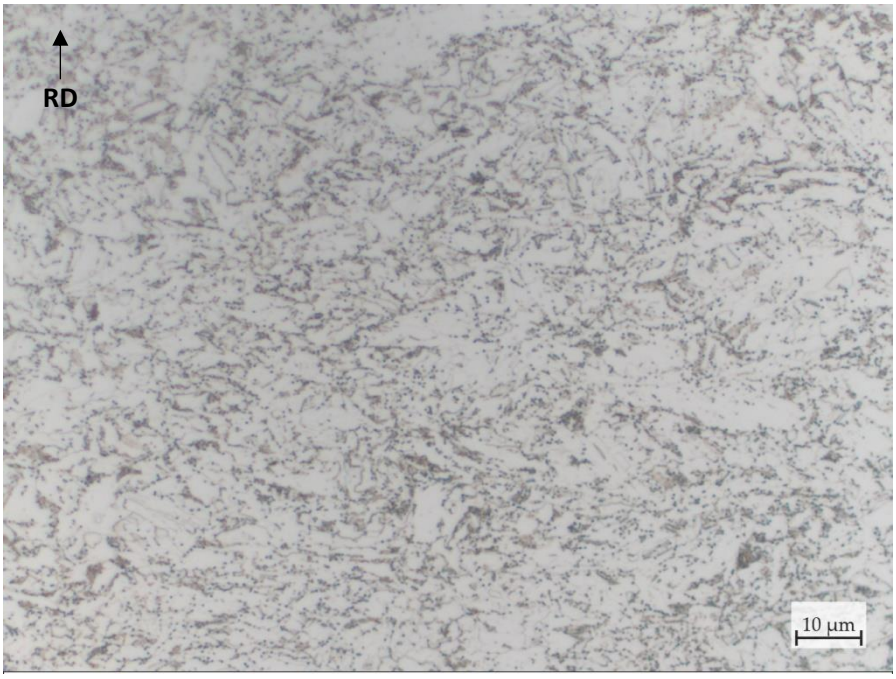

Figure 5.6. Light microscope image of hot rolled microstructure. White background is ferrite with the dark pearlite phase present.

The hot rolled samples have then been cold reduced by 55% to achieve the final material thickness of 1.3mm which is a typical reduction seen on Tata's continuous annealing line. Due to the nature of the cold rolling process, the microstructure becomes elongated in the direction of rolling, and therefore requires heat treatment to allow for grain recrystallisation to achieve the final dual phase structure. The temperatures used for the annealing cycle are shown in table 5.3:

Table 5.3. Annealing processing parameters used for this chapter

Soak (°C)	Conventional Jet Cooling (CGJC) (°C)	Hydrogen Jet Cooling (HGJC) (°C)	Overage (°C)	Strip Speed (mpm)
750	640	325	325-300	140
800	640	325	325-300	140
850	640	325	325-300	140

Soak (°C)	Conventional Jet Cooling (CGJC) (°C)	Hydrogen Jet Cooling (HGJC) (°C)	Overage (°C)	Strip Speed (mpm)
800	640	275	275-250	140
800	640	300	300-275	140
800	640	325	325-300	140
800	640	350	350-325	140

5.2. Effect of Soak temperatures on Mechanical Properties

This section will focus on the soak section of a continuous annealing cycle. The only variable being investigated is the change in temperature of the soak region, with temperatures of 750°C, 800°C and 850°C being investigated.

5.2.1. Metallography

As a DP steel is heating to its soak temperature, the proportion of ferrite to austenite will change. At the lower soak temperature it would be expected that a lower proportion of austenite (martensite on cooling) would be present, whilst as the soak temperature increases so will the proportion of martensite in the final microstructure (53). The light microscope images in Figure 5.7 show the effect of changing soak temperature on the microstructure.

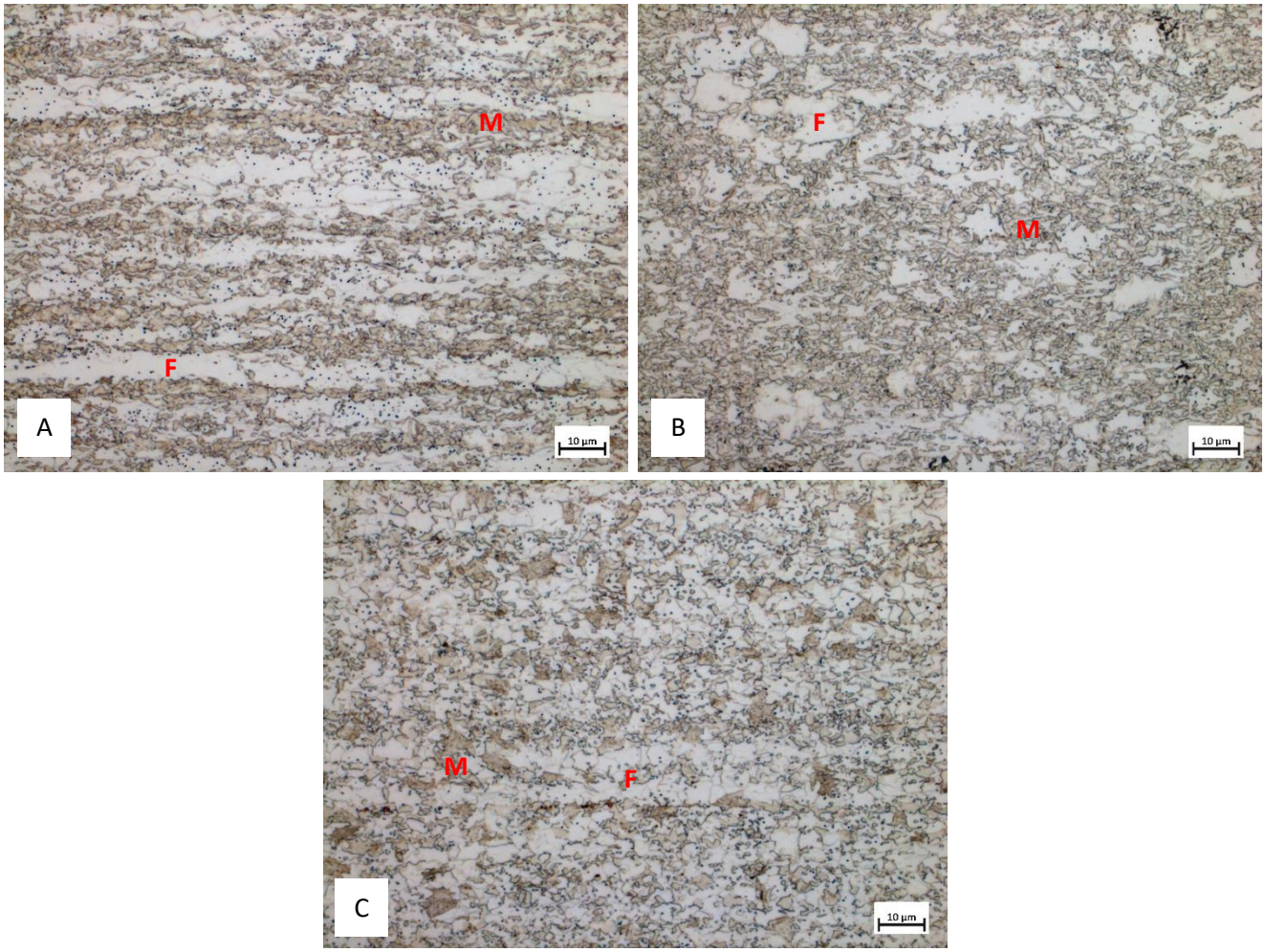

Figure 5.7 Optical images of 750°C (A), 800°C (B) and 850°C (C) soak temperatures and the effect on the microstructure. The white background represents ferrite (F) with the brown areas being martensite (M). Increasing volume fraction of martensite being produced as temperatures increase.

The 750°C soak temperature shows a heavily banded microstructure, with large veins of martensite and ferrite running parallel with the cold rolling direction. The martensite present in the microstructure is also less equiaxed due to the low temperature and short soak time limiting austenite grain growth. The martensite present in the microstructure is very refined, again likely due to the low temperature not providing sufficient energy for austenite grain growth.

Increasing the soak temperature from 750°C to 800°C increased the volume fraction of martensite in the final microstructure from 52% to 55% respectively. There is also less directionality in the microstructure, though some does still exist. Large grains of ferrite are clearly present, so grain growth has occurred as well as new ferrite formation. The increased volume fraction of martensite has also been accompanied with an increased martensite grain size, which has increased from 1.8µm

to 2.7µm. This increase in martensite grain size has also been accompanied with a reduction in ferrite grain size, which has decreased from 4.2µm to 3.1µm.

At 850°C soak temperature there is less banding present and the grains are more equiaxed. The ferrite and martensite phases have become more uniformly distributed and the grain size of the martensite is much larger compared to the lower soak temperatures. The larger ferrite grains present in the lower soak temperatures are also not present, therefore it is likely that the austenite growth is competing with the ferrite, this leads to the average ferrite grain size decreasing from 3.1µm to 2.6µm. The volume fraction of martensite and grain size of martensite is highest at 850°C soak temperature at 65% and 3.3µm respectively.

Figure 5.8 shows the scanning electron microscope (SEM) micrographs of the three different heat treatments.

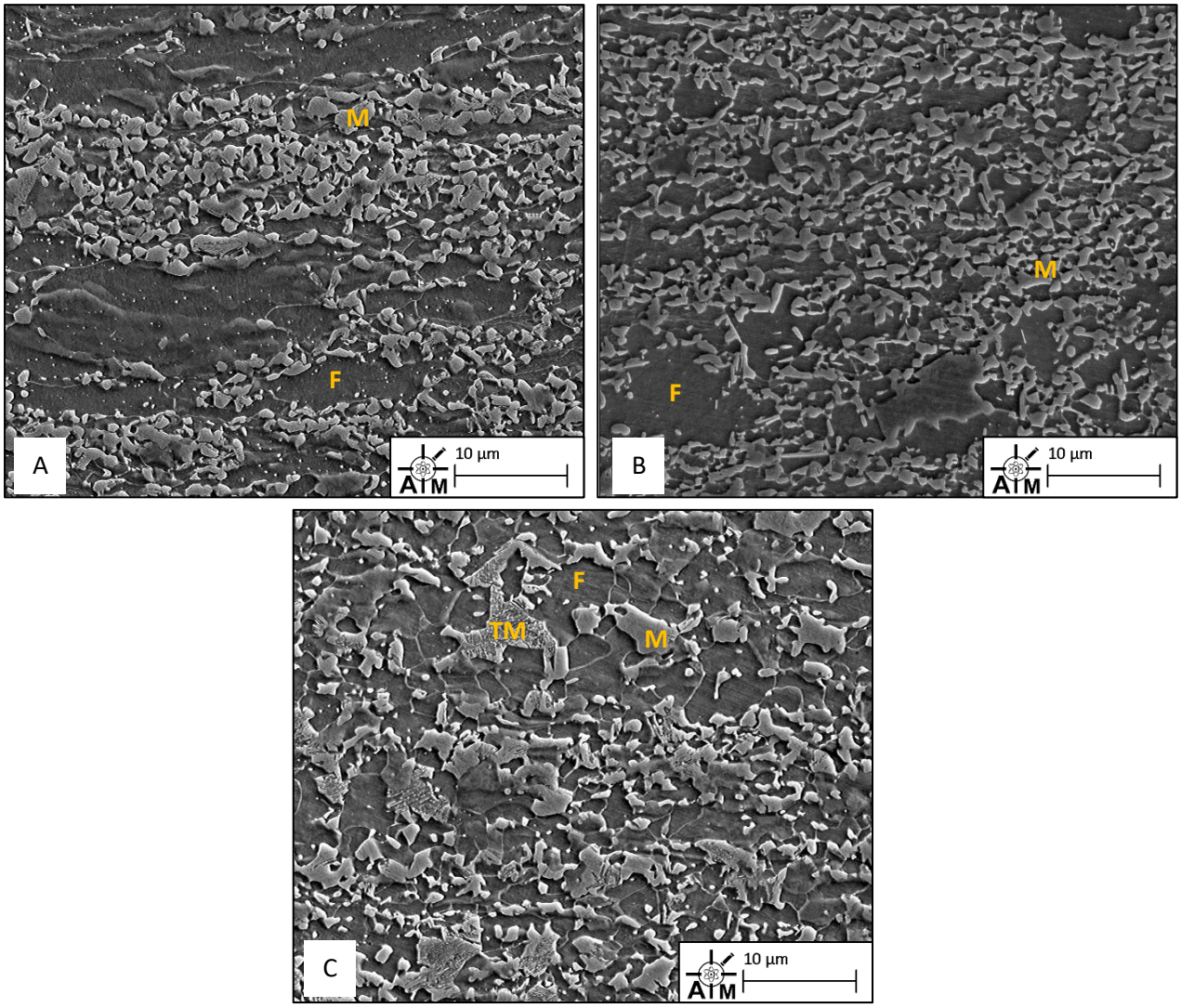

Figure 5.8. Scanning electron microscope images (SEM) of 750°C (A), 800°C (B) and 850°C (C) soak temperatures. Ferrite (F) is shown as the dark background whilst martensite (M) is the lighter phase. Also note the presence of tempered martensite (TM) at higher soak temperature.

From these SEM images shown in figure 5.8 the banding of martensite and ferrite seen in the light microscope images are present at lower magnification. At the higher temperature, the final martensite grains become larger and more equiaxed.

At 850°C the presence of tempered martensite can be seen in the structure. Tempered martensite in the microstructure would likely increase the ductility of the final mechanical properties whilst lowering the tensile strength (8). The grain sizes and phase fraction analysis are shown in table 5.4.

Table 5.4 Phase fraction analysis and grain size analysis on each of the soak cycles. Increasing volume fraction of martensite seen at higher soak temperature, whilst martensite grain size also increases

Soak Temp (°C)	Martensite Phase Volume Fraction (%)	Phase Fraction Error (%)	Ferrite Grain Size Average (µm)	Martensite Grain Size Average (µm)	Grain Size Error (%)
750	52	1.1	4.2	1.8	+/- 5%
800	55	1.6	3.1	2.7	
850	65	2.3	2.6	3.3	

5.2.2. Mechanical Properties

Changes seen in the microstructure under the microscope influences material behaviour during mechanical testing. The values for the following results are shown as averages, with the error bars dictating the minimum and maximum values achieved from the tensile tests.

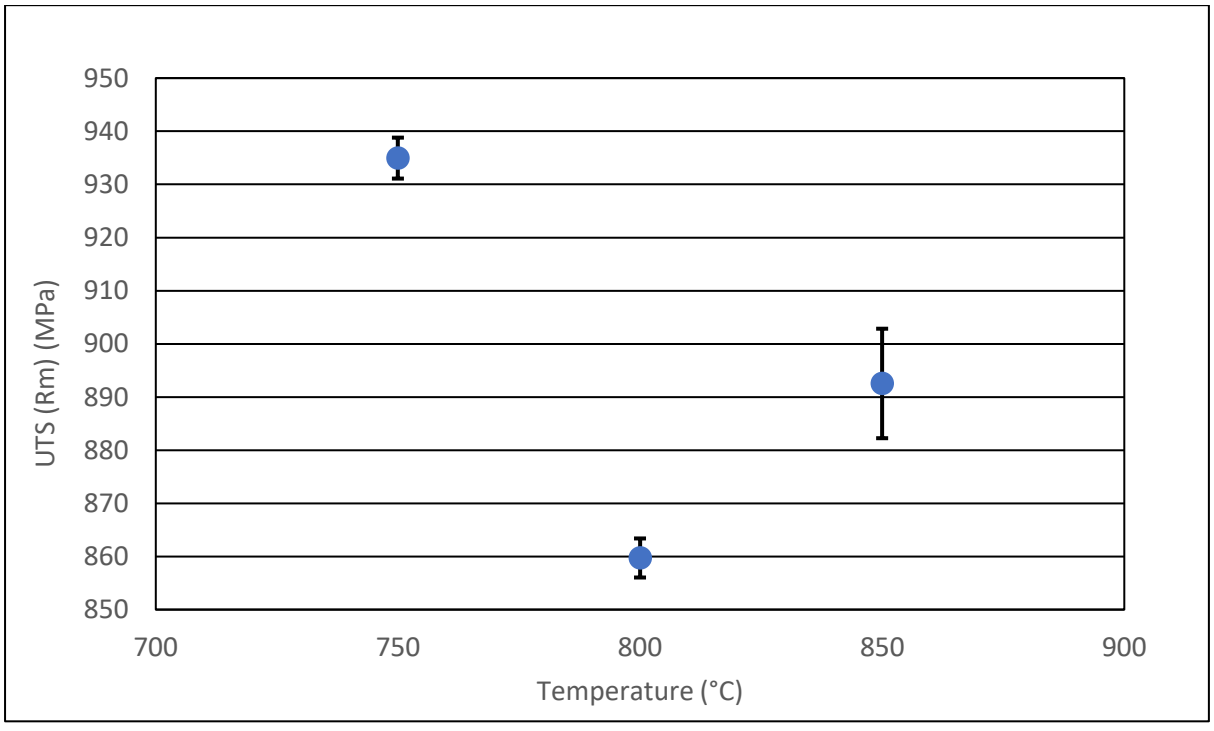

Figure 5.9 Effect of soak temperature on the ultimate tensile strength (UTS).

The tensile test results for UTS in figure 5.9 show highest strength was measured on the sample exposed to the 750°C soak temperature, achieving an average of 935MPa. The second highest strength values were found at 850°C soak temperatures at 893MPa, whilst the medium value of 800°C soak had the lowest strength on average at 860MPa. The highest soak also provided the most variability in results, though all UTS results were shown to be within 20MPa of each other.

On an industry manufactured steel, the material needs to be made to a recognised standard before it is released to a customer. The Euronorm standard which governs the mechanical properties is EN10338 (106), and whilst customers may have their own processing standard to which their requirements are set, the majority are based on these international standard. In terms of tensile strength, each of these soak variants exceed the minimum requirement of 780MPa.

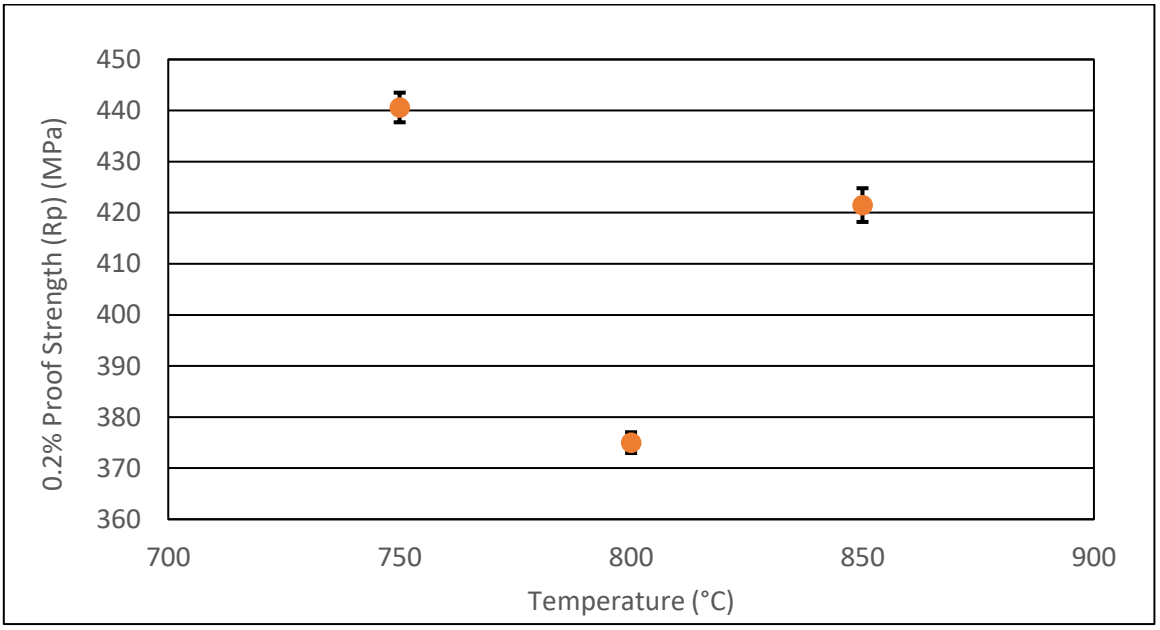

Figure 5.10 Effect of soak temperature on 0.2% proof strength.

The results from the proof strength in figure 5.10 follow the same trend as the UTS results. The highest proof strengths were seen on the 750°C soak, at 441MPa, and 850°C soak, at 422MPa soak temperature. The lowest values were seen at 800°C soak temperature with results of 375MPa.

The minimum requirement for proof strength for DP800 according to the EN10338 standard is between 440-550MPa. Whilst its clear from figure 5.10 that only the low soak temperature cycle

would achieve this, during industrial processing a temper rolling pass would apply within the region of 50-100MPa of additional strength (123), which has not been applied to these samples.

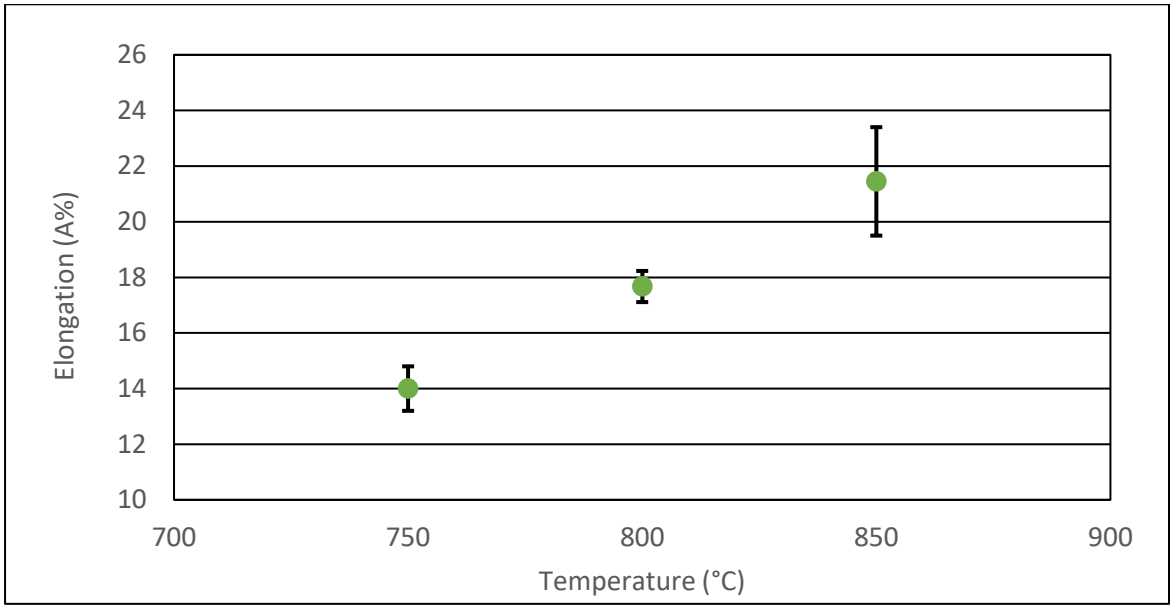

Figure 5.11 Effect of soak temperature on total elongation properties.

Figure 5.11 shows that total elongation values increase with soak temperature. The 750°C soak temperature achieved 14%, which is minimum requirement for the specification. At 800°C the value increased to an average of nearly 18%. The 850°C soak temperature achieved an average of 21% but showed the highest scatter.

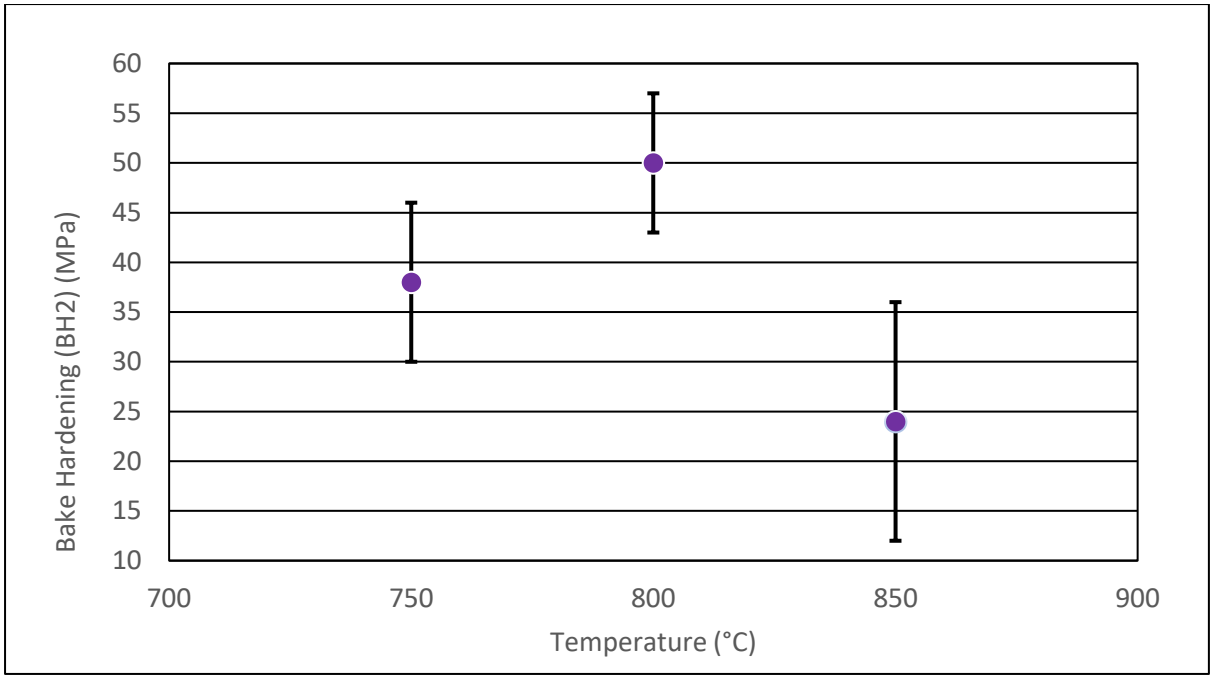

Figure 5.12 Effect of soak temperature on bake hardening properties.

Bake hardening (BH) occurs when an automotive panel is heated to around 150-200°C to cure the paint layer. At this temperature free dislocations become pinned by carbon in Cottrell atmospheres, resulting in an increase in yield strength and is defined as the bake hardening response (68). This increase in yield strength is also accompanied by a return of a yield point, compared to the continuous yielding that is typically seen in DP steels.

BH occurs with ageing of ferrite and the tempering of martensite in the following stages: the formation of Cottrell atmospheres, carbon clustering and growth and tempering of martensite (70).

Similarly, to strength and ductility, there is a requirement in the EN standard for a minimum of 30MPa increase after bake hardening. The values in figure 5.12 show the highest response occurs at the middle range of the soak at 800°C, achieving an average of 50MPa. The worst BH response occurs at 850°C where only a 24MPa increase is obtained. The results show the highest soak temperature also exhibits the highest variability in BH response.

Nano hardness plots were also taken to show the effect of soak temperature on the hardness properties at different soak temperatures. These values are shown in figure 5.13.

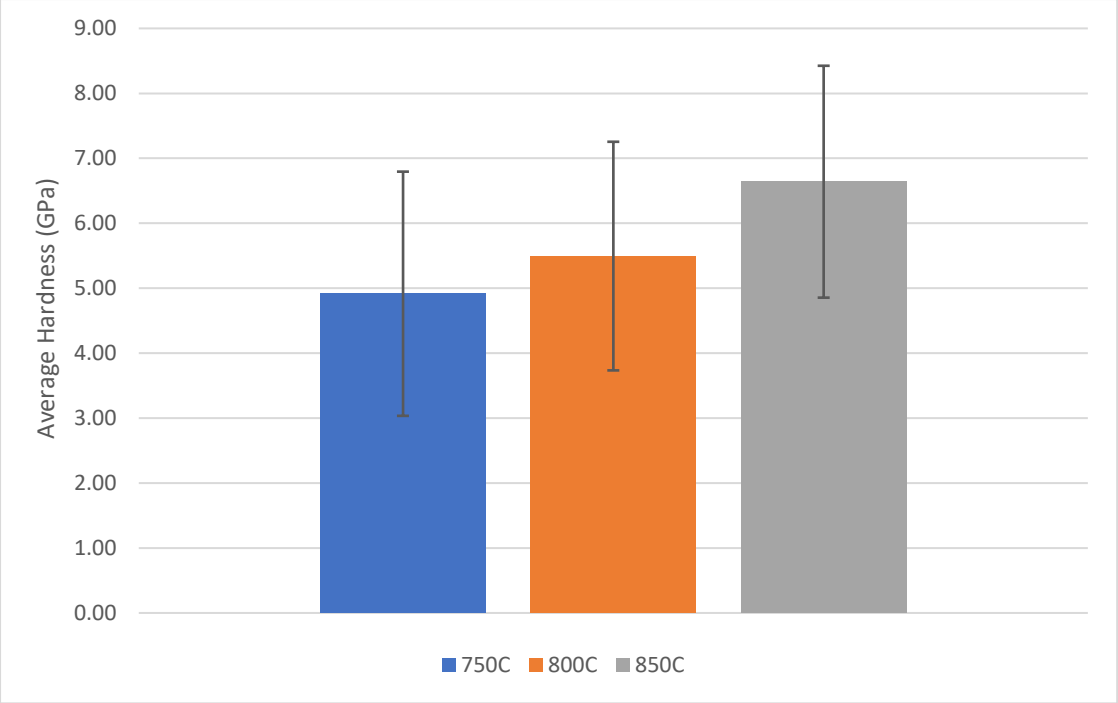

Figure 5.13. Average hardness values at each of the soak temperatures, showing an increase in average hardness when the soak temperature increases.

The results show an increase in average hardness from 750°C, which averaged 4.92GPa, to 5.50GPa at 800°C and then a further increase in average to 6.64GPa at 850°C. The standard deviation of the samples was consistent at around 1.8GPa, this large variation coming from the difference between the hard martensite phase and the ductile ferrite.

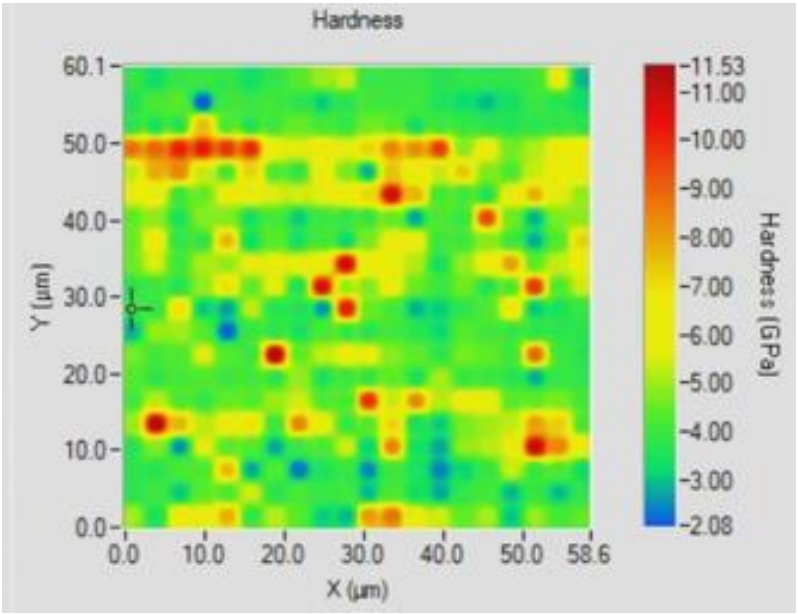

Figure 5.14. XPM plot of 750°C soak temperature. Higher hardness phases shown in red represent martensite which the blue phases showing ferrite.

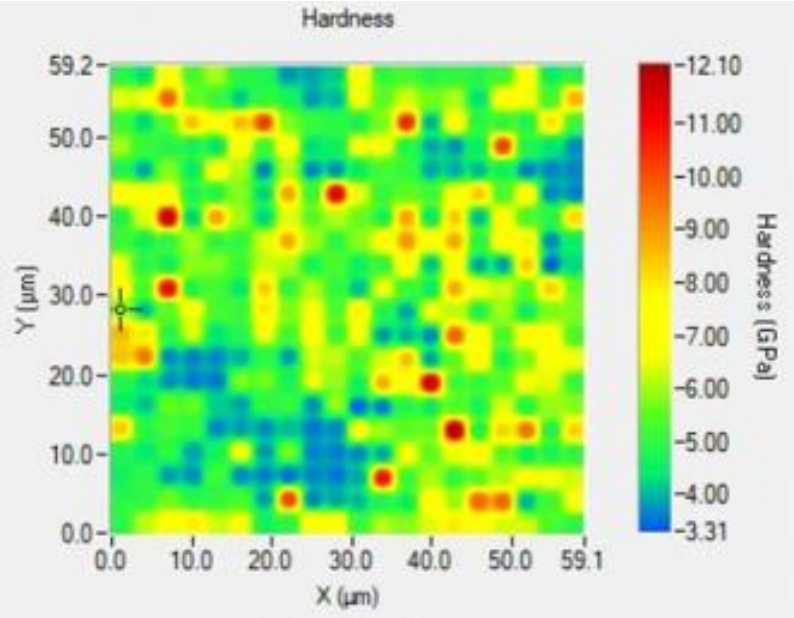

Figure 5.15. XPM plot of 800°C soak temperature. Higher hardness phases shown in red represent martensite which the blue phases showing ferrite

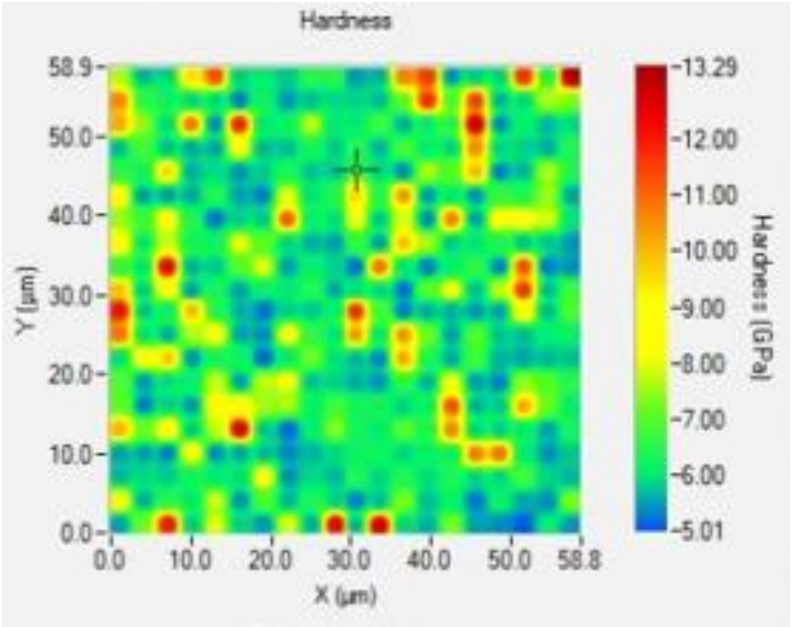

Figure 5.16. XPM plot of 850°C soak temperature. Higher hardness phases shown in red represent martensite which the blue phases showing ferrite. More distinct areas of high and low hardness seen compared to figure 5.14 and 5.15

Figures 5.14 – 5.16 show a XPM hardness plot of the 60x60µm area of indentation. All three images show a lower hardness phase in blue and green, which represents the background ferrite, interspersed with harder orange and red phases, indicating martensite.

Figure 5.14 represents the XPM plot for the 750°C soak and shows the lowest minimum hardness reading of 2.08GPa and the lowest maximum hardness of 11.03GPa of the three soak ranges. These values increase to a minimum hardness of 3.31GPa and maximum of 12.10 in the 800°C soak in figure 5.15 and increase further again to a minimum of 5.01GPa and 13.29GPa maximum in the 850°C soak in figure 5.16.

5.2.3. Discussions

As was discussed in the first section of this chapter, the overall mechanical properties of DP steels are defined by their microstructural constituents, depending on the ratio of each phase, its morphology, and its properties. Each change to the annealing temperature profile and heating and cooling rates plays a role in determining the final mechanical properties of the steel.

5.2.4. Effect of Low Soak temperature (750°C)

The banded microstructure at low soak temperatures is prominent. During the cold rolling process, the grains are deformed in the direction of rolling leading to thin elongated grains that provide high hardness but also poor ductility. The cold rolling process generates dislocations within the grain structure which act as sites for ferrite nucleation during the annealing process.

During the soak stage of the continuous annealing cycle, the time at elevated temperature promotes nucleation of austenite, which occurs primarily at the interphase boundaries of the existing pearlite and ferrite (89). These grain boundaries tend to be more energetically favourable as sites for nucleation than within grains themselves.

The time in which ferrite takes to recrystallise can be restricted by presence of the high levels of manganese, as well as the additions of chromium and niobium. Work done by Garcia and DeArdo (90) show that at low soak temperatures, combined with short soak holding times, allow only for ferrite recovery, rather than recrystallisation. Even at low temperatures, there looks to have been sufficient time to allow for recrystallisation to occur from the annealing cycles used in this investigation.

The growth of austenite along the rolling direction is related to the banding present in the existing cold rolled structure. The potential for manganese to segregate within the pearlite bands can cause regions of high manganese containing pearlite which has been reported to accelerate the transformation of pearlite to austenite (83). Due to the short soak stage which typically lasts less than two minutes during a continuous annealing cycle, the growth of the austenite is limited before the cooling section, thus the size of the austenite is limited, forming a refined final martensite grain size.

One of the major determining factors for the final transformation to austenite to either martensite or bainite is related to its carbon content (88). Typically, a low volume fraction of austenite in the microstructure would lead to austenite that has high levels of carbon present. This increases the hardenability of the austenite (124).

At 750°C soak temperature the stability of the austenite also increases, this being due to the lower volume of austenite becoming enriched with carbon. This means that during cooling the bainite transformation would shift it to slower cooling rates, increasing the likelihood of martensite in the final microstructure. This is shown diagrammatically from Girina et al. (88) in figure 5.17 and 5.18 when comparing low soak temperatures of 760°C to fully austenitic soak temperatures of 930°C.

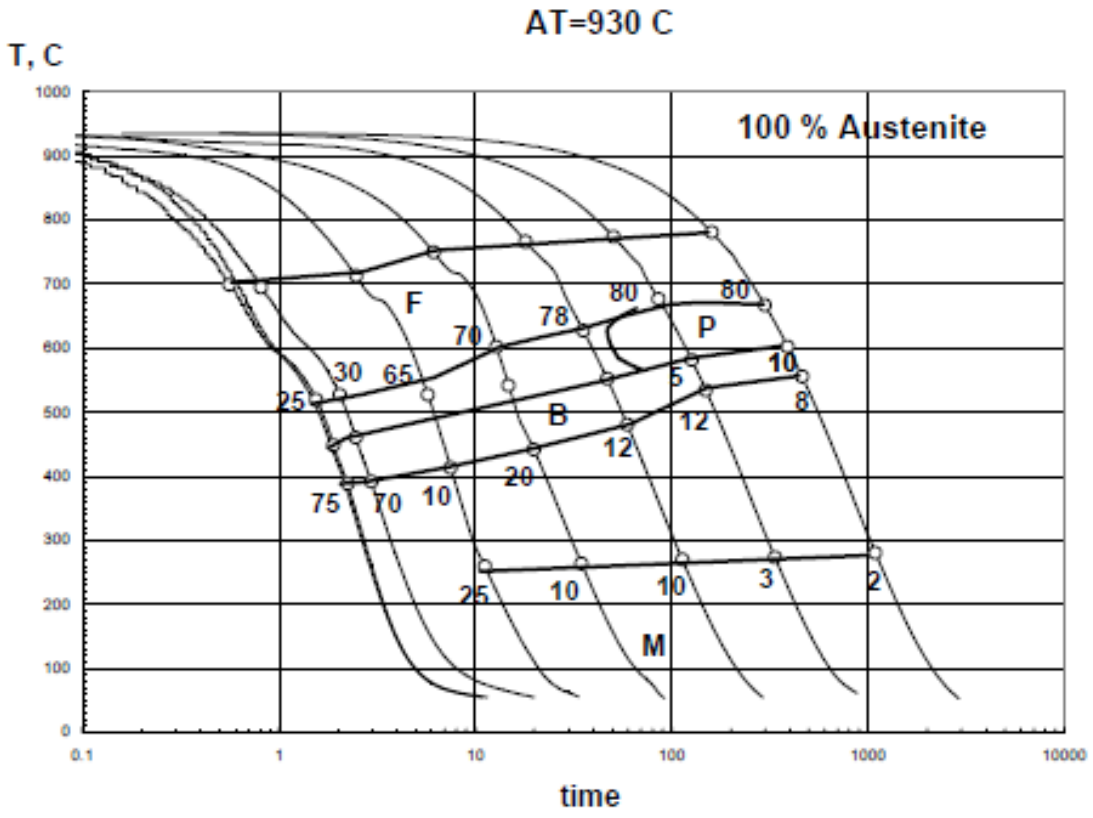

Figure 5.17 Continuous Cooling Transformation (CCT) of fully austenitic soak of DP chemistry and the final phases produced. ferrite (F), pearlite (P), bainite (B) and martensite (M) represented (88)*. The numbers represent the percentage of phase present in the microstructure at a given point in cooling. This example shows bainite cannot be avoided if cooling from a fully austenitic starting microstructure.*

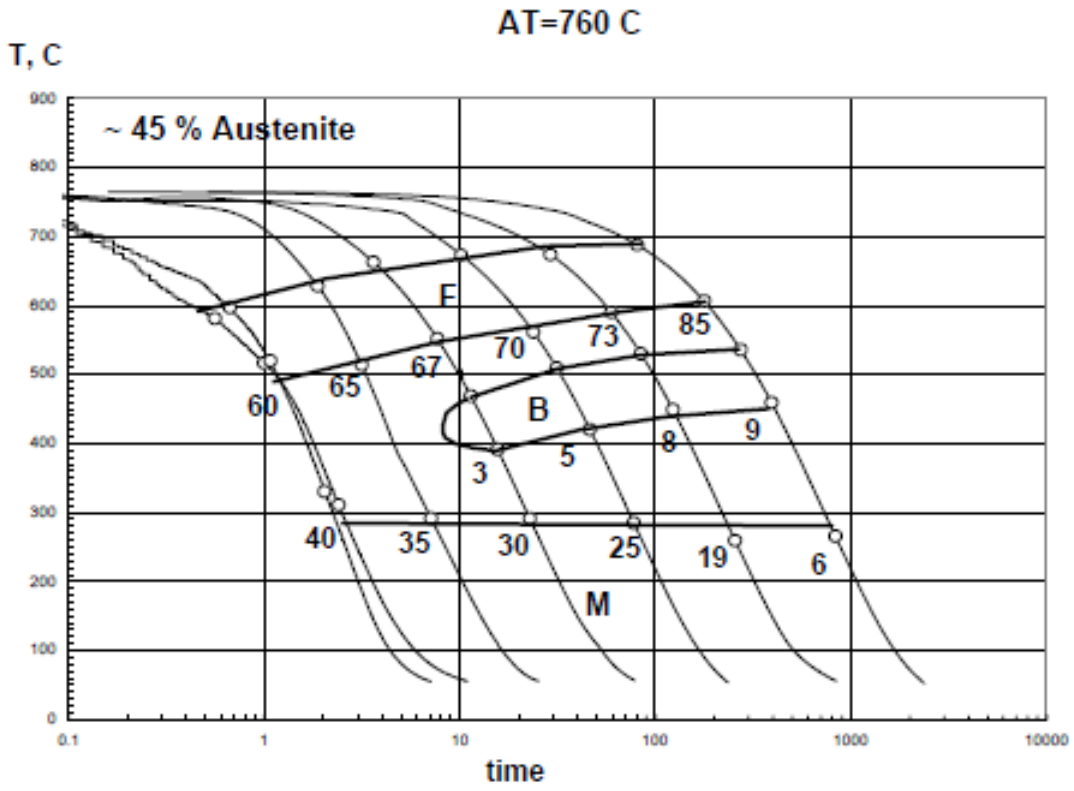

Figure 5.18 Continuous Cooling Transformation (CCT) of intercritical soak of DP chemistry and the final phases produced. ferrite (F), pearlite (P), bainite (B) and martensite (M) represented (88)*. Achieving a 45% austenitic starting microstructure means rapid cooling will avoid the onset of bainite in the microstructure.*

The refinement of the martensite in the final microstructure explains the higher strengths present in the mechanical properties at 750°C soak. Refined martensite, as described above, would have an increased carbon content and increased hardenability that results in the increased strength.

Another advantage of the lower soak temperature can be seen in the CCT diagram in figure 5.3. At lower soak temperature, the B_s and M_s is lower than that of higher soak. During rapid cooling, there will be less chance of hitting the B_s, therefore there would be a lower chance of producing bainite within the final product. Furthermore, the temperature to which the material is cooled in the overage (325°C) is higher than the M_s. With sufficient alloying to stop bainite formation, and the temperature being higher than the M_s means martensite should be produced until the final cool to 190°C, resulting in no bainite or tempered martensite present in the final microstructure.

At the lower soak temperature, there is likely to be anisotropy in the bulk mechanical properties, depending on whether the material is tested in the transverse of longitudinal direction. The trend of highest strength at the lowest soak temperature is observed by Mohanty et al. (82) who noted that

whilst the effect of the heating rate did not have a significant influence on the strength of the material, the soak temperature did.

5.2.5. Effect of Medium Soak temperature (800°C)

At 800°C there is grain growth occurring in the austenite, however this is competing with the recrystallisation of ferrite and is therefore still limited in the direction of rolling. The other notable difference between the 750°C soak and 800°C soak is the presence of large ferrite and martensite grains dispersed throughout the microstructure. These can benefit the ductility of the steel but would also lower the overall strength.

Figure 5.7b shows there is less directionality present in the final microstructure of the 800°C soak compared to the 750°C soak, this, coupled with the increase in grain size of the ferrite and martensite, will allow for an increase in the ductility of the final material.

The samples treated at the 800°C soak temperature exhibit the lowest tensile strength. This temperature is between the 750°C soak temperature, where the lower volume fraction of austenite remains sufficiently enriched with carbon to form martensite after the overage with limited new ferrite in the microstructure, and the 850°C soak, where lower carbon containing austenite produces new ferrite that enriches the surrounding austenite with carbon during the slow cooling section of the continuous annealing cycle.

As shown in the CCT diagram in Figure 5.4, there could be insufficient austenite stability at the overage, therefore it would be expected that some tempered martensite would be present in the microstructure. Similar findings were seen in the work by Girina et al. (88), where low stability of austenite was responsible for lower strengths in comparison to lower soak temperatures. In the same study, increasing the temperature close to the fully austenitic intercritical region showed an increase in strength, primarily due to the refinement of ferrite and the higher volume fraction of martensite.

One noted improvement at the 800°C soak was the bake hardening response. This increase could be due to the limitation of new ferrite in the microstructure. During the rapid cooling, the carbon concentration can be retained within the ferrite, this can then lead to an increase in the strengthening by free carbon pinning dislocations within the ferrite (83).

5.2.6. Effect of High Soak temperature (850°C)

At the highest soak temperature of 850°C there is sufficient energy for complete recrystallisation of ferrite. As the austenite grains grow, there is a restriction of the ferrite growth as the existing pearlitic structure is consumed by the austenite.

As the austenite grain size increases, carbon content and hardenability decreases. During the slow cooling section, the austenite grains that have low carbon content are first to transform to new ferrite. This in turn enriches the remaining austenite as carbon is ejected from the ferrite (95). This is demonstrated in the CCT diagram shown in figure 5.5. Compared to the other two soak temperature, the high temperature soak sample shows the ferrite curve pushed left, allowing for an increased amount of new ferrite growth at the same slow cooling temperature and cooling rate.

Areas of austenite that are supersaturated in carbon sufficiently depress the M_s temperature and transform readily to martensite during the final cooling after the overage section, rather than during the overage section. The increased M_s shown in table 5.2 for high soak temperatures (389°C) means that during the overage section at 325°C, there is likely to be some martensite forming before the final cool . This martensite would spend sufficiently long at high temperature to become tempered. Figure 5.19 shows an example of tempered martensite formed during the overage.

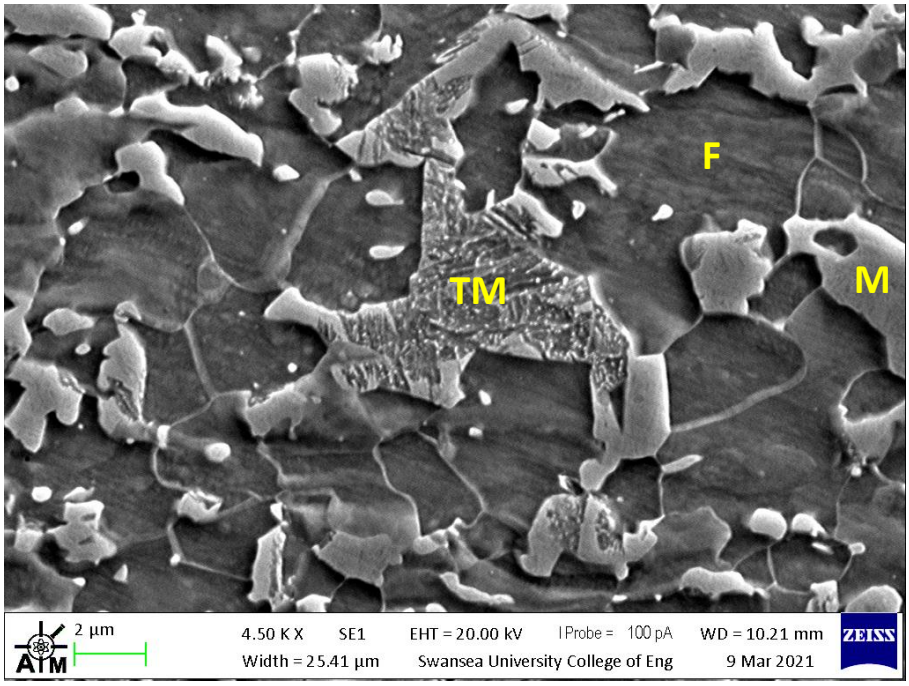

Figure 5.19 Tempered martensite presence after cooling from high soak temperatures. Tempered martensite (TM) shown middle of the image surrounded by ferrite (F) and martensite (M) islands.

The presence of bainite can also lower the overall strength of a DP steel. Work by Fonstein et al (125) suggest that bainite has a 30% lower strengthening than martensite. In the same work, it is suggested that the presence of bainite leads to an improved yield strength and elongation. Tempered martensite would also have a similar effect.

Along with equiaxed ferrite, the presence of bainite or tempered martensite can account for the higher levels of elongation shown in comparison to the 750°C and 800°C soak. Typically, a larger grain size can also contribute to higher levels of ductility too. As previously mentioned, larger martensite grains contain less carbon, which reduces its hardenability but increases its ductility.

The higher strength observed in the 850°C in comparison to the 800°C soak temperature is likely to due to the 10% increase in the volume fraction of martensite present in the final microstructure. Whilst a small fraction may be tempered, there is sufficient martensite present to increase the overall strength of the steel by 33MPa, this can also be combined with the fact that the ferrite grain size is more refined than that of both the 800°C and 750°C soak temperatures, due to the increasing martensite volume fraction.

One of the biggest areas for concern for processing at the highest soak temperature is the relatively low bake hardening values. As seen in figure 5.12, at the highest soak temperature, the requirement of 30MPa is not met, and there is a lot of scatter in the results.

At 850°C it is likely that the increase in new ferrite in the microstructure occurring during cooling from a higher soak temperatures would reject carbon, therefore leading to significant enrichment of the surrounding portion of austenite with carbon (83). The enrichment of the surrounding austenite would increase its hardenability and also delay the onset of bainite transformation. Conversely, the interstitial free ferrite would have insufficient free carbon to pin dislocations in the ferrite, this in turn would lower the BH response.

The increased levels of hardness as the soak temperature increases can be attributed to the increased volume fraction of martensite in the microstructure, and is in good accordance with other research showing an increase in hardness as the intercritical temperature increases (126).

As well as the increase volume fraction of martensite, the 850°C soak also has a smaller ferrite grain size. This has also been shown to cause an increase in nano-hardness, with larger ferrite grains leading to lower hardness values (127)

5.3. Effect of Cooling and Over-aging temperatures

Whilst the soak region of the continuous annealing cycle plays a major part in the volume of ferrite and austenite produced, it is the cooling section that provides the transformation from austenite to martensite or other phases such as bainite.

This section will focus on the rapid cooling (HGJC) and overage region of the annealing cycle, whilst keeping the simulated line speed and soak temperature constant.

5.3.1. Metallography

Figure 5.20 shows the visual similarities between all four HGJC temperatures under an SEM. All show a largely refined microstructure with martensite islands in a ferrite matrix. As was seen in the 800°C soak temperature in the section previously, there are larger ferrite and martensite grains in the microstructure.

Even though the microstructures look very similar, some differences do exist. The 275°C HGJC temperature exhibits the largest volume fraction of martensite at nearly 44%, which drops progressively as the HGJC temperature increases to 350°C HGJC temperature which has nearly 39%.

Whilst the variations in soak temperatures showed a considerable difference in microstructure, the subtle change in microstructure drives a big change in mechanical properties when looked at under greater magnification, these changes will be described later in this section.

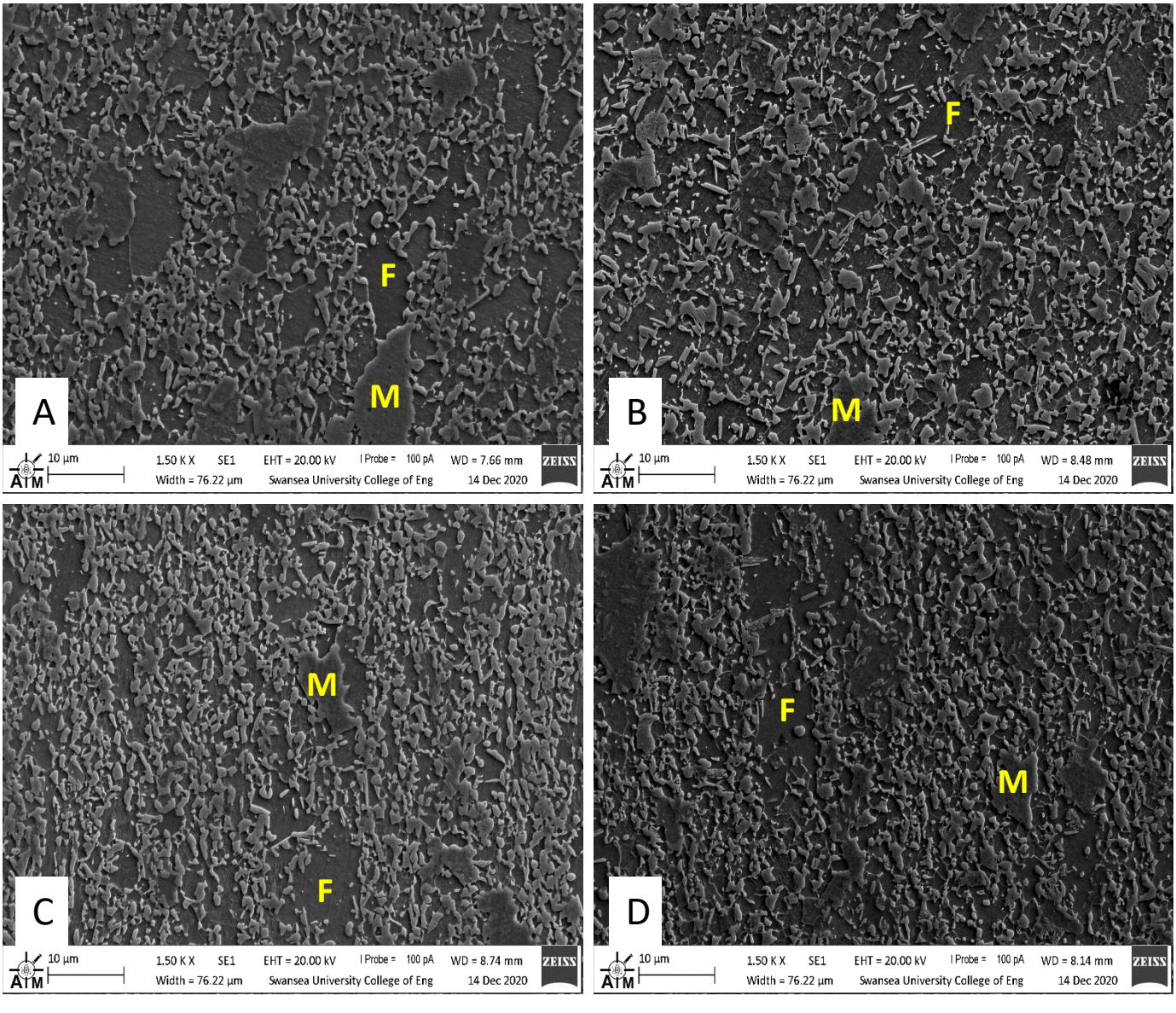

Figure 5.20 Effect of HGJC temperature on microstructure. 275°C (A), 300°C (B), 325°C (C), 350°C (D) shown with little visual difference seen. Martensite (M) islands within a ferrite (F) matrix

An overview of the volume fractions and the grain size analysis for each HJGC temperature is detailed in Table 5.5.

Table 5.5 Phase fraction analysis and grain size analysis on each of the HGJC cycles

HGJC Temp (°C)	Martensite Phase Volume Fraction (%)	Phase Fraction Error (%)	Grain Size Average (µm)	Grain Size Error (%)
275	62.8	0.4	1.71	+/- 6
300	61.3	0.6	1.88	
325	60.9	0.7	2.04	
350	60.1	1.8	2.07	

5.3.2. Mechanical Properties

By keeping the soak temperature consistent, the HGJC temperature can be adjusted to show the effect that the cooling temperature has on the mechanical properties of the steel.

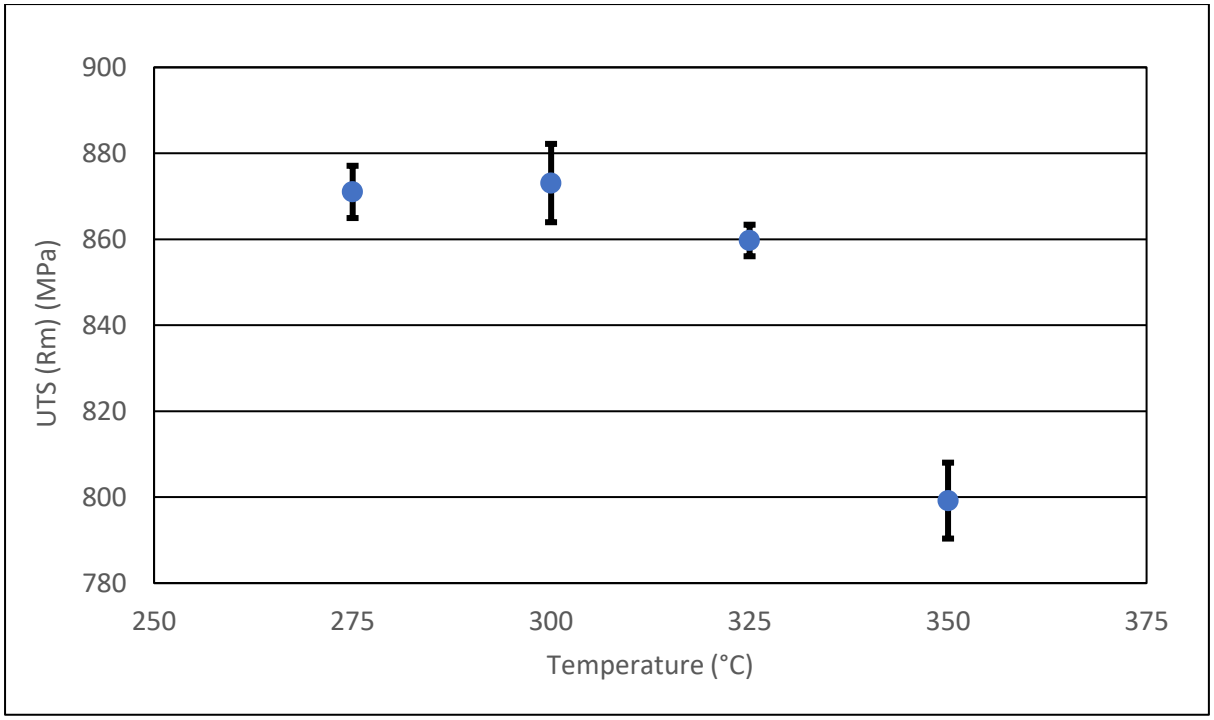

Figure 5.21 Effect of HGJC temperature on UTS, a decrease in strength seen as temperature increases.

As can be seen from Figure 5.21, the highest tensile strengths are achieved from the 275°C HGJC temperature range. Similar values of 870 to 875MPa are seen between 275°C and 300°C respectively, from there the strength drops off slightly at 325°C to 860MPa and then significantly drops at 350°C to around 800MPa.

The area between 275-325°C suggests a region of stability, where operating within these temperature ranges would have a limited effect on the tensile strength, however at higher temperatures the strength of the material reduces, as much at 60MPa for a 25°C drop.

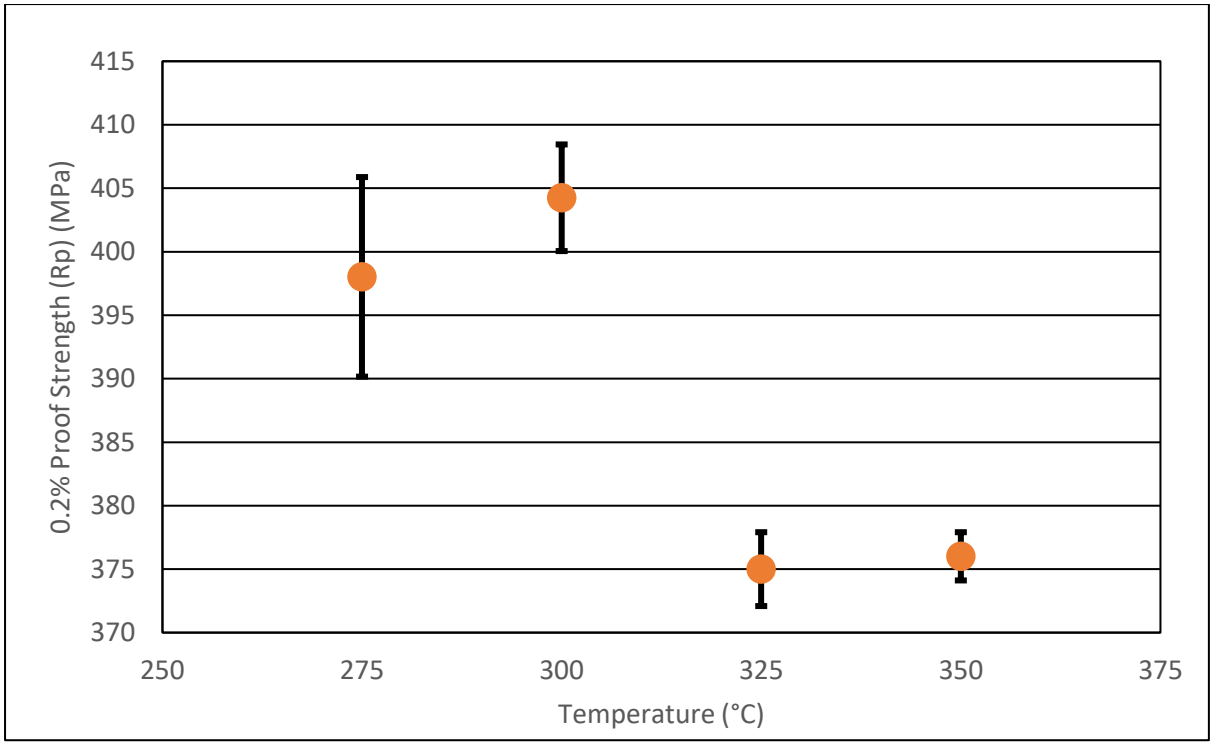

Figure 5.22 Effect of HGJC temperature on Proof Strength. High proof typically seen at low HGJC temperature with a step change seen at 325°C.

Like the tensile strength, the higher proof strength values were seen at the lower HGJC temperature range. Averages of 400MPa and 405MPa were seen at 275°C and 300°C respectively. Whilst the drop was not as significant as the strength, the proof strength dropped at 325°C and 350°C HGJC to around 375MPa.

Large error bars at the lower HGJC temperatures indicate a wider range of values, this could also indicate that the proof strength could be more susceptible to process variability. As was stated section 5.2.2 for proof strength, the values shown here would not achieve the standard requirements of 440MPa, but with in-line temper rolling the increase should be sufficient for all of these to achieve 440MPa as a minimum.

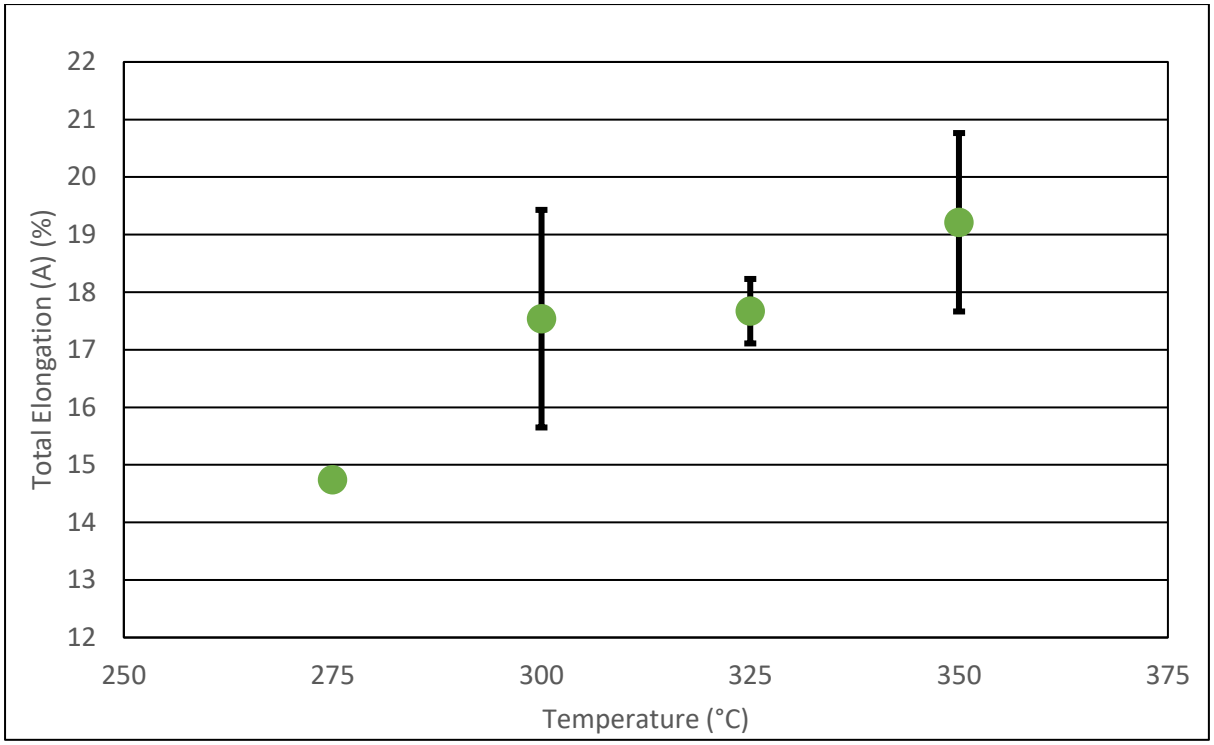

Figure 5.23 Effect of HGJC temperature on total elongation, higher ductility seen as temperatures increase.

Conversely to the tensile strength, the highest elongations were found at higher HGJC temperatures. The 275°C HGJC consistently achieved just above the standard requirement for total elongation, which is 14% as a minimum (106). The highest HGJC temperatures achieved just above 19% on average, whilst the 300°C and 325°C were also well within the standard requirements, averaging about 17.5%.

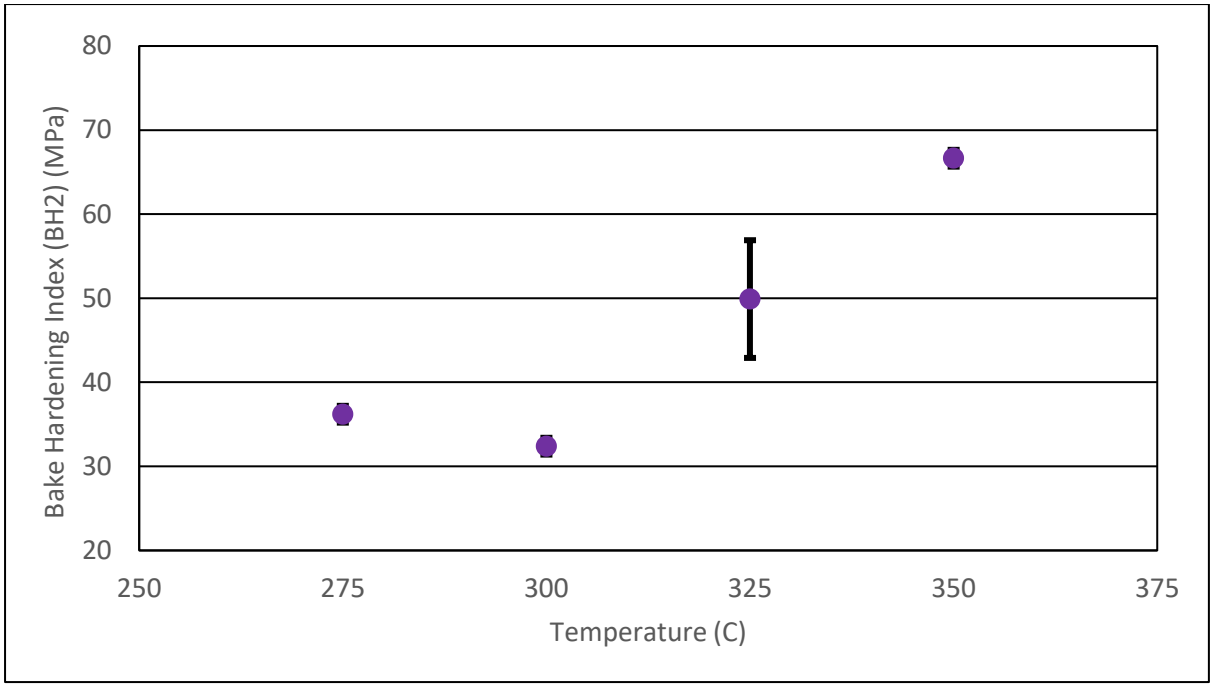

Figure 5.24 Effect of HGJC temperature on bake hardening, limited effect on BH seen at low HGJC, but increase occurs as temperatures pass 325°C.

As with the elongation values, the lowest BH values are found at the lowest HGJC temperatures. Average values of 36MPa and 32MPa were achieved for 275°C and 300°C HGJC temperatures respectively. Whilst both values do achieve the 30MPa minimum requirement of the standard, small changes in the manufacturing process may mean they drop below this limit.

As the HGJC temperature increases so does the BH values. At 325°C an average of 50MPa was achieved, and at 350°C the value rose to around 65MPa.

5.3.3. Discussions

A continuous annealing line is set up to produce various grades of steel. Each chemistry will have different temperature and time considerations to achieve specific microstructures and mechanical properties. The large overage section, which at line speeds of 140mpm are around 5 minutes from start to end, were built to allow for maximisation of carbon out of solid solution, this allows sufficient time for carbide precipitates to form and grow, which leads to a reduction in the ageing effect on the steel (52).

Ensuring that the DP steel is sufficiently alloyed with elements that increase the hardenability of austenite, such as manganese (42), mean transformation upon cooling to the overage section should be limited, allowing for the austenite to remain untransformed through the overage and to transform on final cooling to martensite. Any austenite that transforms to martensite at this stage would be kept at sufficient time and temperature to become tempered, which would impact the final mechanical properties.

As shown in Figure 5.2, there are two cooling sections in the continuous annealing cycle, a slow cooling section (CGJC) and a rapid cooling section (HGJC). Both of these sections can influence the final mechanical properties, however the HGJC is the focus of this investigation.

The CGJC cools from the soak temperature to, in this case, 640°C. Typically cooling rates in this section are between 3.5-6°C/s, depending on the thickness of the material. It is during this section that new ferrite can occur during cooling. The slower the cooling in this section, the more ferrite can be produced. This new ferrite has a two-fold effect on the microstructure. Firstly, the new ferrite growth restricts austenite growth, refining the austenite. Secondly, the new ferrite rejects carbon, and it significantly enriches the surrounding portion of austenite with the carbon (83).

Whilst the CGJC can be of significance, as will be shown in a later chapter for achieving high yield DP products, for this chapter the focus is on the HGJC and the overage temperature. The HGJC cools from the CGJC at a rate of between 25-50°C/s, depending on the thickness of the material which dictates the speed the line is running at. It is at the end of this cooling section that the austenite, if insufficiently saturated with carbon, will transform to bainite or tempered martensite when hitting the overage temperature target.

5.3.4. Strength characteristics

As seen in Figure 5.21 the lower HGJC temperatures have the highest tensile strength values. The strength is likely being contributed from the increased martensite present in the microstructure at these lower temperatures.

Table 5.5 does show an increase in the volume fraction of martensite at lower HGJC, but there is a limited difference between 275°C, 300°C and 325°C. A larger change is seen in average grain size,

which increases from 1.71µm at 275°C to 2.07µm at 350°C, this suggests a more refined grain structure which is known to increase strength.

A sudden drop in strength is seen between 325°C and 350°C, whilst there is a larger grain structure, the amount of martensite in the microstructure remains consistent. Therefore, revisiting the microstructure was necessary to indicate whether the martensite had become tempered at the elevated temperature.

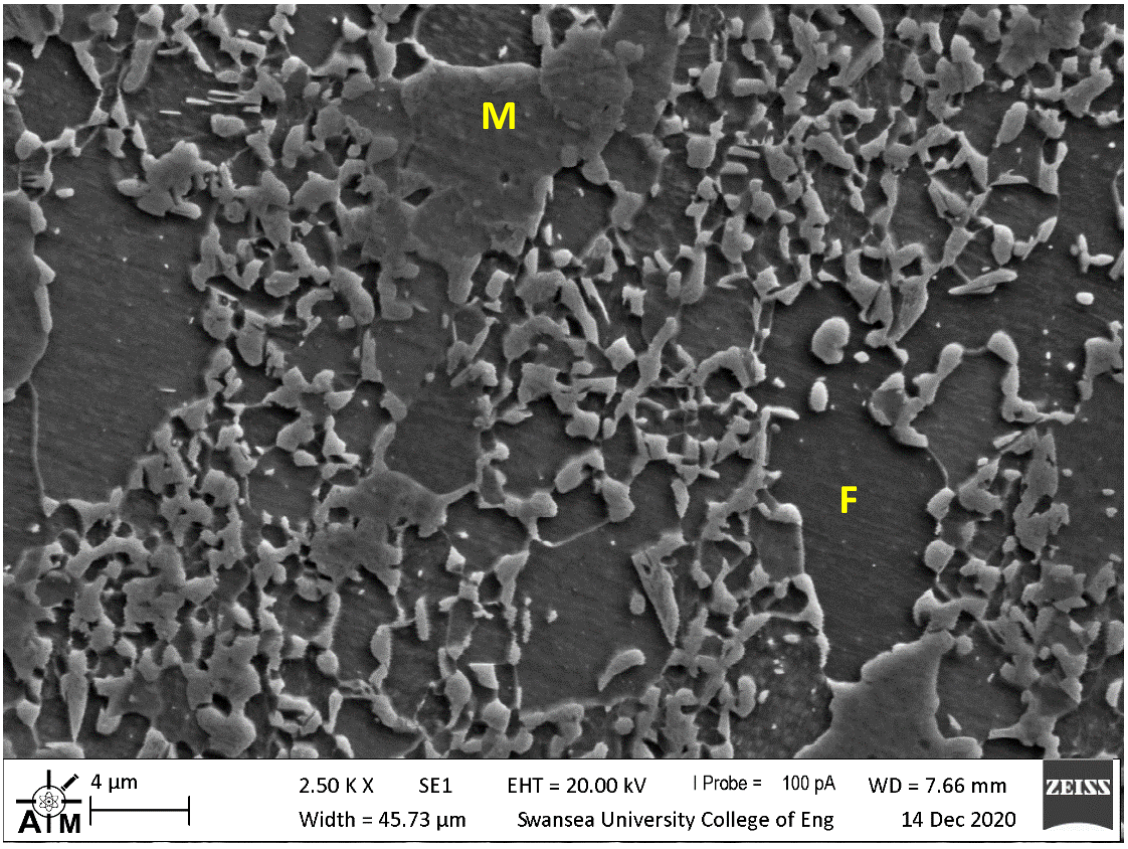

Figure 5.25 SEM image of microstructure at 275°C HGJC. Martensite (M) and Ferrite (F) with no presence of tempered martensite in microstructure

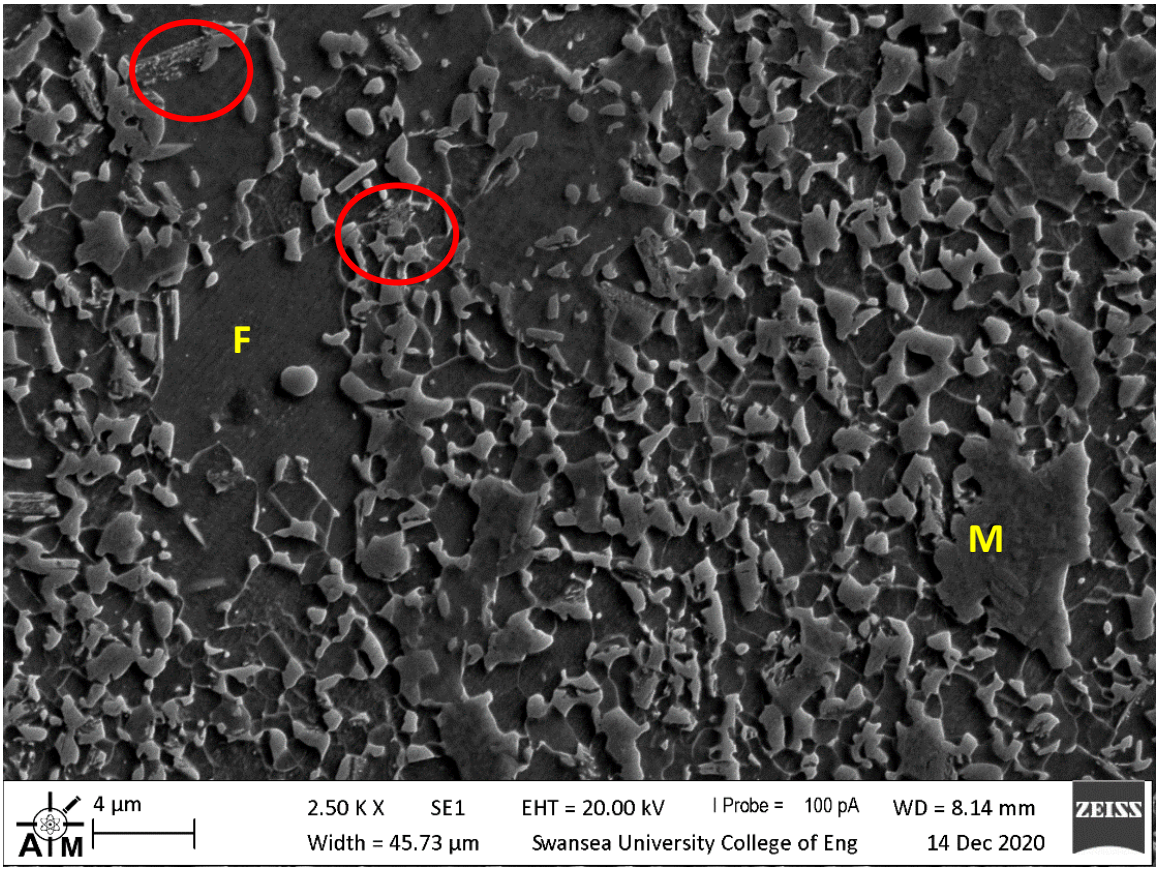

Figure 5.26. SEM image of microstructure at 350°C HGJC. Martensite (M) and ferrite (F) with instances seen of tempered martensite in microstructure (circled)

Evidence of this is shown by a comparison of the microstructure in Figure 5.25, taken at low HGJC of 275°C and figure 5.26, taken at 350°C. It's clear that there is some decomposition of martensite occurring, this reduces the martensite volume fraction (53).

The cooling rate can also play a part as to how much bainite is formed in the microstructure during cooling. Cooling from the CGJC through the HGJC typically takes around 8 seconds processing at line speeds of 140mpm, therefore, to achieve lower overage temperatures a higher cooling rate is required. This increased cooling rate can mean less time in the region in which bainite is produced. Whilst achieving 275°C would require a cooling rate of 48°C/s through the HGJC, achieving 350°C requires a 38°C/s cooling rate, a difference of 10°C/s. This slower cooling rate can allow for decomposition of austenite to form bainite, which would lower the strength of the final product (8).

The yield strength results were more varied than expected, though the trend of highest yield strengths at lowest HGJC is expected, dropping at the higher HGJC temperatures. This would be due to the increase in martensite at the lower HGJC temperatures (128), this theory aligns with the

simple law of mixtures, where a higher volume fraction of the harder phase provides an increase in strength.

Another indication of the tempering of martensite comes in the form of the proof strength to tensile strength ratio (PS/TS). For the 275°C the PS/TS ratio was 0.457, however as the temperature was increased to 350°C the PS/TS ratio rose to 0.471. Work by Fonstein et al. (95) suggests that as result of tempering there is a pinning of dislocations within ferrite and also a relaxation of residual stresses there is an expectant increase in the PS/TS ratio.

5.3.5. Ductility characteristics

As has been seen in the previous chapter with regards to soak temperature, the total elongation values are lower where higher levels of martensite are present. Tempering of martensite at higher HGJC levels can also bring about a relaxation of stresses present in the microstructure, this would benefit the overall ductility.

The supersaturated carbon atoms that are in the martensite phase would dissolve at higher HGJC temperatures and segregate to the mobile dislocations around the ferrite / martensite interface. This dissolution decreases the martensite hardness and increases the elongation due to the increase of plastic deformation coordination (129).

Nano-hardness values taken from samples at 275°C HGJC temperature and 350°C HGJC temperature show that the average hardness values decreased from 5.70GPa to 5.60GPa, these values compliment the decrease in tensile strength and conversely the increase in ductility as the HGJC temperature is increased. As the phase fraction analysis shows the martensite content remains consistent across the HGJC temperatures, however the average hardness has dropped as the temperature increases.

5.3.6. Bake hardening characteristics

The effect of bake hardening is more pronounced during the HGJC and overage section of the continuous annealing cycle. The overaging section allows for carbon to precipitate out of solution, which leads to a reduction in the solute carbon content.

An important aspect for BH response is related to the degree of supercooling that occurs from the intercritical region. The lower the slower the rate of cooling, for example in achieving higher HGJC temperatures, means carbide precipitation becomes inhibited. Therefore, Cottrell atmosphere formation and carbide precipitation during the baking process are promoted due to an increase in solute carbon atoms, allowing for an increase in BH response (129).

Conversely, the faster cooling rate to achieve lower HGJC temperatures leads to a greater carbide nucleation rate. This, combined with an increase in dislocations due to the transformation of austenite to martensite, means that there is a limitation on free solute carbon atoms to pin the dislocations during bake hardening (130), limiting the BH response.

The tempered martensite also lowers the dislocation density in comparison to untempered martensite. The decomposition of the martensite during tempering allows for diffusion of carbon atoms which can in turn provide further pinning of dislocations and further increase the BH response (63).

5.4. Conclusion

As the soak temperature is raised there is a clear increase in the volume fraction of austenite, transforming to martensite from 52% to 65%, in the final microstructure of the material. As the soak temperature is increased, so too is the grain size of martensite, whilst the grain size of ferrite decreases.

The highest strength values were found at the lowest soak temperatures, this being primarily due to the refined martensite with high hardenability. Conversely, this refined structure also provides the lowest ductility.

It was found that the best strength and ductility combination was at the highest soak temperatures. The highest soak temperature contained the highest volume fraction of martensite, but also the

largest grain size. The large volume fraction of martensite can provide the strength whilst the increased grain size also provides the structure with ductility.

Whilst it was shown that the highest soak temperatures provide the best strength and ductility, the low BH values mean that it would not achieve standard requirements. Due to the low soak having excessive strength and low ductility, the optimum soak temperature would be around the 800°C range, where there is a trade-off between optimising the tensile strength and ductility over the bake hardening response of the steel.

For the HGJC work it was shown that the highest strengths were found at the lowest temperatures, this is due to the increase in martensite volume fraction which ranged from 43% at 275°C to 38% at 350°C. Conversely, the total elongation increased as the HGJC temperature increased.

Finally, the BH response was shown to be highest at increased HGJC temperatures, this being due to the tempered martensite in the microstructure, as well as sufficient free solute carbon atoms to provide pinning of free dislocations and the formation of Cottrell atmospheres, which in turn lead to an improved BH response.

6. Effect of silicon on the mechanical properties of DP800 steel

The work in chapter 5 focusses on the adjustments that can be made to time and temperature through the annealing of DP steels. Understanding how time and temperature effects the microstructure and mechanical properties can help create an ideal processing window to maximise the mechanical properties through CAPL.

Adjusting the chemistry is another route for improving mechanical properties. Section 2.4 shows the effect that chemical elements have in steel, one alloying element that has had limited investigation for industrially processed DP steel is silicon. The allowable additions of silicon to a DP steel according to EN 10388 is to 0.8wt% (106). At the time of writing this work, the internal steel grade used for production of DP800 at Tata has a maximum limit of 0.4wt%, with a current aim of 0.25wt% added. Therefore it was decided to produce three chemistries with 0wt%, 0.25wt% and 0.4wt%, sufficient enough of a change to investigate its effect through industrial processing.

Silicon is a ferrite stabilising element in steel (131). Its addition can help influence the recrystallisation process and hardenability during quenching (132). The effect of silicon on mechanical properties and microstructure of hot rolled DP steels was investigated by Cai et al (97), concluding the tensile strength to ductility balance was improved by increasing silicon. Drumond et al. (124) also investigated silicon's effect on mechanical properties and microstructure for annealed DP steel, the research showed the addition of silicon favoured the formation of a homogeneous austenite of higher hardenability, which resulted in a higher volume of martensite in the final structure.

There has been limited research on the how silicon can affect a DP steel through a continuous annealing line, and in particular its effect on bake hardenability. Therefore, this chapter will investigate the effect of silicon additions on the microstructure and mechanical properties of DP steels, replicating conditions used for an industrial continuous annealing process. This work is subject to another journal paper which is subject to approval at time of writing.

6.1. Methods

Three 50kg casts of a typical DP steel chemistry was made with varying silicon content as shown in table 6.1. The material has been cast to ingots in a vacuum induction melting furnace (VIM) and then rolled to transfer bar thickness of 34cm.

Table 6.1 Cast Chemistries with varying silicon content (wt%)

Alloy	C	Mn	Si	Ti	Cr	Nb
Low Si	0.14	1.838	0.013	0.029	0.547	0.025
Med Si	0.137	1.825	0.253	0.031	0.54	0.026
High Si	0.139	1.826	0.407	0.03	0.549	0.026

The blocks have then been processed to cold rolled sheets and annealed using the CASIM, as has been described in section 4. Metallographic, phase fraction and grain size analysis has also been undertaken, which has also been described in section 4.

Changing the chemical composition will influence the starting and finishing temperatures of the intercritical region of steel. To have an indication as to the effect changing the silicon content will have, the Andrews' empirical equation can be used (24).

Table 6.2. Calculation of A_{c1} and A_{c3} start temperatures. Increasing silicon content leading to increase Ac1 and Ac3 start temperatures.

	A_{c1} (°C)	A_{c3} (°C)
Low silicon	712	835
Med silicon	719	846
High silicon	724	852

Increasing the silicon content raises both the A_{c1} and A_{c3} temperatures, as can be seen in table 6.2. This will impact on the starting temperature at which austenite will be produced at the intercritical temperature, but should reduce variation of austenite volume fractions with temperature (43).

6.2. Results and Discussions

6.2.1. Effect of silicon additions on hot rolling of DP steel

The aim of the hot rolling process is to produce the softest steel possible to maximise the capacity of cold reduction. The target microstructure for hot rolling is to achieve a ferrite and pearlite mix, which has a lower strength compared to the final product that consists of ferrite and martensite (20). Research has shown that there is benefits in using a ferrite-martensite initial microstructure, which brings benefits in terms of high density of nucleation sites for austenite formation, which enhances the efficient of pinning the migration of ferrite grain boundaries during the intercritical anneal (133).

However, during industrial processing, limitations of rolling loads on the cold mill can prohibit rolling of material that is very high in strength, meaning the majority of reduction has to be made at the hot rolling stage. Therefore, to minimise the loads experienced on the cold mill, the reduction from hot mill to cold mill in these tests has been kept at 55% for DP800 type material.

To replicate the hot rolling process, each of the samples is heated up to 1250°C in a reheat furnace before passing through a set of rollers seven times, with each pass progressively deforming the steel to achieve the final thickness of 3.5mm. During the rolling process, the strip temperature reduces from around 1000°C to approximately 800°C. From here a set of water sprays controls the final aim temperature to 600°C. Keeping the finishing temperature this high allows for a final ferrite / pearlite microstructure to develop, as shown in figure 6.1.

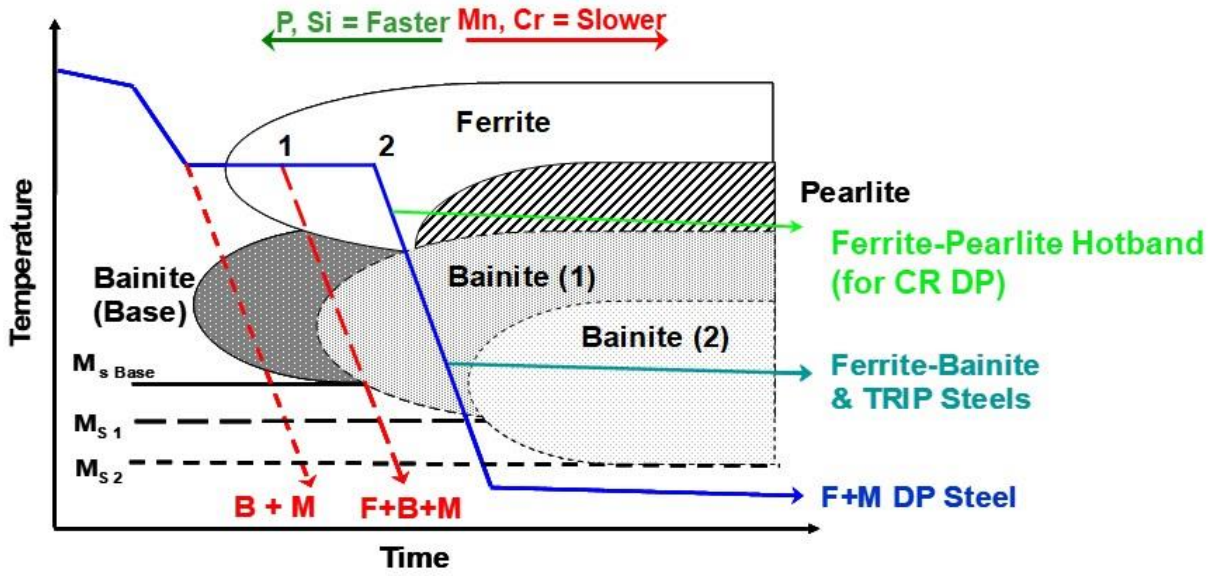

Figure 6.1 Continuous cooling diagram for DP production. Note the green pathway for hot rolling to achieve a ferrite-pearlite aim (4). 'F' represents ferrite, 'M' represents martensite and 'B' represents bainite. Addition of certain elements such as Mn or Cr delays the onset of bainite, therefore allowing cooling directly to martensite

The effect of silicon on the hot rolled microstructure is evident from the light microscope images shown in figure 6.2.

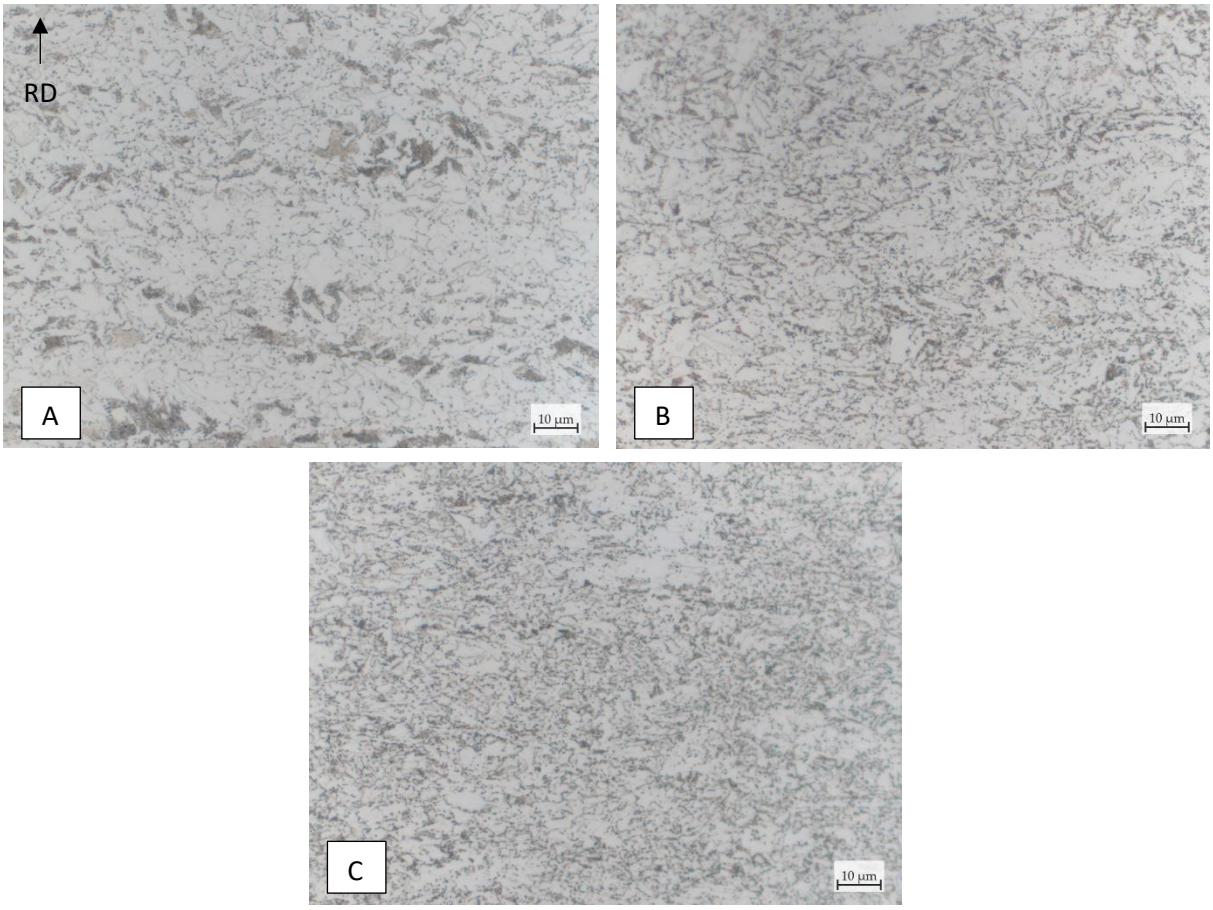

Figure 6.2. Light microscope images of hot rolled samples. Lighter regions are ferrite while the darker regions are pearlite. A = low silicon, B = medium silicon, C = high silicon. Samples show progressive refinement of microstructure as silicon content is increased.

As can be seen from figure 6.2, as the silicon levels increase so does the refinement of the microstructure. Much larger ferrite and pearlite grains are seen in figure 6.2A which contains low silicon, whilst there is some rolling directionality still present, particularly in the pearlite grains.

As the silicon levels increase in the medium silicon sample, figure 6.2B, there is a refinement of the pearlite whilst larger ferrite grains still exist in the microstructure, though the ferrite microstructure is still more refined than in the low silicon sample.

At the highest silicon levels in figure 6.2C there is further refinement of the microstructure, with both the ferrite and the pearlite grains being much smaller than the low and medium silicon containing samples. The refinement is also shown in the grain size analysis in table 6.3.

Silicon is a ferrite stabiliser, it reduces the recrystallisation temperature of ferrite. In the low silicon containing steel, it is evident that the austenite has been restricted to growth along the direction of deformation during hot rolling and sufficient energy has allowed large grain growth to occur in a banded structure.

The formation of refined and equiaxed ferrite as the silicon addition increases has been seen in other bodies of work (97)(134). Silicon inhibits carbide formation by increasing the activity of carbon in austenite, which allows for increased austenite to ferrite transformation (135).

Inhibiting carbide formation with the addition of silicon allows the austenite adjacent to ferrite to become enriched with carbon, which increases its stability on cooling and add to its strength (136).

The refinement in the microstructure as the silicon content increases will lead to a more refined microstructure post cold rolling. The smaller grains will increase the grain boundary surface energy and should generate a higher thermodynamic potential for ferrite recrystallisation (100).

Figures 6.3-6.5 show the mechanical properties for each of the silicon variants, each result is an average of two tensile tests with error bars showing the variability.

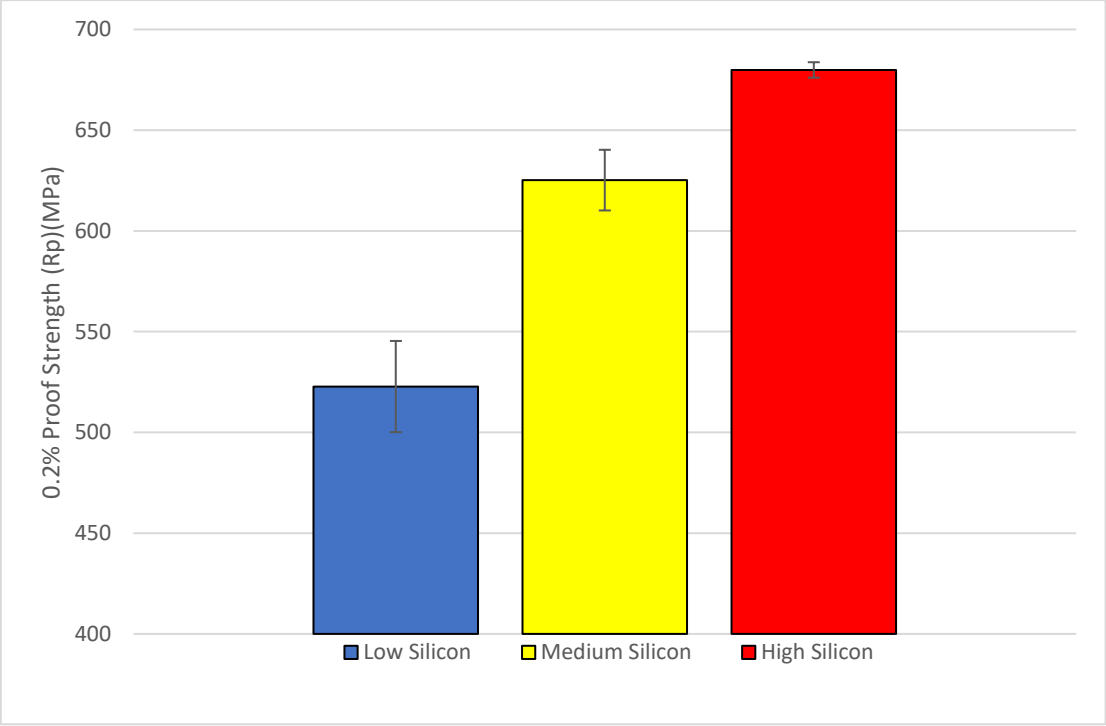

Figure 6.3. Proof strength for hot rolled low, medium and high silicon containing DP chemistry.

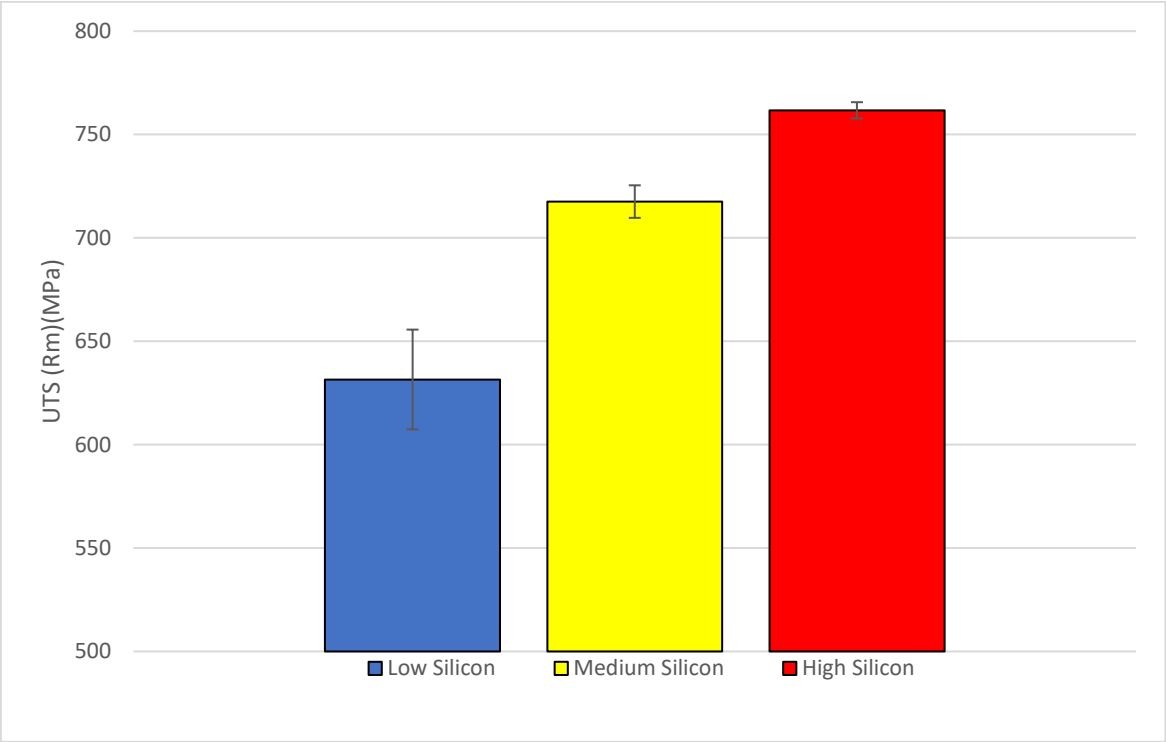

Figure 6.4. Ultimate tensile strength for hot rolled low, medium and high silicon containing DP chemistry.

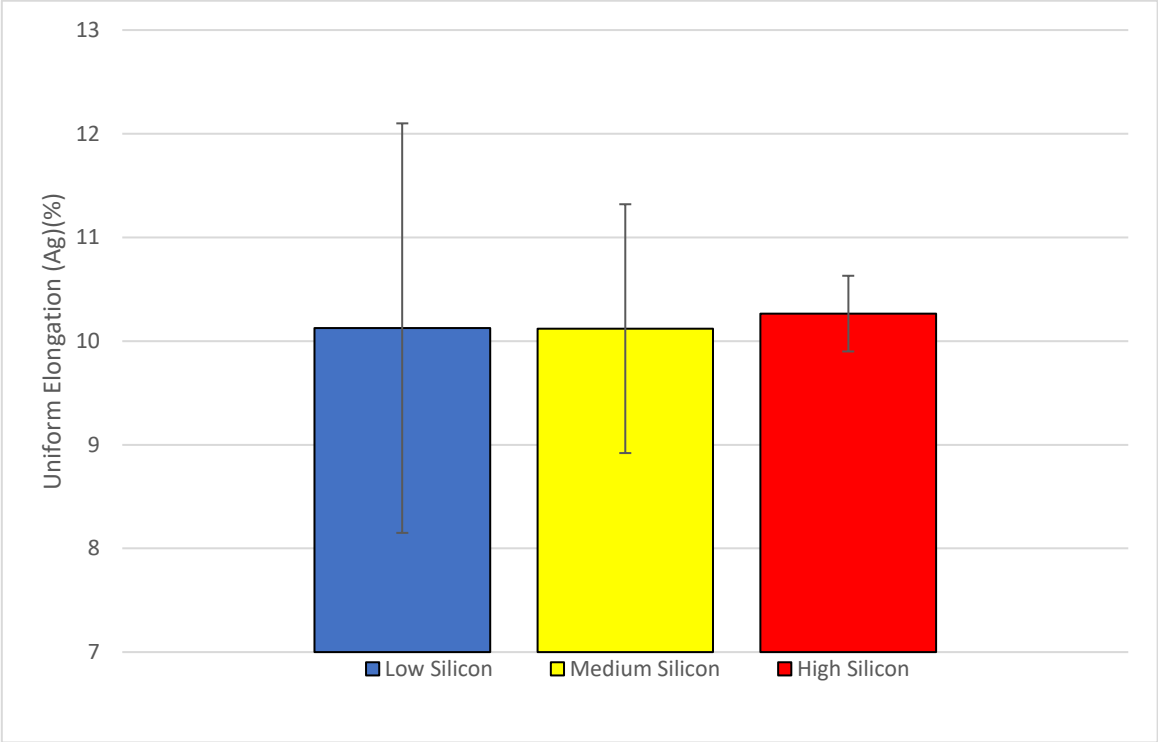

Figure 6.5. Uniform elongation for hot rolled low, medium and high silicon containing DP chemistry.

Increasing the silicon content has led to an increase in both the proof and tensile strength of the hot band steel, whilst maintaining its ductility. The average proof strength increased from 522MPa in the low silicon hot rolled material to 680MPa in the high silicon hot rolled material. UTS increased by 130MPa from an average of 631MPa in the low silicon to 761MPa in the high silicon material. On average a small increase in elongation was seen from 10.1% in the low silicon to 10.3% in the high silicon. The error bars become smaller as the silicon content increases, this indicates that the strength and ductility results become more consistent as the silicon levels increase.

The biggest contributing factor to the strength increase would be due to the refinement of the microstructure, both for the ferrite but primarily the pearlite. Typically in metals, the finer the grain size, the higher the resulting yield stress. An equation by Hall and Petch is typically used which led to the following relationship between yield strength and grain size (15):

$$\sigma_y = \sigma_0 + k_y d^{-1/2}$$

Where σ_y represents yield stress, σ_0 is friction stress, d is grain size and k_y is a constant. Additional to the grain refinement, phase fraction analysis shows an increase in the volume fraction of pearlite as the silicon levels increase, as shown in table 6.3.

Table 6.3 Phase Fraction Analysis of Hot Rolled Samples, showing increase in pearlite as silicon content increases as well as a decrease in pearlite grain size.

Silicon Content	Ferrite (%)	Pearlite (%)	Error (%)	Grain Size Average (µm)	Error (%)
Low	55.2	44.8	1.3	3.54	4.6
Medium	48.6	51.4	2.1	2.79	7.7
High	47.6	52.4	2.6	2.63	9.8

This increase in pearlite increases the strength of the steel (137). Therefore, the increase in the yield and tensile strength seen in figures 6.3 and 6.4 can also be related to the increase in the pearlite within the microstructure, increases from 44.8% to 52.4% from low to high silicon content.

There is limited difference in the elongation properties of the steel as the silicon content increases. Due to enhanced partitioning of carbon to austenite with increasing silicon content, the ferrite

should have less interstitial carbon present (95). This would have a twofold effect, allowing for increased ductility in the ferrite phase, which would contribute to increased overall ductility but also allow more carbon to saturate the surrounding austenite, increasing hardenability.

Further work by Fonstein et al. (96), has also shown that there is a general trend of a better balance between the tensile strength and the elongation when the silicon content is increased, this could also be a reason for increased strength whilst maintaining ductility, where a typical trend in steel would be for ductility to decrease as the tensile strength increases.

6.2.2. Effect of silicon on the microstructure of cold rolled annealed DP steel

To elevate the stresses brought about by the cold rolling process and to achieve the final dual phase microstructure, the steel passes through an annealing cycle. Chapter 5 shows the effect of soak temperature and HGJC, or the rapid cooling section of the furnace, with its effects on the microstructure and mechanical properties. From that work, it was decided to look at varying the HGJC temperatures, whilst keeping the remainder of the annealing cycle consistent. Figure 6.6 shows the variations of the annealing cycle that have been used for this chapter.

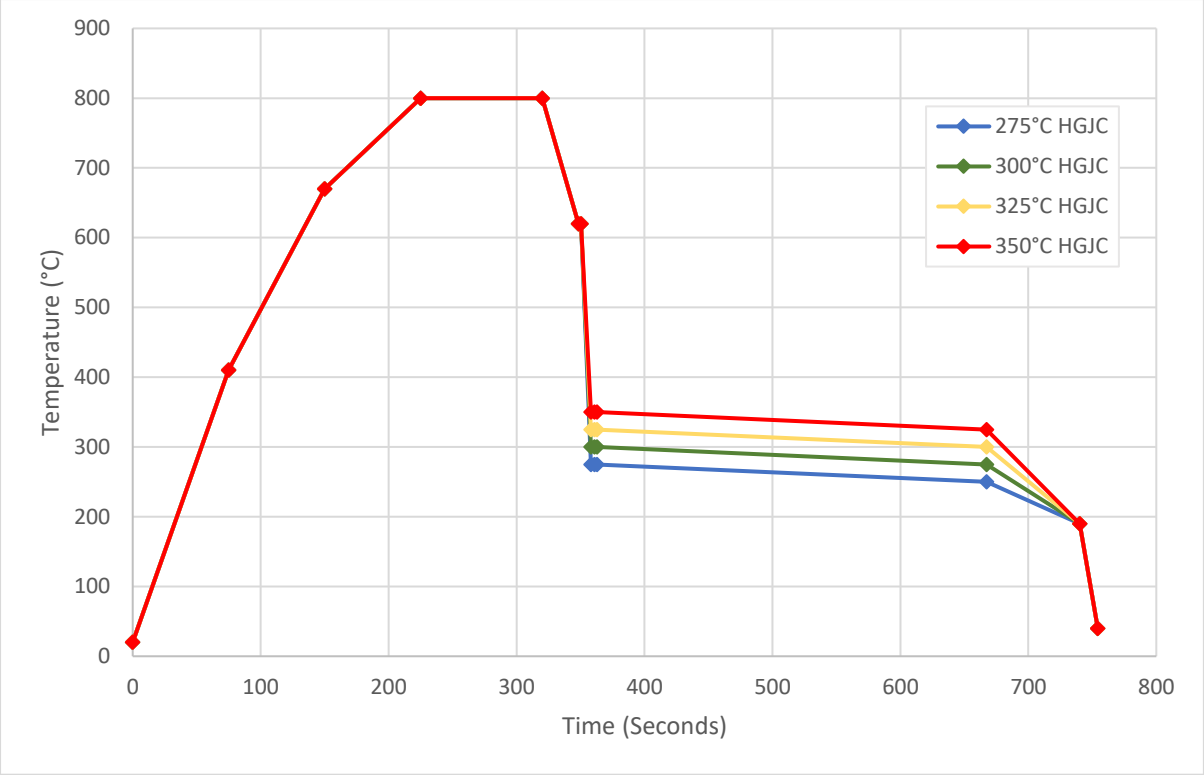

Figure 6.6 Variations in HGJC temperatures used for experimentation.

The effect on the final annealed microstructure is not a pronounced as the effect on the hot band microstructure. There are subtle differences between the three different silicon levels in figure 6.7.

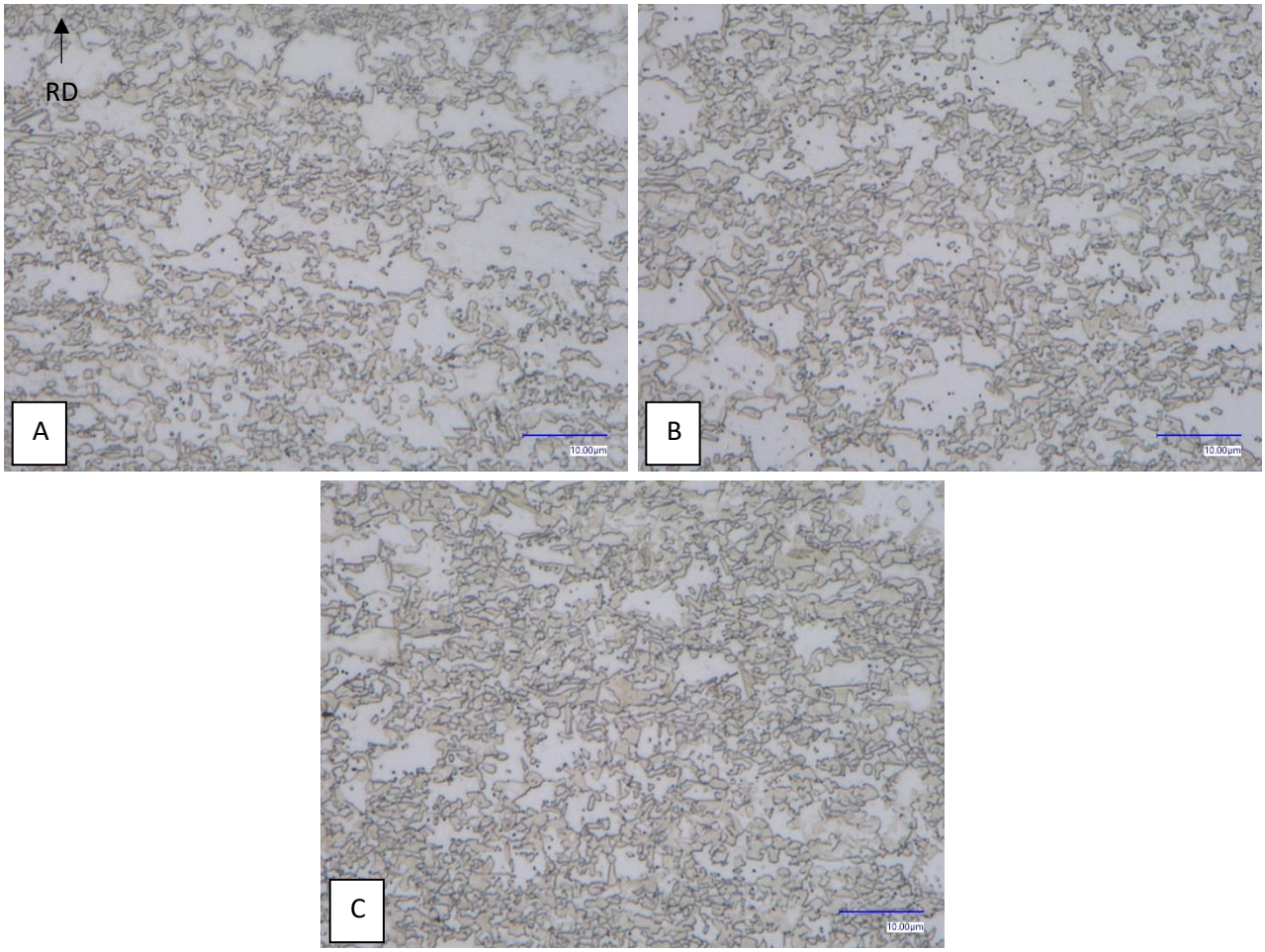

Figure 6.7. Light microscope of (A) low silicon (B) medium silicon and (C) high silicon. All processed with the same annealing conditions at 250°C HGJC temperature. White regions represent ferrite and darker regions are martensite.

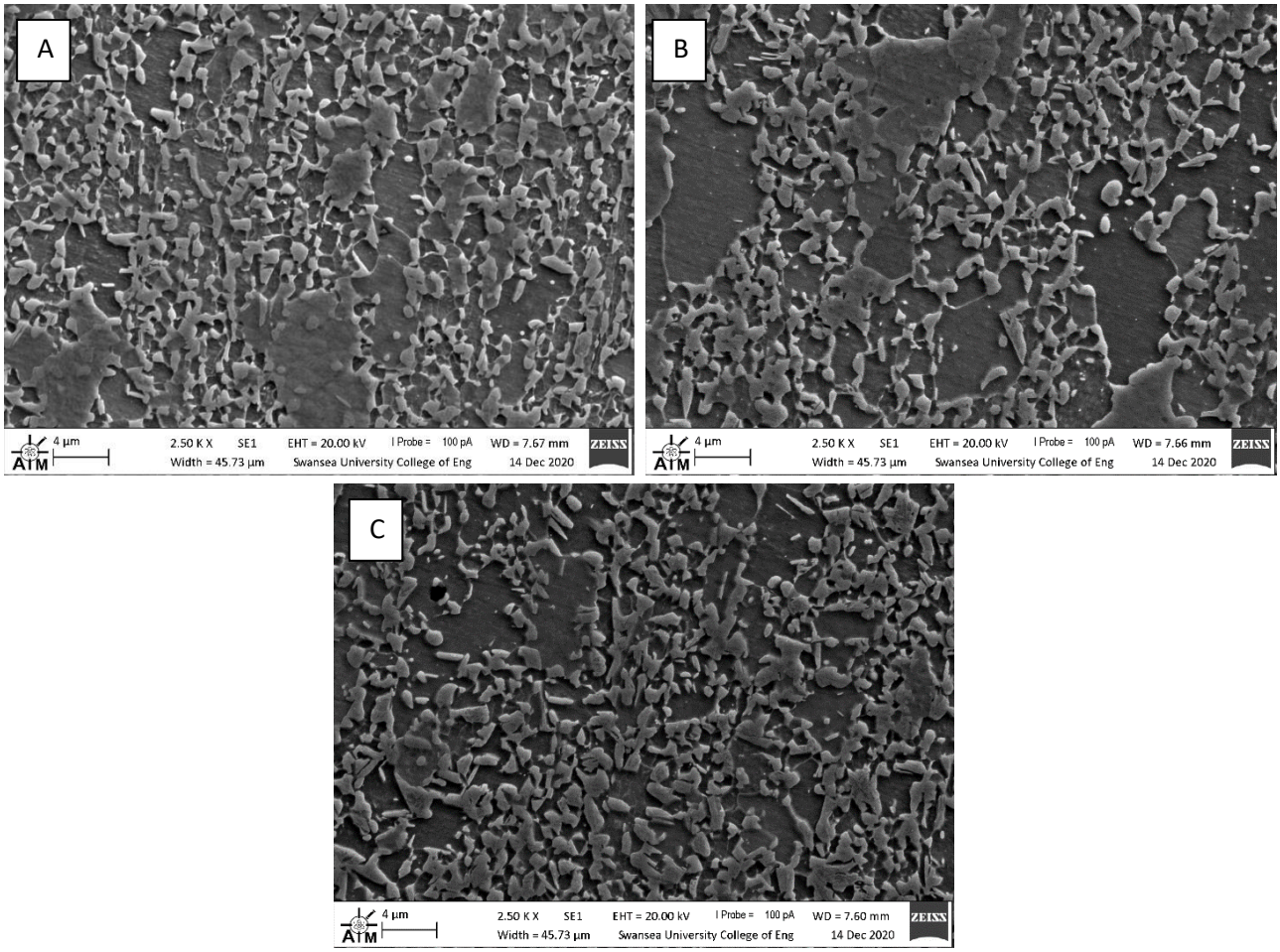

Figure 6.8 SEM microscope of (A) low silicon (B) medium silicon and (C) high silicon. All processed with the same annealing conditions at 250°C HGJC temperature. The lighter regions represent martensite whilst the darker regions are background ferrite.

As the silicon levels increase from 6.7A to 6.7C, so does the volume fraction of martensite. Therefore, the increase in martensite has led to a decrease in the volume fraction of ferrite. Furthermore, the larger grains of ferrite in the microstructure have also decreased. The increase in silicon has led to a progressively more refined microstructure. This can also be seen in figure 6.8A to 6.8C

Research has shown that the nucleation of austenite during the heating of a DP steel with a starting microstructure of ferrite and pearlite occurs predominantly at the interphase boundaries between pearlite colonies and ferrite grains, followed by nucleation at recrystallized ferrite grain boundaries (89). A more refined initial microstructure, combined with higher pearlite volume fraction in the higher silicon samples should allow for multiple nucleation sites for austenite growth which creates a more uniform and refined final microstructure, this can be seen in figures 6.7 - 6.9.

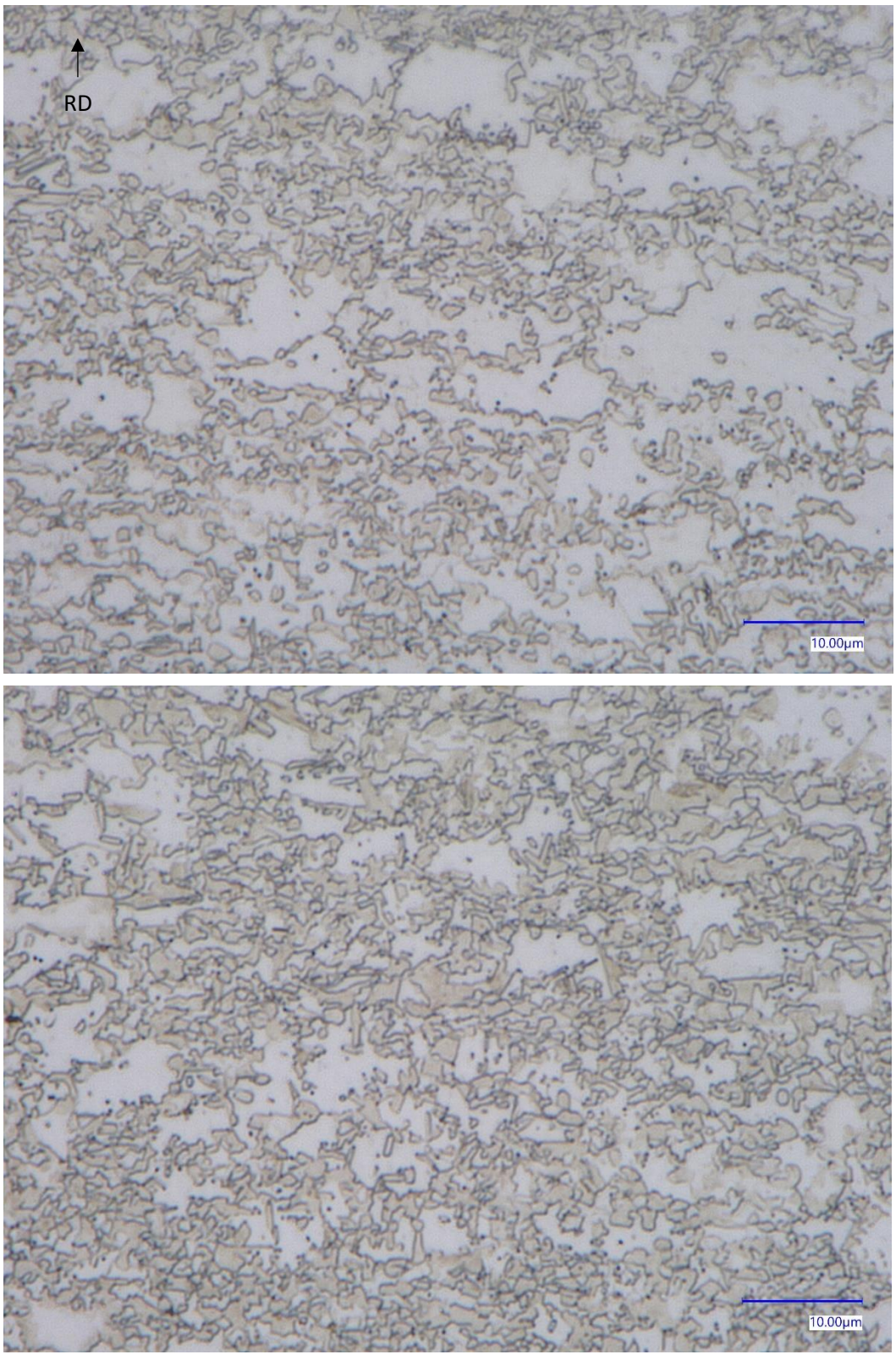

Figure 6.9. Image of low silicon steel (top) and high silicon steel (bottom). White areas represent ferrite whilst the darker areas represent martensite. Processed with the same annealing conditions at 250°C HGJC temperature. Note a more refined microstructure at higher silicon content (bottom).

Figure 6.9 shows that there is less observable directionality present in steel as the silicon content is increased. Directionality can lead to mechanical properties that are anisotropic, meaning unwanted variation in mechanical properties dependant on whether the material is tested in a longitudinal or transverse direction.

The directionality present can be linked to the initial hot rolled microstructure. Areas of pearlite colonies in the rolling direction can be seen in the low silicon images of figure 6.2a. It's likely that during the reheating stage of the annealing process that the initial nucleation and growth of austenite would occur at those areas of high carbon containing pearlite colonies, therefore would continue to grow along the existing lines of the rolling direction.

Another consideration is the effect that the silicon will have on the recrystallisation of ferrite and the formation of austenite. The growth of austenite is dictated by the competition between austenite formed at pearlite areas its simultaneous nucleation at newly recrystallised ferrite boundaries (82). This process is not only controlled by the diffusion of carbon, but also by substitutional elements present in the alloy.

Because silicon is a ferrite forming element, it can be expected that its addition will promote recrystallisation of ferrite at lower temperatures. Therefore, it can be expected that as austenite nucleation takes place, the ferrite will recrystallise earlier during reheating compared to the low silicon containing material, this facilitates multiple austenite nuclei along the ferrite grain boundaries (124). This allows for competition between the austenite nucleating in former pearlite regions and at ferrite boundaries, leading to a more refined microstructure.

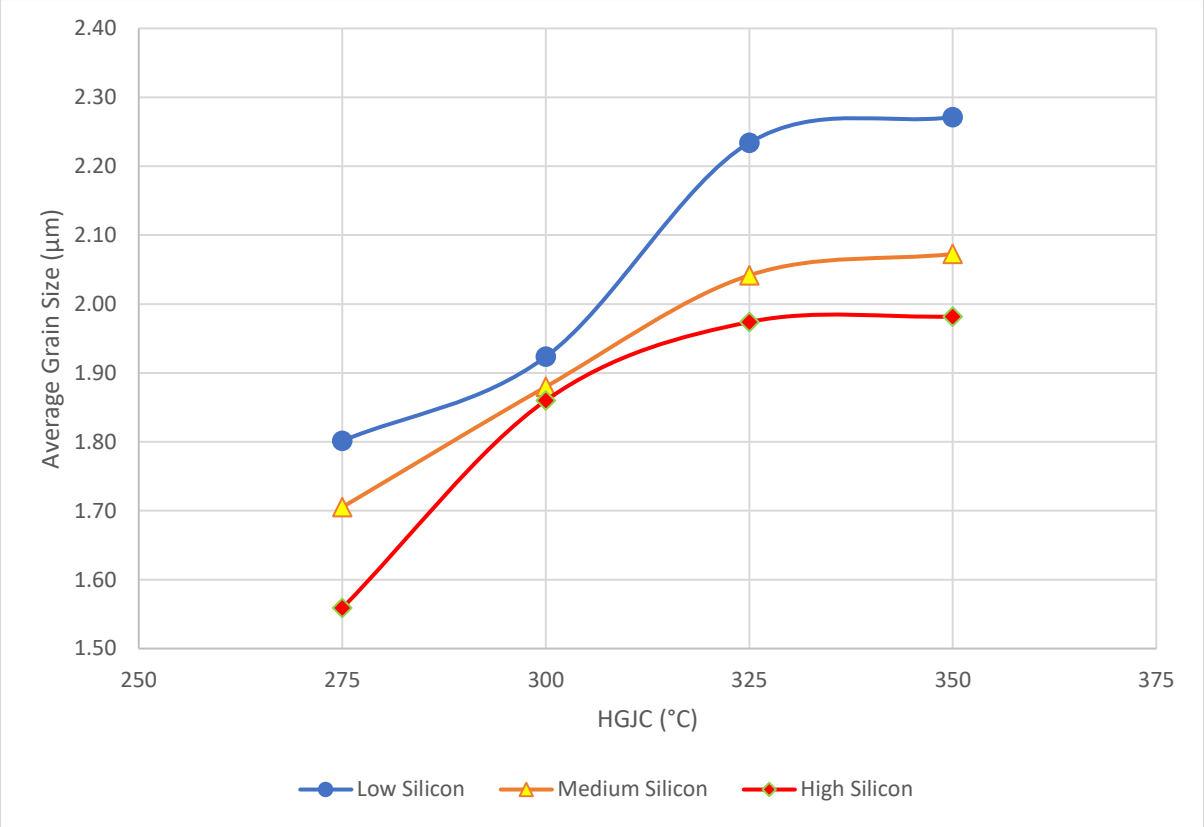

Figure 6.10. Average grain size calculated using mean linear intercept method. Grain size for each silicon variant at each HGJC temperature. Measurement error calculated to +/-0.14µm.

Figure 6.10 shows a larger average grain size as the HGJC temperature is increased. It is also clear that as the silicon content is increasing the average grain size decreases, therefore the silicon is refining the microstructure.

Silicon free DP steel will require a longer time at temperature for the ferrite grains to recrystallise when compared to silicon containing DP steel. This leads to the growth of austenite in carbon rich pearlite regions which do not compete with grain boundary austenite due to its delayed nucleation, producing coarse elongated islands of austenite along the rolling direction (124) as shown in figure 6.9 (top).

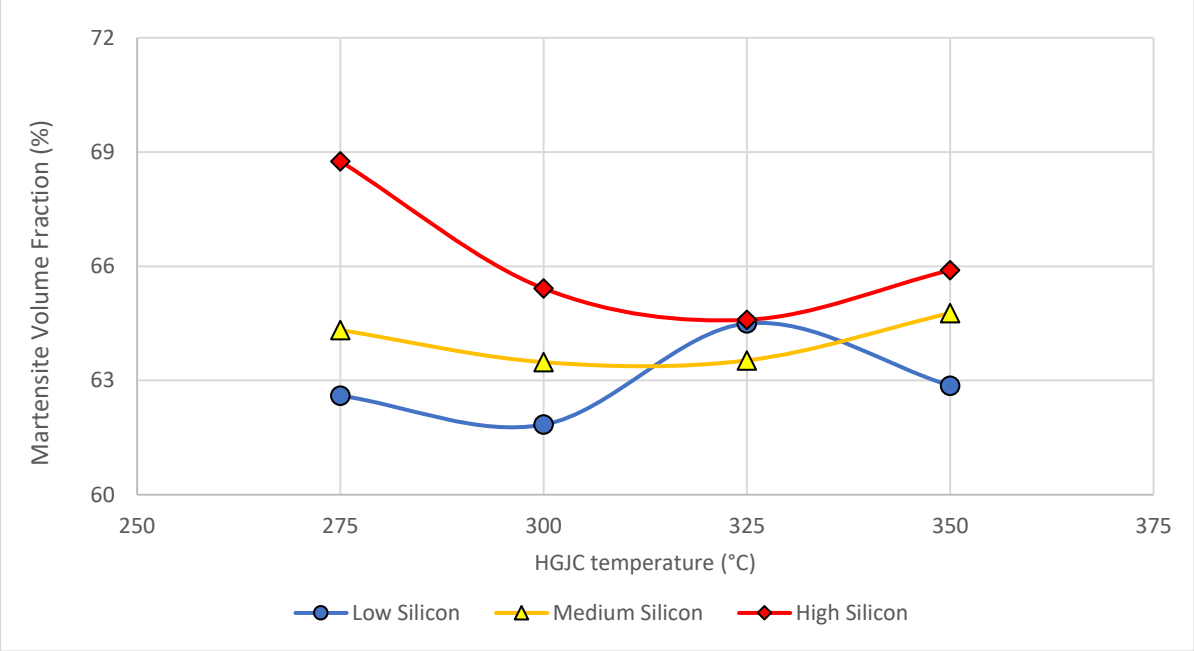

Figure 6.11. Average martensite volume fraction for each silicon content at each HGJC temperature. Error calculated within approximately +/-2%

Figure 6.11 shows the higher silicon content contains a greater volume fraction of martensite in the final microstructure compared to the lower silicon containing steels tested here. The larger volume fractions of the harder martensitic phase observed as a function of Si content, leads to the higher measured strengths which is shown in figure 6.12.

6.2.3. Effect of silicon on the mechanical properties of cold rolled annealed DP steel

The cooling rate has a profound effect on the final mechanical properties of dual phase steels. Figure 6.12 shows the effect of HGJC temperature soak on the ultimate tensile strength of each of the alloy investigated. A lower soak temperature in the HGJC significantly increases the final tensile strength of the material, regardless of the silicon content. Typically, a ~100MPa increase is seen in UTS from a low HJGC temperature of 275°C to the higher HGJC temperature of 350°C. This increase can be attributed to a higher volume fraction of ferrite in the microstructure as well as an increase in the volume fraction of tempered martensite present.

As these tests reflect a continuous annealing line running at a constant processing speed, the cooling rate required to achieve a HGJC temperature of 350°C requires cooling of 38°C/s, compared to 275°C which requires 48°C/s. This change is sufficient to change the type of second phase constituent from un-tempered martensite to a tempered martensite and bainite. The comparatively lower strength of bainite can decrease the overall tensile properties of the material (88).

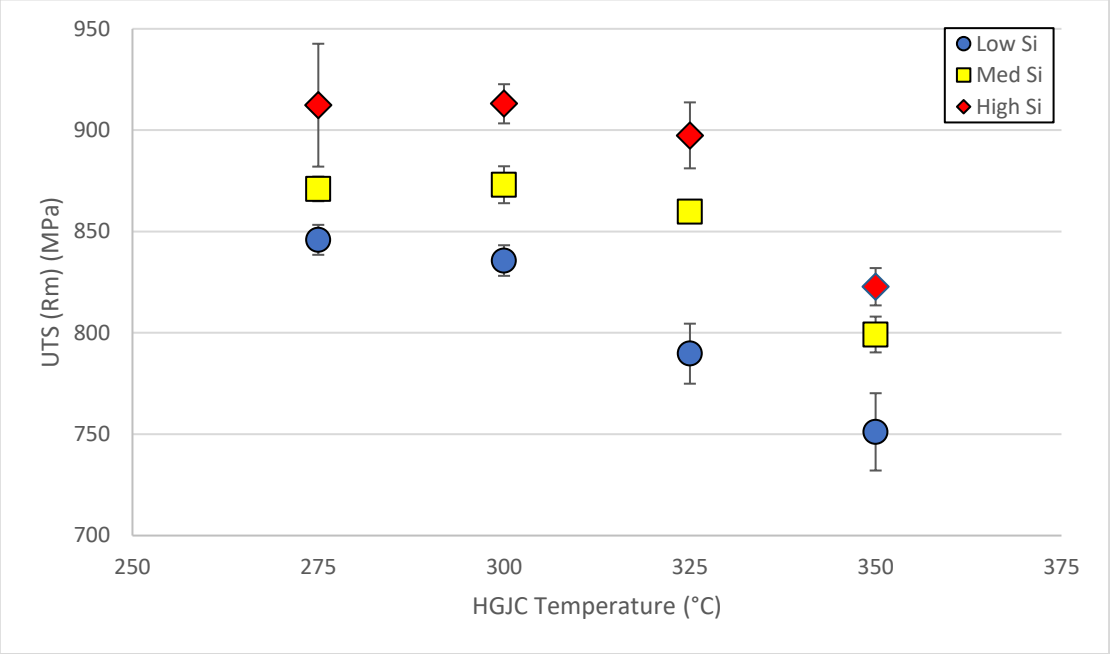

Figure 6.12 Tensile strength at varying HGJC cooling temperatures and silicon contents, an increase in tensile strength seen as silicon content increases.

The trend of decreasing UTS with increased soak temperature is repeated for each silicon content. This can be linked directly a higher volume fraction of ferrite being present at lower silicon content for each soak temperature. The UTS is shown to increase with the addition of silicon at each HGJC temperature. The higher the silicon content, the higher the measured UTS.

Literature agrees that an increase in silicon does improve the tensile strength of DP steels (135)(138), and work by Drumond et al. (100) states that the increase in silicon content increases the strength of DP steels owing to the formation of a high volume of homogenous austenite with high hardenability. This gives rise to a higher volume fraction of martensite in the final structure (100). This is complemented by a refinement in the microstructure of both ferrite and martensite, which is known to give an improvement in the strength characteristics of a material as per a typical Hall-Petch relationship (139).

An improvement in the strength at higher silicon content was also noted by Cai et al. (97). This was linked to the formation of fine equiaxed grains, where silicon increases the nucleation rate of ferrite. This is driven by increased activity of carbon in austenite by inhibiting carbide formation, driving the change from austenite to ferrite.

Similarly, silicon increases the formation of new ferrite. This allows for the enrichment and stabilisation of austenite with carbon and has been shown not only to lower the martensite start temperature, but to also retard the bainite reaction. This leaves a higher proportion of the remaining austenite turning to martensite upon final cooling (7). A refined grain size, as shown in figure 6.10, also improves strength.

Another benefit of silicon is that it is known to retard the martensite tempering reactions (140). The tempering of martensite means that any austenite that transforms to martensite during the overage section would be less likely to decompose and therefore retain its strength.

The relationship between proof strength and Si levels is shown in Figure 6.13. There is a subtle increase in strength with increasing silicon content. An increase in temperature gives a reduction in proof strength for the higher silicon containing grades, however a sharp increase is noted in the low silicon grade.

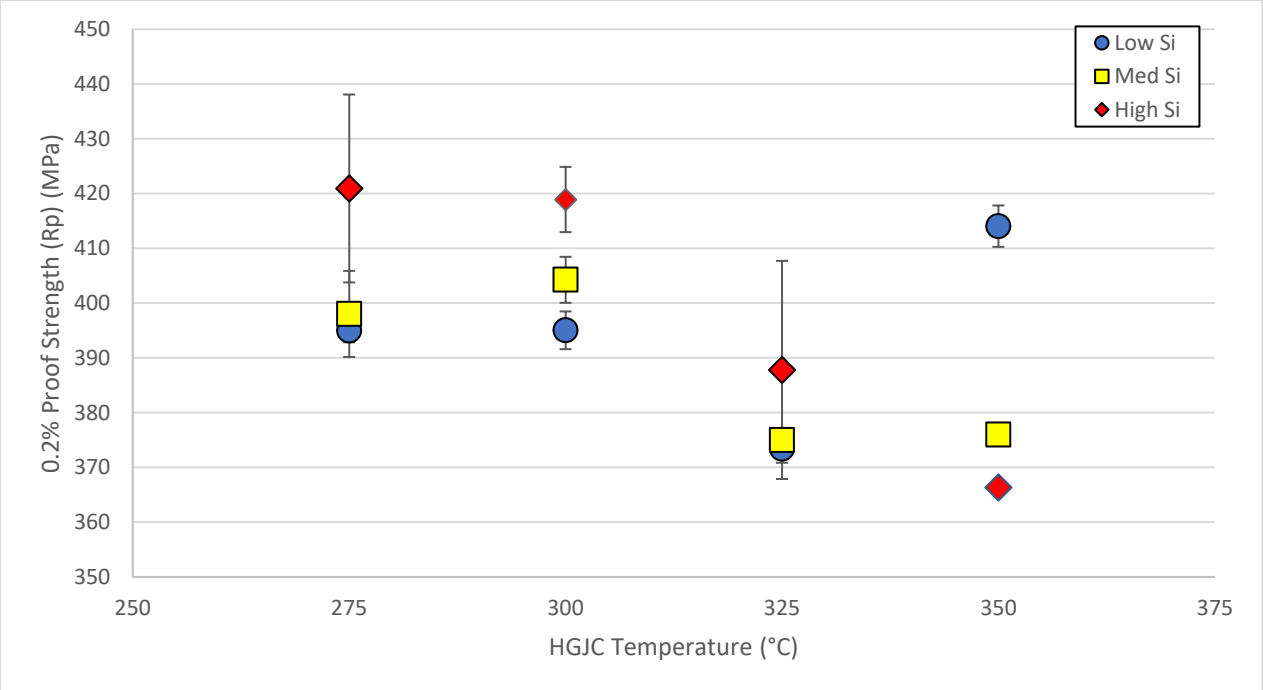

Figure 6.13. Proof Strength at varying HGJC cooling temperatures and silicon contents. Slight increase in proof strength is seen as silicon increases, with the exception of 350°C where a spike is seen for the low silicon results.

The relationship between proof stress and HGJC can be explained due to the increase in tempered martensite and bainite with increasing soak temperature. Typical DP steels have a low proof strength (PS) to tensile strength (TS) ratio in the region of 0.4-0.5, this is due to the expansion of grains during the transformation from austenite to martensite which deforms the ferrite and creating a high density of mobile dislocations (7). Replacing martensite with either tempered martensite or bainite not only reduces the strain hardening rate, but also increases the PS/TS ratio (8). This increase can be seen in Figure 6.14, which shows the difference between proof strength and tensile strength.

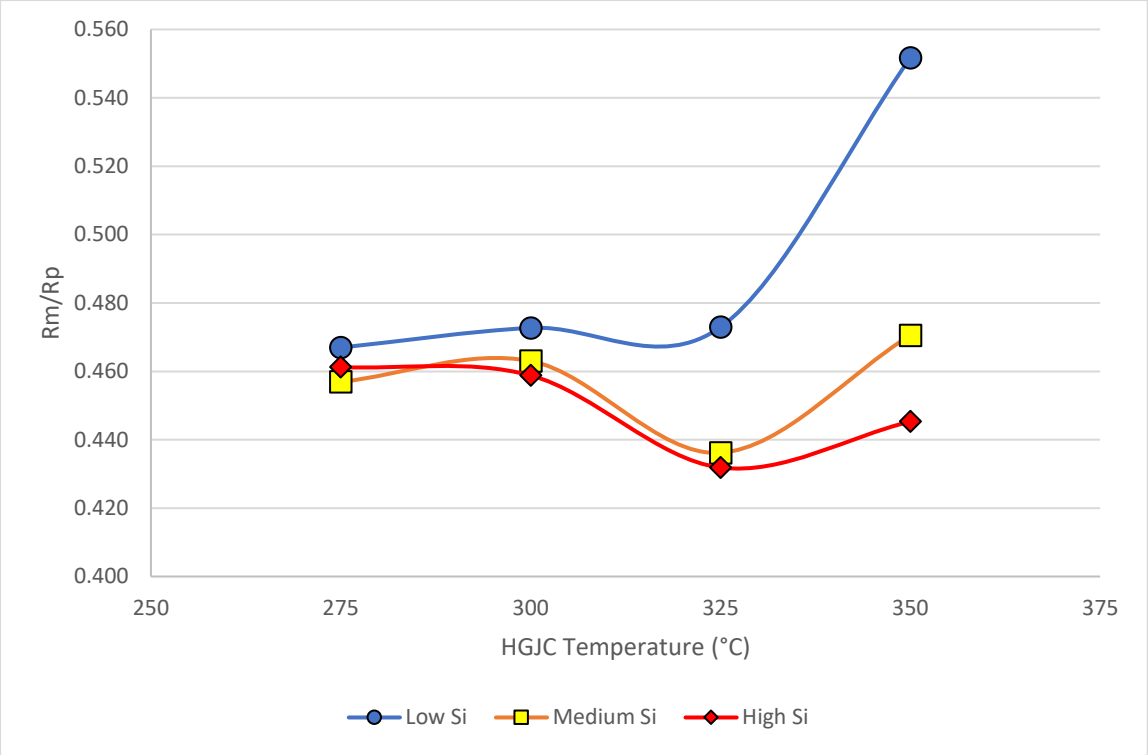

Figure 6.14. PS/TS ratio at varying HGJC cooling temperatures and silicon contents. An increase in the PS/TS ratio can indicate a different microstructural presence such as bainite.

The relatively consistent PS/TS ratio shown at the lower HGJC for all silicon contents indicates that the microstructure of the steel is primarily ferrite and martensite. As the soak temperature increases a higher volume fraction of bainite or tempered martensite is present, increasing the PS/TS ratio. A return of yield point was seen for the low silicon content at 350°C HGJC temperature, another indicator of the presence of bainite or tempered martensite in the material.

Increased tempered martensite in the microstructure would lead to a decrease in dislocation density and remove residual stresses around ferrite, this combination of events can cause a reappearance of the discontinuous yield point (141). The increase silicon content has been shown in literature to eject interstitial elements such as carbon from ferrite (98), which would enrich the surrounding austenite. This would lower the Ms temperature and retain a high dislocation density around ferrite and could explain the lack of definitive yield point in the higher silicon results. Figure 6.15 shows the returning yield point.

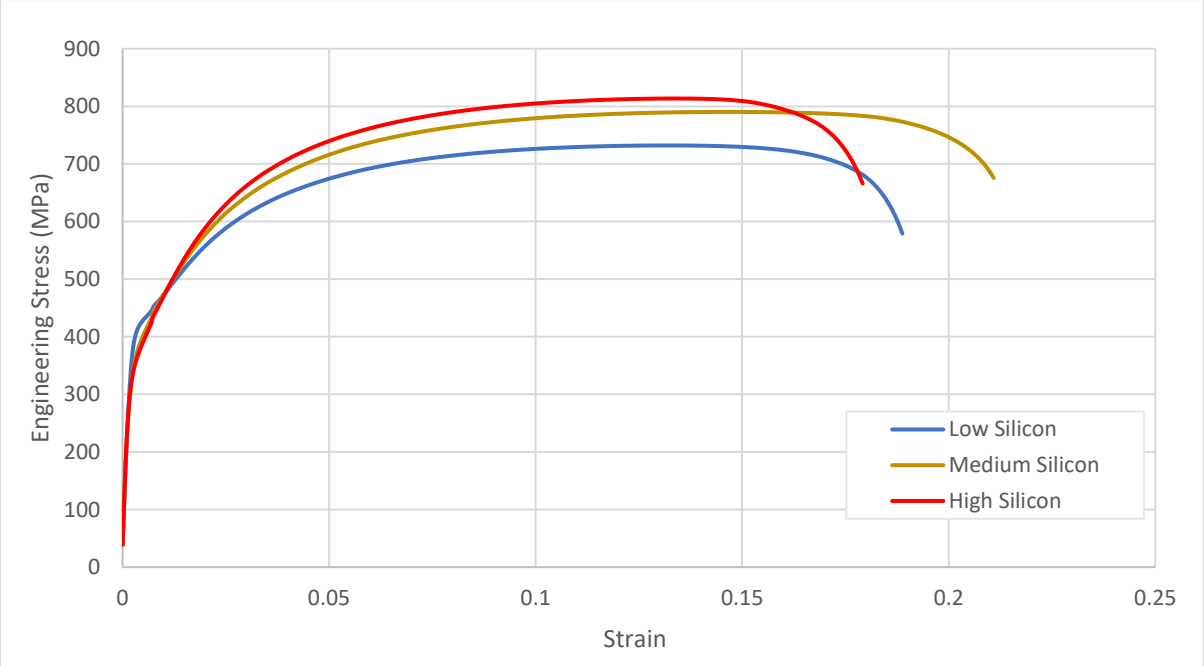

Figure 6.15. Tensile test curves for low, medium and high silicon at 350C HGJC temperature. Note the return of yield point visible on the low silicon curve, an indicator of bainite presence.

Figure 6.16 shows the measured elongation for the increasing Si levels treated at different HGJC temperatures. As the HGJC temperature increases, an increase in ferrite is seen in the microstructure, accompanied by an increase in ductility.

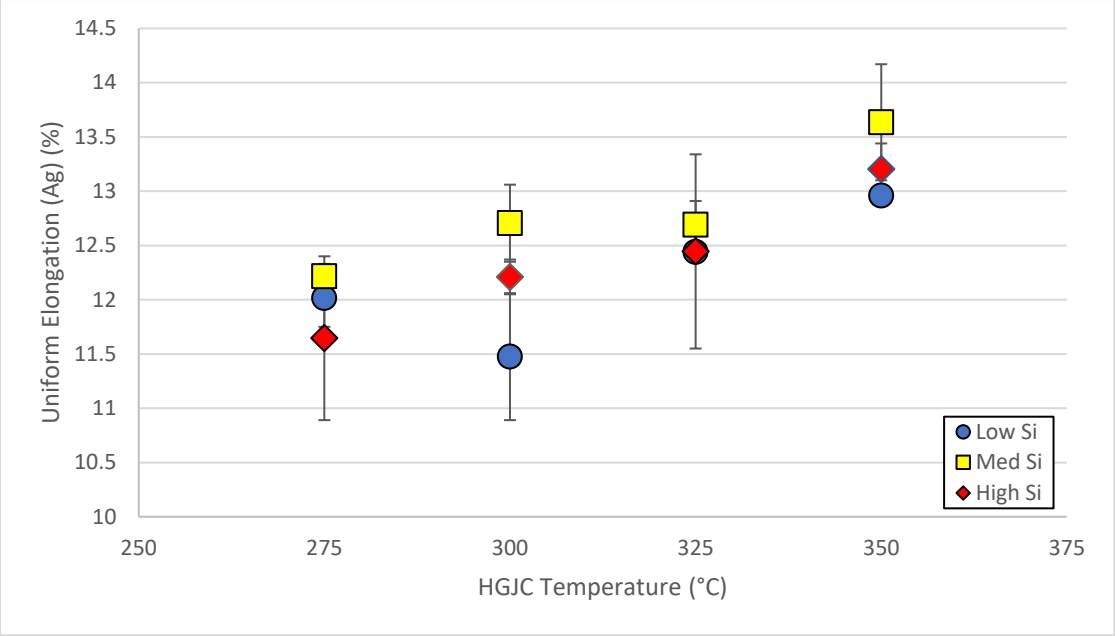

Figure 6.16. Uniform elongation properties at varying HGJC cooling temperatures and silicon contents. Similar results are seen for all silicon contents, with medium silicon being slightly higher in elongation for all temperatures.

The results show that increasing the silicon content not only increases the strength of the material but also retains the ductility, as seen in figure 6.16 and 6.17. The increase in uniform elongation can be linked to the increase in strain hardening rate, which is increased through the addition of silicon. This is illustrated by an increasing n-value and the difference between total and uniform elongation, which is smallest at the lower HGJC, which is shown by higher proportion of martensite in the microstructure.

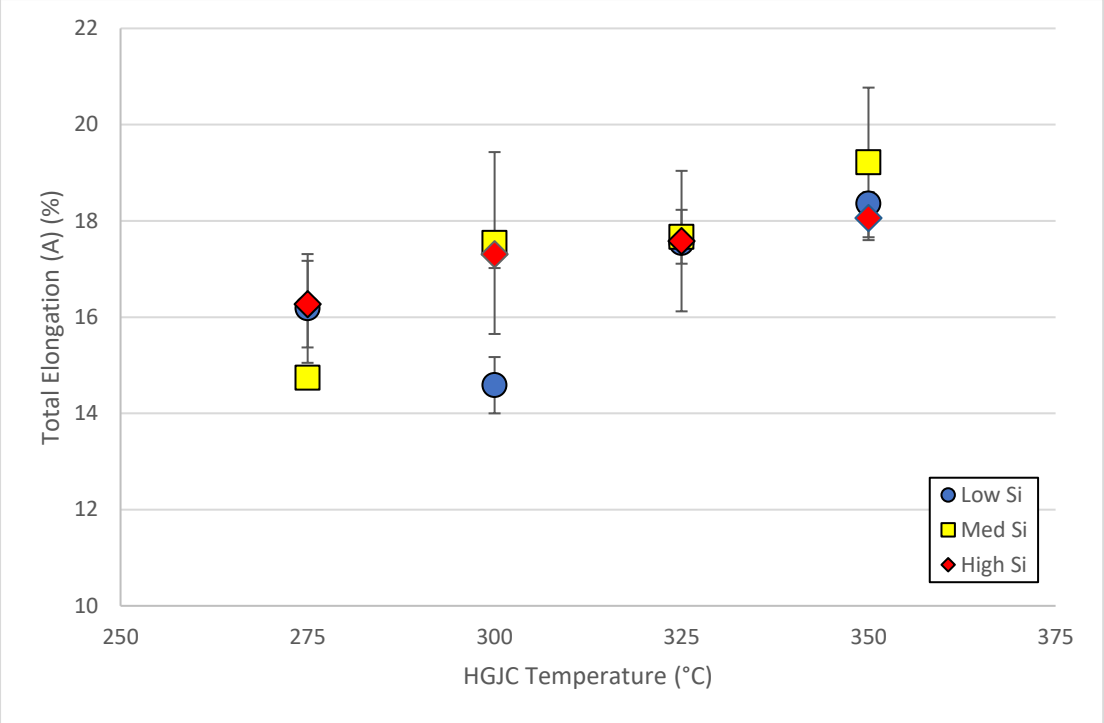

Figure 6.17. Total elongation properties at varying HGJC and silicon content. Little difference is seen in total elongation as silicon content is increased, general trend of increased ductility as HGJC temperature increases is observed.

Another possible reason for the increased ductility at higher HGJC temperatures is the refinement and fine dispersion of the martensite. This gives improvement to both uniform and total elongation due to the martensite having smaller voids in the microstructure, therefore delaying their coalescence to form the crack that would cause material fracture as described by Erdogn et al. (142).

To show the improvement of strength and ductility, the values can be multiplied together and shown in figure 6.18. The higher the value seen, the better the strength / ductility combination.

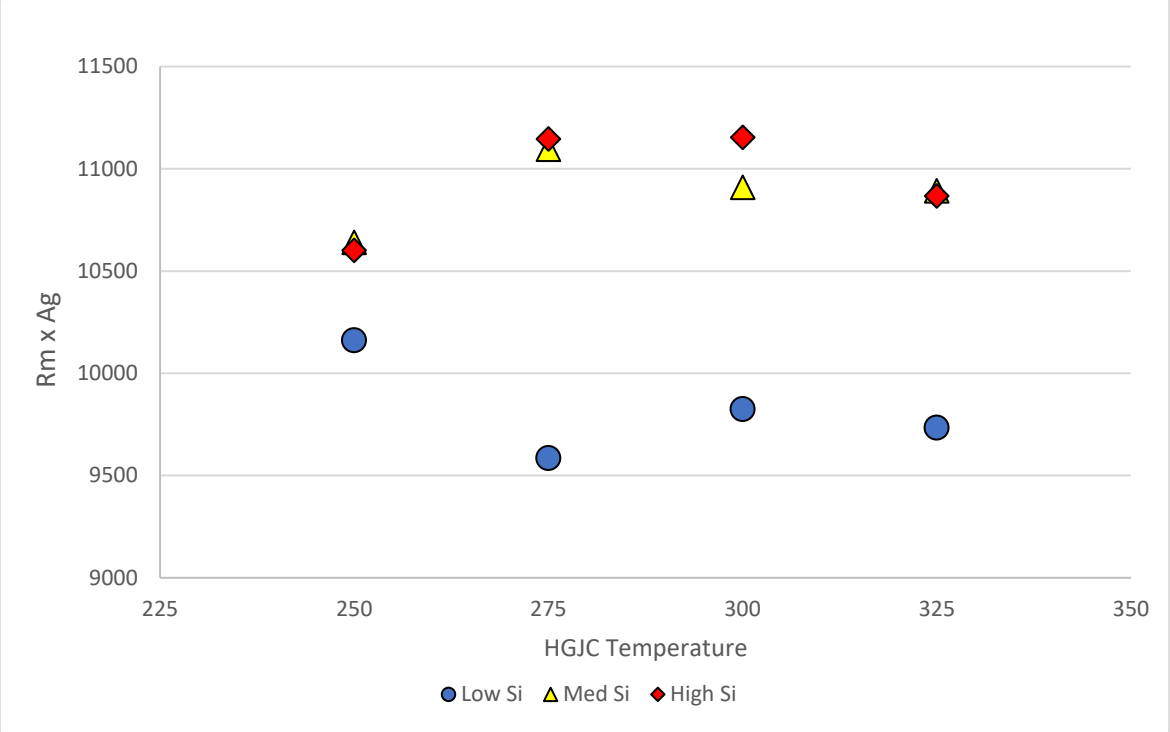

Figure 6.18. UTS x Uniform elongation for each chemistry variant plotted against HGJC temperature. An increased ratio indicates a higher strength to ductility ratio which has been seen in other bodies of work (96)

There is a clear indication that the medium and high silicon additions to DP steel are beneficial to the strength / ductility balance, with the benefits of adding silicon also noted in work by Fonstein et al. (96). Figure 6.18 shows these results match other literature where an improvement in the strength to ductility balance was seen and is particularly prevalent at higher HGJC temperatures when increased silicon additions are added.

A further requirement for a DP steel is the ability to improve yield strength post part pressing and paint curing, known as bake hardening. For DP steel that is produced against an industrial standard, typically the Euronorm EN 10338, there is a requirement of achieving a 30MPa increase post bake hardening. The results from the BH testing are shown in figure 6.19.

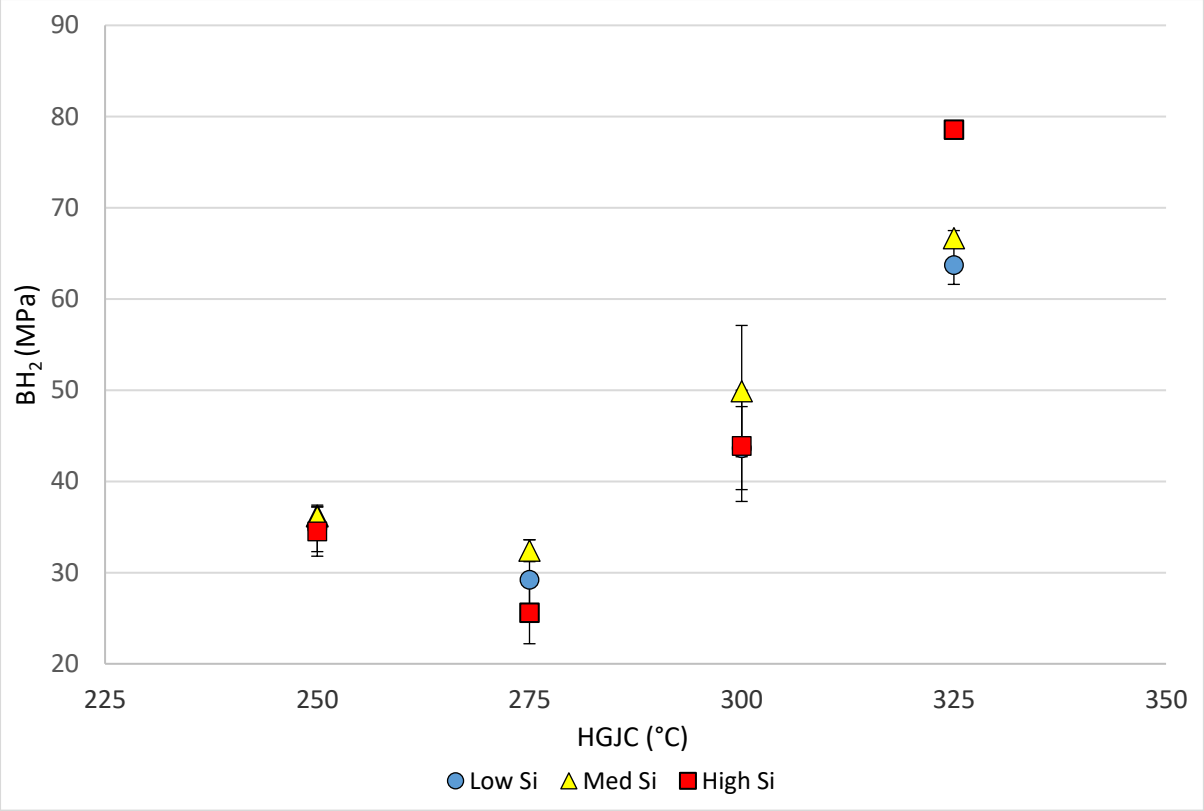

Figure 6.19. Bake Hardening results for each silicon variant against the HGJC temperature. Limited impact noted from increasing silicon content.

It has been established that the BH response is related to the degree of supercooling that occurs from the intercritical region. At higher supercooling rates, where the HGJC temperature is lower, the rate of carbide nucleation is greater during the overage section. This combined with a large volume of dislocations limits the amount of solute carbon atoms free to pin the dislocations leading to a lower BH response (130).

Due to lower carbide precipitation during the overage section, the higher HGJC temperatures have higher free solute carbon concentration during the bake hardening. Therefore, Cottrell atmosphere formation and carbide precipitation during the baking process is promoted leading to an increase in the observed BH response (129).

The effect of silicon additions on bake hardening seems to be limited. A small increase in BH response of around 10MPa is seen as the HGJC temperature is increased to 350°C for the highest silicon content. Work by Hanai et al. (143) has suggested that silicon gives rise to an increase in the solute carbon content, as well as providing grain refinement. This has shown to be beneficial to BH

response and is likely to be a reason for some improvement in response at the higher HGJC temperature.

The decrease in grain size can be seen in figure 6.10. Refined ferrite grain size has been noted to improve bake hardenability due to accelerated carbon diffusion to grain boundaries (144). The refined grain size means shorter diffusion paths for carbon in ferrite to enable the pinning of dislocations present in the ferrite / martensite interface. For example, at 325°C HGJC temperature, the average grain size decreased from 2.23 µm to 1.97µm.

Conversely to the benefits of refinement, silicon also increases the cleanness of ferrite, by enhancing partitioning of carbon to austenite (95). Therefore it can be expected that increasing the silicon content would increase the carbon content of martensite (135). Partitioning of carbon from ferrite means it has a lower carbon content, so a lower BH response could be expected particularly from within the ferrite grains.

Whilst an improvement in BH might be seen from a refined microstructure, the partitioning of carbon from ferrite may also reduce the BH response during a BH test, so any benefit may be lost. This could explain the reason silicon does not show an improvement on BH for this work.

6.3. Conclusions

An increase in the HGJC temperature leads to a drop in strength and an increase in ductility. An increase in silicon levels improves both the tensile strength and the yield strength at all HGJC temperatures, without impairing ductility.

The benefit is derived from the hot rolling process where silicon increases grain refinement and a higher volume fraction of pearlite. The finely dispersed pearlite allows for an increase in nucleation sites where it can transform to austenite during the soak section. This leads to a more finely dispersed and higher volume fraction of austenite which on cooling transforms to martensite. The low silicon composition had larger, elongated martensite which is detrimental to strength and ductility.

Limited improvement of BH response was seen by increasing the silicon content. The refinement of the microstructure should improve the BH response, however literature suggests the addition of

silicon partitions carbon from ferrite to austenite, therefore leaving reduced carbon in ferrite to provide the pinning of dislocations.

7. Optimising DP1000 for continuous galvanising

7.1. DP1000 through a continuous galvanising line

A dual phase, DP1000 product is currently being produced at Tata Steel, utilising cold rolled hard iron substrate produced at Tata Steel's IJmuiden plant. There is demand from the automotive industry for this type of advanced high strength steel, that enables further downgauging of automotive components, therefore saving weight and emissions. The capability to produce a galvanised DP1000 product in the UK is therefore desirable.

Owing to its higher strength, demand for the DP1000 product tends to be limited in application for the automotive industry. Therefore, lower volumes compared to commodity grades require the product to be made using a single chemistry that can be processed on both a continuous annealing line and a continuous galvanising line. This introduces complexity as the annealing lines have different heat treatment cycles which are used to achieve the same product, shown in figure 7.1.

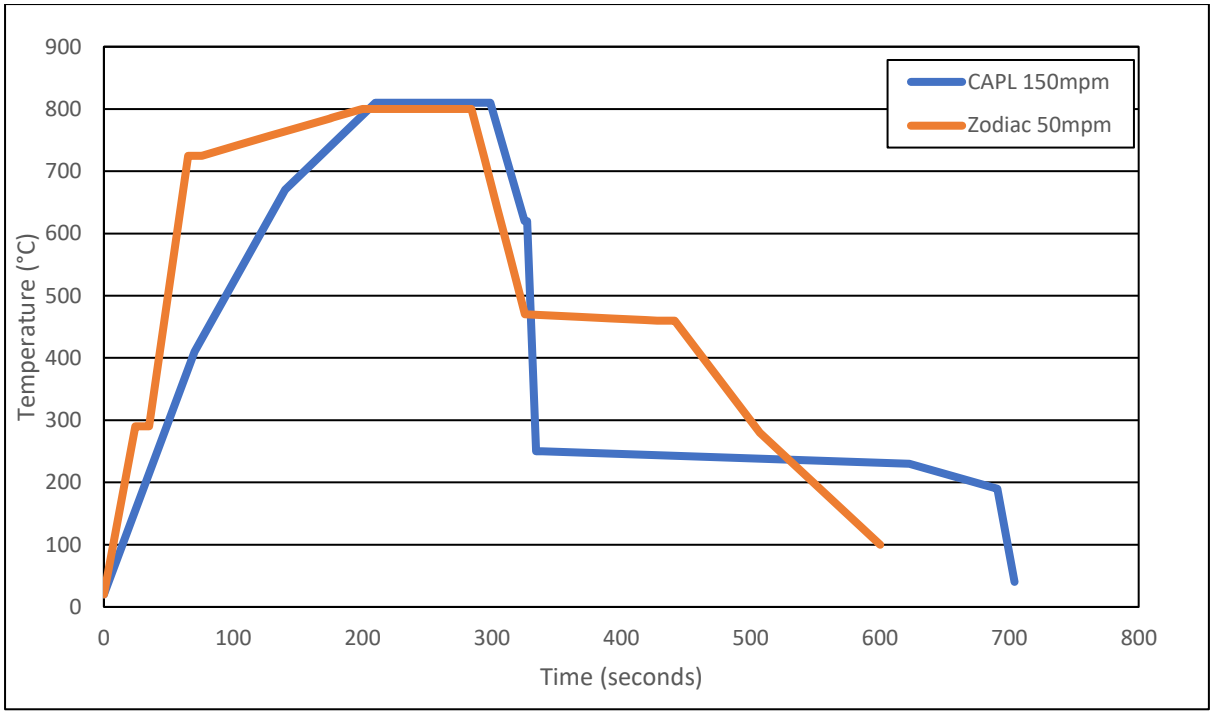

Figure 7.1 Example of each annealing cycle and the differences in time, temperature and speed to achieve the same DP product.

A viable DP1000 chemistry and product is currently produced on Tata's continuous annealing line, labelled grade DP1 in table 7.1. Whilst this grade provides sufficient mechanical properties for use on the continuous annealing line, internal trials using annealing parameters on its continuous galvanising line have shown that the chemistry does not achieve the mechanical property requirements of a DP1000 product (145).

Tata Steel Ijmuiden do have a viable DP1000 product that can be galvanised. This work investigates the potential to process the Ijmuiden chemistry, labelled DP2 in table 7.1, on the Zodiac galvanising line in South Wales.

Table 7.1 Chemistry of DP1000 grades, with Si additions being the most notable difference.

Grade	C (wt%)	Mn (wt%)	Si (wt%)	Ti(wt%)	Cr(wt%)	Nb (wt%)
DP2	0.149	2.242	0.102	0.015	0.552	0.015
DP1	0.160	2.178	0.057	0.027	0.540	0.016

Whilst the two grades listed in table 7.1 are chemically similar, the increase in silicon in DP2, a solid solution strengthener (146)(7), may provide a stable and consistent product that can be processed on Zodiac. This work will evaluate the DP2 grade and assess its suitability for the UK continuous galvanising line.

Several 1200mm width steel sheets of 1mm thickness cold rolled unannealed DP1 chemistry were received from Tata Steel IJmuiden steel works. These samples have then been annealed on the CASIM and tensile tested in the same procedure stated in section 4.

To accurately measure the A_{c1} and A_{c3} temperature, three cold rolled unannealed samples of 20mm x 5mm were heated in a Netzsch DIL 402 dilatometer, and an average taken. The samples were heated up at a rate of 35°C/min to a temperature of 1200°C. The A_{c1} temperature measured to be 719°C and the A_{c3} temperature 847°C. These values can then be used to determine the intercritical temperatures for the experiments, taking this information and using a processing window within the galvanising line capability, the temperatures and times tested for the continuous galvanising cycle are shown in Table 7.2.

Table 7.2. Variations of annealing cycles for continuous galvanising processing route

Direct Fire Furnace Temperature (ºC)	**Soak Temperature (ºC)**	**Overage Start- Finish Temperature (ºC)**
725 / 735	780 / 810 / 840	470-460 500-480

7.2. Results and Discussions

7.2.1. Effect of processing parameters on the microstructure

A hot rolled substrate is produced with a ferrite / pearlite microstructure. This allows for the softest microstructure when processing through the cold mill to minimise the rolling loads during cold rolling. The cold rolling process then reduces the hot band thickness by around 50%-60% dependant on the final customer gauge. The initial cold rolled substrate DP2 is shown in figure 7.2:

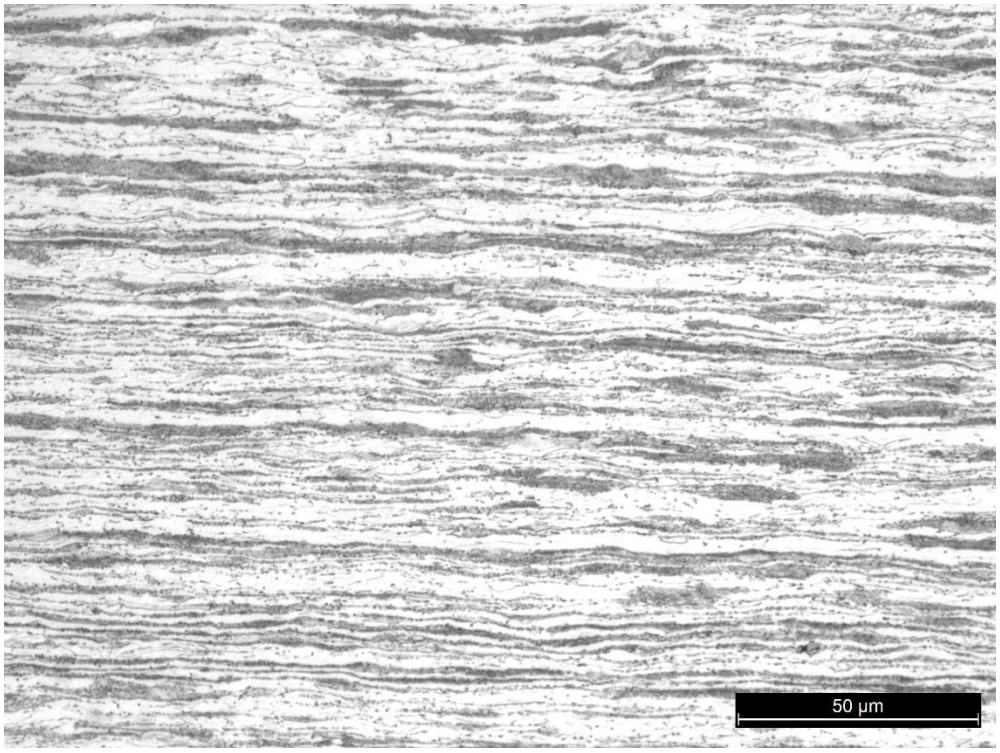

Figure 7.2 Initial cold rolled hard iron microstructure for chemistry DP2. Highly deformed microstructure in the rolling direction, lighter regions are ferrite, whilst the darker regions are pearlite.

Light microscopy has been undertaken to reveal any differences that may exist between the two DP1000 type chemistries. As expected, with the same processing conditions, the similarity under the microscope is very similar, as seen in figure 7.3.

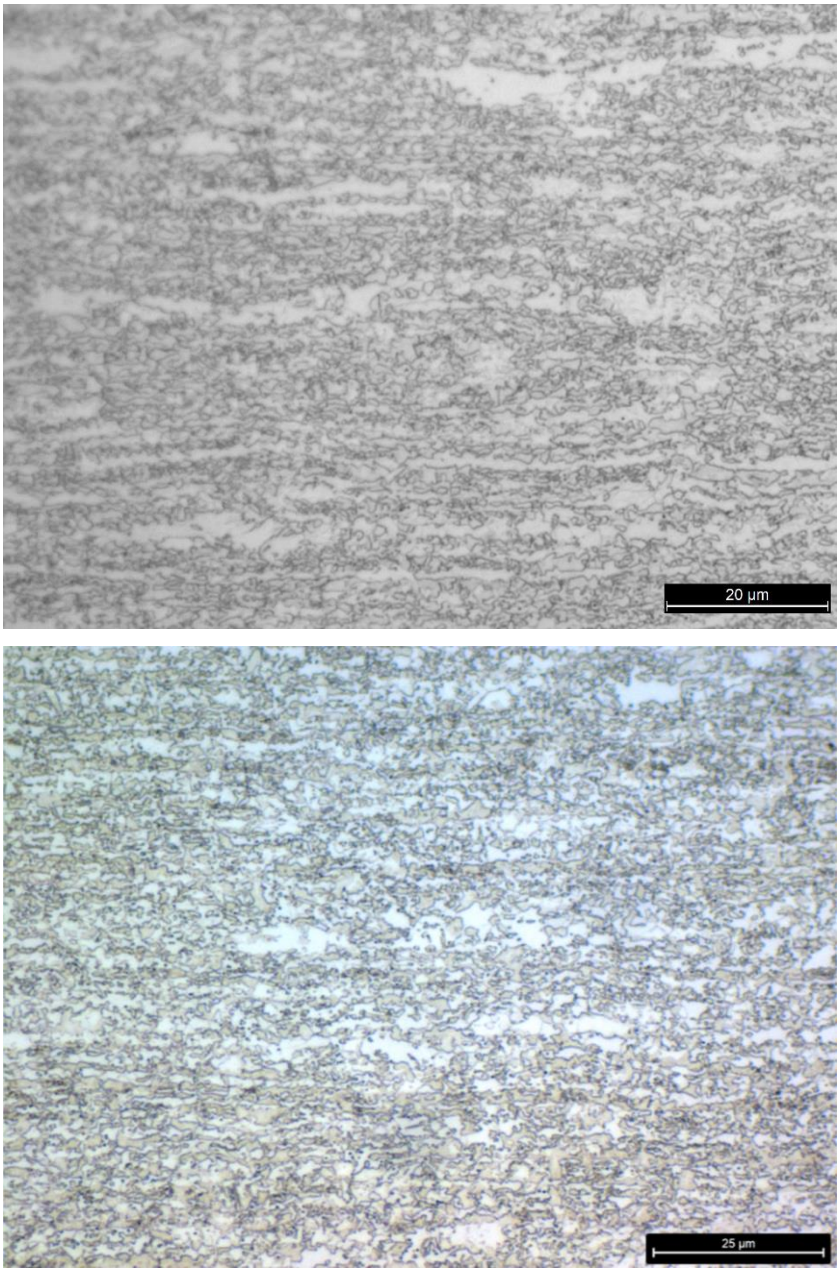

Figure 7.3. Light Microscope comparison between existing DP1 grade (top) and DP2 grade (bottom) at low intercritical soak temperature of 780°C. The white background phase is ferrite whilst the brown phase is martensite.

The examples in figure 7.3 have both processed with a low soak temperature of 780°C and an overage temperature of 460°C. The lower soak temperature shows directionality present in the microstructure from the cold rolling process, this would lead to anisotropic mechanical properties (147).

Larger ferrite grains are also seen at lower soak temperatures, it is likely that grain growth is occurring from the initial cold rolled ferrite, causing an enlargement of ferrite grains, rather than the recrystallisation of ferrite which is shown to occur at higher annealing temperatures. It is clear from

these images that there is a high-volume fraction of refined martensite present in the microstructure, with a smaller amount of ferrite.

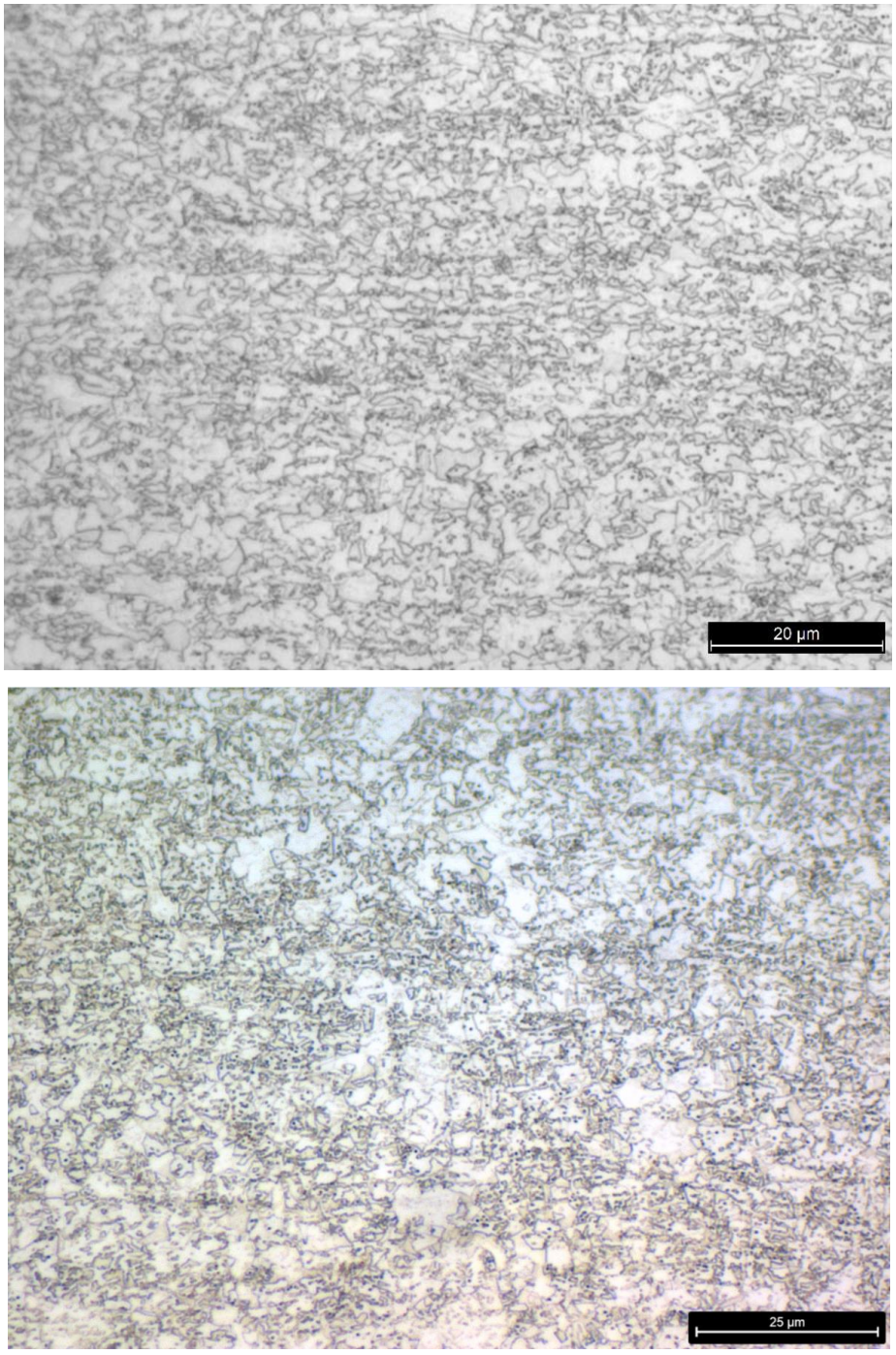

Figure 7.4. Light Microscope comparison between existing DP1 grade (top) and DP2 grade (bottom) at higher intercritical temperature of 840°C. The white background phase is ferrite whilst the brown phase is martensite.

Whilst the higher annealing temperatures shown in figure 7.4 shows less directionality, it exhibits an increase in the ferrite grain size in comparison to the lower intercritical temperature. The higher temperature provides an increase in energy needed for grain growth. This can be seen more clearly in the SEM images in figure 7.5.

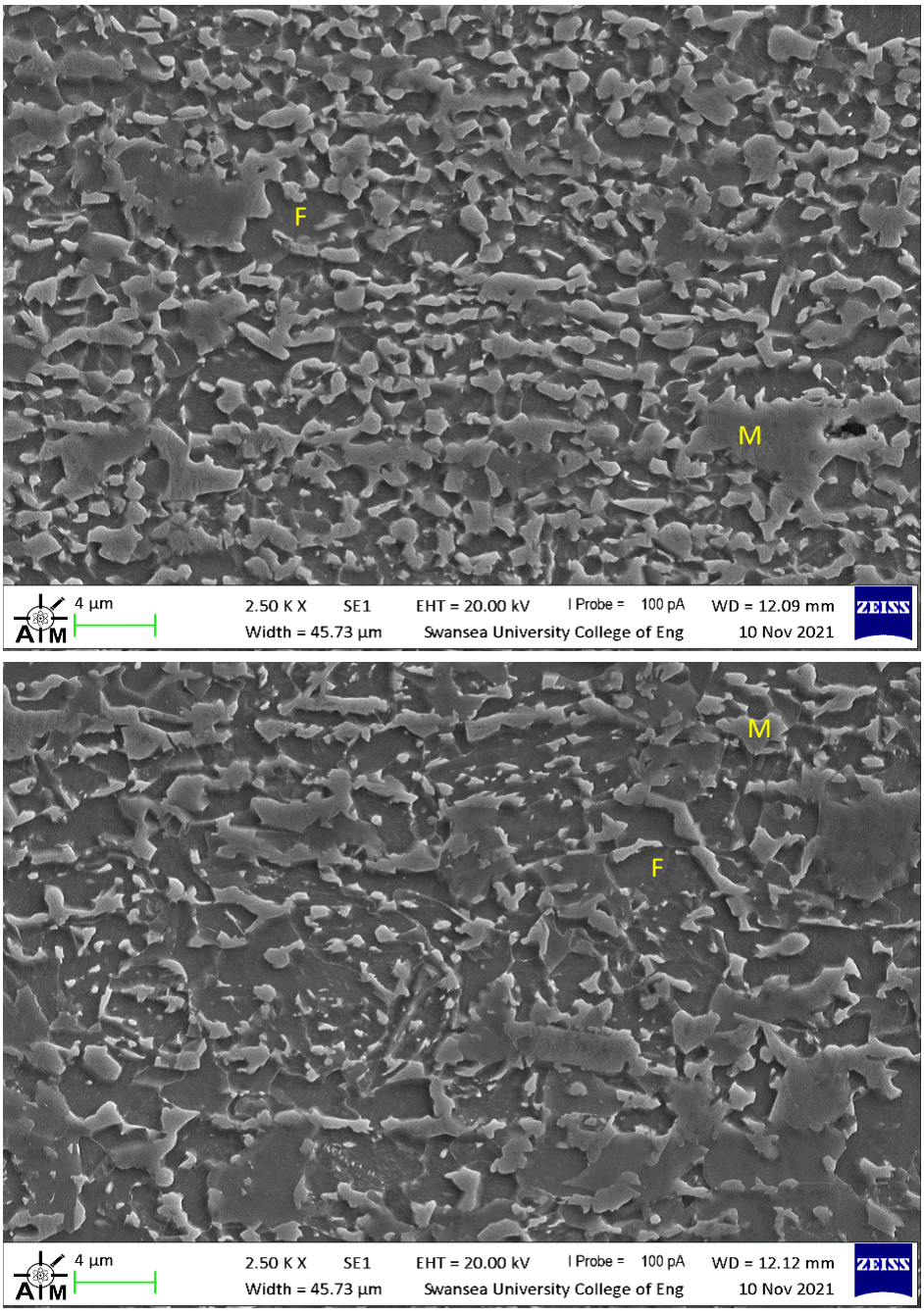

Figure 7.5. SEM image of 780°C soak (top) and 840C soak (bottom). The darker background represents ferrite (F) with martensite (M) islands dispersed over the top.

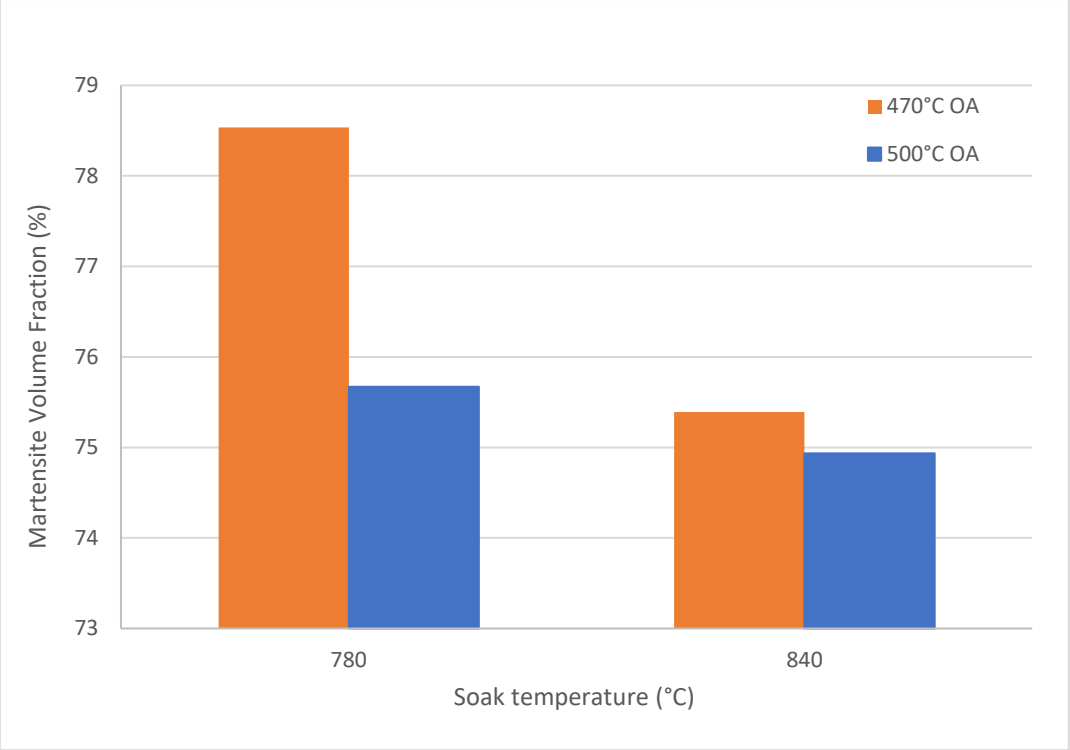

Figure 7.6. Martensite volume fraction present at soak temperatures for each overage temperature, showing an increase at lower soak temperature.

Figure 7.6 shows that there is a slight increase in martensite volume fraction of 3% at the lower soak temperature of 780°C when compared to the higher soak temperature of 840°C. This would seemingly be counter intuitive compared to work shown in previous chapters as the higher the soak temperature within the intercritical region, there is typically an increase in the volume fraction of austenite, hence martensite.

However, an increase in the martensite volume fraction seen at the lower soak temperatures would lead to an increase in the overall strength of the steel. As the soak temperature increases, so will the ferrite content, leading to a decrease in strength.

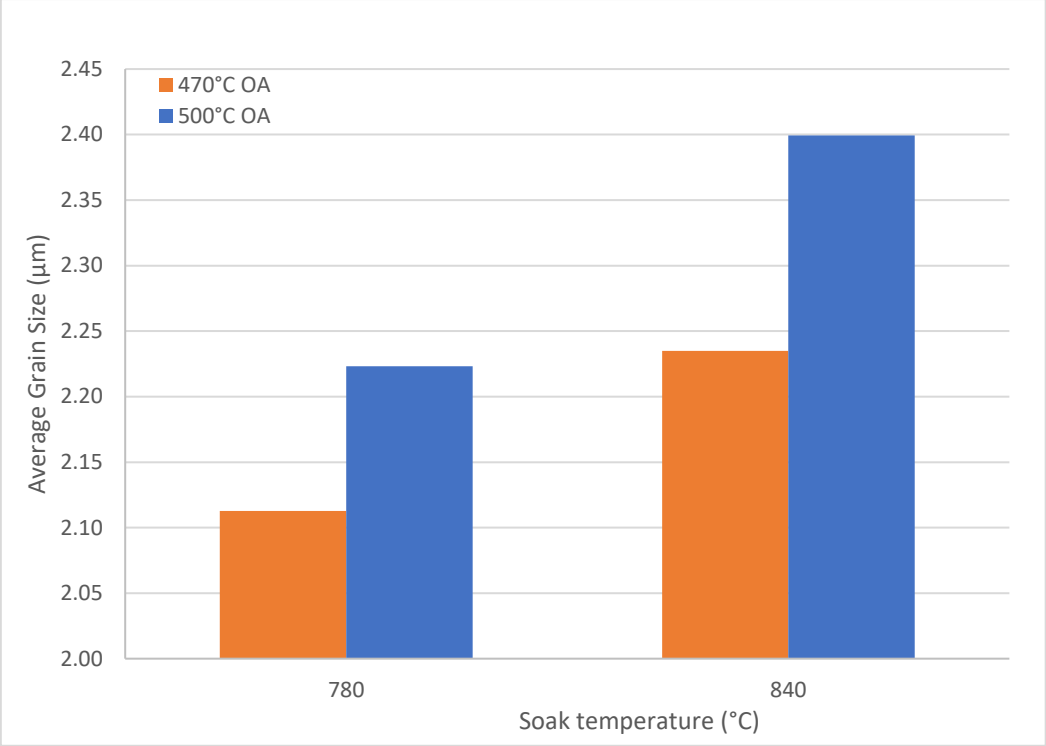

Figure 7.7. Average grain size at soak temperatures for each overage temperature, increasing as soak temperature increases.

As seen in figures 7.3 and 7.4, the increasing soak temperature leads to an increase in grain size. A larger grain size typically gives an increase ductility, therefore combining this with a decrease in martensite volume fraction would mean lower strength as soak temperatures are increased, as demonstrated in figure 7.7.

7.2.2. Effect of Direct Fire Furnace (DF) temperature on mechanical properties

The initial heating section at Zodiac uses direct burner heating to rapidly increase the strip temperature from room temperature to over 700°C, providing a controlled furnace atmosphere the also helps clean the strip surface, allowing for good zinc adhesion during coating. Two temperatures were tested, 725°C and 735°C, whilst this is a small range, the accuracy of the annealing simulation should allow for any differences to be shown, which may not appear in a more variable temperature scenario across a strip profile in the industrial rolling mill.

Work from the New Product Development team in Tata Steel utilising DP1 grade has shown that a temperature of 720°C or above should provide stability in terms of mechanical properties. Below this temperature leads to a drop in tensile strength and an increase in elongation (148).

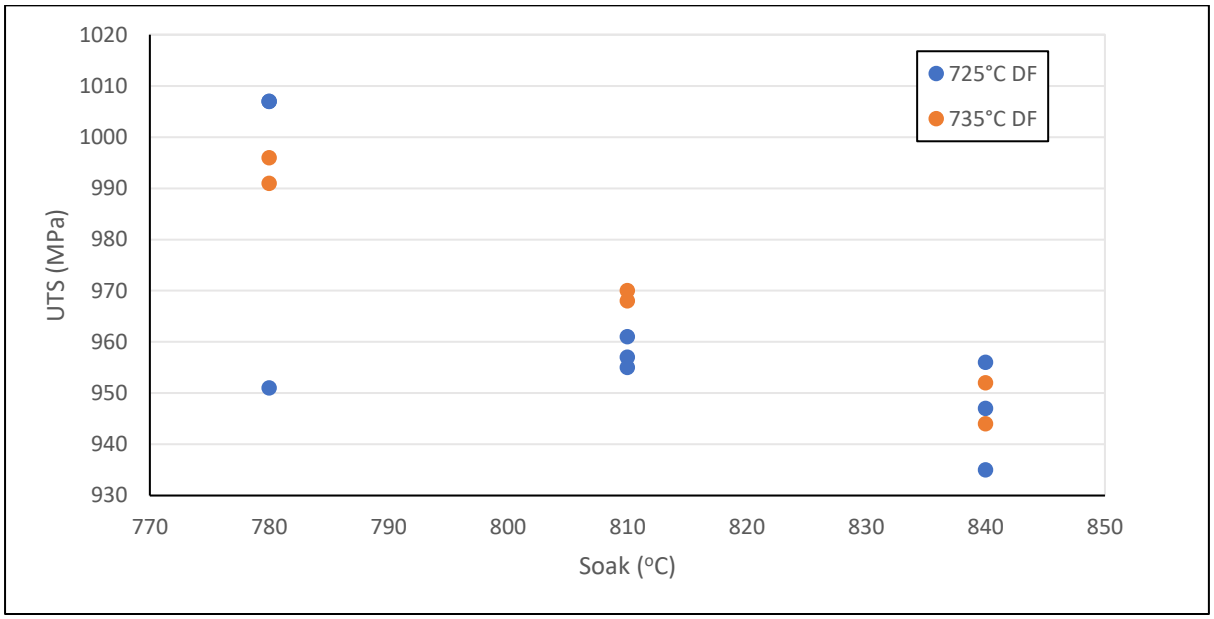

Figure 7.8 Effect of direct fire furnace temperature on ultimate tensile strength

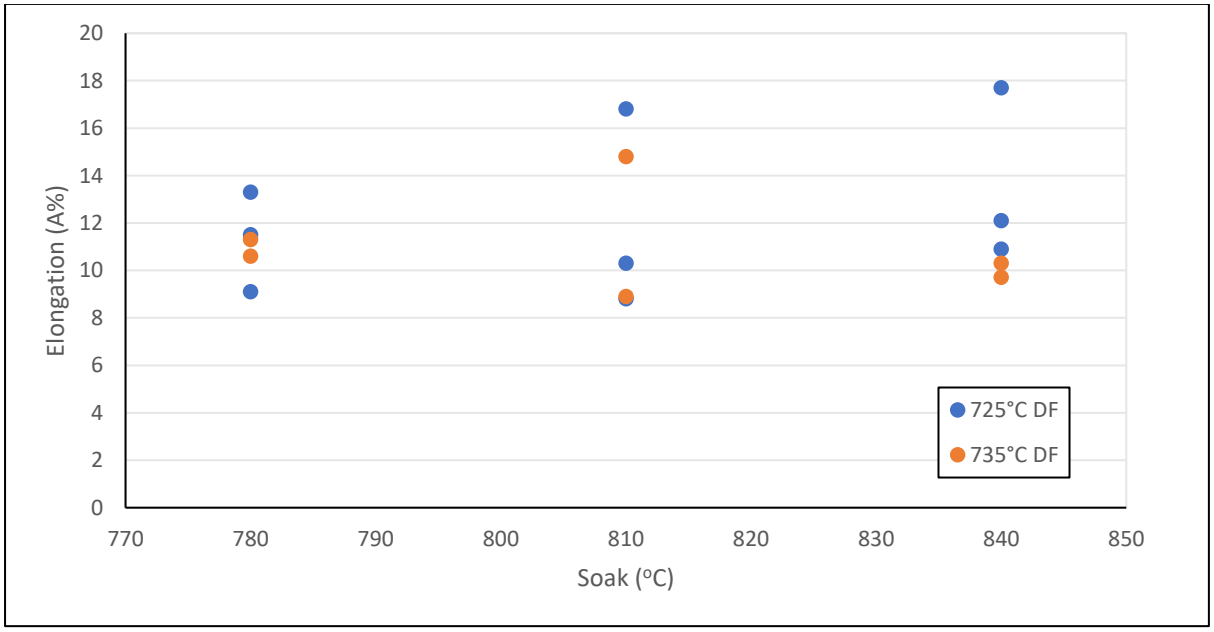

Figure 7.9. Effect of direct fire furnace temperature on elongation properties

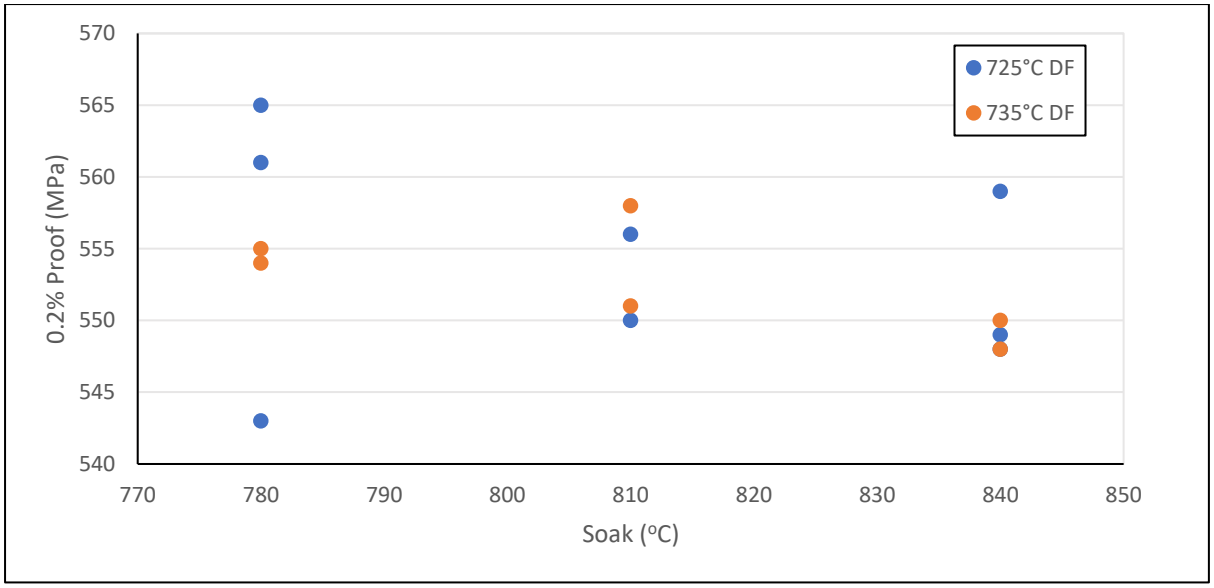

Figure 7.10. Effect of direct fire furnace temperature on yield strength, with two tests taken per variant

Overall, the properties over this range of DF temperatures with variation of 10°C will be consistent. Whilst there is some inherent variability in tensile test results, the above graphs show that processing at 725-735°C has minimal impact compared to the effect of soak temperature across all the mechanical properties. These findings also match those from the NPD trials that were run on the DP1 grade (145).

7.2.3. Effect of soak temperature on mechanical properties

Once past the DF furnace, the strip moves through a radiative tube furnace. For dual phase steels this is a critical part of the process, it is here the material is held at what is known as the intercritical temperature. This part of the cycle industrially is more commonly referred to as the soak, and typically for DP's occurs at around 800°C. For this DP chemistry the A_{c1} and A_{c3} temperature have been determined as 719°C and 847°C respectively. Therefore, soak temperatures between this region should influence the phase fraction and the grain size of the product.

The limitations of the overage temperature before the galvanising pot restrict the capability of the line in producing higher strength DP's, which will be discussed further in chapter 7.2.4. Therefore, the biggest effects on the final mechanical properties are often achieved during the soak region on conventional continuous galvanising lines.

For this section, three soak temperatures were chosen in line with the dilatometer results calculated for this chemistry, allowing for processing at a low (780°C), medium (810°C) and high (840°C) temperature within the A_{c1}/A_{c3} intercritical temperature range. Each of the points represents the average values of three tests, with the minimum and maximum values shown as error bars.

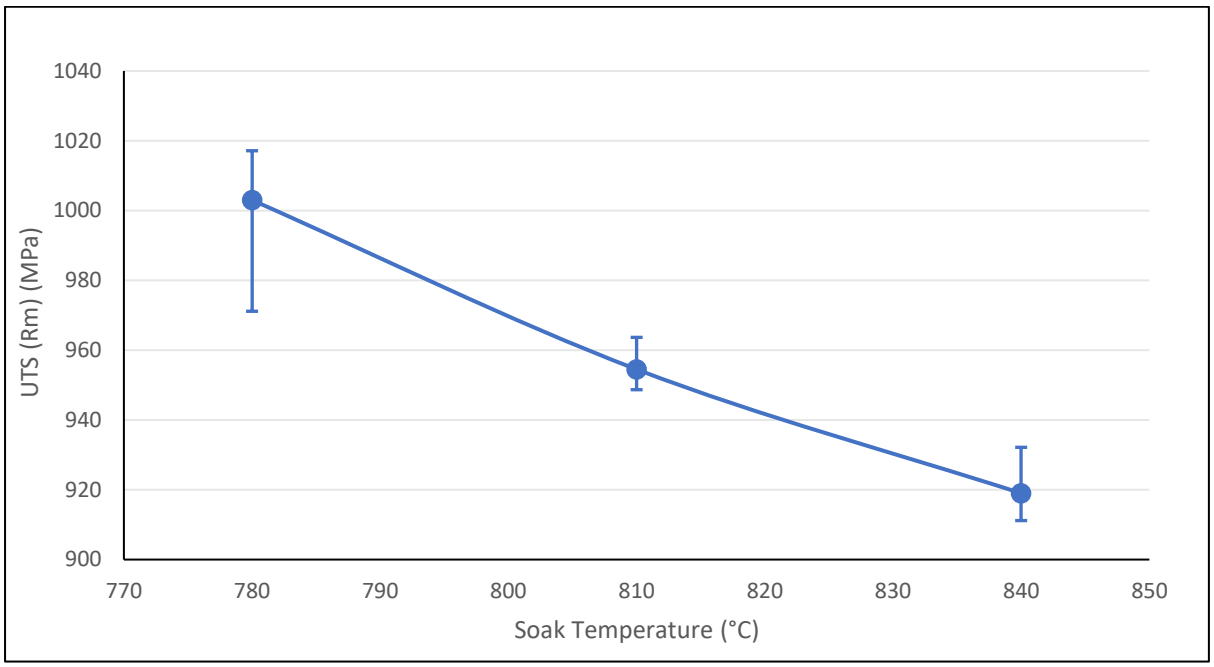

Figure 7.11 Effect of Soak temperature on UTS taken at a simulated 50mpm line speed. UTS decreases as soak temperature increases.

Figure 7.11 shows the UTS results with respect to soak time. The results show highest tensile strengths of just over 1000MPa are achieved at the lowest soak temperature of 780°C. The strength then decreases linearly as the soak temperature increases, averaging just under 920MPa at 840°C.

At lower soak temperature the austenite will become enriched with carbon, stabilising it to lower temperatures. It is therefore less likely to form bainite, or the bainite reaction is delayed. Bainite is softer than martensite, so avoiding bainite is desirable to maximise the martensite content from the austenite transformation, and therefore achieve the required DP microstructure.

Another reason for the increase in strength at low soak temperature is the grain size, with lower temperature producing a more refine microstructure. Grain refinement will lead to the inhibition of dislocation movement during tensile loading, and therefore increase the strength characteristics of the material.

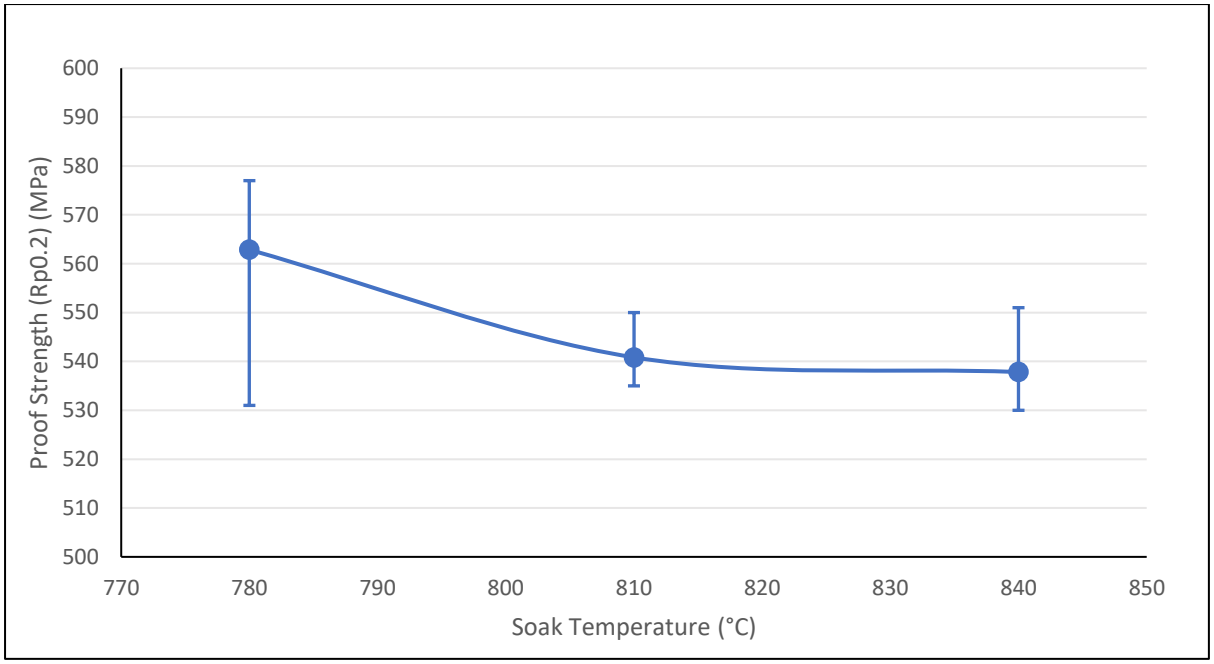

Figure 7.12. Effect of soak temperature on proof strength taken at 50mpm, proof strength decreases as soak increases, though a lot of scatter is seen in the results.

As is typical with DP steels, continuous yielding was seen throughout tensile testing. The increase in yield strength at lower soak temperatures could be attributed to the higher volume fraction of non-recrystallised ferrite in the microstructure (124).

As the soak temperature increases the yield strength plateaus, there is little difference between the medium and high soak temperature. Typically, DP microstructures with a purely martensite / ferrite microstructure would have a low yield to tensile strength ratio (Ys/Ts). The average Ys/Ts ratio for these results were 0.56, 0.57 and 0.59 for the low, medium, and high soak temperature respectively. An indication for increase in the Ys/Ts ratio in DP's is typically associated with an increase in additional phases in the microstructure such as bainite. Substitution of martensite with bainite can lead to an increase in the yield strength of DP steels whilst lowering the tensile strength (125), which is indicated by a drop in tensile strength but retaining yield strength values at higher soak temperatures shown in figure 7.11 and 7.12.

This investigation shows that the yield strength values can be produced with very consistent values, within 20MPa, if run at the fastest line speeds. It's worth noting at this point that the requirement for minimum yield strength for the current Euronorm specification at the time of writing would be 590MPa (149), this is achieved with temper rolling being applied to the material, which can add over 100MPa to the yield strength values when subjected to typical temper rolling forces of 0.5% (123).

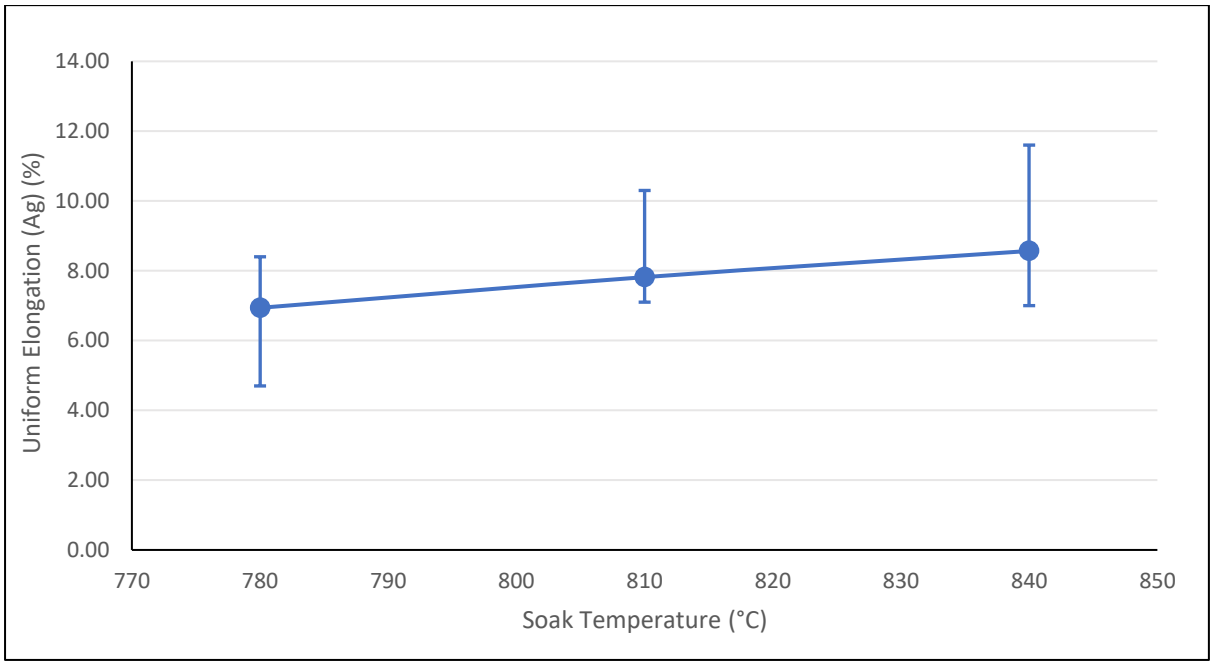

Figure 7.13. Effect of soak temperature on uniform elongation taken at 50mpm

As seen in Figure 7.13, the typical trend for elongation is opposite to that of strength. As the strength of a product increases, it tends to be accompanied with a drop in the elongation values. Interestingly, the higher line speed seems to be most beneficial in terms of elongation properties, which seems to contradict the usual increase in strength / decrease in ductility normally associated with steel. As with the tensile strength, the elongation values are at the highest when processed at the fastest possible line speed.

7.2.4. Effect of overage temperature on mechanical properties

The primary purpose of the overage section is to allow for carbon to precipitate out of solution, this is required for certain grades of steel to increase resistance to the ageing effect (52). The time at temperature during this section allows precipitate growth which influences the mechanical properties of the material (129). During the overage, the ideal temperature for DP steels is to drop below the bainite nose, the start of bainite formation. Typically with DP steel, an avoidance of bainite would be beneficial to the strength of the material. Therefore, the steel needs to be cooled

rapidly to a temperature where bainite can be avoided, or to have sufficient alloying additions to delay the onset of bainite. An example of this is shown diagrammatically in figure 7.14.

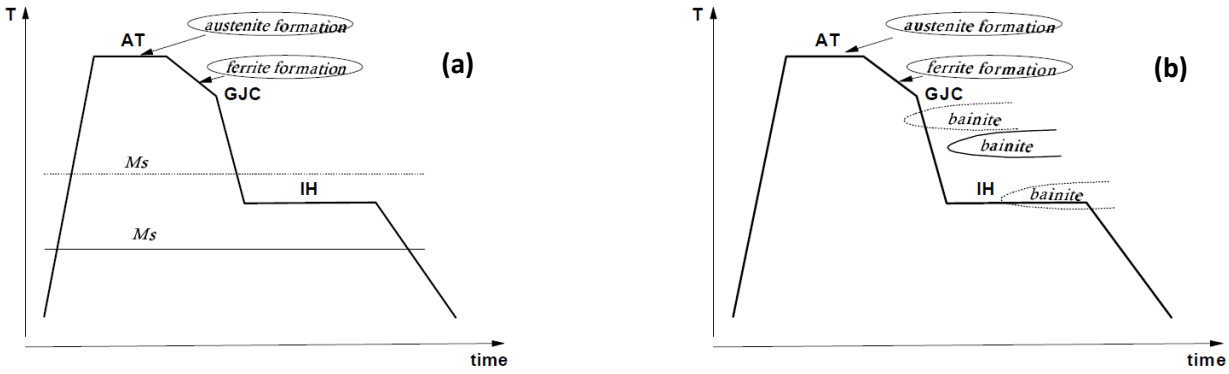

Figure 7.14 Typical DP annealing cycle, with annealing temperature (AT) / soak, gas jet cooling (GJC) and isothermal hold (IH) / overage . Martensite start temperature examples shown in (a), whilst the bainite formation is shown in (b) (12). The importance of avoiding bainite formation by alloying is observed.

Whilst this example is typical for a DP annealing cycle, the overage temperature on a galvanised cycle would typically be 100-150°C higher than that of an annealing line. On Zodiac the temperature of the overage is typically around 460-470°C, which is around the same temperature as the liquid zinc galvanising bath, and therefore has limited flexibility for increasing and decreasing the temperature. CAPL has an overage temperature of approximately 325°C and because it does not have the limitation of a zinc pot the temperatures can be varied between 250-400°C.

The bath temperature therefore imposes a minimum temperature for the overage section, which makes it difficult to fully avoid the formation of bainite. Therefore, sufficient alloying additions are required to retard the growth of bainite at this elevated temperature, and typically this can be achieved with an addition of typically 1-2% manganese (150). The overage section of the galvanising line is also a lot shorter than the overage on the continuous annealing line. Strip processed at a line speed of 100mpm would spend one minute in the overage section on the galvanising line compared to just over seven minutes on the continuous annealing line. The advantage of lesser time at temperature is that if martensite is formed during the overage section, due to insufficient carbon saturation of austenite, then there is a limited time for which tempered martensite would form.

With the temperature limitations in mind, it was decided to see look at two overage temperatures of 470°C and 500°C, both of which are within the capability of the galvanising line.

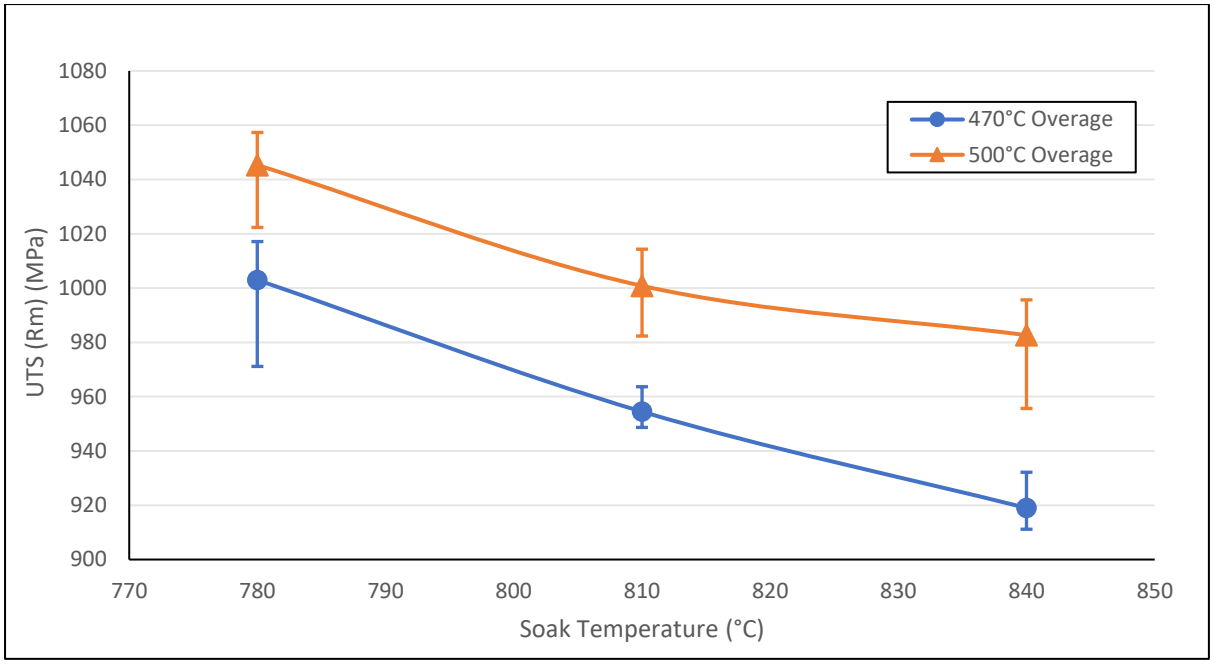

Figure 7.15. Effect of overage and soak temperature on UTS. Higher overage temperatures show benefit to strength.

It can be seen from Figure 7.15 that the UTS values can be greatly enhanced when the overage temperature is increased to 500°C, with each of the soak temperatures being comfortably above the Euronorm specification requirement which is 980MPa (149). Compared to this, the 470°C overage temperature only achieved the requirement at the lowest soak temperature. The increased overage temperature produced consistent UTS values even at higher soak temperatures, with there being little variation in results from 810°C to 840°C. This means the material has a large processing window where the soak temperature can fluctuate without having a significant impact on tensile strength.

The mechanical property variability is higher at the lower soak temperature, this is the same for both the 470°C and the 500°C overage temperature. This would indicate that processing at the lower soak temperature of 780°C would give greater variability between tests.

The likelihood is that at the lower overage temperature there would be an increase in the volume fraction of bainite, which is known to lower the strength of the final product. The CCT diagram in figure 7.16 shows that processing at a higher overage should lower the volume fraction of bainite in the final microstructure by keeping the temperature above the bainite nose, meaning a higher fraction of austenite should transform to martensite on final cooling, provided cooling past the zinc bath is sufficiently rapid enough.

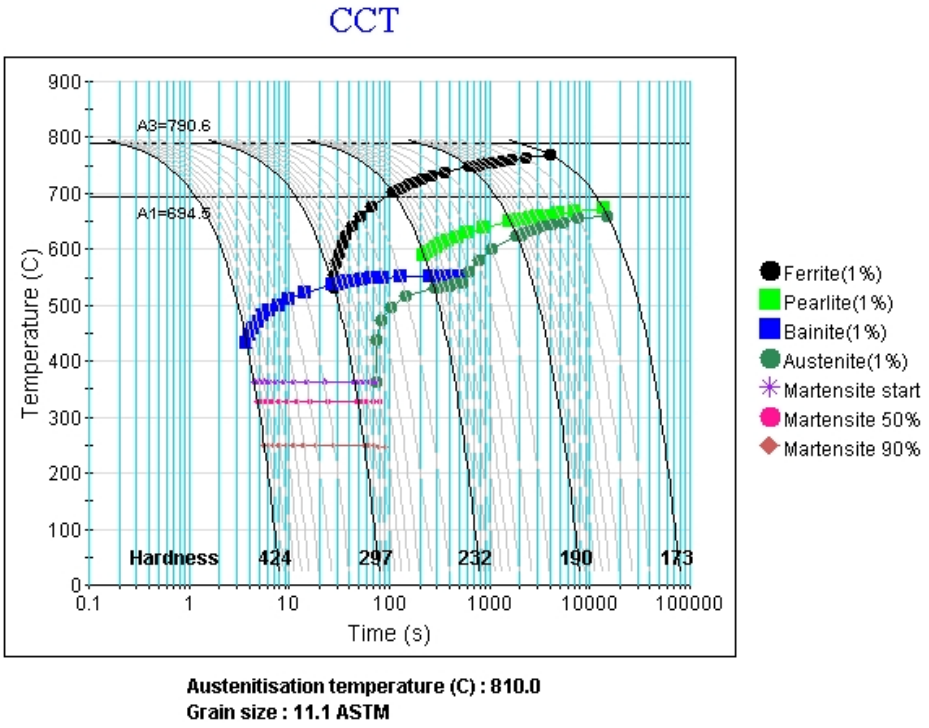

Figure 7.16. CCT diagram from JMatPro using DP2 chemistry. Blue line representing bainite formation around 450°C during rapid cooling.

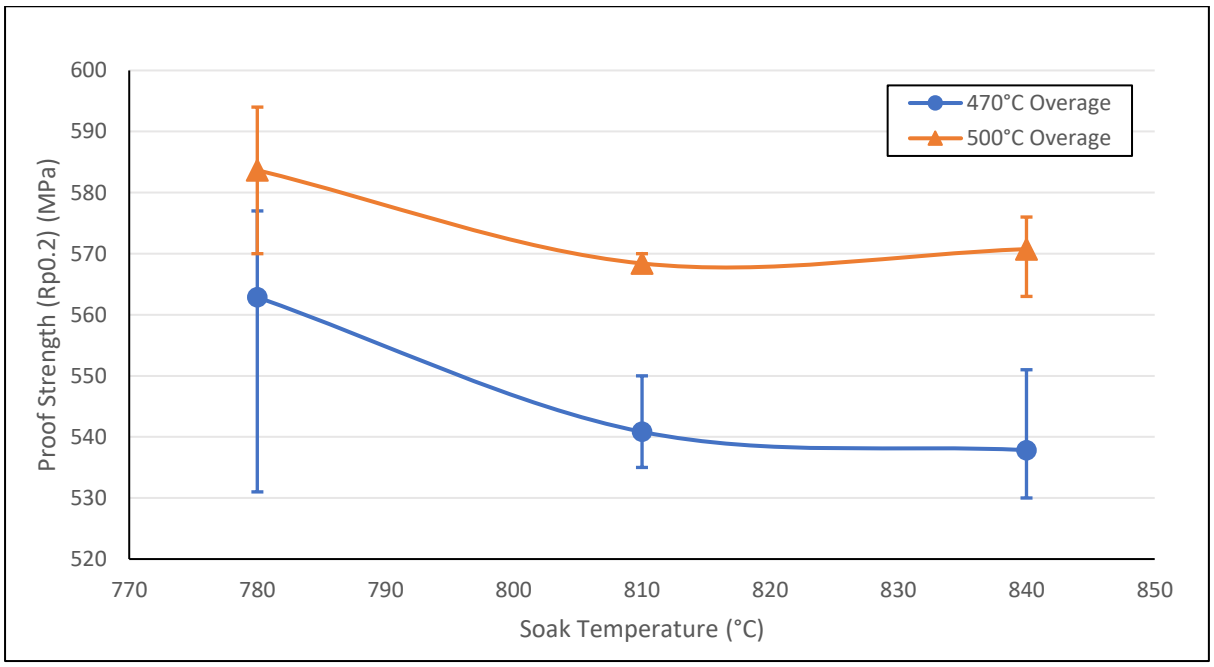

Figure 7.17. Effect of overage and soak temperature on yield strength, increased proof strength is seen from increasing overage temperature.

As with the UTS, the increased overage temperature gives benefits in terms of yield strength of the as can be seen in figure 7.17. The yield strength is highest at 780°C soak temperature, achieving on average 585MPa, which is then reduced to around 570MPa at both 810°C and 840°C. One of the primary reasons for the increase in proof strength is the increase in volume fraction of martensite as shown in figure 7.6, which would benefit both the UTS and proof strength.

The averages suggest that consistent yield strengths can be achieved across a broad range of temperatures, with little difference seen between 810°C and 840°C. This is ideal to achieve consistent yield strength across the length of a full-size coil.

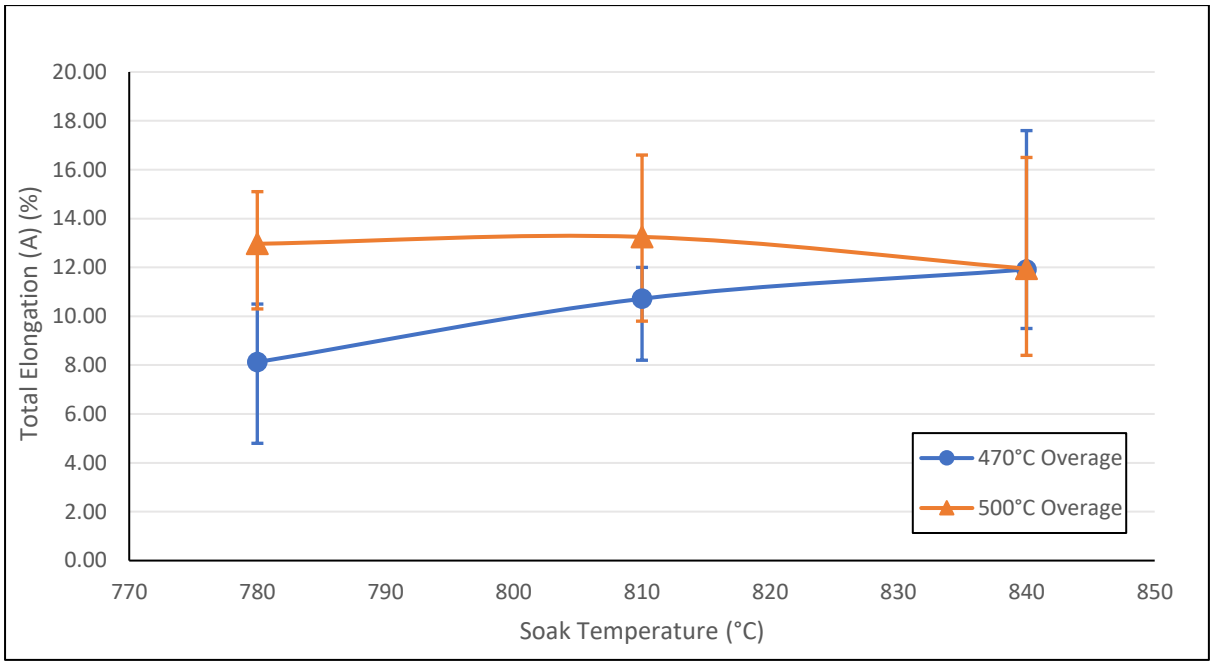

Figure 7.18. Effect of overage and soak on elongation properties. Higher ductility seen at increased overage temperature, particularly at lower soak temperatures. Little difference seen as soak temperature is increased.

As can be seen in Figure 7.18, utilising the 500°C overage temperature provides benefits for elongation at the lower soak temperature range, where 13% elongation has been achieved. As the soak temperature increases to 840°C there is little difference between the 470°C overage temperature and 500°C, both averaging 12% total elongation.

As with the DP1 grade, whilst most of the results achieve the minimum specification requirement of 10% (149), there are several tests which fall below the requirement, regardless of overage temperature. The only temperature range that achieves the 10% minimum consistently is the 780°C soak at 500°C overage.

7.2.5. Effect of line speed on mechanical properties

Another consideration of processing on a continuous galvanising or continuous annealing line is the line speed. On an industrial annealing line, it is typical that material of a heavier gauge, typically 1.3 to 2mm is processed through the line more slowly compared to thinner gauge material, typically between 0.6-1.3mm. Processing of heavier gauge material will require more time in the furnace to allow for the correct temperature to be reached throughout the body of the material. Thinner gauge material does not need as much time to achieve the required temperature, therefore it is processed through the line at a quicker speed. Similarly increased widths would also impact speed. A wider width of material would require more time at temperature to ensure a consistent strip temperature profile is achieved.

Line speed is typically measured in metres per minute. For the continuous galvanising line at Tata, running at 50mpm would mean processing through annealing stage within 600 seconds. 100mpm consequently would take 300 seconds whilst the fastest speeds used for DP grades of 150mpm would take 200 seconds.

The time at temperature can play a pivotal role in the final microstructure and mechanical properties of a DP steel. For real world application, DP steels can typically range from 0.5mm to around 2mm in thickness, therefore this next section will see what influence a change in line speed would have on the mechanical properties.

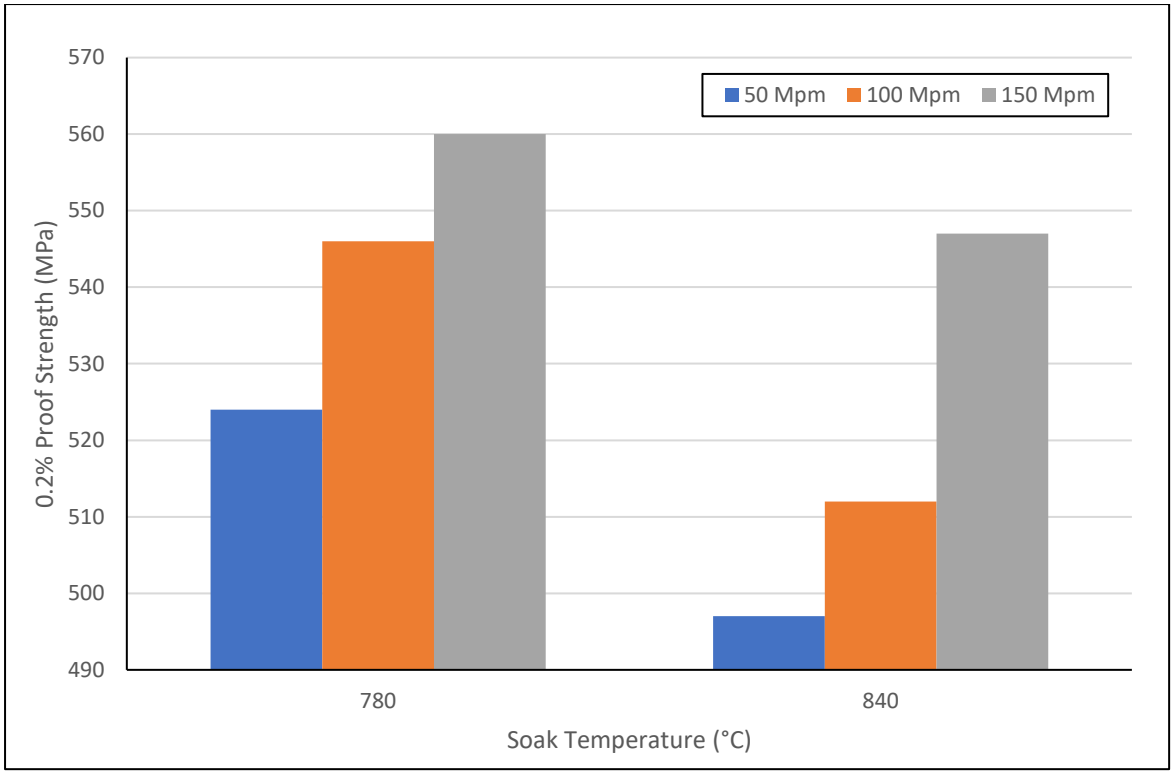

Figure 7.19 Effect of line processing speed on 0.2% proof strength. Speed increase gives highest proof strengths. Averages taken of three tests.

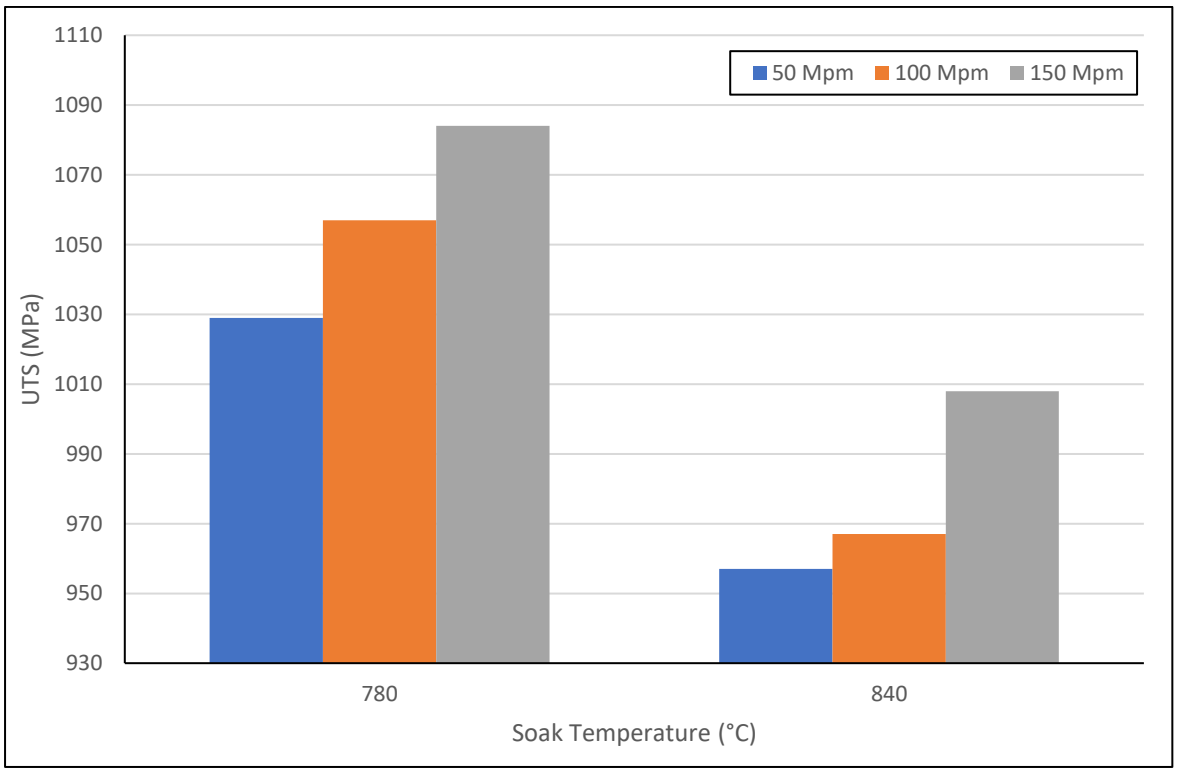

Figure 7.20. Effect of line processing speed on UTS. Increasing speed achieves the highest UTS. Averages taken of three tests.

From figure 7.19 and 7.20 it is clear to see that the trend of decreasing strength as the soak temperature increases is still present. It is also noted that the faster the material is processed through the line, the higher the strength characteristics are, for example the increase of line speed from 50mpm to 150mpm increased tensile strength by 50MPa at 780°C soak. By processing at 150mpm the required strength of a DP1000 specification is achievable for even the 840°C soak temperature.

At slower line speeds there is a longer time at temperature during the annealing stage, therefore the grain size will increase compared to material processed at a faster line speed. The refined grain size leads to an increase in strength, hence the increase in proof and tensile strength as the line speed is increased.

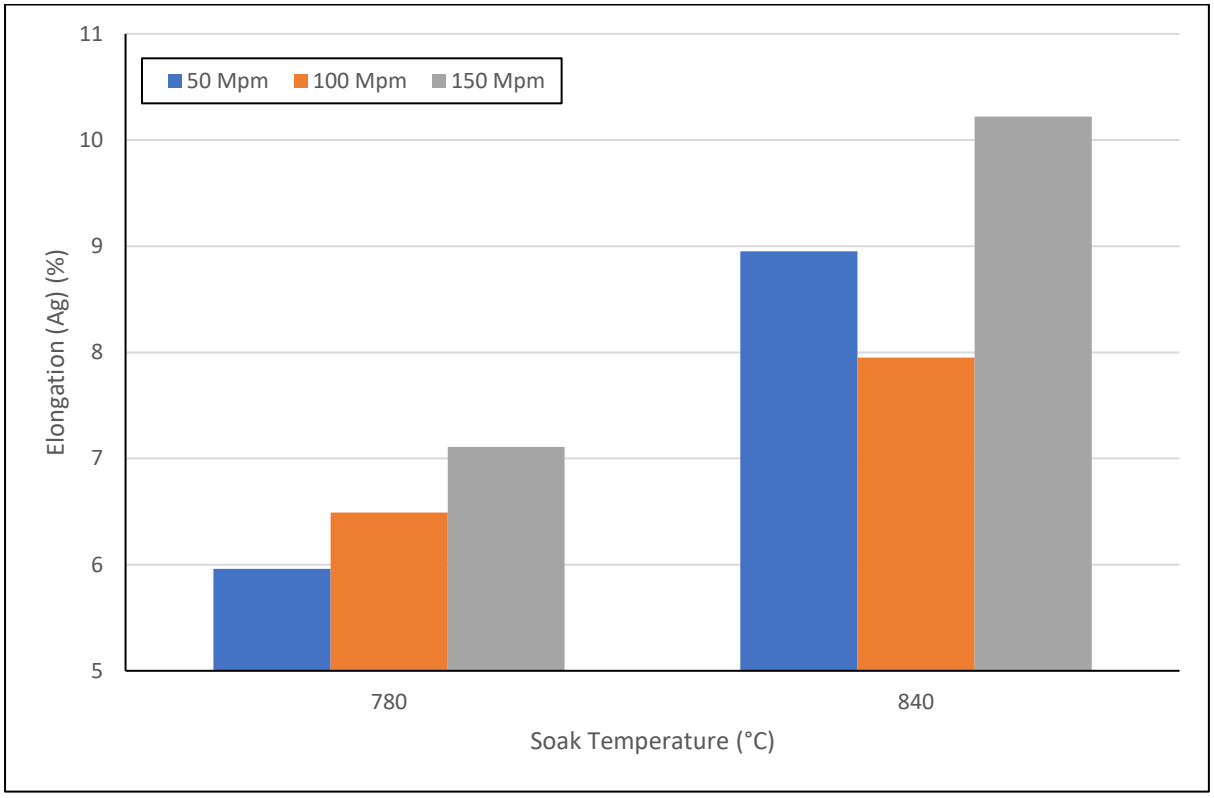

Figure 7.21. Effect of line processing speed on uniform elongation. Typically, the faster processing speed was shown to increase ductility. Averages taken of three tests.

All line speeds show an increase in ductility as the soak temperature is increased. It would typically be expected that the additional time at soak would aid the recrystallisation and promote grain growth which in turn will lead to an increase in ductility, however in these results the highest ductility was seen at the fastest line speeds, which is opposite to the trend seen in other work (53).

Whilst grain refinement might decrease ductility, a more finely dispersed martensite microstructure can exhibit a higher ductility due to higher uniform elongation and smaller voids present in the martensite matrix. This delays the coalescence of smaller cracks to form the main crack after reaching the ultimate tensile strength (7).

The effect of line speed can be seen in figure 7.22. Processing at 50mpm has left larger ferrite and martensite grains due to an increase time at soak temperature. As the speed has been increased to 150mpm the grain size of both ferrite and martensite is more refined. It is also noticeable that at increased speed there is more directionality visible in the microstructure, where recrystallisation has occurred along the pre-existing cold rolled pearlite bands. Because less time is spent at soak the recrystallisation has become retarded, allowing for a refined and banded microstructure (151).

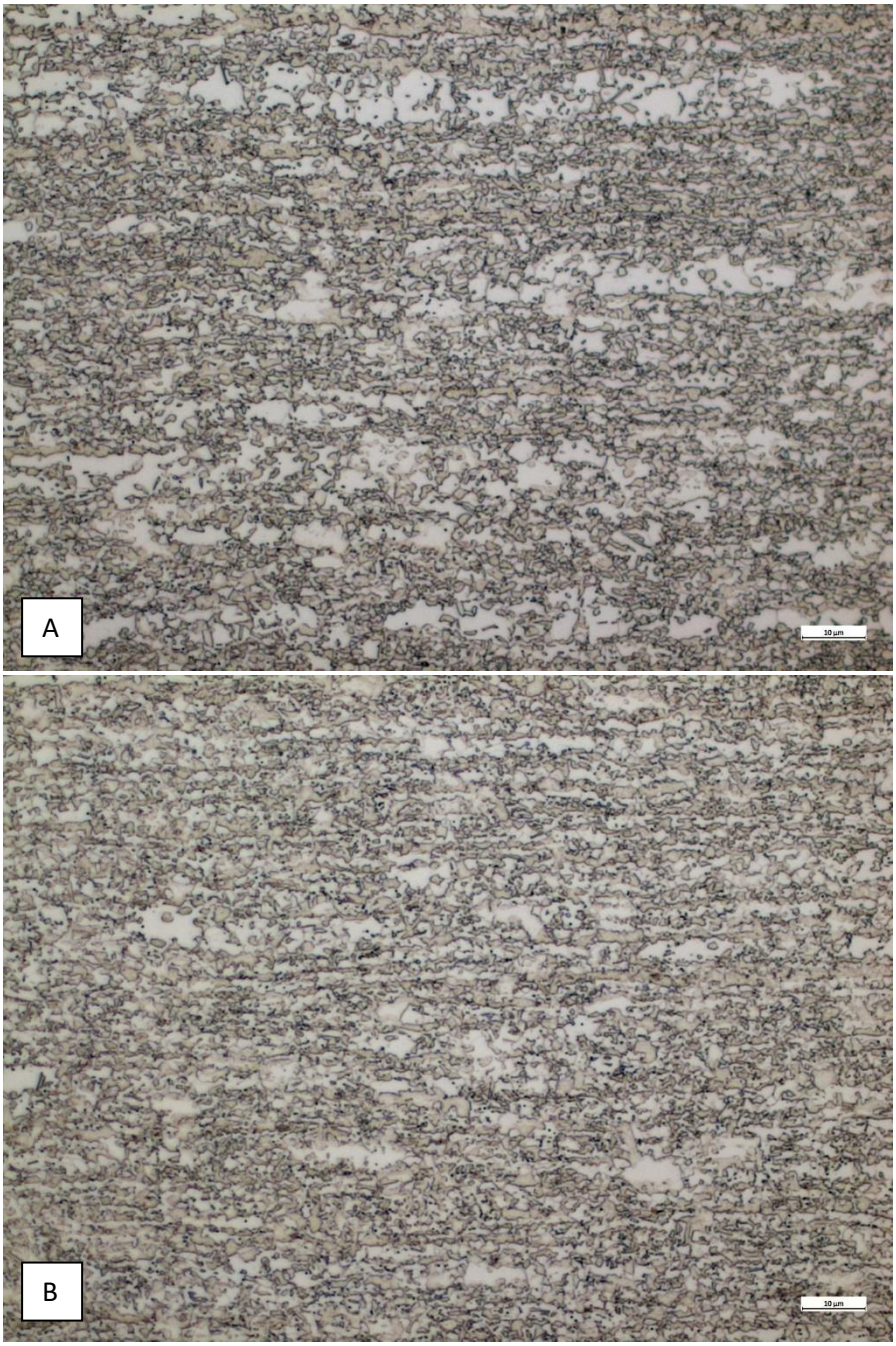

Figure 7.22. Effect of line speed on the microstructure of DP2. Top image (A) shows line speed of 50mpm and (B) shows 150mpm. Both with identical annealing temperatures of 780°C soak and 460°C overage.

7.2.6. Mechanical Property comparison – DP1 vs. DP2

A comparison between DP1 and DP2 compositions reflecting the time and temperature on the continuous galvanising line is shown in figures 7.23-7.25, with the averages shown from two tensile tests.

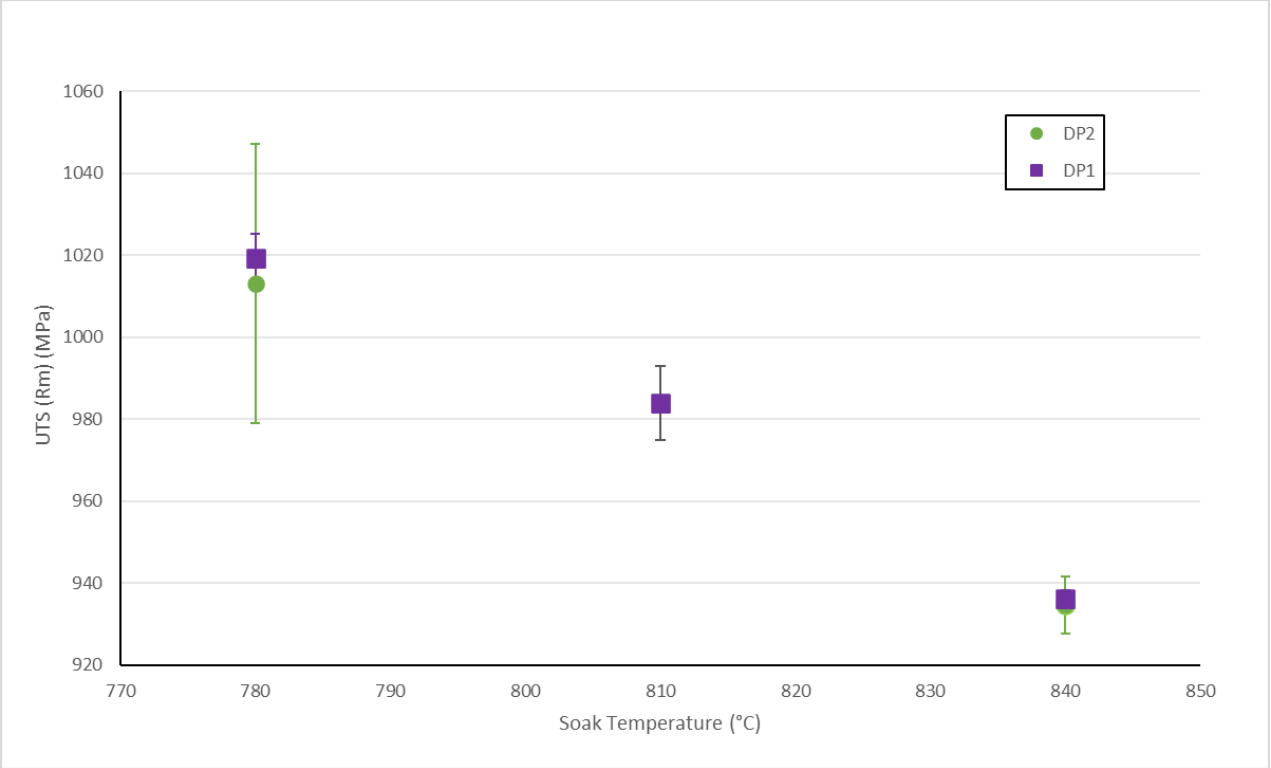

Figure 7.23 Effect of soak temperature on UTS for both DP1 and DP2 chemistry.

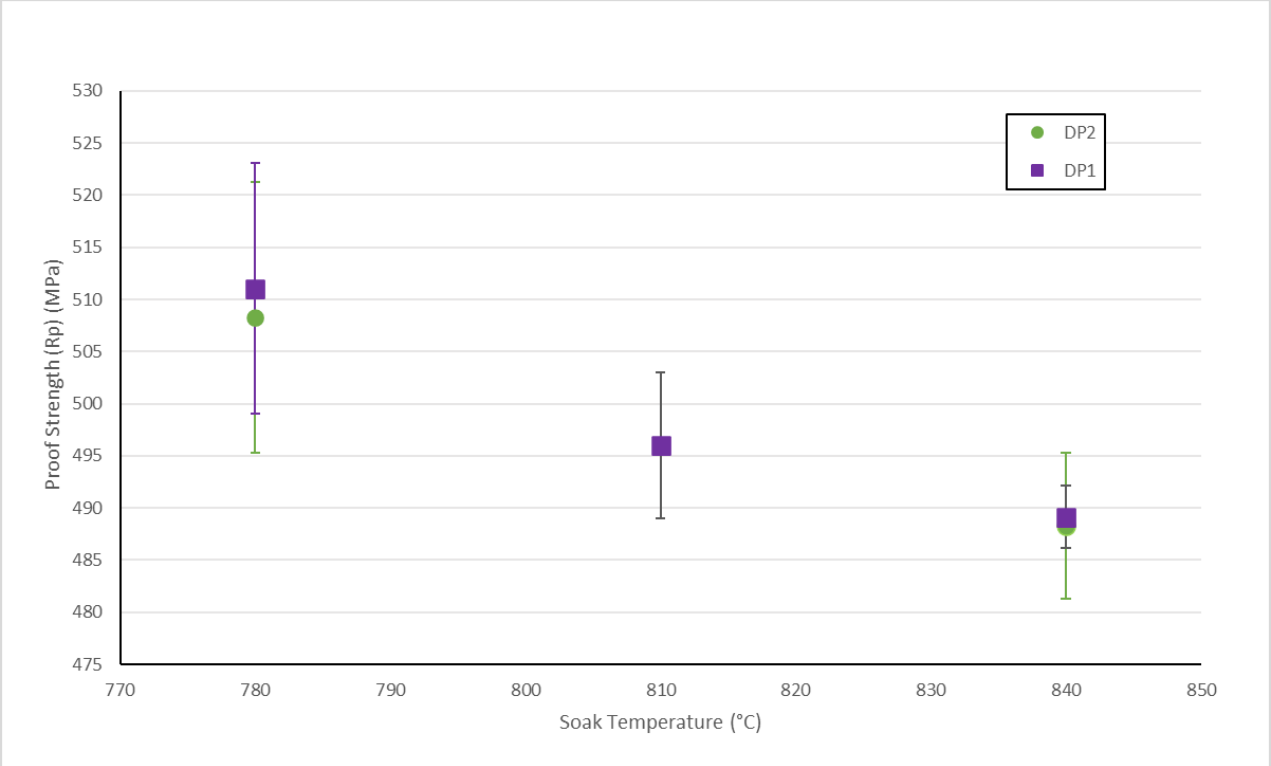

Figure 7.24. Effect of soak temperature on proof strength of both DP1 and DP2 chemistry

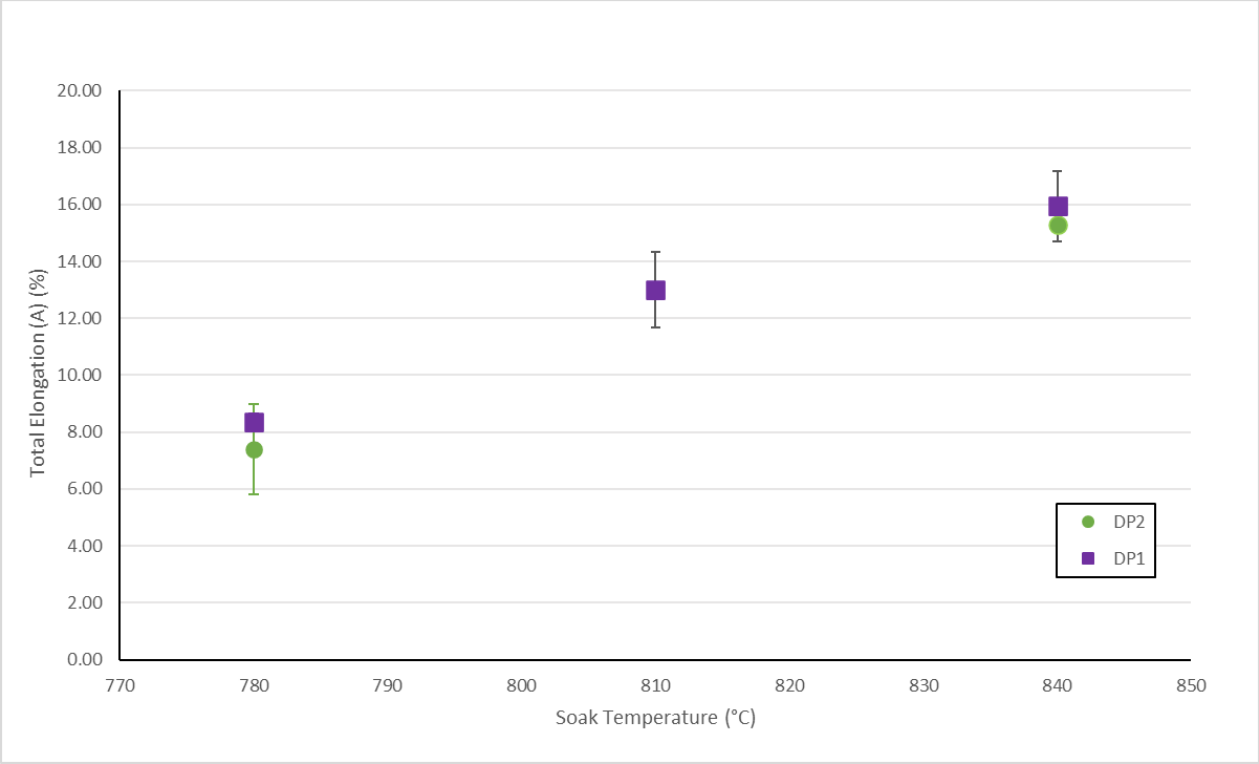

Figure 7.25. Effect of soak temperature on total elongation for both DP1 and DP2 chemistry

It can be clearly seen from figures 7.23-7.25 that the small addition of silicon (0.045wt%) and manganese (0.06wt%) is insufficient to improve the mechanical properties. It is worth noting at this point that steel grades that are cast industrially have a set of limits to which the steel is produced too. Whilst both of these chemistries have the same carbon aim requirement, it can be seen from the chemistry in table 1 that there is an increase in carbon of 0.1wt% in DP1 compared to DP2.

This difference is small, but an increase in carbon would increase the volume fraction of martensite and hence tensile strength of the material (39). This increase in carbon may have masked any benefit that could be seen with the small silicon and manganese addition.

This work has shown that producing a viable DP1000 product through Tata's UK galvanising line is not viable by adjusting temperature and time parameters within the mill capability. Therefore an alloying increase is required to improve the mechanical properties sufficiently enough to make a viable DP1000 through the continuous galvanising line in the UK.

7.3. Conclusions

The main outcome from this chapter is that the current IJmuiden DP2 chemistry would not achieve a viable DP1000 product if produced in the UK. Whilst the strength requirements can be achieved by using a low soak temperature, the elongation values would not achieve the required specification.

The higher the overage temperature, the better the overall mechanical properties are in terms of both strength and ductility, with the 500°C overage achieving a viable product at both 780°C and 800°C soak temperatures. Whilst this would be beneficial for mechanical properties, a higher overage temperature can lead to issues in the galvanising bath, where the incoming strip into the galvanising pot can be too hot, causing coating adhesion issues.

The fastest line speed showed to be beneficial for both strength and ductility, operating consistently at fast line speeds would produce the best mechanical properties overall. Whilst this may be possible for DP material at thinner gauge, the heavier gauge material would not have sufficient time to achieve the correct microstructure if processed at too high line speed.

The increase in strength seen at the highest line speed can be linked back to the Hall Petch relationship, where less time in the furnace has allowed for more refined grains, providing the increase in strength seen in the results.

8. Creating a high yield DP1000 for continuous annealing

The current DP1000 product produced on Tata Steel's Continuous Annealing Processing Line (CAPL) utilises cold rolled unannealed coil from Tata's European steelworks based in IJmuiden. This grade, termed DP1, is produced specifically for the UK to achieve a viable DP1000 product. The Ijmuiden works produce several variants of the DP1000 type chemistry to achieve differing mechanical properties on their continuous galvanising lines.

There is demand from the automotive sector for a DP1000 material that has higher yield performance, as well as the current lower yield grade that is currently produced at Tata in the UK. This type of differentiated product is of interest not only to the automotive manufacturers, but also to Tata themselves, allowing them to diversify their product offering to the marketplace.

Therefore, this chapter will investigate processing parameters of one of the Ijmuiden DP1000 chemistries, DP2, with the view to achieving a commercially viable DP1000 product through the CAPL route. Furthermore, this DP2 chemistry will be tested for its capability of producing a DP1000 high yield variant, which is yet to be commercialised in the UK.

Because the DP2 grade is already cast for use in Ijmuiden, it means that a reduced lead time should be required for casting and rolling, therefore lessening the time is takes to get the material to the UK, as well as allowing the DP1 grade to be rationalised as a variant.

8.1. Processing conditions for DP1000

The grade chemistry that will be used for in this chapter is the same as was used in chapter 7 of this body of work and is shown in table 8.1. The DP2 chemistry will then be subjected to the existing processing conditions used on CAPL for DP1, allowing for a comparison between the two.

Table 8.1 Chemistry of DP2 material with the DP1000 low yield (DP1000LY) and DP1000 high yield (DP1000HY) specification limits of EN 10338 specification (bottom section) to which this material would be produced against. DP1000HY allows for a higher carbon content compared to DP1000LY

Grade Chemistry	**C (wt%)**	**Mn (wt%)**	**Si (wt%)**	**Ti(wt%)**	**Cr(wt%)**	**Nb (wt%)**
DP2	0.149	2.242	0.102	0.015	0.552	0.015
Specification	**C (wt%) Max**	**Mn (wt%) Max**	**Si (wt%) Max**	**Ti+Nb (wt%) Max**	**Cr+Mo(wt%) Max**	
DP1000LY DP1000HY	0.20 0.23	2.9	1.0	0.15	1.4	

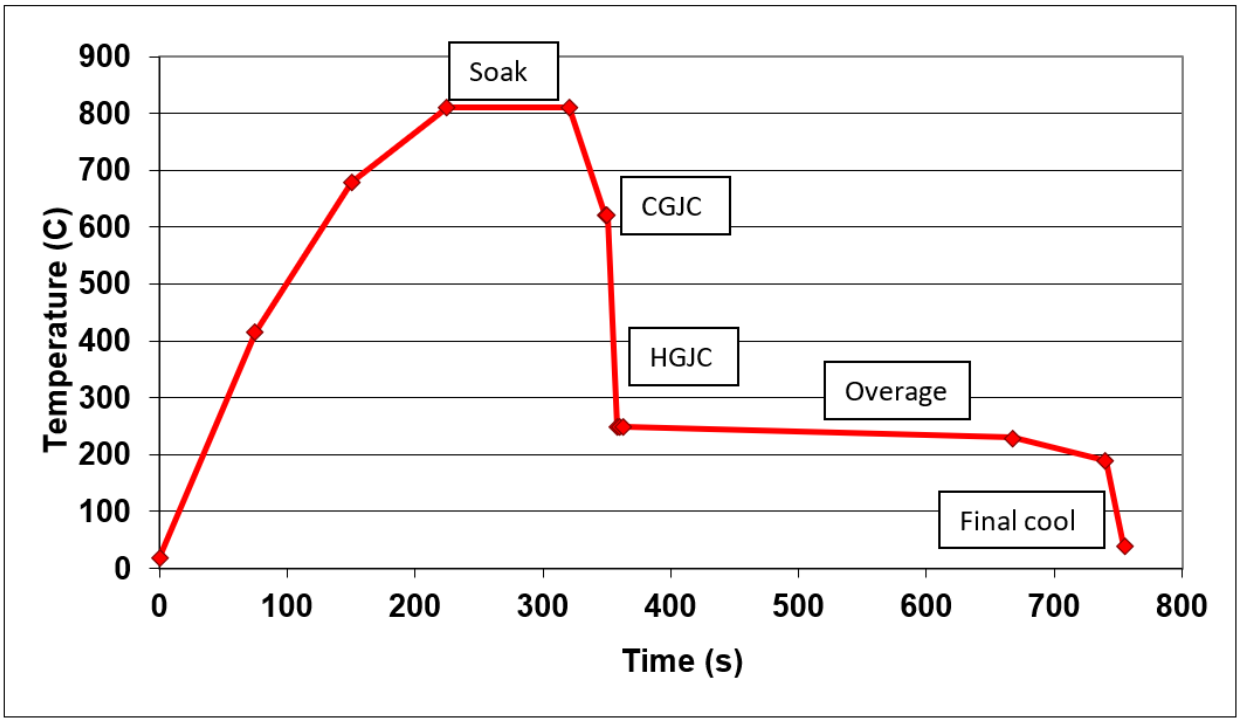

Figure 8.1 Example of DP1000 annealing cycle on CAPL with the soak, conventional gas jet cooling (CGJC), hydrogen gas jet cooling (HGJC) and overage sections.

Whilst both CAPL and Zodiac (continuous galvanising line) achieve similar soak temperatures of around 800°C, the ability to rapidly cool down <300°C for martensite formation means that it is

easier to achieve a dual phase product with a leaner chemistry via CAPL. The Zodiac galvanising line is restricted in its cooling ability to ~460°C at which temperature it enters the molten zinc pot.

Previous work by Evans et al. (48) suggest that the two main areas where the mechanical properties can be most affected are by variation of the line speed, and by adjusting the hydrogen gas jet cooling (HGJC) temperature. The initial section of this work will focus on the mechanical property behaviour of the DP2 grade by varying the speed at which the material passes through the line, whilst the second part will focus on the conventional gas jet cooling (CGJC) section, shown in Figure 8.1, and adjusting these temperatures to produce a high yield version of DP1000.

As with chapter 7, several full width steel sheets of 1mm thickness cold rolled unannealed DP2 were received from IJmuiden. These samples were sheared to 360mm x 100mm plates ready for annealing. The annealing process was simulated on both a continuous annealing simulator (CASIM) and the Gleeble 3500 thermomechanical simulator, the tests were set up using a standard annealing processing route for the current DP1 chemistry and is shown in table 8.2.

Table 8.2 Processing Conditions of DP1000LY and DP1000HY trials. Both DP1000HY and DP1000LY material uses the same DP2 chemistry.

Chemistry	Test ID	Simulated Line Speeds (mpm)	Soak Temperature (°C)	CGJC Temperature (°C)	HGJC Temperature (°C)	Overage Temperature (°C)
DP2	DP1000LY	90 / 120 / 150	810	620	250	230
DP2	DP1000HY	120	810	680	250	230

Once annealed, samples were metallographically tested along with grain size and phase fraction analysis which has been described in chapter 4.

8.2. DP1000 low yield results and discussions

An established DP1 chemistry has been utilised on Tata's CAPL line for several years. This chemistry has had various trials through product development to determine the optimum processing

parameters through CAPL to achieve the final products mechanical properties, which are shown in table 8.3.

The current processing temperatures used for processing DP1 grade will be used to allow for direct comparison with the DP2 chemistry, these are shown in line one of table 2. The only important variable that will required to be changed will be line speed, ie. The time in which the material is processed through the furnace. The line speed is not typically consistent on an industrial annealing line and will vary depending on the products final gauge requirements. Typically heavier gauge material of 1.5-2mm will be processed at a slower line speed, more typical of 90-100mpm, whilst light gauge material of 0.8-1.2mm is processed quicker, typically up to 150mpm. Therefore it is important to see the effect adjust line speed will have on the final mechanical properties of the steel.

The Euronorm specification for DP1000 is EN 10338. This specification is the basis of the chemistry and property requirements that must be met to classify the material as DP1000 product. The current DP1 grade is established and the plant can consistently achieve the required mechanical properties. The chemistry requirements for this specification are comfortably met for DP2, as is shown in table 8.1.

The target mechanical properties are shown in table 8.3. To consider this material a success, each of these mechanical property requirements must be achieved.

Table 8.3 Minimum mechanical property requirements of DP1000 as specified on Euronorm standard EN 10338 (2)

Proof Strength (Rp) **MPa**	**Tensile Strength (Rm)** **MPa**	**Elongation (A)** **%**
590-740	980	10

Figure 8.2 Light microscope image of DP2 showing a very refined, high martensite containing microstructure. White phases show ferrite and brown regions show martensite.

Figure 8.2 shows the microstructure of the DP2 material processed equivalent to 120mpm. The lighter regions in the image show the ductile ferrite phase, whilst the brown regions are the harder martensite phase. The image shows a large volume fraction of martensite with refined regions of ferrite interspersed. The phase fraction analysis is shown in table 8.4.

Table 8.4. Phase fraction analysis of DP2 taken at 120mpm

Ferrite (%)	Martensite (%)	Error (%)
17	83	+/-1

A large volume fraction of martensite should be beneficial to tensile strength, allowing for a DP1000 to be achieved. To prove this tensile testing was undertaken with the mechanical property results below shown as averages. The error bars dictate the minimum and maximum values achieved from the tensile tests.

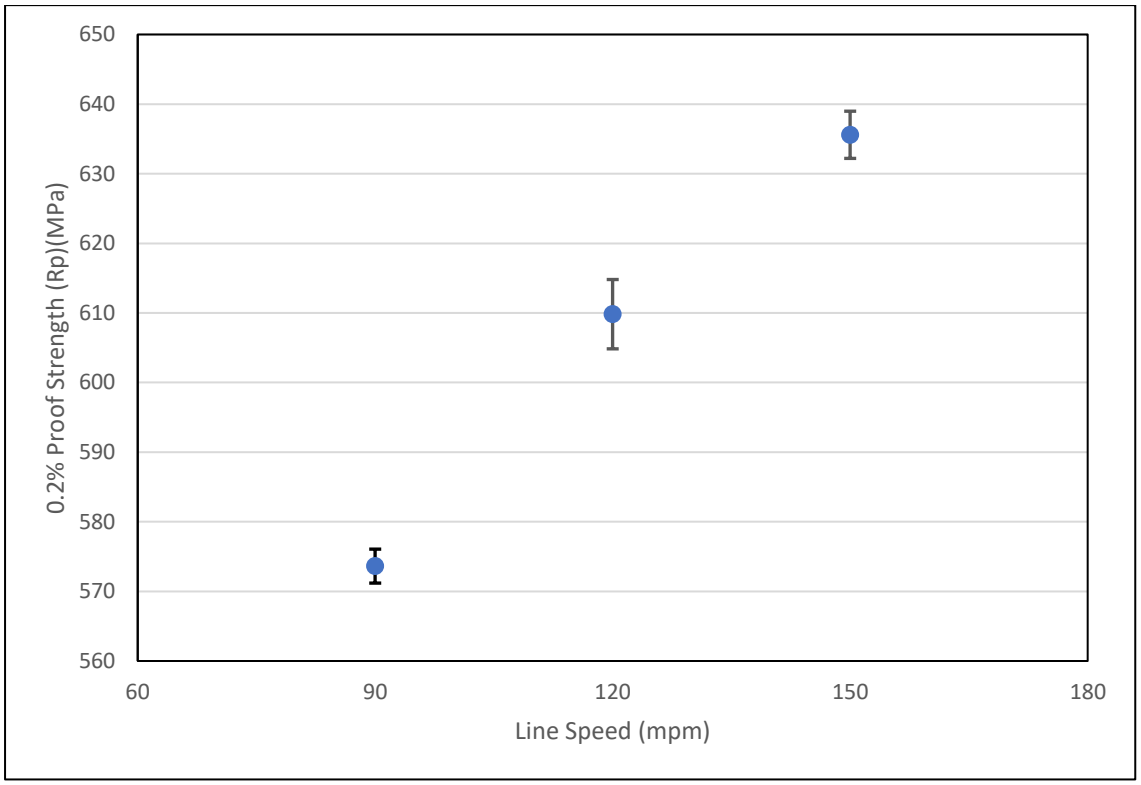

Figure 8.3. Effect of line speed on the yield strength, increasing proof strength as line speed increases

Figure 8.3 shows a trend typical for DP steels across both the CAPL and Zodiac lines, in which the faster the material is processed, the higher the final overall strength of the material. The average yield strength rose from 574MPa at 90mpm to 610MPa at 120mpm, whilst the maximum strength was achieved at 150mpm, where an average of 635MPa is seen.

Whilst the values at 90mpm do fall below the minimum requirement for the EN 10388 specification, it is worth noting that during industrial processing the material passes through a temper mill. The additional temper mill elongation that is applied to the strip as it passes through will give an additional 10MPa increase on the yield strength for each 0.1% applied from temper rolling (123), with typically a 0.4-0.5% being applied to production material.

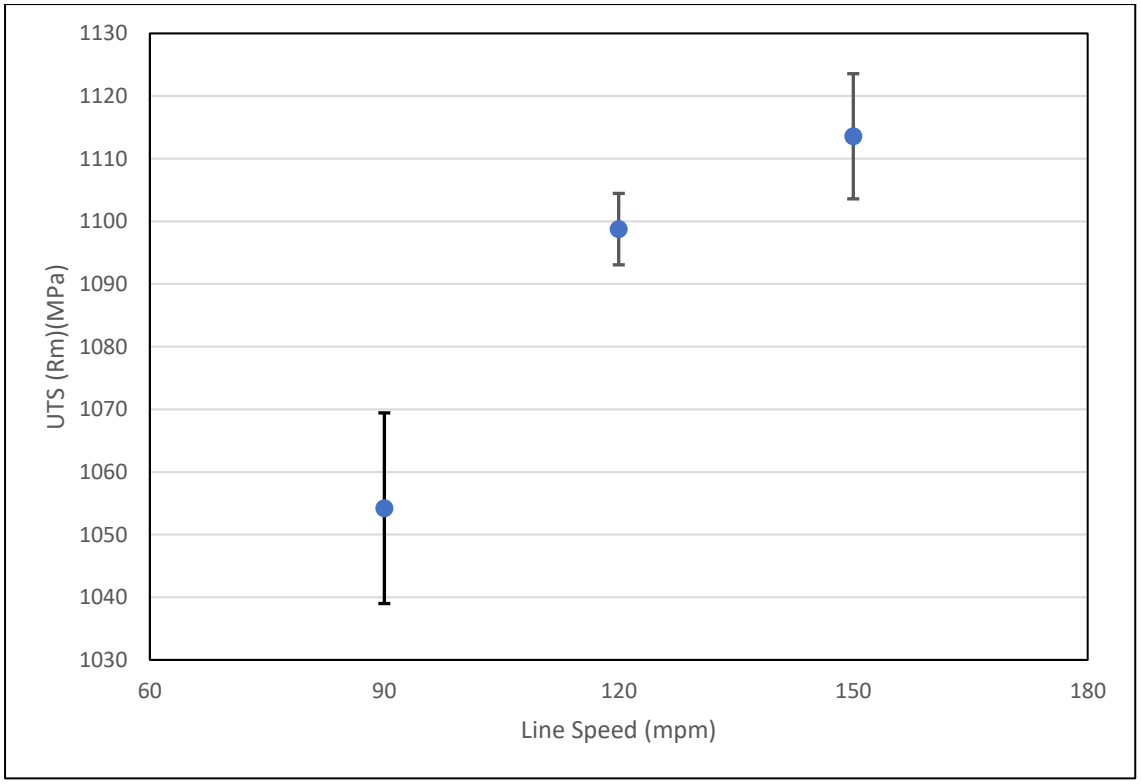

Figure 8.4. Effect of line speed on the tensile strength. Increase in UTS seen as line speed increases.

As with the proof strength, the tensile strength values seen in figure 8.4 show improved strength characteristics as the line speed is increased. The lowest UTS values are seen at 90mpm, where an average of 1055MPa was achieved, increasing to 1098MPa at 120mpm and further increased to 1114MPa at 150mpm. At each line speed the UTS is comfortably achieved within the 980MPa minimum requirement of the EN10388 specification.

Work from Kong et al. (53) has shown that the strength, both proof and UTS, is affected by the speed the material passes through the furnace(53). Longer dwell times in cooling section lead to lower volume fractions of martensite being produced. Additionally, a slower line speed will also lead to a longer time in the overage section, which will allow for an increased likelihood of decomposition of martensite due to a longer time at temperature.

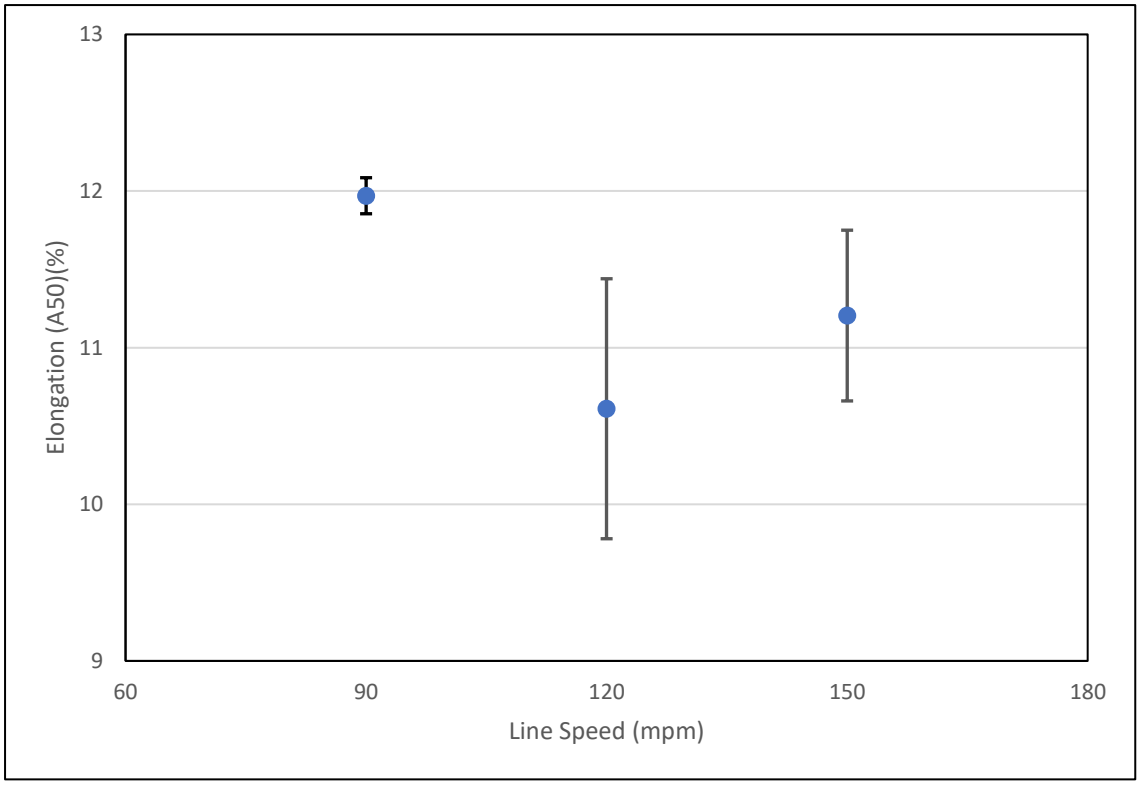

Figure 8.5. Effect of line speed on the elongation. 90mpm line speed has best elongation values, which then drops and increases at fastest line speed of 150mpm.

A relatively small variation is seen in the elongation at different speeds. The slowest line speed has shown to be the most beneficial for ductility, with an average of nearly 12% at 90mpm. A drop is seen at 120mpm to 10.5%, whilst at 150mpm the average was 11.25%.

Typically, when the strength of steel increases the ductility decreases. A concern for the DP2 grade would be its proximity to the minimum requirement for elongation. At 120mpm, the minimum level drops below the 10% specification requirement, and whilst the other line speeds do not drop below 10%, they are close to it.

The following graphs compare the average mechanical properties of the DP1 and DP2 grade processed on the CASIM, in addition to line produced material using the DP1 grade (CAPL).

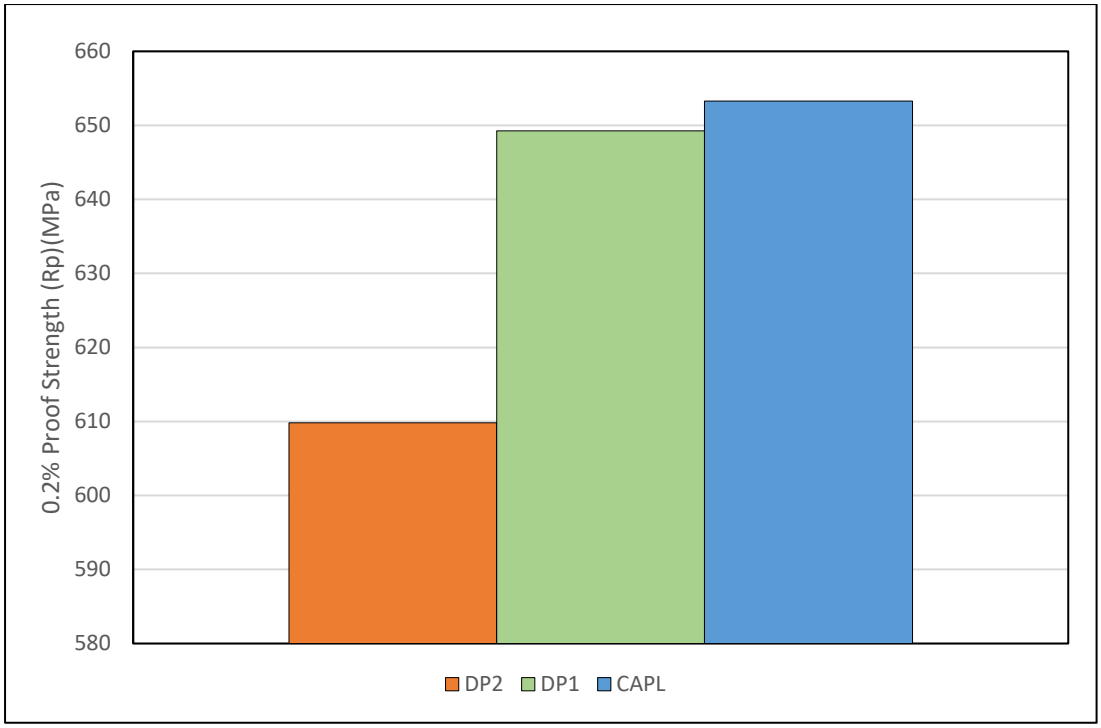

Figure 8.6. Proof strength of DP2 trial material vs. DP1 and CAPL production material, using the same annealing parameters. Note DP2 has not has temper rolling applied, which explains the difference compared to DP1 and CAPL material.

Figure 8.6 shows a lower yield strength achieved from the DP2 trial grade when compared to DP1 and CAPL production material. However, both DP1 and CAPL material have had a 0.4% temper mill extension applied to the material, which has allowed for an increase in the overall yield strength of the material.

As stated earlier in this work, an additional 0.4% extension applied to the DP2 material should allow for an increase of around 40MPa, this would mean the overall yield strength would be raised to 650MPa on average, matching that of the DP1 material.

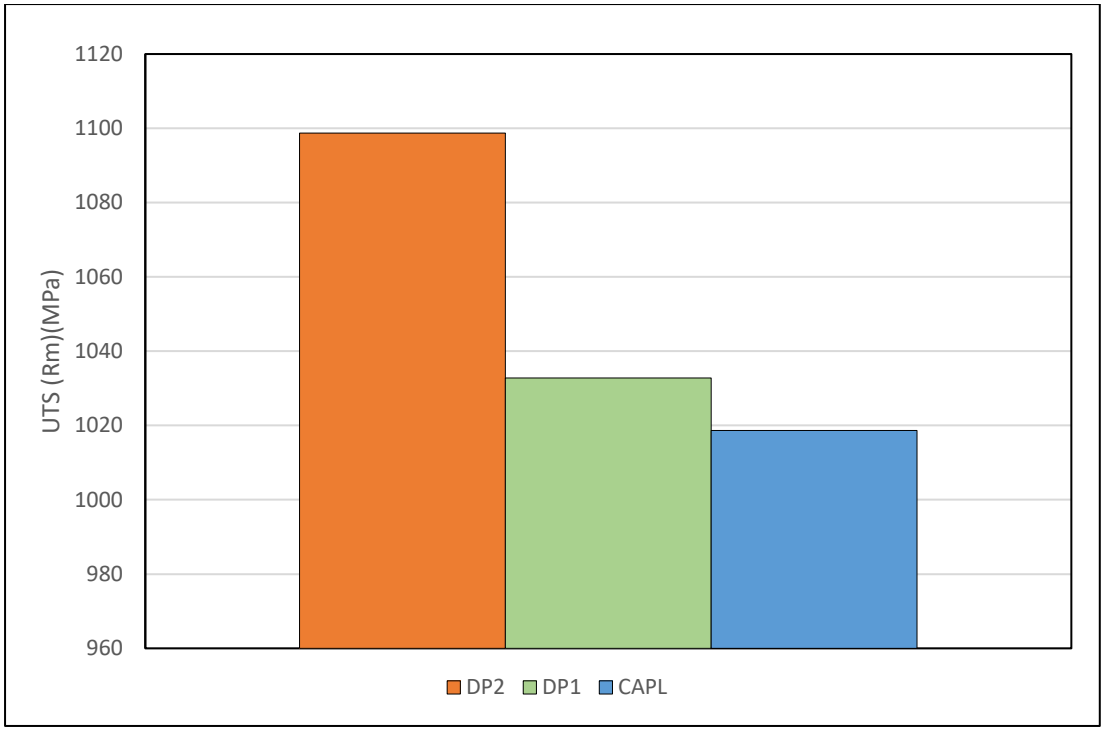

Figure 8.7. Tensile strength of DP2 trial material vs. DP1 and CAPL production material, using the same annealing parameters. A notable increase in UTS seen using the DP2 material compared to DP1 and CAPL production material.

The UTS results in figure 8.7 show DP2 trial material averages close to 1100MPa, 70MPa higher than the DP1 material which achieves an average of 1030MPa. The CAPL material only achieves slightly lower than this at 1020MPa. Each of the tests achieve above the minimum specification requirement of 980MPa on average.

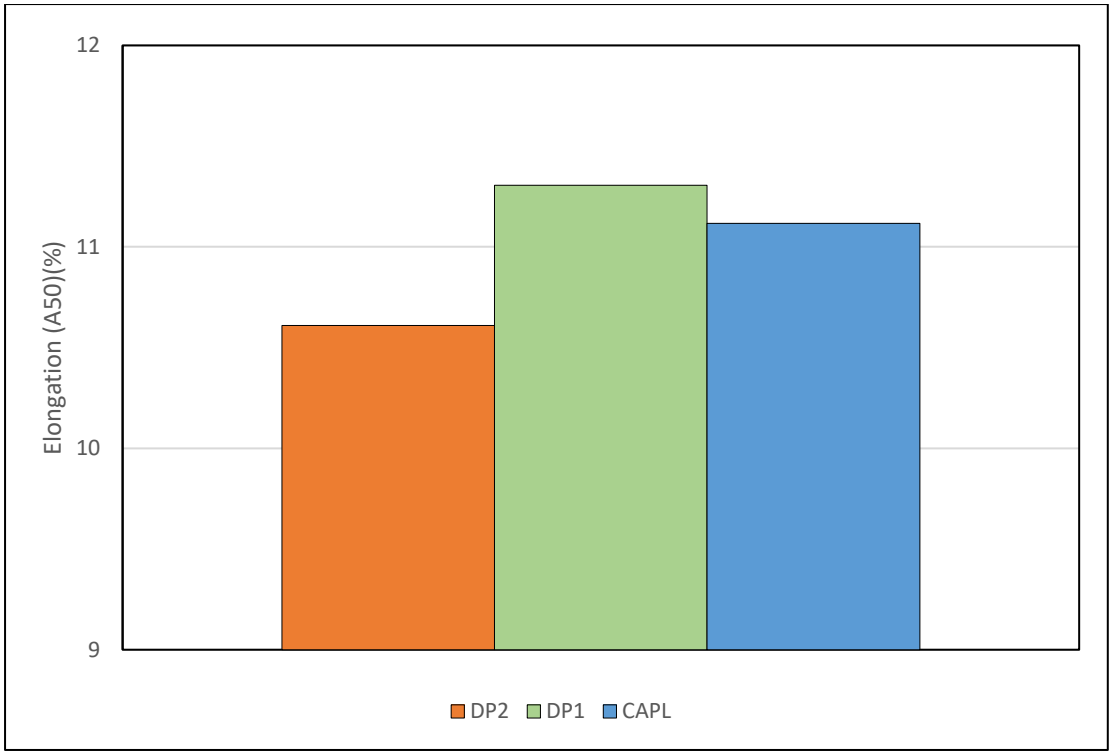

Figure 8.8. Elongation properties of DP2 trial material vs. DP1 and CAPL production material, using the same annealing parameters. Slight decrease in average elongation for DP2 compared to DP1 and CAPL material.

As can be expected, an increase in the tensile strength has led to a reduction in the ductility when compared to DP1 and CAPL material. The DP2 material achieving on average just over 10.5% whilst the DP1 and CAPL material achieve over 11%.

8.3. DP1000 low yield conclusion

The DP2 chemistry would be sufficient to achieve a viable DP1000 product on CAPL. The proof strength and the tensile strength would fall comfortably within the EN10388 specification during the standard DP1000 annealing cycle.

Whilst the elongation value averages achieve over the 10% minimum requirement, the minimum values achieved at 120mpm drop just below the limit. The inherent variability in the industrial annealing process can lead to temperatures and speeds that are more scattered than lab based testing. Therefore, the next step for trialling this material would be to see what effect other

annealing parameters would have on the mechanical properties, and whether varying the standard annealing cycle temperatures would be more beneficial to the DP2 chemistry.

8.4. DP1000 high yield

Building from the work in the section above for the DP1000 low yield, further experimentation was done in relation to adjustments of the CGJC temperature to try and achieve a high yield strength variant of DP1000, utilising the DP2 chemistry.

Internal trials by Tata Ijmuiden R&D showed promise when the temperature in the slow cooling region is increased. This increased the volume fraction of martensite and bainite in the microstructure, which in turn led to an increase in yield and tensile strength at the cost of lower ductility (152). This means that a differentiated product could be achieved by adjusting the furnace temperatures on the annealing line but keeping the chemistry of the material consistent.

It was from this work that it was decided that an increased slow cooling temperature would be trialled, raising the CGJC temperature from 620°C to 680°C. Whilst this increase was shown to benefit the DP1000 product via the DVL galvanising lines in IJmuiden, the processing conditions of CAPL are different, again due to the galvanising requirement for the DVL lines. However, this increase should be significant enough to show whether an improvement in yield strength can be achieved in the UK. The specification requirements for high yield DP1000 are shown in table 8.5.

Table 8.5 Mechanical property requirements of DP1000HY as specified on Euronorm standard EN 10338 (2)

Proof Strength (Rp) **MPa**	**Tensile Strength (Rm)** **MPa**	**Elongation (A)** **%**	**Bake Hardening (BH2)** **MPa**
700-850	980	8	30

8.5. DP1000LY vs. DP1000HY – results and discussions

The results in this section of work compare DP1000LY, processed with a CGJC of 620°C, and DP1000HY, with a CGJC temperature of 680°C as shown in table 2. For consistency, simulated line speeds are 120mpm for both sets of tests. To compare the changes in CGJC, light microscopy and SEM imaging was undertaken, with the high yield being designated DP1000HY and the low yield as DP1000LY. The differences between the tests are shown from figures 8.9-8.12.

Figure 8.9 DP1000LY with the white regions representing ferrite and the brown areas showing martensite.

Figure 8.10. DP1000HY with the white regions representing ferrite and the brown areas showing martensite. Small volume fraction of ferrite seen under light microscope image.

Both figure 8.9 and figure 8.10 consist of a ductile ferrite and harder martensite regions. Due to the refinement of the grains, it is difficult to see differences between the DP1000HY and the DP1000LY materials, though from these images there is seemingly a higher fraction of ferrite present in the DP1000LY material.

Using the SEM the differences between the microstructures become more apparent, as shown in figures 8.11 and 8.12:

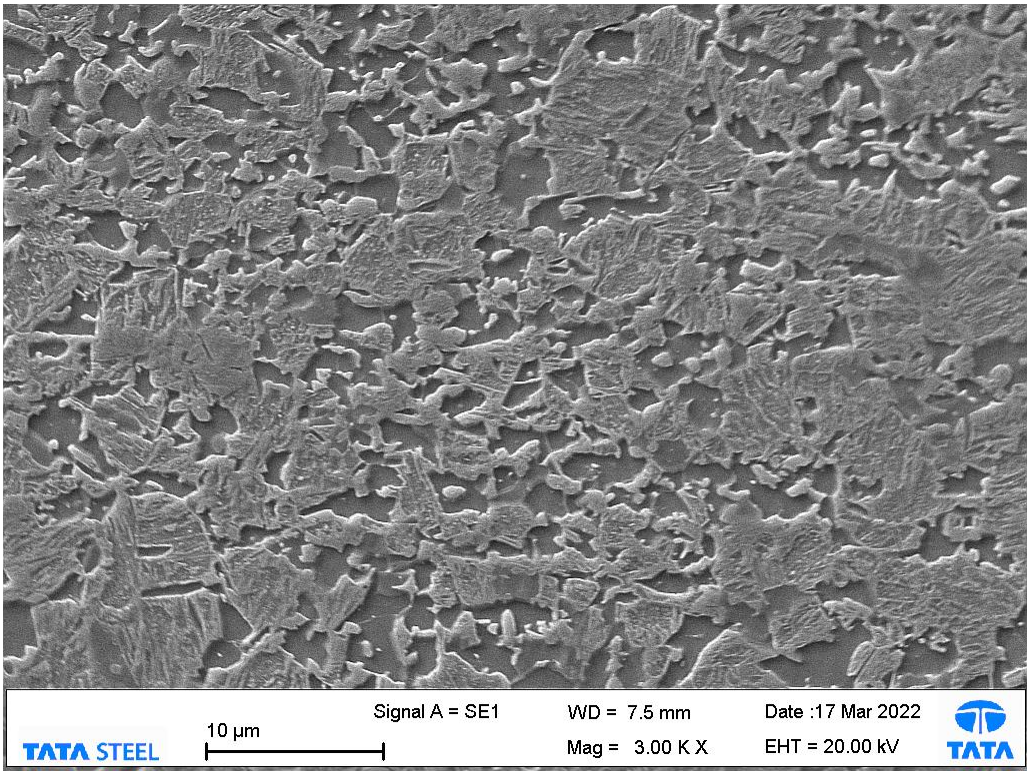

Figure 8.11. DP1000LY with the background as ferrite and martensite phase on top. The martensite has formed a skeletal structure with smaller regions of ferrite present within.

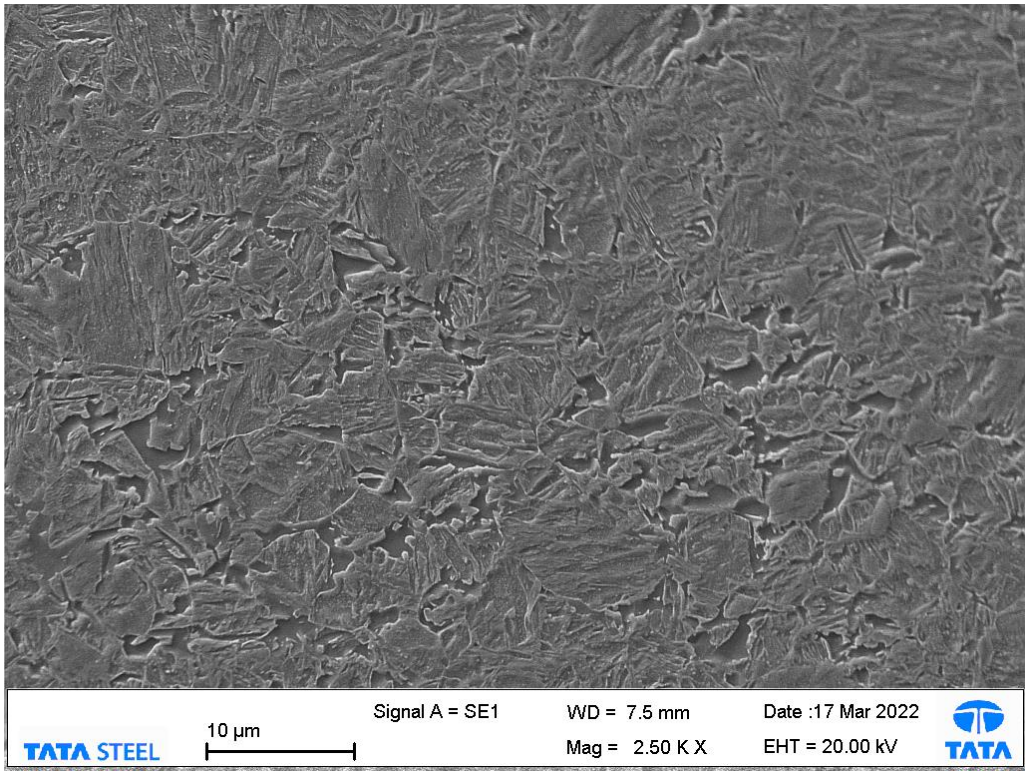

Figure 8.12. DP1000HY with background ferrite and a large volume fraction of martensite present. At such high volume the martensite forms a skeletal structure of martensite with small regions of refined ferrite present.

Whilst the microstructures of both the DP1000HY and DP1000LY are similar, with large volumes of martensite and small fractions of ferrite present, it is clear to see that the DP1000HY contains a higher volume fraction of martensite. The martensite also looks like it has started to temper more in the DP1000HY, this can be expected as the higher volume of martensite will retain lower carbon content. This means that during the cooling stage it is more likely to start tempering during the overage section. The volume fractions of both the DP1000LY and DP1000HY are shown in table 8.6.

Table 8.6. Phase fraction analysis of DP1000LY and DP1000HY

Sample	Martensite Average (%)	Ferrite Average (%)	Error +/- (%)
DP1000 LY	83	17	1.1
DP1000 HY	95	5	1.2

Whilst there is an increase in the volume fraction of martensite from 83% to 95%, it is also noted that the overall grain size has increased. These measurements are shown in table 8.7.

Table 8.7. Grain size analysis using the mean linear intercept method. Increased average grain size due to larger martensite in DP1000HY, whilst DP1000LY contains more refined martensite grains.

Sample	Grain Size Average (µm)	Grain Size Error (+/-) (µm)
DP1000 LY	2.8	0.05
DP1000 HY	4.11	0.36

The average grain size has increased from the DP1000LY from 2.8µm to 4.11µm. Typically, an increase in grain size would lead to an increase in ductility and lower strength (153), however this would be offset due to the large increase in volume fraction of martensite present in the microstructure.

Manual grain measurements of the ferrite phase in each sample show that the average ferrite grain size decreases from 2.39µm in the DP1000LY sample to 1.46µm in the DP1000HY sample. This reduction would contribute to an increase in the strength of the ferrite phase, whilst likely to be overshadowed by the contribution of strengthening from the martensite, a refined ferrite phase would increase strength.

The following graphs in figures 8.13 to 8.16 show the effect of increasing the CGJC. Each graph shows the average with the minimum and maximum shown as the error bars.

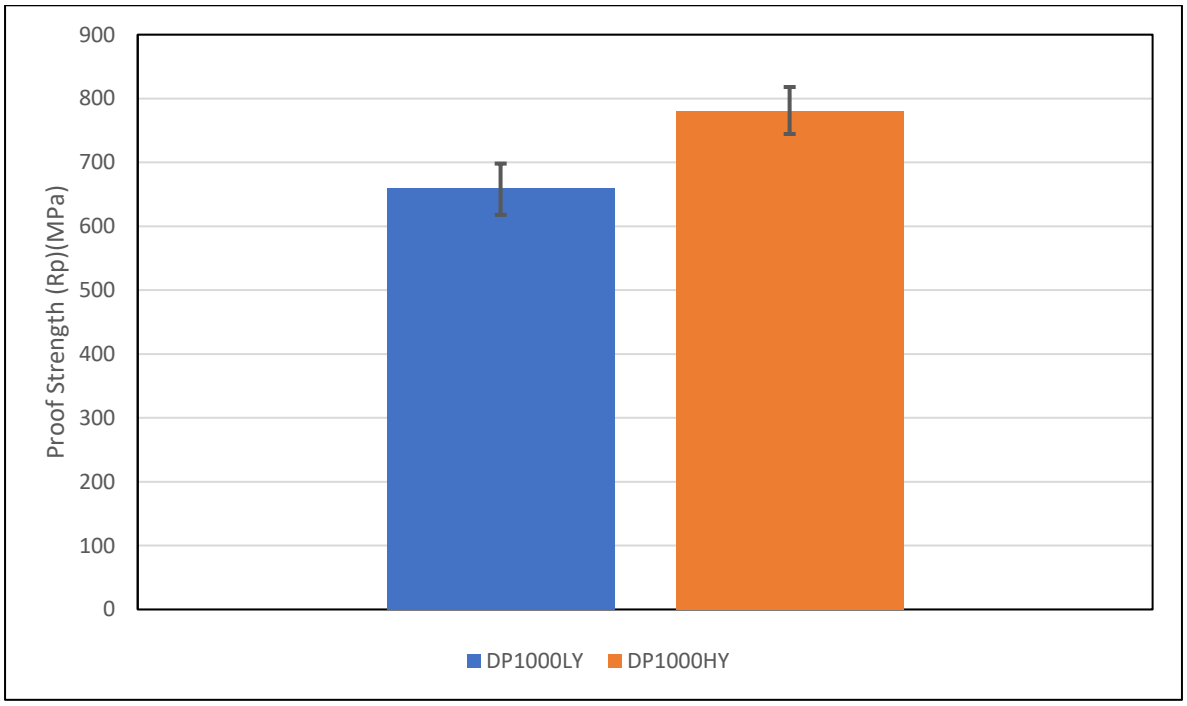

Figure 8.13. DP1000LY and DP1000HY showing the effect of CGJC temperature difference on the proof strength. Proof strength increased by 120MPa in DP1000HY compared to DP1000LY.

The DP1000LY averaged around 660MPa whereas the DP1000HY averaged 780MPa, an increase of 120MPa. An increase in the volume fraction of martensite will lead to an increase in the proof strength of the steel, as is seen in DP1000HY.

Due to the lower carbon content in austenite, which will occur with an increased martensite content, there will be a higher martensite start temperature (M_s). This increased M_s means that tempering of martensite is more likely to occur during the overage process of the annealing cycle (95). This will lead to a decrease in the strength of the martensite due to tempering, and will therefore increase the yield strength in the steel (154).

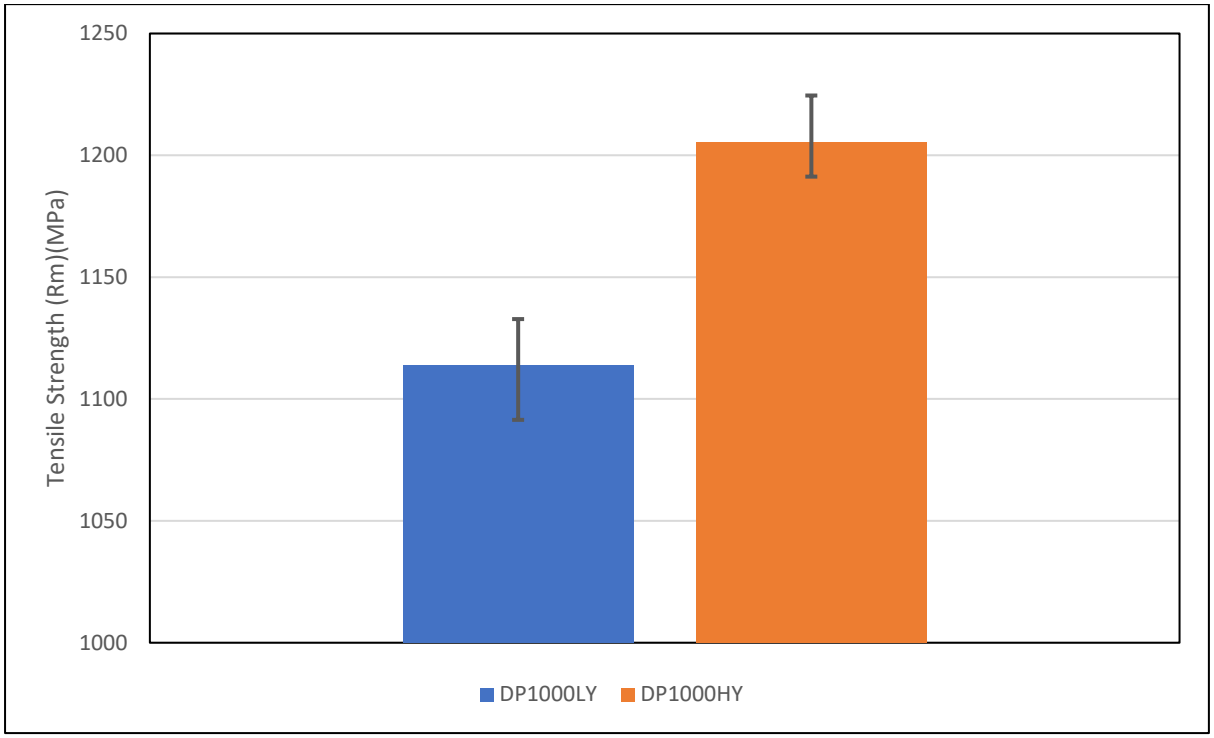

Figure 8.14. DP1000LY and DP1000HY showing the effect of CGJC temperature difference on the tensile strength. Considerable increase in strength seen from DP1000LY to DP1000HY.

As with yield strength, an increase in the volume fraction of martensite will lead to an increase in tensile strength. This is seen in figure 8.14, where the average of DP1000LY is 1110MPa and the increased martensite volume fraction in DP1000HY has led to an increased average tensile strength of 1200MPa, an increase of 90MPa.

The increase in volume fraction of martensite present in the DP1000HY has led to an increase in strength. Whilst more martensite may be tempered in comparison to the DP1000LY, the increased volume fraction will negate this difference. Additionally, the refine grains of the ferrite would add to the increased strength in comparison to the larger ferrite grains seen in the DP1000LY (155).

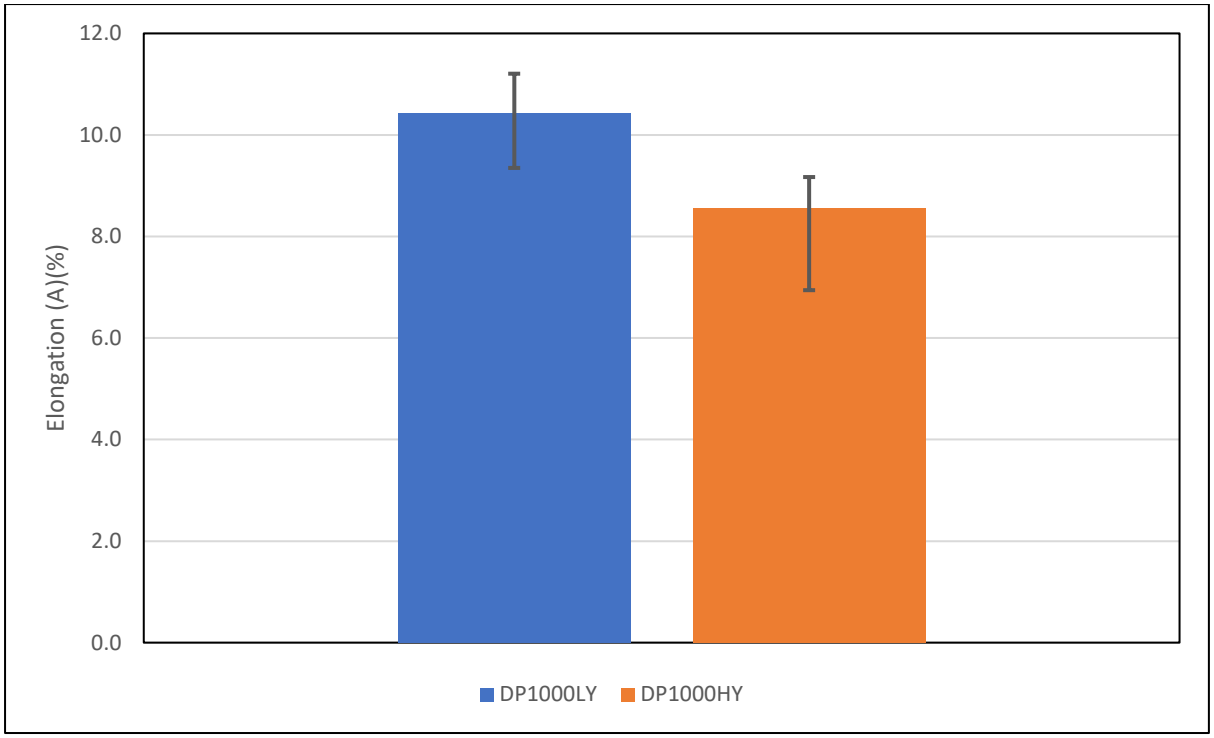

Figure 8.15. DP1000LY and DP1000HY showing the effect of CGJC temperature difference on the elongation. Decrease in elongation for DP1000HY compared to DP1000LY.

As expected, the increase in strength of the DP1000HY has led to a decrease in the elongation properties, which is seen in figure 8.15. The DP1000LY achieved on average 10.4% whilst the DP1000HY had an average of 8.5%. This decrease will again be related to the increase in martensite volume fraction of the DP1000HY.

Whilst the average elongation is above the minimum specification requirement of 8%, the lowest value recorded of 6.9% falls below the requirement, therefore the variability of the elongation properties and its proximity on average to the specification requirement means that on an industrial processing line it would be difficult to achieve the required properties.

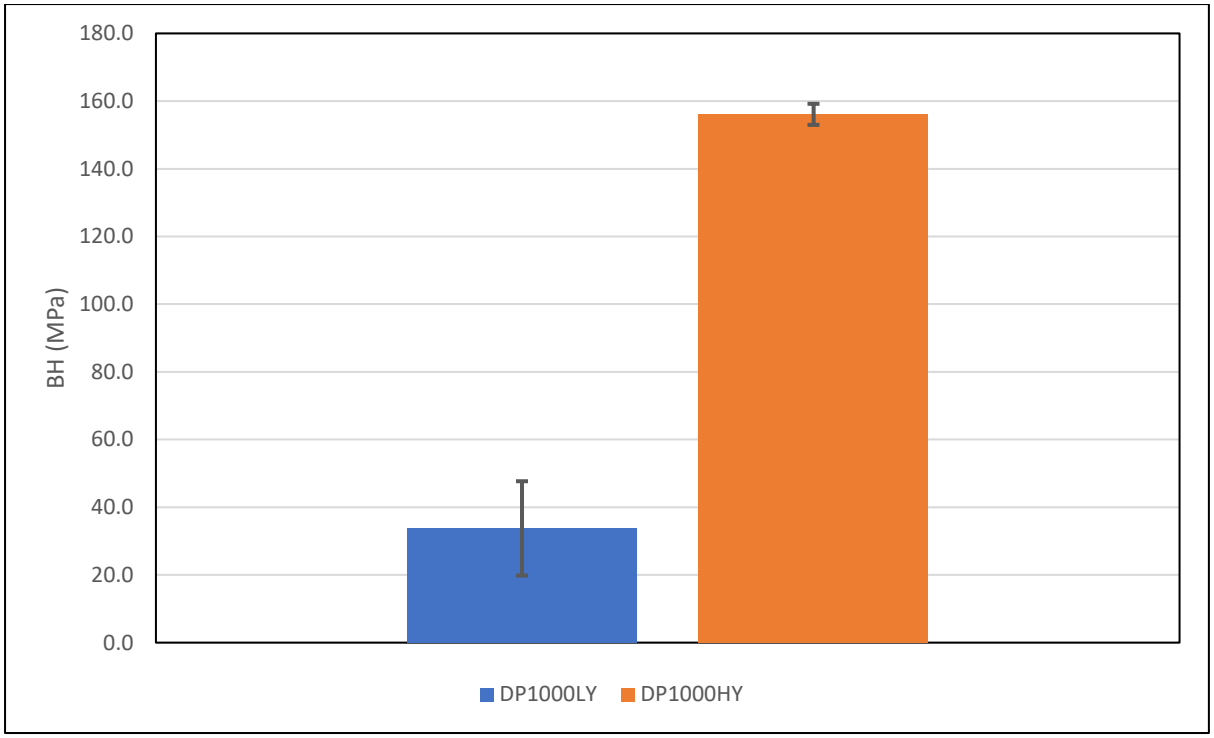

Figure 8.16. DP1000LY and DP1000HY showing the effect of CGJC temperature difference on the bake hardening.

The biggest improvement seen in mechanical properties is the increase in bake hardening response. The average BH response for the DP1000LY was 33MPa. Whilst this is over the 30MPa requirement in the EN standard, the variability of the BH response means it often falls below what is required.

Conversely, the DP1000HY achieved on average 156MPa, far exceeding the 30MPa requirement. There are likely to be several contributing factors to this, firstly, an increase in volume fraction of martensite has been shown to positively effect the BH response due to stronger dislocation pinning occurring at the ferrite – martensite interfaces (156)(157)

The higher volume fraction of martensite will lead to a lower carbon in the martensite present in the DP1000HY. Therefore, it can be expected that during the overage section that tempering of the martensite would occur. This tempered martensite allows for an increased free carbon content, allowing for further pinning of dislocations in the ferrite / martensite interface, increasing the BH response.

8.6. DP1000 high yield conclusion

Increasing the CGJC temperature from 620°C to 680°C has shown promise. The yield strength improved from an average of 660MPa in the DP1000LY to 780MPa in the DP1000HY, an increase of 120MPa. The tensile strength also increased from 1100MPa in the DP1000LY to 1200MPa in the DP1000HY, a 90MPa increase. Conversely, the elongation dropped on average from 10.4% in the DP1000LY to 8.5% in the DP1000HY.

Whilst the strength characteristics are sufficient to achieve a viable DP1000HY product, the elongation values are close to, and on occasion below, the requirement of the specification. Further experimentation would be required adjusting the CGJC temperature, it would be expected that decreasing the temperature would lower the strength but increase the ductility due to an increase ferrite phase volume fraction, finding a balance that would achieve the required specification limits.

9. Conclusions

Chapter five of this work was dedicated to understanding the effects industrial processing can have on a DP steel's microstructure and mechanical properties.

- It was concluded that 800°C was optimum mechanical property range for soak temperature, whilst 325°C provided the best combination of properties as a HGJC temperature. This combination provides the best strength and ductility, whilst allowing for sufficient bake hardening to achieve the required 30MPa specification limit.

In chapter six, the effect of silicon additions on the mechanical properties and microstructure of DP800 steel was investigated.

- It was found that an increase in silicon improved the tensile strength and yield strength for all HGJC temperatures, whilst the elongation values were kept constant.
- The improvement in mechanical properties seen from increasing silicon content is linked back to the hot rolling process, where the silicon additions increased the volume fraction of pearlite, as well as its grain refinement.

Chapter seven investigated whether a DP chemistry (DP2) with increased Si and C would produce a viable DP1000 product through Tata's continuous galvanising line, Zodiac.

- The investigation showed the biggest effect on mechanical properties came from varying soak temperature and line speed.
- No set of processing parameters was found to produce a DP1000 product that would consistently achieve the Euronorm requirement.

Chapter eight investigated whether the DP chemistry (DP2) would produce a viable DP1000 product through Tata's continuous annealing line, CAPL.

- Trials showed a DP1000 low yield specification was easily achievable with this chemistry using current DP1000 processing conditions.
- Additionally, an adjustment to the cooling during the annealing cycle showed promise for a novel DP1000 high yield product could be created using the DP2 chemistry, a potential differentiated product for Tata.

10. Further Work

This thesis has highlighted the benefits of silicon additions to the chemistry of DP800 steel. By increasing the level of silicon from 0.2% to 0.4%, an increased strength can be achieved while retaining the ductility. The specification limitations of silicon content could look to be increased to 0.7wt%, which could show to produce a greater benefit, this could be a potential avenue for further investigation.

This work has shown the benefits that can be achieved for the mechanical properties, however additional work was initially planned around the galvanic coating. Research suggests that increasing the Si content by up to 0.5wt% worsens the wettability of the coating, by generating $MnSiO_3$ and Mn_2SiO_4 oxides (103). As already alluded to previously in this work, both CAPL and Zodiac use the same steel chemistry to produce a DP800 product. This means that trialling the effect that the increased silicon content has on the wettability of the steel would be critical before such a change could be made to the grade. Due to time and equipment constraints, this work was not able to be fully achieved, with only a few coating trials undertaken.

An initial investigation to identifying the effects of silicon on the nano hardness of the DP microstructure was made in this thesis. It was hoped that being able to accurately measure the impact silicon was having on the ferrite and martensite microstructure would further prove the theory read in literature, where silicon has been shown to provide solid solution strengthening to ferrite. Due to steel sample production delays, this piece of work was started late into this doctorate, limiting the amount of work that could be done. Future work could establish individual grain measurements and measure individual phase strength as a function of silicon content using the nano indentor.

The processing window identified in this work has been set up at Tata to produce DP800 through CAPL, using the soak temperature and HGJC temperature to produce the best combination of mechanical properties. This work recommends an increase in the silicon content for an improvement in the strength characteristics of DP800 through CAPL. This change should improve the rejection rate for mechanical properties, particularly for bake hardening where the current product falls close to the 30MPa limit.

Changing the chemistry to the current DP1 chemistry to using DP2 should also bring benefits to the DP1000 product through CAPL. Whilst this work shows a viable product is not possible through Zodiac, using the DP2 grade will mean a Tata UK specific chemistry can be replaced with a chemistry

that is already used in Ijmuiden, which should improve the lead time for production. Additionally, using the grade has shown promise to produce a DP1000 high yield product, which would add to Tata's current offering as a differentiated product.

Whilst industrial competitors have different processing capabilities and chemistries to produce DP800 and DP1000 grades, this body of work would be transferrable for the identification and improvement in processing conditions through continuous annealing and continuous galvanising lines, as well as showing the benefits of silicon additions to processing of DP material.

11. References

1. Rynikiewicz C. The climate change challenge and transitions for radical changes in the European steel industry. J Clean Prod. 2008;16(7):781–9.

2. Keeler S, Kimchi M, J. Mooney P. Advanced High-Strength Steels Application Guidelines Version 6.0. 2017;(September):314.

3. Rowe J. Advanced materials in automotive engineering. J R, editor. Cambridge: Woodhead Publishing; 2012. 340 p.

4. Mayyas AT, Qattawi A, Mayyas AR, Omar MA. Life cycle assessment-based selection for a sustainable lightweight body-in-white design. Energy. 2012;39(1):412–25.

5. Ungureanu CA, Das S, Jawahir IS. Life-cycle Cost Analysis : Aluminum versus Steel in Passenger Cars. Miner Met Mater Soc. 2007;11–24.

6. Frees N. Crediting Aluminium Recycling in LCA by Demand or by Disposal. Int J Life Cycle Assess. 2007;13(3):212–8.

7. Fonstein N. Dual-phase steels. Automotive Steels: Design, Metallurgy, Processing and Applications. 2016. 169–216 p.

8. Saeidi N, Ekrami A. Comparison of mechanical properties of martensite/ferrite and bainite/ferrite dual phase 4340 steels. Mater Sci Eng A. 2009;523(1–2):125–9.

9. Shah K, Kumar R, Sahoo S, Pais RS, Chakrabarti D, Chakraborti N. Optimization of annealing cycle parameters of dual phase and interstitial free steels by multiobjective genetic algorithms. Mater Manuf Process. 2017;32(10):1201–8.

10. Thomas G. The Physical Metallurgy and Alloy Design of Dual Phase Steels. 1983;

11. Pereloma E, Timokhina I. Bake hardening of automotive steels [Internet]. Automotive Steels: Design, Metallurgy, Processing and Applications. Elsevier Ltd; 2016. 259–288 p. Available from: http://dx.doi.org/10.1016/B978-0-08-100638-2.00009-2

12. Bouaziz O, Zurob H, Huang M. Driving force and logic of development of advanced high strength steels for automotive applications. Steel Res Int. 2013;84(10):937–47.

13. Tata Steel. HyperForm [Internet]. 2022 [cited 2022 Oct 12]. Available from: https://www.tatasteeleurope.com/automotive/key-products/hyperform

14. Davies G. Materials for Automobile Bodies. 2nd, editor. Butterworth-Heinemann; 2012.

15. Callister WD, Rethwisch DG. Materials Science and Engineering [Internet]. 8th ed. Welter J, editor. Materials Science and Engineering A. New Jersey: John Wiley & Sons; 2011. 213 p. Available from: http://linkinghub.elsevier.com/retrieve/pii/S0928493108002312

16. Bhadeshia H, Honeycombe R. Steels: Microstructure and Properties. 4th ed. Kent C, editor. Steels: Microstructure and Properties. Oxford: Butterworth-Heinemann; 2006. 135–137 p.

17. Sheyaa Alwan A, Abbass M, Jalil JM. Parametric Study of Metallurgical and Heat Transfer Characteristics of Manual Metal Arc Welding Process FRICTION STIR WELDING View project Effect Effect of Cerium Addition on Mechanical properties and Microstructure of Al-12%Si Alloys View project. 2009;(February 2016). Available from: https://www.researchgate.net/publication/293333803

18. El-Sesy IA, El-Baradie ZM. Influence carbon and/or iron carbide on the structure and properties of dual-phase steels. Mater Lett. 2002;57(3):580–5.

19. Hamada S, Sasaki D, Ueda M, Noguchi H. Fatigue limit evaluation considering crack initiation for lamellar pearlitic steel. Procedia Eng [Internet]. 2011;10:1467–72. Available from:

http://dx.doi.org/10.1016/j.proeng.2011.04.245

20. Wang X, Zurob HS, Xu G, Ye Q, Bouaziz O, Embury D. Influence of microstructural length scale on the strength and annealing behavior of pearlite, bainite, and martensite. Metall Mater Trans A Phys Metall Mater Sci. 2013;44(3):1454–61.

21. Reed-Hill R AR. Physical Metallurgy. Phys Metall Princ [Internet]. 1991;3. Available from: http://www.sciencedirect.com/science/article/pii/B9780444537706000228

22. Krauss G. Principles of Heat Treatment of Steel. Ohio: American Society for Metals; 1980. 14–15 p.

23. Erdogan M. Effect of austenite dispersion on phase transformation in dual phase steel. Vol. 48, Scripta Materialia. 2003. p. 501–6.

24. Krauss G. Steels: Processing, Structure, and Performance. ASM International. 2015. 63–65 p.

25. Mayer D. Why are some stainless steels magnetic? | VGO Inc. [Internet]. VGO. [cited 2018 Feb 27]. Available from: http://vgoinc.com/general/why-are-some-stainless-steels-magnetic

26. Han K, G M. van G, Bottger A. Initial stages of Fe-C martensite decomposition. Philos Mag A. 2001;81(3):741–57.

27. Bhadeshia HKD. Tempered Martensite [Internet]. University of Cambridge. 2004 [cited 2022 Oct 12]. Available from: https://www.phase-trans.msm.cam.ac.uk/2004/Tempered.Martensite/tempered.martensite.html

28. Azuma M, Goutianos S, Hansen N, Winther G, Huang X. Effect of hardness of martensite and ferrite on void formation in dual phase steel. Mater Sci Technol [Internet]. 2012;28(9–10):1092–100. Available from: http://www.tandfonline.com/doi/full/10.1179/1743284712Y.0000000006

29. Yang ZG, Fang HS. An overview on bainite formation in steels. Curr Opin Solid State Mater Sci. 2005;9(6):277–86.

30. Mehl R. Hardenability of Alloy Steels. In: ASM. Ohio; 1939. p. 1–54.

31. Bramfitt BL, Speer JG. A perspective on the morphology of bainite. Metall Trans A. 1990;21(3):817–29.

32. Edmonds D., Cochrane R. Structure-property relationships in bainitic steels. Metall Trans A. 1990;21:1527–40.

33. Takahashi M, Bhadeshia HKD. Model for transition from upper to lower bainite. Mater Sci Technol. 1990;(7):592–603.

34. Bhadeshia HKD. Bainite in Steels. 2nd ed. London: Maney Publishing; 2001. 1–600 p.

35. Bhadeshia HKDH. Novel Steels for Rails. Encycl Mater Sci Technol. 2002;1–7.

36. Goodall AL. Effect of initial microstructure and tempering parameters on the precipitation characteristics and mechanical properties of alloyed quenched and tempered steel plates. Birmingham; 2019.

37. Dossett JL, Boyer HE. Fundamentals of the Heat Treating of Steel. In: Practical Heat Treating, Second Edition. 2nd ed. ASM International; 2006. p. 296.

38. Maffei B, Salvatore W, Valentini R. Dual-phase steel rebars for high-ductile r.c. structures, Part 1: Microstructural and mechanical characterization of steel rebars. Eng Struct. 2007;29(12):3325–32.

39. de la Concepción VL, Lorusso HN, Svoboda HG. Effect of Carbon Content on Microstructure and Mechanical Properties of Dual Phase Steels. Procedia Mater Sci. 2015;8:1047–56.

40. Deeley P.D, Kundig K.J.A SJH. Ferroalloys & Alloying Additives Handbook. 1st ed. New York: Metallurg Alloy Corporation; 1981. 54–59 p.

41. Calcagnotto M, Ponge D, Raabe D. Ultrafine Grained Ferrite/Martensite Dual Phase Steel Fabricated by

Large Strain Warm Deformation and Subsequent Intercritical Annealing. ISIJ Int. 2008;48(8):1096–101.

42. Calcagnotto M, Ponge D, Raabe D. On the effect of manganese on grain size stability and hardenability in ultrafine-grained ferrite/martensite dual-phase steels. Metall Mater Trans A Phys Metall Mater Sci. 2012;43(1):37–46.

43. Girina OA, Fonstein NM. Influence of Al Additions on Austenite Decomposition in Continuously Annealed Dual-Phase Steels. Mater Sci Technol. 2005;(January 2005):65–76.

44. Garfias-Mesias LF, Sykes JM, Tuck CDS. The effect of phase compositions on the pitting corrosion of 25 Cr duplex stainless steel in chloride solutions. Corros Sci. 1996;38(8):1319–30.

45. Zhao J, Jiang Z. Thermomechanical processing of advanced high strength steels. Prog Mater Sci. 2018;(94):174–242.

46. Llewellyn D. Steels: Metallurgy & Applications. 2nd ed. Oxford: Butterworth-Heinemann; 1994. 22–23 p.

47. Lee K, Han J, Park J, Kim B, Ko D. Prediction and control of front-end curvature in hot finish rolling process. Adv Mech Eng. 2015;7(11):1–10.

48. Evans P., Jones L., Brown A, Gladwyn G, Grabham B. DP800CR Review of Through Process Effects. 2017.

49. Volkers A. Introduction to cold rolling [Internet]. Q8 Oils. 2018 [cited 2021 Oct 5]. Available from: https://www.q8oils.com/metalworking/introduction-cold-rolling/

50. Bhav Singh B, Sivakumar K, Balakrishna Bhat T. Effect of cold rolling on mechanical properties and ballistic performance of nitrogen-alloyed austenitic steels. Int J Impact Eng [Internet]. 2009;36(4):611–20. Available from: http://dx.doi.org/10.1016/j.ijimpeng.2008.07.082

51. Davies I. Development of a processing route for producing galvanised dual phase steel at the Zodiac Galvanising Line. Swansea University; 2010.

52. Wigley NR. Property Prediction of Continuous Annealed Steels. 2012.

53. Kong Z, Zhang J, Li H, Kong N. Effects of Continuous Annealing Process Parameters on the Microstructure and Mechanical Properties of Dual Phase Steel. Steel Res Int. 2018;89(8):1–10.

54. García De Andrés C, Caballero FG, Capdevila C, Álvarez LF. Application of dilatometric analysis to the study of solid-solid phase transformations in steels. Mater Charact. 2002;48(1):101–11.

55. Hashiguchi K. Effects of alloying elements and cooling rate after annealing on mech props of dual phase sheet steel. Kawasaki Steel Tech Rep. 1980;(1):70–8.

56. Herring PR. Group 2 Steels: Medium Carbon Alloy Steels (0.25-0.55% C) [Internet]. 2017. Available from: http://slideplayer.com/slide/4630237/

57. Girina O, Fonstein N, Yakubovsky O, Panahi D. The Influence of Mo, Cr and B Alloying on Phase Transformation and Mechanical Properties in Nb Added High Strength Dual Phase Steels. In: HSLA Steels 2015. 2015. p. 237–45.

58. Campbell F. Inspection of Metals: Understanding the basics. Ohio: ASM International; 2013. 117 p.

59. BSI. BS EN ISO 2566-1. European Commitee for Standardization; 1999.

60. Wyatt O, Dew-Hughes D. Metals, Ceramics and Polymers. 1st ed. London: Cambridge University Oress; 1974. 146–150 p.

61. Danilov VI, Gorbatenko V V, Zuev LB, Orlova D V, Danilova L V. Luders deformation of low-carbon steel. Steel Transl [Internet]. 2017;47(10):662–8. Available from: https://www.scopus.com/inward/record.uri?eid=2-s2.0-85040924300&doi=10.3103%2FS0967091217100035&partnerID=40&md5=d683ce394122b87e4ca9764bd47b5651

62. Calcagnotto M, Ponge D, Demir E, Raabe D. Orientation gradients and geometrically necessary dislocations in ultrafine grained dual-phase steels studied by 2D and 3D EBSD. Mater Sci Eng A. 2010;527(10–11):2738–46.

63. Gündüz S. Effect of chemical composition, martensite volume fraction and tempering on tensile behaviour of dual phase steels. Mater Lett. 2009;63(27):2381–3.

64. Çavuşoğlu O, Toros S, Gürün H. Microstructure based modelling of stress–strain relationship on dual phase steels. Ironmak Steelmak. 2017;9233.

65. Higgins R. Properties of Engineering Materials. 2nd ed. Industrial Press Inc.; 1994. 74–75 p.

66. Sakata K, Satoh S, Kato T, Hashimoto O. Metallurgical principles and applications for producing extra-low carbon IF steels with deep drawability and bake hardenability. Int Forum Phys Metall IF Steels. 1994;279–88.

67. Ballarin V, Soler M, Perlade A, Lemoine X, Forest S. Mechanisms and modeling of bake-hardening steels: Part I. Uniaxial tension. Metall Mater Trans A Phys Metall Mater Sci. 2009;40(6):1367–74.

68. Das S, Singh SB, Mohanty ON, Bhadeshia HKDH. Understanding the complexities of bake hardening. Mater Sci Technol [Internet]. 2008;24(1):107–11. Available from: http://www.tandfonline.com/doi/full/10.1179/174367507X247511

69. Cottrell AH, Bilby BA. Dislocation theory of yielding and strain ageing of iron. Proc Phys Soc Sect A. 1949;62(1):49–62.

70. Waterschoot T, De AK, Vandeputte S, de Cooman BC. Static strain aging phenomena in cold-rolled dual-phase steels. Metall Mater Trans A Phys Metall Mater Sci. 2003;34(13):781–91.

71. Timokhina IB, Pereloma E V., Ringer SP, Zheng RK, Hodgson PD. Characterization of the Bake-hardening Behavior of Transformation Induced Plasticity and Dual-phase Steels Using Advanced Analytical Techniques. ISIJ Int [Internet]. 2010;50(4):574–82. Available from: http://www.scopus.com/inward/record.url?eid=2-s2.0-77953632182&partnerID=tZOtx3y1

72. Krieger M, Estrin Y, Janecek M, Niemeyer M, Paul S. Mechanical Properties and Bake Hardening Behaviour of two Cold Rolled Multiphase Sheet Steels subjected to CGL Heat Treatment Simulation. Steel Res Int. 2006;77(9–10):668–74.

73. Shimada S, Takada Y, Lee J, Tanaka T. Trial to Evaluate Wettability of Liquid Zn with Steel Sheets Containing Si and Mn. ISIJ Int. 2008;48(9):1246–50.

74. Prabhudev S, Swaminathan S, Rohwerder M. Effect of oxides on the reaction kinetics during hot-dip galvanizing of high strength steels. Corros Sci [Internet]. 2011;53(7):2413–8. Available from: http://dx.doi.org/10.1016/j.corsci.2011.03.027

75. Kim Y, Lee J, Jeon SH, Chin KG. The influence of Mn content on the wettability of dual-phase high-strength steels by liquid Zn-0.23 % Al. J Mater Sci. 2012;47(24):8477–82.

76. Kalhor A, Mirzadeh H. Tailoring the Microstructure and Mechanical Properties of Dual Phase Steel Based on the Initial Microstructure. Steel Res Int. 2017;88(8):1–8.

77. Satjabut P, Kalhor A, Uthaisangsuk V, Mirzadeh H. Microstructure and Mechanical Properties of Dual-Phase Steels by Combining Adjusted Initial Microstructures and Severe Plastic Deformation. Steel Res Int. 2022;93(5):1–9.

78. Deng Y gang, Di H shuang, Misra RDK. On significance of initial microstructure in governing mechanical behavior and fracture of dual-phase steels. J Iron Steel Res Int [Internet]. 2018;25(9):932–42. Available from: https://doi.org/10.1007/s42243-018-0133-0

79. Meng Q, Li J, Li P. Effect of heating rate and temperature on microstructure evolution of cold rolled dual phase steel. Int Heat Treat Surf Eng. 2014;8(3).

80. Deng YG, Li Y, Di H, Misra RDK. Effect of Heating Rate during Continuous Annealing on Microstructure

and Mechanical Properties of High-Strength Dual-Phase Steel. J Mater Eng Perform. 2019;28(8):4556–64.

81. Valdes-Tabernero MA, Celada-Casero C, Sabirov I, Kumar A, Petrov RH. The effect of heating rate and soaking time on microstructure of an advanced high strength steel. Mater Charact. 2019;155:1–34.

82. Mohanty RR, Girina OA, Fonstein NM. Effect of heating rate on the austenite formation in low-carbon high-strength steels annealed in the intercritical region. Metall Mater Trans A Phys Metall Mater Sci. 2011;42(12):3680–90.

83. Fonstein N. Advanced High Strength Sheet Steels. Advanced High Strength Sheet Steels. 2015. 34–35 p.

84. Hüseyin A, Havva KZ, Ceylan K. Effect of Intercritical Annealing Parameters on Dual Phase Behavior of Commercial Low-Alloyed Steels. J Iron Steel Res Int. 2010;17(4):73–8.

85. Maleki M, Mirzadeh H, Zamani M. Effect of Intercritical Annealing on Mechanical Properties and Work-Hardening Response of High Formability Dual Phase Steel. Steel Res Int. 2018;89(4).

86. Alfirano, Samdan W, Maulud H. Effect of intercritical annealing temperature and holding time on microstructure and mechanical properties of dual phase low carbon steel. Appl Mech Mater. 2014;493:721–6.

87. Rai PK, Kumar DS, Balachandran G. Effect of composition and inter-critical annealing parameters on microstructure and mechanical properties of DP steel. Sadhana - Acad Proc Eng Sci [Internet]. 2022;47(3). Available from: https://doi.org/10.1007/s12046-022-01886-3

88. Girina O. Effect of Annealing Parameters on Austenite Decomposition in a continuously Annealed {Dual-Phase} Steel. 41th {MWSP}. 2003;(January 2003):403–14.

89. Speich GR, Demarest VA, Miller RL. FORMATION OF AUSTENITE DURING INTERCRITICAL ANNEALING OF DUAL-PHASE STEELS. Metall Trans A, Phys Metall Mater Sci. 1981;

90. Garcia CI, Deardo AJ. FORMATION OF AUSTENITE IN 1. 5 PCT Mn STEELS. Metall Trans A, Phys Metall Mater Sci. 1981;12 A(3):521–30.

91. Bandi B, Van Krevel J, Srirangam P. Interaction Between Ferrite Recrystallization and Austenite Formation in Dual-Phase Steel Manufacture. Metall Mater Trans A Phys Metall Mater Sci [Internet]. 2022;53(4):1379–93. Available from: https://doi.org/10.1007/s11661-022-06597-2

92. Andrews KW. Empirical formulae for the calculation of some transformation temperatures. JISI. 1965;203:721–7.

93. Geib M, Matlock D, Krauss G. The effect of intercritical annealing temperature on the structure of niobium microalloyed dualphase steel. Metall Trans A. 1980;11:1683–9.

94. Bhadeshia HKDH, Edmonds D V. Analysis of mechanical properties and microstructure of high-silicon dual-phase steel. Met Sci. 1980;14(2):41–9.

95. Fonstein N. Advanced high strength sheet steels: Physical metallurgy, design, processing, and properties. Advanced High Strength Sheet Steels: Physical Metallurgy, Design, Processing, and Properties. 2015. 43 p.

96. Fonstein N. Evolution of advanced high strength steels (ahss) for automotive industry. Tech Contrib to 50th Roll Semin – Process Roll Coat Prod November, 18th to 21s. 2013;

97. Cai MH, Ding H, Lee YK, Tang ZY, Zhang JS. Effects of Si on microstructural evolution and mechanical properties of hot-rolled ferrite and bainite dual-phase steels. ISIJ Int. 2011;51(3):476–81.

98. Davies R. Formable HSLA and Dual Phase Steels. In: Formable HSLA and Dual Phase Steels. 1981.

99. Hayami, T Furukawa HG. Recent developments in formable hot and cold rolled HSLA including dual-phase steels. In: Formable HSLA and dual-phase steels. 1979.

100. Drumond J, Girina O, da Silva Filho JF, Fonstein N, de Oliveira CAS. Effect of Silicon Content on the

Microstructure and Mechanical Properties of Dual-Phase Steels. Metallogr Microstruct Anal. 2012;

101. Mein A. Hot Rolled Multiphase Steels. Swansea University; 2012.

102. Saleh MH, Priestner R. Retained austenite in dual-phase silicon steels and its effect on mechanical properties. J Mater Process Technol. 2001;113(1–3):587–93.

103. Kim Y, Lee J, Park J, Jeon SH. Effect of Si content on wettability of dual phase high strength steels by liquid Zn-0.23 wt.%Al. Met Mater Int. 2011;17(4):607–11.

104. Meschut G, Böhne C, Rethmeier M, Biegler M, Frei J, Dahmene F, et al. Combined Reports - AHSS Implementation Solutions: Liquid Metal Embrittlement Study. 2020;(June):220.

105. Ghatei Kalashami A, DiGiovanni C, Razmpoosh MH, Goodwin F, Zhou NY. The effect of silicon content on liquid-metal-embrittlement susceptibility in resistance spot welding of galvanized dual-phase steel. J Manuf Process [Internet]. 2020;57(May):370–9. Available from: https://doi.org/10.1016/j.jmapro.2020.07.008

106. BSI. BS EN 10338:2015. London: British Standards Institution; 2015. p. 10.

107. Davis JR. Tensile testing. 2nd ed. Tensile testing. ASM International; 2004. 44 p.

108. WorldAutoSteel. Bake Hardenable - AHSS Guidelines [Internet]. 2021. Available from: https://ahssinsights.org/metallurgy/steel-grades/ahss/bake-hardenable-steel/

109. Bogner A, Jouneau PH, Thollet G, Basset D, Gauthier C. A history of scanning electron microscopy developments: Towards “wet-STEM” imaging. Micron. 2007;38(4):390–401.

110. Saunders N, Guo Z, Li X, Miodownik AP, Schillé JP. Using JMatPro to model materials properties and behavior. Jom. 2003;55(12):60–5.

111. Arganda-Carreras I, Kaynig V, Rueden C, Eliceiri KW, Schindelin J, Cardona A, et al. Trainable Weka Segmentation: A machine learning tool for microscopy pixel classification. Bioinformatics. 2017;33(15):2424–6.

112. BSI Standards Publication. BS EN ISO 643-2020 - Steels — Micrographic determination of the apparent grain size. 2020.

113. Ayres J, Penney D, Evans P, Underhill R. Effect of intercritical annealing on the mechanical properties of dual-phase steel. Ironmak Steelmak [Internet]. 2022;1–7. Available from: https://doi.org/10.1080/03019233.2022.2062163

114. Movahed P, Kolahgar S, Marashi SPH, Pouranvari M, Parvin N. The effect of intercritical heat treatment temperature on the tensile properties and work hardening behavior of ferrite-martensite dual phase steel sheets. Mater Sci Eng A. 2009;518(1–2):1–6.

115. Alibeyki M, Mirzadeh H, Najafi M. Fine-grained dual phase steel via intercritical annealing of cold-rolled martensite. Vacuum. 2018;155(June):147–52.

116. Nouroozi M, Mirzadeh H, Zamani M. Effect of microstructural refinement and intercritical annealing time on mechanical properties of high-formability dual phase steel. Mater Sci Eng A [Internet]. 2018;736(August):22–6. Available from: https://doi.org/10.1016/j.msea.2018.08.088

117. Ghaemifar S, Mirzadeh H. Enhanced mechanical properties of dual-phase steel by repetitive intercritical annealing. Can Metall Q. 2017;56(4):459–63.

118. Li Z, Wu D, Lü W, Yu H, Shao Z, Luo L. Effect of holding time on the microstructure and mechanical properties of dual-phase steel during intercritical annealing. J Wuhan Univ Technol Mater Sci Ed. 2015;30(1):156–61.

119. Zeytin HK, Kubilay C, Aydin H. Investigation of dual phase transformation of commercial low alloy steels: Effect of holding time at low inter-critical annealing temperatures. Mater Lett. 2008;62(17–18):2651–3.

120. Balbi M, Alvarez-Armas I, Armas A. Effect of holding time at an intercritical temperature on the microstructure and tensile properties of a ferrite-martensite dual phase steel. Mater Sci Eng A [Internet]. 2018;733(February):1–8. Available from: https://doi.org/10.1016/j.msea.2018.07.029

121. Pichler A, Traint S, Arnoldner G, Werner E, Pippan R, Stiaszny P. Phase transformation during annealing of a cold-rolled dual phase steel grade. 42Nd Mech Work Steel Process Conf Proc. 2000;38(October):573–93.

122. Erişir E, Bilir OG. Effect of intercritical annealing temperature on phase transformations in medium carbon dual phase steels. J Mater Eng Perform. 2014;23(3):1055–61.

123. Evans P., Jones L, Grabham B, Gladwyn G, Brown A. Review of Process Windows for Zodiac Dual Phase Grades. 2017.

124. Drumond J, Girina O, da Silva Filho JF, Fonstein N, de Oliveira CAS, Cai MH, et al. Effects of Silicon and Manganese Addition on Mechanical Properties of High-strength Hot-rolled Sheet Steel Containing Retained Austenite. ISIJ Int. 2012;113(3):587–93.

125. Fonstein N, Jun HJ, Huang G, Sriram S, Yan B. Effect of bainite on mechanical properties of multiphase ferrite-bainite-martensite steels. Mater Sci Technol Conf Exhib 2011, MS T'11. 2011;1(January 2011):634–41.

126. Ghaheri A, Shafyei A, Honarmand M. Effects of inter-critical temperatures on martensite morphology, volume fraction and mechanical properties of dual-phase steels obtained from direct and continuous annealing cycles. Mater Des [Internet]. 2014;62:305–19. Available from: http://dx.doi.org/10.1016/j.matdes.2014.04.073

127. Basantia SK, Bhattacharya A, Khutia N, Das D. Influence of microstructural parameters on nanohardness of various dual-phase steels: Experiment, Finite Element simulation and Statistical analysis. Mater Today Commun [Internet]. 2022;30(January):103125. Available from: https://doi.org/10.1016/j.mtcomm.2022.103125

128. Tamura I, Tomota Y, Akao A, Yamaoka Y, Ozawa M, Kanatani S. On the Strength and Ductility of Two-Phase Iron Alloys. Trans Iron Steel Inst Jap. 1973;13(4):283–92.

129. Kuang C fu, Zheng Z wang, Zhang G ting, Chang J, Zhang S gen, Liu B. Effects of overaging temperature on the microstructure and properties of 600 MPa cold-rolled dual-phase steel. Int J Miner Metall Mater. 2016;23(8):943–8.

130. Kuang C fu, Zhang S gen, Li J, Wang J, Liu H fei. Effects of pre-strain and baking parameters on the microstructure and bake-hardening behavior of dual-phase steel. Int J Miner Metall Mater. 2014;21(8):766–71.

131. Nouri A, Saghafian H, Kheirandish S. Effects of Silicon Content and Intercritical Annealing on Manganese Partitioning in Dual Phase Steels. J Iron Steel Res Int [Internet]. 2010;17(5):44–50. Available from: http://linkinghub.elsevier.com/retrieve/pii/S1006706X10600982

132. Gao B, Chen X, Pan Z, Li J, Ma Y, Liu M, et al. A high-strength heterogeneous structural dual-phase steel. J Mater Sci [Internet]. 2019;54(19):12898–910. Available from: https://doi.org/10.1007/s10853-019-03785-1

133. Pan Z, Gao B, Lai Q, Chen X, Cao Y, Liu M, et al. Microstructure and Mechanical Properties of a Cold-Rolled Ultrafine-Grained Dual-Phase Steel. Materials (Basel). 2018;11:1–11.

134. Cai MH, Ding H, Zhang J, Long L. Effect of silicon and prior deformation of austenite on isothermal transformation in low carbon steels. Acta Metall Sin (English Lett [Internet]. 2009;22(2):100–9. Available from: https://doi.org/10.1016/S1006-7191(08)60076-9

135. Zhou L yu, Zhang D, Liu Y zheng. Influence of silicon on the microstructures, mechanical properties and stretch-flangeability of dual phase steels. Int J Miner Metall Mater. 2014;21(8):755–65.

136. Leslie W., Rauch G. Precipitation of carbides in low-carbon Fe-AI-C alloys. Metall Trans A.

1978;9(3):343–9.

137. Jr WMG. Steels : Classifications. Encycl Mater Sci Technol. 2001;8840–3.

138. Pan F, Ding P, Zhou S, Kang M, Edmonds D V. Effects of silicon additions on the mechanical properties and microstructure of high speed steels. Acta Mater. 1997;45(11):4703–12.

139. Calcagnotto M, Ponge D, Raabe D. Effect of grain refinement to 1µm on strength and toughness of dual-phase steels. Mater Sci Eng A [Internet]. 2010;527(29–30):7832–40. Available from: http://dx.doi.org/10.1016/j.msea.2010.08.062

140. Kozeschnik E, Bhadeshia HKDH. Influence of silicon on cementite precipitation in steels. Mater Sci Technol. 2008;24(3):343–7.

141. Smith A, Luo H, Hanlon DN, Sietsma J, Van Der Zwaag S. Recovery processes in the ferrite phase in C-Mn steel. ISIJ Int. 2004;44(7):1188–94.

142. Erdogan M. The effect of new ferrite content on the tensile fracture behaviour of dual phase steels. J Mater Sci. 2002;37(17):3623–30.

143. Hanai S, Tokunaga Y, Mizuyama Y, Takemoto N. Effect of Grain Size and Solid Solution Strengthening Elements on the Bake Hardenability of Low Carbon Aluminum-Killed Steel. Trans Iron Steel Inst Japan. 1984;24(1):17–23.

144. Ormsuptave N, Ã VU. Effect of Fine Grained Dual Phase Steel on Bake Hardening Properties. 2017;83(3):1–8.

145. Evans P., Jones L., Grabham B. Tata Steel Internal Report - DP1000 GI. 2017.

146. Davies RG. Influence of silicon and phosphorous on the mechanical properties of both ferrite and dual-phase steels. Metall Trans A. 1979;

147. Ahmad E, Manzoor T, Hussain N. Thermomechanical processing in the intercritical region and tensile properties of dual-phase steel. Mater Sci Eng A. 2009;508(1–2):259–65.

148. Evans P., Jones L., Grabham B. Tata Steel Internal Report - Bake Hardening of DP800 Steel. 2017.

149. BSI. EN10346:2015. 2015.

150. Goulas C, Mecozzi MG, Sietsma J. Bainite Formation in Medium-Carbon Low-Silicon Spring Steels Accounting for Chemical Segregation. Metall Mater Trans A Phys Metall Mater Sci. 2016;47(6):3077–87.

151. Chatterjee S, Koley S, Sarkar RB, Behera N, Manna M, Mukherjee S, et al. Design and Development of Galvannealed Dual-Phase Steel: Microstructure, Mechanical Properties and Weldability. J Mater Eng Perform [Internet]. 2019;28(1):231–41. Available from: https://doi.org/10.1007/s11665-018-3804-x

152. Kop T, Lansbergen M. DP1000GI Volume trial 410 with 3FAD. Ijmuiden; 2015.

153. Avendaño-Rodríguez D, Granados JD, Espejo-Mora E, Mujica-Roncery L, Rodríguez-Baracaldo R. Fracture mechanisms in dual-phase steel: Influence of martensite volume fraction and ferrite grain size. J Eng Sci Technol Rev. 2018;11(6):174–81.

154. M.S R, B.V.N R. Tempering characteristics of a vanadium containing dual phase steel. Metall Trans A. 1982;13:1679–86.

155. Li H, Gao S, Tian Y, Terada D, Shibata A, Tsuji N. Influence of Tempering on Mechanical Properties of Ferrite and Martensite Dual Phase Steel. Mater Today Proc. 2015;2(0):S667–71.

156. Türkmen M, Gündüz S. Bake-hardening response of high martensite dual-phase steel with different morphologies and volume fractions. Acta Metall Sin (English Lett. 2014;27(2):279–89.

157. Asadi M, De Cooman BC, Palkowski H. Influence of martensite volume fraction and cooling rate on the properties of thermomechanically processed dual phase steel. Mater Sci Eng A [Internet].

2012;538(2012):42–52. Available from: http://dx.doi.org/10.1016/j.msea.2012.01.010